

This file is part of the following work:

Kanakaraju, Devagi (2013) *Photochemical and solar degradation of pharmaceuticals in water*. PhD Thesis, James Cook University.

Access to this file is available from:

<https://doi.org/10.25903/0mab%2Ddv77>

Copyright © 2013 Devagi Kanakaraju

The author has certified to JCU that they have made a reasonable effort to gain permission and acknowledge the owners of any third party copyright material included in this document. If you believe that this is not the case, please email

researchonline@jcu.edu.au

ResearchOnline@JCU

This file is part of the following reference:

Kanakaraju, Devagi (2013) *Photochemical and solar degradation of pharmaceuticals in water*. PhD thesis, James Cook University.

Access to this file is available from:

<http://researchonline.jcu.edu.au/40321/>

The author has certified to JCU that they have made a reasonable effort to gain permission and acknowledge the owner of any third party copyright material included in this document. If you believe that this is not the case, please contact

*ResearchOnline@jcu.edu.au and quote
<http://researchonline.jcu.edu.au/40321/>*

**PHOTOCHEMICAL AND SOLAR DEGRADATION OF
PHARMACEUTICALS IN WATER**

**Thesis submitted by
Devagi Kanakaraju M.Sc
November 2013**

**For the degree of Doctor of Philosophy
School of Pharmacy and Molecular Sciences
James Cook University**

STATEMENT OF CONTRIBUTION OF OTHERS

The work reported in this thesis was conducted under the supervision of Assoc. Prof. Dr Michael Oelgemöller (School of Pharmacy and Molecular Sciences at James Cook University) and Prof. Dr Beverley D. Glass (School of Pharmacy and Molecular Sciences at James Cook University).

Dr Joy Morgan (School of Pharmacy and Molecular Sciences at James Cook University) provided training to the candidate on the use of high performance liquid chromatography.

Dr Cherie Motti from Australian Institute of Marine Sciences (AIMS) is acknowledged for providing training on the use of liquid-chromatography mass spectrometry, for collecting fourier transform-ion cyclotron resonance-mass spectrometry data and also for expert advice for mass spectrometry data analyses.

Dr Shane Askew at the Advanced Analytical Centre, James Cook University collected the scanning electron microscopy, energy dispersive spectroscopy and x-ray diffraction for integrated photocatalytic adsorbent samples reported in this thesis.

Financial assistance was provided by the Graduate Research Scheme (GRS 2011 and 2012) (James Cook University).

Townsville Laboratory Services (Douglas Water Treatment Plant) analysed the water quality parameters of river and drinking water used in this thesis.

STATEMENT OF ACCESS

I, the undersigned, the author of the thesis, understand that James Cook University will make it available for the use within the University Library and, by microfilm or other means, allow access to users in other approved libraries.

All users consulting this thesis will have to sign the following statement:

In consulting this thesis, I agree not to copy or closely paraphrase it in whole or in part without the written consent of the author, and to make proper public written acknowledgement for any assistance which I have obtained from it.

Beyond this, I do not wish to place any restriction on access to this thesis.

Signature

Date

STATEMENT OF SOURCES

DECLARATION

I declare that this thesis is my own work and has not been submitted in any form for another degree or diploma at any university or other institution of tertiary education. Information derived from the published or unpublished work of others has been acknowledged in the text and a list of reference is given.

Signature

Date

Acknowledgements

First and foremost, I would like to thank the Ministry of Higher Education Malaysia and Universiti Malaysia Sarawak for the Doctorate Training Award.

The completion of this work would have not been possible without the support of many people.

First and foremost, I offer my sincere gratitude to my principal supervisor, Assoc. Prof. Dr Michael Oelgemöller. Thank you for being a wonderful and cool supervisor. Thank you for the guidance and allowing me to work in my own way.

I also owe my deepest gratitude to my co-supervisor, Prof. Beverley D. Glass, for her endless patience and willingness to help me whenever I needed her advice and support.

My sincere thanks also go to Dr Cherie Motti from AIMS, who bailed me out from the mass spectrometry trauma and also when Louie, the HPLC, was completely down for months. Thank you for your help, guidance and meaningful advice. Also, for patiently answering all my questions, correcting my drafts and I have learnt much stuffs from you.

I also wish to extend my thanks to Assoc. Prof. Dr Bruce Bowden, Dr Dana Roberts and Mr David for their help. Also, not forgetting, Ohlu and Hines Maree.

I had the opportunity to meet exchange students from Germany, France and Japan. Tiffany, Manuela, Kilian, Alkit, Katrin, Adeline, Christina, Shin and Jordi, to name few. I had wonderful moments, especially our long coffee breaks in the lunch room and will cherish every moment in the coming years. Also, I will not forget our adventurous road trip to Crystal Creek with Assoc. Prof. Dr Michael Oelgemöller, Oksana, Caro and little Tia. Thanks to Jordi and Johnny for joining me in sky diving at Mission Beach, which was one of my best experiences in Australia.

I also have to thank my friends from the Molecular Sciences, Dr Ioana Bowden, Dr Bernhard, Simon Hu and Shiyoh for good company, fun and laughter and also to Jutta Kockler. My dearest friend, Dhanya, who has been there for me during my ups and downs and also thanks for her cooking and our wonderful road trips.

Another special 'person' who I would like to thank is my dear *Louie*, the HPLC. I had a great bonding with Louie these past 3 years although he betrayed me for some time.

My biggest thanks go to the man in my life, my husband, Ir. Thilagar Suberamaniam who supported me throughout this journey. Without his support, love, sacrifice and motivation nothing would have

been possible. I'm greatly indebted to him for taking good care of our little master, Sachiv Thilagar. And last but not least, to God who has been always been with me and kind to me.

This work is dedicated to my father.

Abstract

Active pharmaceutical ingredients (APIs), despite their beneficial effects on human or animal health, have emerged as an environmental pollutant due to their increased use and subsequent continuous entry into the aquatic environment. Existing wastewater treatment technologies are not designed to handle this specific class of pollutants and inadequate removal is commonly observed. Even in trace levels, APIs can trigger deleterious effects in terrestrial and aquatic organisms. This has resulted in APIs being recognized as an increasingly important environmental pollutant. This concern has necessitated the search for effective technologies to deal with this continuous accumulation of APIs in the environment.

The application of photochemical treatments, namely homogeneous and heterogeneous photocatalysis based on ultraviolet (UV) and sunlight, for the removal of APIs in water has been highlighted. Of these, titanium dioxide (TiO₂) photocatalysis has emerged as an effective treatment methodology for pharmaceutical removal. Its widespread application on large scales has been hindered by unfavourable kinetics, low degrees of mineralization and also high costs related to the use of artificial light and the recovery of TiO₂ nanoparticles. These issues need to be addressed now to ensure its adaptation for water treatment in the near future.

The aim of this study was to investigate the effects of direct photolysis and TiO₂ photocatalysis in combination with sunlight, a sustainable and low-cost light source and also UV light for the degradation of diclofenac (DCF), naproxen (NPX) and their mixtures in different water matrices. The efficiency of immobilized TiO₂ was furthermore assessed for amoxicillin (AMX) degradation.

In most cases, direct photolysis by UV irradiation allowed complete degradation for individual and mixture APIs. Lower degradation rates were observed when drinking water and river water were used compared to distilled water suggesting that the water matrix affects the efficiency of this process. The role of UV/TiO₂ photocatalysis in degrading DCF and NPX were examined by varying experimental parameters such as concentrations of APIs, TiO₂ loadings, solution pH and water matrices, with all parameters influencing the degradation of the APIs to some extent. A significant relationship between water matrix and the effectiveness of TiO₂ photocatalytic process has been observed. For mineralization, UV/TiO₂ photocatalysis led to higher oxidation rates compared to direct photolysis, although overall mineralization rates were incomplete. Studies using DCF and NPX mixtures revealed that degradation of NPX was slowed down in most cases in the presence of DCF. The degradation rates of both, DCF and NPX, in drinking water were suppressed in the presence of anions.

Solar degradation studies showed comparable performances with those undertaken under laboratory conditions although longer exposure times were generally required for the degradation of APIs. A

dependency of the removal efficiency on the water matrix was also found. Although differing sunlight intensities somehow impacted on the performances of solar photolysis and solar TiO₂ photocatalysis, the results showed that sunlight can be used as an inexpensive source of photons for API degradation.

Various degradation products were identified following the TiO₂ photocatalytic treatment of DCF, NPX and their mixtures by liquid-chromatography mass spectrometry (LC-MS) and fourier transform-ion cyclotron resonance-mass spectrometry (FT-ICR-MS). The degradation of DCF and NPX produced a total of eight degradation products, mainly as a result of decarboxylation and hydroxylation. Degradation of DCF and NPX mixtures produced fifteen degradants corresponding to degradations of the individual APIs, while two degradation products with much higher molecular weight than the parent APIs were identified.

Integrated photocatalytic adsorbents (IPA) were prepared from TiO₂, synthesized by a sol-gel method and natural zeolite, characterized and used for AMX degradation. The prepared IPA material from pre-treated acid-alkali zeolite calcined at 300°C under nitrogen optimally degraded AMX. The superior performance of this IPA material was confirmed by scanning electron microscope (SEM), energy-dispersive spectroscopy (EDS) and x-ray diffraction (XRD). SEM analysis showed an uneven surface structure as a result of TiO₂ cluster deposition. This increase in the surface roughness caused an increase in surface area, which then provides more active sites for adsorption and degradation to occur. XRD results showed that peaks from anatase, which are known to have a higher photocatalytic activity, were prominent in the IPA material calcined at 300°C. EDS analyses also confirmed the presence of higher amounts of TiO₂ in this material. The overall performance of the IPA material to degrade AMX was attributed to the adsorption capability of both the zeolite and photocatalytic activity of TiO₂. The immobilization of the synthesized TiO₂ on the surface of zeolite did not have a deleterious effect on the photoactivity of TiO₂.

This study confirms the findings from previous studies that the water matrices have a large effect on the performance of direct photolysis and TiO₂ photocatalysis for APIs degradation. TiO₂ photocatalysis can be efficient in degrading APIs; however, its performance is influenced by various operating parameters. The results obtained from TiO₂ photocatalytic degradations of API mixtures suggest that individual API components can hinder the degradation efficiency of other ones. This effect may be more pronounced when numerous APIs are present in real wastewater. Utilization of the same reactor for both solar and laboratory studies allowed a reasonable comparison although the “photon source” significantly contributed to the degradation efficiency. UV/TiO₂ photocatalysis, while efficiently degrading parent APIs, resulted in the formation of numerous degradation products. Thus, attention needs to be paid when applying this advance technology for real wastewater treatment as these degradants may be persistent or toxic themselves. Immobilized TiO₂ on natural zeolite can be

used for the degradation of APIs. In addition, it can be recovered and reused for subsequent degradations.

This study has clearly demonstrated that TiO_2 photocatalysis can be applied to degrade APIs in both surface and drinking water and offers an attractive option for small-scale pharmaceutical water treatment. The complex nature of real effluents with co-existing pollutants and higher levels of organic and inorganic matter however calls for coupling of biological processes as pre- or post-treatment to improve their biodegradability.

List of Publications

Book Chapter

D. Kanakaraju, B. D. Glass, M. Oelgemöller. Heterogeneous Photocatalysis for Pharmaceutical Wastewater Treatment; in: *Green Materials for Energy, Products and Depollution (Environmental Chemistry for a Sustainable World, Vol. 3)*, E. Lichtfouse, J. Schwarzbauer, D. Robert (Eds.), Springer, Dordrecht (2013), Chapter 3, 69-133.

Journal Articles

D. Kanakaraju, B. D. Glass, M. Oelgemöller. Heterogeneous photocatalysis application in pharmaceutical wastewater remediation. *Environmental Chemistry Letters* (2013). DOI: 10.1007/s10311-013-0428-0 (by invitation of the editors).

D. Kanakaraju, C. A. Motti, B. D. Glass, M. Oelgemöller. Photolysis and TiO₂-catalyzed degradation of diclofenac in surface and drinking water using circulating batch photoreactors. *Environmental Chemistry* (2014) DOI: 10.1071/EN13098 (accepted).

J. Kockler, D. Kanakaraju, B. D. Glass, M. Oelgemöller. Solar photochemical and photocatalytic degradation of diclofenac and amoxicillin in water. *Journal of Sustainability Science and Management* (2012). 7(1). 23-29

Conference Presentations

D. Kanakaraju, B. D. Glass, M. Oelgemöller. TiO₂ photocatalytic degradation of naproxen in water and the competitive effect of diclofenac. *3rd European Symposium on Photocatalysis* (25-27 September 2013), Portoroz, Slovenia.

D. Kanakaraju, B. D. Glass, M. Oelgemöller. Photocatalytic degradation of diclofenac and amoxicillin in water. *European Symposium on Photocatalysis* (29 & 30 September 2011), Bordeaux, France.

Awards

Best student poster presentation. Photochemical degradation of naproxen in water. *North Queensland Festival of Life Sciences*. JCU Townsville. 30 October 2012.

Queensland Tropical Health Alliances (QTHA) *Travel Awards Scheme for Students and Early Career Researchers 2012*.

Best oral presentation (runner-up). Degradation of Pharmaceuticals in Water via Photolysis and Photocatalysis. *North Queensland Festival of Life Sciences*. JCU Townsville. 3 November 2010.

Contents

Chapter 1. Introduction	1
1.1. Background	1
1.2. Objectives.....	3
1.3. Relevance	4
1.4. Thesis organization.....	5
Chapter 2. Literature Review	7
2.1. Pharmaceutical pollution	7
2.2. Overview of advanced oxidation processes (AOPs)	11
2.3. UV light and sunlight for degradation of pharmaceuticals.....	18
2.4. Photochemical degradation	20
2.4.1. Homogeneous photodegradation: Photolysis	21
2.4.2. Heterogeneous photodegradation: Photocatalysis	22
2.5. Photocatalyst features of titanium dioxide	24
2.5.1. General mechanism of TiO ₂ photocatalysis	25
2.6. Photochemical degradation of pharmaceuticals	27
2.7. Parameters affecting TiO ₂ photocatalysis.....	32
2.7.1. TiO ₂ concentration.....	32
2.7.2. Initial substrate concentration.....	33
2.7.3. Solution pH.....	33
2.7.4. Photon flux	34
2.7.5. Temperature.....	34
2.7.6. Electron acceptors	35
2.7.7. Water composition.....	36
2.8. NSAID model compound I: Diclofenac	36
2.8.1. Occurrence of diclofenac.....	36
2.8.2. Photolytic and photocatalytic degradation of diclofenac by UV and sunlight	37
2.8.3. Degradation pathway of diclofenac	41
2.9. NSAID model compound II: Naproxen	44
2.9.1. Occurrence of naproxen	44
2.9.2. Photolytic and photocatalytic degradation of naproxen by UV and sunlight	44
2.9.3. Degradation pathway of naproxen.....	47
2.10. Antibiotic model compound: Amoxicillin.....	49
2.10.1. Photolytic and photocatalytic degradation of amoxicillin	49
2.10.2. Degradation pathway of amoxicillin	53
Chapter 3. Materials and Methods	55
3.1. Reagents	55
3.2. River water and drinking water samples	55
3.3. Properties of the active pharmaceutical ingredients	56
3.4. Adsorption experiments	56
3.5. Photochemical degradation procedures	57
3.5.1. Immersion-well reactor	57
3.5.2. Demonstration-scale loop reactor.....	59
3.6. Solar exposures: Immersion-well reactor	61

3.7. Analytical methods.....	62
3.7.1. High performance liquid chromatography (HPLC).....	62
3.7.2. Mass spectrometry.....	66
3.7.3. UV-Vis spectroscopy.....	67
3.7.4. pH.....	67
3.7.5. Dissolved oxygen.....	67
3.7.6. Light intensity.....	67
3.7.7. Chloride ion.....	68
3.7.8. Determination of mineralization.....	68
3.8. Kinetic analysis.....	69

Chapter 4. Photochemical degradation of diclofenac, naproxen and their mixtures by UV light70

4.1. Introduction.....	70
4.2. HPLC method.....	70
4.2.1. HPLC method for individual compound analysis.....	70
4.2.2. HPLC method for diclofenac and naproxen mixture analysis.....	74
4.3. Photophysical properties.....	76
4.3.1. Diclofenac.....	77
4.3.2. Naproxen.....	78
4.3.3. Diclofenac and naproxen mixtures.....	80
4.4. Direct photolysis.....	80
4.4.1. Direct photolysis using an immersion-well reactor.....	80
4.4.2. Direct photolysis using a loop reactor.....	87
4.5. Photocatalytic degradation of diclofenac using an immersion-well reactor.....	89
4.5.1. Adsorption experiments.....	89
4.5.2. Effect of initial concentration.....	89
4.5.3. Effect of TiO ₂ concentration.....	90
4.5.4. Effect of air bubbling.....	92
4.5.5. Effect of solution pH.....	93
4.5.6. Effect of water matrix.....	95
4.5.7. TiO ₂ type and immersion-well tube material.....	97
4.6. Photocatalytic degradation of naproxen using an immersion-well reactor.....	98
4.6.1. Adsorption experiments.....	98
4.6.2. Effect of initial concentration.....	98
4.6.3. Effect of TiO ₂ concentration.....	99
4.6.4. Effect of solution pH.....	101
4.6.5. Effect of water matrix and anions.....	103
4.7. Photocatalytic degradation of diclofenac and naproxen mixtures using an immersion-well reactor.....	106
4.8. Mineralization in the immersion-well.....	109
4.9. TiO ₂ photocatalytic degradation using a loop reactor.....	111
4.9.1. Diclofenac.....	111
4.9.2. Naproxen.....	112
4.9.3. Diclofenac and naproxen mixtures.....	112
4.10. Mineralization in the loop reactor.....	113
4.11. Conclusions.....	115

Chapter 5. Solar photolytic and TiO₂ photocatalytic degradation of pharmaceuticals	117
5.1. Introduction	117
5.2. Solar degradation of diclofenac	117
5.3. Solar degradation of naproxen	123
5.4. Solar degradation of diclofenac and naproxen mixtures	129
5.5. Conclusions	136
Chapter 6. Identification of photoproducts and elucidation of degradation pathways	138
6.1. Introduction	138
6.2. Degradation products of diclofenac	138
6.3. Degradation products of naproxen	144
6.4. Degradation products of diclofenac and naproxen mixtures	150
6.5. Conclusions	155
Chapter 7. Integrated photocatalytic adsorbents for the degradation of amoxicillin	156
7.1. Introduction	156
7.2. Optimising titanium dioxide's photocatalytic activity	156
7.3. Integrated photocatalytic adsorbents	157
7.4. Titanium dioxide supported on Ca-alginate	159
7.5. Materials and method	159
7.5.1. Reagents and chemicals	159
7.5.2. Pre-treatment of natural zeolite	160
7.5.3. Preparation of IPA	160
7.5.4. Characterization	162
7.5.5. Point of zero charge	162
7.5.6. Dark adsorption	162
7.6. Preparation of Ca-alginate and immobilization of TiO ₂	162
7.7. Photocatalytic assessment on amoxicillin using immobilized TiO ₂	164
7.8. Degradation monitoring and identification of degradation products	166
7.9. Results and discussion	166
7.9.1. Preliminary degradation of amoxicillin	166
7.9.2. Characterization of integrated photocatalytic adsorbent	168
7.9.3. Point of zero charge measurement	171
7.9.4. Photocatalytic degradation of amoxicillin	171
7.9.5. Effect of catalyst concentration	174
7.9.6. Catalyst recycling	174
7.9.7. Mineralization	175
7.10. Amoxicillin degradation with TiO ₂ -gel beads	176
7.11. Degradation products of amoxicillin	177
7.12. Conclusions	181
Chapter 8. Conclusions and recommendation for future research	182
8.1. Summary	182
8.2. Conclusions	183
8.2.1. Photochemical degradation of diclofenac, naproxen and their mixtures by UV light	183
8.2.2. Solar photolytic and TiO ₂ photocatalytic degradation of pharmaceuticals	184
8.2.3. Identification of photoproducts and elucidation of degradation pathways	185

8.2.4. Integrated photocatalytic adsorbent for the degradation of amoxicillin	186
8.3. Recommendations for future research.....	187
8.3.1. Photochemical degradation of diclofenac, naproxen and their mixtures by UV light.....	187
8.3.2. Solar photolytic and TiO ₂ photocatalytic degradation of pharmaceuticals	188
8.3.3. Identification of photoproducts and elucidation of degradation pathways.....	188
8.3.4. Integrated photocatalytic adsorbent for the degradation of amoxicillin	188
References	190
Appendix	198

List of Figures

Chapter 1

Fig.1.1 Overall framework of work presented in this study	5
---	---

Chapter 2

Fig.2.1 Sources and routes of pharmaceuticals in the environment (modified from Nikolaou <i>et al.</i> [14] and Mompelat <i>et al.</i> [4])	8
Fig.2.2 Statistics of publications based on country occurrence of pharmaceuticals in the environment (Scopus database for search “Occurrence of pharmaceuticals AND environment” in all subject areas).....	9
Fig.2.3 Types of AOPs for pharmaceutical wastewater treatment	12
Fig.2.4 Spectral distribution of different lamps [89].....	18
Fig.2.5 Solar spectrum based on data by the American Society for Testing and Materials (ASTM) (http://www.astm.org/ASTM)	19
Fig.2.6 Commonly used lamps in pharmaceutical degradation studies.....	20
Fig.2.7 Photocatalytic processes on TiO ₂ semiconductor	25
Fig.2.8 Degradation products of direct photolysis of DCF [139, 161, 171].....	42
Fig.2.9 TiO ₂ photocatalytic degradation pathway of DCF [149]	43
Fig.2.10 Photolysis degradation products of NPX	48
Fig.2.11 TiO ₂ photocatalytic degradation products of NPX [126].....	48
Fig.2.12 Photocatalytic degradation of AMX [190].....	53
Fig.2.13 Proposed degradation pathway for AMX [193, 194].....	54

Chapter 3

Fig.3.1 Schematic representation and picture of immersion-well photoreactor setup.....	57
Fig.3.2 Spectral distribution of Heraeus TQ 150 medium pressure Hg lamp (manufacturer data) [198]	58
Fig.3.3 Loop reactor (Laboclean®, Tandem UV, a.c.k. aqua concept GmbH).....	60
Fig.3.4 (a) Solar degradation experimental setup (b) close-up of photoreactor (c) pump for water circulation	61
Fig.3.5 (a) HPLC (b) close-up of column unit and (c) close-up of autosampler	62
Fig.3.6 (a) LC-MS and (b) FT-ICR-MS	66

Chapter 4

Fig.4.1 DCF chromatogram with 80/20 MeOH/water (pH 4) (20 µL; λ = 274 nm; 0.8 mL/min, column: C18 Pursuit XRs (250 × 4.6 mm, 5 µm)).....	71
Fig.4.2 NPX (10 mg/L) chromatogram with 60/40 MeOH/1% CH ₃ COOH (20 µL; λ = 230 nm; 0.8 mL/min, column: C18 Pursuit XRs (250 × 4.6 mm, 5 µm)).....	72
Fig.4.3 Calibration curves for (a) DCF and (b) NPX	73
Fig.4.4 HPLC chromatogram of DCF and NPX mixture standard with 80/20 MeOH/0.01 M KH ₂ PO ₄ at pH 3.1 (20 µL; λ = 230 nm; column: C18 Phenomenex 150 × 4.6 mm, 2.6 µm)	74

Fig.4.5 HPLC chromatogram of DCF and NPX mixtures with 70/30 MeOH/0.01 M KH ₂ PO ₄ at pH 3 ($\lambda_{\text{DCF}} = 274 \text{ nm}$ and $\lambda_{\text{NPX}} = 230 \text{ nm}$; 20 μL ; column: C18 Phenomenex 150 \times 4.6 mm, 2.6 μm)	75
Fig.4.6 Calibration curves of NPX ($\lambda = 230 \text{ nm}$) and DCF ($\lambda = 274 \text{ nm}$) in a 1:1 mixture (NPX:DCF)	76
Fig.4.7 Molar absorption coefficients of DCF in water and medium pressure Hg lamp main emission lines (manufacturer data).....	77
Fig.4.8 Absorption spectra of DCF in water at different pHs	78
Fig.4.9 Molar absorption coefficients of NPX in water and medium pressure Hg lamp main emission lines (manufacturer data).....	78
Fig.4.10 Absorption spectra of NPX in water at different pHs	79
Fig.4.11 DCF and NPX mixture (1:1) ($C_0 = 30 \text{ mg/L}$) in water.....	80
Fig.4.12 Effect of immersion-well tube type on direct photolysis of individual DCF and NPX ($C_0 = 30 \text{ mg/L}$) in distilled water with time ($n=3$).....	81
Fig.4.13 Direct photolysis of DCF and NPX in the mixture ($C_0 = 30 \text{ mg/L}$) with pyrex immersion-well tube in distilled water ($n = 3$).....	81
Fig.4.14 HPLC chromatogram of direct photolysis of DCF ($C_0 = 30 \text{ mg/L}$) using pyrex immersion- well tube.....	83
Fig.4.15 HPLC chromatogram of direct photolysis of NPX ($C_0 = 30 \text{ mg/L}$) using pyrex immersion- well tube.....	83
Fig.4.16 UV spectra changes of direct photolysis of individual (a) DCF (b) NPX and (c) DCF and NPX mixtures (1:1) ($C_0 = 30 \text{ mg/L}$)	84
Fig.4.17 Effect of water matrix on direct photolysis of (a) DCF (30 mg/L) (b) NPX (30 mg/L)	85
Fig.4.18 Effect of initial concentration on the photolytic degradation of (a) DCF and (b) NPX in distilled water ($n=3$).....	86
Fig.4.19 Formation of chloride ions during DCF photolysis in distilled water ($C_0 = 30 \text{ mg/L}$)	87
Fig.4.20 Direct photolysis of individual compound (a) DCF ($C_0 = 30 \text{ mg/L}$), (b) NPX ($C_0 = 30 \text{ mg/L}$) and (c) DCF:NPX (1:1) mixtures ($C_0 = 30 \text{ mg/L}$) in the loop reactor (Laboclean®).....	88
Fig.4.21 Effect of DCF initial concentration (a) 10 and 30 mg/L and (b) 50-70 mg/L on photocatalytic reaction kinetics (0.1 g/L TiO ₂ P25, pH = 6, $T_{\text{max}} 29^\circ\text{C}$).....	89
Fig.4.22 Effect of TiO ₂ concentrations (0.01-2 g/L) on DCF photocatalytic degradation ($C_0 = 30 \text{ mg/L}$) in distilled water with a medium pressure Hg lamp.....	91
Fig.4.23 Photocatalytic degradation of DCF with TiO ₂ P25 and TiO ₂ P25/DO ($C_0 = 30 \text{ mg/L}$, TiO ₂ = 0.1 g/L, air flow rate = 55.5 mL/min)	92
Fig.4.24 Dissolved oxygen profile for the photocatalytic degradation of DCF($C_0 = 30 \text{ mg/L}$; TiO ₂ = 0.1 g/L; air flow rate = 55.5 mL/min)	93
Fig.4.25 Effect of initial solution pH on DCF photocatalytic degradation	94
Fig.4.26 Effect of initial solution pH on rate constant (k_{app}) of DCF photocatalysis	95
Fig.4.27 Effect of water matrix on DCF degradation by UV/TiO ₂ and UV/TiO ₂ /H ₂ O ₂ ($C_0 = 30 \text{ mg/L}$; TiO ₂ = 0.1 g/L; H ₂ O ₂ = 250 mg/L)	96
Fig.4.28 Kinetics of DCF degradation by UV/TiO ₂ and UV/TiO ₂ /H ₂ O ₂ oxidation in different water matrices.....	96
Fig.4.29 Comparison of photocatalytic degradation with different photocatalysts and filters.....	97
Fig.4.30 Effect of NPX concentrations on TiO ₂ photocatalytic degradation	99
Fig.4.31 Effect of TiO ₂ concentration (0.01-2 g/L) on fixed NPX concentration ($C_0 = 30 \text{ mg/L}$)....	100
Fig.4.32 Effect of solution pH on NPX degradation ($C_0 = 30 \text{ mg/L}$; TiO ₂ = 0.1 g/L)	102
Fig.4.33 Pseudo-first-order kinetics of NPX photocatalytic degradation at different pHs.....	102

Fig.4.34 Effect of anions on photocatalytic degradation of NPX (30 mg/L, TiO ₂ P25 0.1 g/L,) (a) river water (20 mg/L of phosphate and chloride) (b) drinking water (20 mg/L of chloride)	104
Fig.4.35 Photocatalytic degradation of DCF and NPX mixture (1:1) (C ₀ = 30 mg/L; TiO ₂ P25 0.1 g/L) in distilled water and drinking water.....	106
Fig.4.36 Photocatalytic degradation of DCF and NPX mixtures (a) DCF:NPX (2:1) and (b) DCF:NPX (1:2) in distilled water.....	107
Fig.4.37 Effect of anions on TiO ₂ photocatalysis of DCF:NPX (1:1) mixtures in drinking water (C ₀ = 30 mg/L DCF and NPX; TiO ₂ 0.1 g/L ; 20 mg/L phosphate and chloride).....	108
Fig.4.38 DOC removal in the immersion-well during TiO ₂ photocatalysis of (a) DCF and (b) NPX in distilled water and drinking water.....	109
Fig.4.39 DOC removal during direct photolysis and TiO ₂ photocatalysis of DCF and NPX mixtures in distilled water.....	110
Fig.4.40 Photocatalytic oxidation (UV/TiO ₂ and UV/TiO ₂ /H ₂ O ₂) of DCF in distilled water and drinking water in the loop reactor.....	111
Fig.4.41 TiO ₂ photocatalysis of NPX in distilled water and drinking water in the loop reactor (C ₀ = 30 mg/L; TiO ₂ = 0.1 g/L).....	112
Fig.4.42 TiO ₂ photocatalysis of DCF and NPX (1:1) mixtures in the loop reactor (a) distilled water and (b) drinking water (C ₀ = 30 mg/L; TiO ₂ = 0.1 g/L)	113
Fig.4.43 DOC removal in the loop reactor for (a) DCF, (b) NPX and (c) DCF and NPX (1:1) mixtures	114

Chapter 5

Fig.5.1 Solar degradation of DCF by (a) solar photolysis and (b) solar/TiO ₂ photocatalysis (solar/TiO ₂ and solar/TiO ₂ /H ₂ O ₂) in different water matrices at natural pH (C ₀ = 30 mg/L; TiO ₂ = 0.1 g/L; H ₂ O ₂ = 250 mg/L).....	119
Fig.5.2 COD reduction of DCF during solar photolysis and solar/TiO ₂ photocatalysis	119
Fig.5.3 Pseudo-first-order kinetics for solar photolysis and TiO ₂ photocatalysis (solar/TiO ₂ and solar/TiO ₂ /H ₂ O ₂) of DCF in drinking water and river water	121
Fig.5.4 Typical variation of lux and temperature in the reactor on (a) 8 th October 2012 during TiO ₂ photocatalysis (solar/TiO ₂) of DCF in distilled water, and (b) 12 th November 2012 (during TiO ₂ photocatalysis (solar/TiO ₂ /H ₂ O ₂) of DCF in drinking water	122
Fig.5.5 Solar photolysis of NPX in different water matrices	124
Fig.5.6 Solar light intensity measured during solar photolysis of NPX in different water matrix	125
Fig.5.7 COD reduction during solar photolysis and solar TiO ₂ photocatalysis of NPX	126
Fig.5.8 Solar TiO ₂ photocatalysis of NPX in (a) distilled water and drinking water; (b) river water (C ₀ = 30 mg/L; TiO ₂ = 0.1 g/L; chloride = 20 mg/L; phosphate = 20 mg/L).....	127
Fig.5.9 Kinetics of solar TiO ₂ degradation of NPX in drinking water (a) pseudo-first-order kinetic, and (b) second-order-kinetic	127
Fig.5.10 UV absorbance changes during solar TiO ₂ photocatalysis of NPX in drinking water	128
Fig.5.11 Solar photolysis of DCF and NPX mixtures in distilled water	130
Fig.5.12 Solar photolysis of DCF and NPX mixtures in drinking water.....	130
Fig.5.13 Solar photolysis of DCF and NPX mixtures in river water.....	131
Fig.5.14 Absorbance spectra of DCF, NPX and global solar spectrum (ASTM)	131
Fig.5.15 UV absorbance changes during solar photolysis of (a) drinking water and (b) river water	132

Fig.5.16 Solar TiO ₂ photocatalysis degradation of mixtures in (a) distilled water, (b) drinking water and (c) river water	133
Fig.5.17 Solar TiO ₂ photocatalysis degradation of mixtures in drinking water in the presence of chloride anions (C ₀ = 30 mg/L; TiO ₂ = 0.1 g/L; chloride = 20 mg/L)	134
Fig.5.18 COD reduction in the DCF and NPX mixtures by solar (a) TiO ₂ photocatalysis and (b) photolysis	135

Chapter 6

Fig.6.1 LC-MS ions of DCF standard (a) (-)-ESI mode and (b) (+)-ESI mode. The top spectrum in each figure is the UV chromatogram, also shown is the BPC. EICs show the ions formed under ESI conditions	139
Fig.6.2 Isotopic distribution of the sodiated ion of DCF, C ₁₄ H ₁₁ O ₂ NCl ₂ , [M + Na ⁺] ⁺ a) observed distribution for [M + Na ⁺] ⁺ by LC-MS b) observed distribution for [M + Na ⁺] ⁺ by FT-ICR-MS and c) theoretical distribution calculated for [M + Na ⁺] ⁺	140
Fig.6.3 TiO ₂ photocatalytic degradation pathways of DCF as confirmed by both LC-MS ^a and FT-ICR-MS ^b	141
Fig.6.4 LC-MS data of TiO ₂ photocatalysis of DCF (a) in (-)-ESI mode and (b) (+)-ESI mode. The top spectrum in each figure is the UV chromatogram, also shown is the BPC. EICs show the retention times and masses of the degradation products	142
Fig.6.5 Profile of chloride evolution and degradation of DCF by TiO ₂ photocatalysis	143
Fig.6.6 Photolytic degradation of DCF in distilled water.....	144
Fig.6.7 LC-MS ions of NPX standard (a) (-)-ESI mode and (b) (+)-ESI mode. The top spectrum in each figure is the UV chromatogram, also shown is the BPC. EICs show the ions formed under ESI conditions	145
Fig.6.8 LC-MS data of TiO ₂ photocatalysis of NPX (a) in (-)-ESI and (b) (+)-ESI. The top spectrum in each figure is the UV chromatogram, also shown is the BPC. EICs show the retention times and masses of the degradation products	147
Fig.6.9 Proposed TiO ₂ photocatalytic degradation pathway of NPX	148
Fig.6.10 LC-MS ion of DCF and NPX mixture standard (a) (-)-ESI mode and (b) (+)-ESI mode. The top spectrum in each figure is the UV chromatogram, also shown is the BPC. EICs show the ions formed under ESI conditions	151
Fig.6.11 UV chromatogram and BPC (-)-ESI and (+)-ESI of DCF and NPX mixtures	153
Fig.6.12 LC-MS data of common ions in the TiO ₂ photocatalysis of DCF and NPX mixtures in (a) (-)-ESI and (b) (+)-ESI. The top spectrum in each figure is the UV chromatogram, also shown is the BPC. EICs show the retention times and masses of the degradation products.....	154

Chapter 7

Fig.7.1 Structure of zeolite [250]	158
Fig.7.2 TiO ₂ /zeolite IPA preparation process.....	161
Fig.7.3 Synthesized TiO ₂ /zeolite from acid-alkali activated zeolites after oven drying (before homogenisation)	161
Fig.7.4 Preparation of TiO ₂ -gel beads based on method A	163
Fig.7.5 Immobilized TiO ₂ -gel beads	163
Fig.7.6 Differences between method A and method B applied to the preparation of TiO ₂ -gel beads.....	164

Fig.7.7 Absorbance spectrum of AMX in water	164
Fig.7.8 Schematic presentation and picture of immersion-well photoreactor setup.....	165
Fig.7.9 Comparison of TiO ₂ /zeolite calcined under nitrogen and air at 300°C for the degradation performance on AMX.....	167
Fig.7.10 SEM images of the materials: (a) natural zeolite, (b) acid-treated zeolite, (c) acid-alkali treated zeolite, (d) TiO ₂ /zeolite acid-alkali (300°C) and (e) TiO ₂ /zeolite acid (300°C)	169
Fig.7.11 XRD pattern of TiO ₂ /zeolite calcined at 300°C and 450°C and bare zeolite (A = anatase and R = rutile)	170
Fig.7.12 Point of zero charge for TiO ₂ /zeolite	171
Fig.7.13 Degradation of AMX under different conditions(C ₀ = 30 mg/L; catalyst concentration: 2 g/L)	172
Fig.7.14 Effect of catalysts concentration on the degradation of 30 mg/L AMX	174
Fig.7.15 Performance of recycled TiO ₂ /zeolite for AMX degradation	175
Fig.7.16 DOC removal during direct photolysis and photocatalysis (TiO ₂ P25, TiO ₂ /zeolite and TiO ₂ only) on AMX.....	176
Fig.7.17 Degradation of AMX (30 mg/L) with TiO ₂ -gel beads (10% v/v) from method A and method B.....	176
Fig.7.18 LC-MS ion of AMX standard in (+)-ESI mode. The top spectrum in each figure is the UV chromatogram, also shown is the BPC. EICs show the ions formed	178
Fig.7.19 UV (274 nm) and BPC (+)-ESI of TiO ₂ /zeolite photocatalysis of AMX. (A) After hydrolysis and (B) after 240 min of irradiation	179
Fig.7.20 Hydrolysis products of AMX confirmed by LC-MS analyses prior to irradiation under TiO ₂ /zeolite photocatalytic conditions	180

List of Tables

Chapter 2

Table 2.1 Application of different types of AOPs on pharmaceuticals degradation	13
Table 2.2 Band gap energy and minimum wavelength for selected photocatalysts [108, 109]	23
Table 2.3 Characteristics comparing of TiO ₂ P25 to other commercial photocatalysts	25
Table 2.4 Photolytic and photocatalytic oxidation of pharmaceuticals	28
Table 2.5 Summary of photolytic and TiO ₂ photocatalytic studies on DCF	38
Table 2.6 Summary of photolytic and TiO ₂ photocatalytic studies on NPX	45
Table 2.7 Summary of photolytic and TiO ₂ photocatalytic studies on AMX	50

Chapter 3

Table 3.1 Water quality characteristics of river water and drinking water	55
Table 3.2 APIs focused on in this study	56
Table 3.3 Tested parameters in photodegradation studies of individual APIs and their mixtures in an immersion-well photoreactor with a medium pressure Hg lamp	59
Table 3.4 Tested parameters in photodegradation studies of individual APIs and their mixtures in a loop reactor (Laboclean®) equipped with a medium pressure Hg lamp	60
Table 3.5 Selected solar degradation studies of DCF (C ₀ = 30 mg/L)	63
Table 3.6 Selected solar degradation studies of NPX (C ₀ = 30 mg/L)	64
Table 3.7 Selected solar degradation studies of DCF and NPX mixtures (DCF:NPX 1:1) (C ₀ = 30 mg/L)	65

Chapter 4

Table 4.1 HPLC conditions employed for DCF and NPX detection in this study	72
Table 4.2 Validated parameters of HPLC methods used for DCF and NPX	73
Table 4.3 Results of recovery (± standard deviation, SD) for DCF and NPX	74
Table 4.4 Results of the linear study for DCF and NPX mixtures	76
Table 4.5 Molar absorption coefficient values of DCF in water at different wavelengths	77
Table 4.6 Molar absorption coefficient values of NPX in water at different wavelengths	79
Table 4.7 Comparison of direct photolysis on degradation rate constants (k) between individual and API mixtures using different immersion-well tubes (C ₀ = 30 mg/L)	82
Table 4.8 Kinetic parameters for TiO ₂ photocatalytic degradation of different initial concentrations of DCF	90
Table 4.9 Pseudo-first-order rate constant for photocatalytic degradation of DCF with different TiO ₂ concentrations	91
Table 4.10 Kinetic parameters for TiO ₂ photocatalytic degradation of different initial concentration of NPX	99
Table 4.11 Extended effect of TiO ₂ concentration (0.01-2.0 g/L) on NPX degradation (5 - 50 mg/L)	100
Table 4.12 Rate constants for TiO ₂ photocatalytic degradation of NPX in the presence of anions in river water and drinking water	104

Table 4.13 Rate constants (k_{app}) of UV/TiO ₂ degradation of DCF and NPX mixtures ($C_0 = 30$ mg/L) in distilled water and drinking water (UV/TiO ₂ and UV/TiO ₂ + anions)	107
--	-----

Chapter 5

Table 5.1 Summary of solar degradation studies on DCF.....	118
Table 5.2 Summary of solar degradation studies of NPX	123
Table 5.3 Summary of solar degradation studies of DCF and NPX mixtures.....	129

Chapter 6

Table 6.1 Degradation products of DCF resulting from UV/TiO ₂ with a medium pressure Hg lamp identified by a combination of (+/-)-ESI LC-MS and FT-ICR-MS techniques.....	141
Table 6.2 Degradation products of NPX from UV/TiO ₂ with a medium pressure Hg lamp identified by a combination of (+/-)-ESI LC-MS and FT-ICR-MS techniques	146
Table 6.3 Degradation products of DCF and NPX mixtures resulting from UV/TiO ₂ with a medium pressure Hg lamp identified by a combination of (+/-)-ESI LC-MS and FT-ICR-MS techniques	152

Chapter 7

Table 7.1 Composition of Escott natural zeolite	160
Table 7.2 Quantitative analysis of IPA with EDS	168
Table 7.3 Hydrolysis products of AMX detected by LC-MS in (+)-ESI mode	180

Chapter 1. Introduction

1.1. Background

The past two decades, since the 1990s, have witnessed extensive research directed towards pharmaceuticals in the environment, and these compounds are now classified as emerging organic contaminants. The renewed interest from the scientific community in pharmaceuticals has stemmed as a result of advancement in analytical methods permitting detection down to parts per trillion (ng/L) of such contaminants in environmental samples [1]. Such advancement has laid the foundation for the detection of a wide spectrum of pharmaceutical substances in the environment, originating from human and veterinary use. Despite this advancement, information on the behaviour, fate, effects and chronic toxicity of these substances in the environment is still limited.

Drug products (pharmaceuticals) containing active pharmaceutical ingredients (APIs), despite being originally designed as drugs to treat a variety of ailments in humans and animals, have in fact turned out to have negative environmental impact due to their excessive use and subsequent occurrence in surface water, groundwater, urban wastewater and also drinking water. Among the numerous available APIs on the market, an environmentally important groups of pharmaceuticals includes non-steroidal anti-inflammatory drugs, antibiotics, beta-blockers (β -blockers), antiepileptics, blood lipid-lowering agents, antidepressants, hormones, antihistamines [2] and X-ray contrast media [3]. When discharged from hospitals, households, industries and pharmacies, these pharmaceuticals may enter wastewater treatment plants (WWTPs). Due to the considerable variation in physico-chemical properties of pharmaceuticals and the configuration of WWTP facilities, the efficiency of treatments can vary significantly requiring a broad range of removal protocols [4, 5]. The non-biodegradable nature and relatively high solubility of the APIs renders conventional biological and chemical treatments ineffective, thus leading to an increased presence of the parent drugs and their metabolites into both the aquatic and terrestrial environments. Veterinary medicines are also known to directly increase APIs levels in the soil and groundwater. Consequently, their concentrations, which are commonly reported in trace levels (ng/L to $\mu\text{g/L}$) [6] have the potential to harm terrestrial and aquatic organisms [7]. Hence, APIs have been recognized as important environmental pollutants necessitating the search for effective technologies to reduce their increasing concentration in the environment.

Among water treatment technologies employed thus far, Advanced Oxidation Processes (AOPs) present a great potential for treating a wide range of emerging contaminants, such as pharmaceuticals. AOPs are all based on the *in-situ* generation of highly reactive and short-lived reactive oxygen species (ROS) with low selectivity such as hydroxyl radicals (HO^\bullet), H_2O_2 , O_3 and

superoxide anion radical ($O_2^{\cdot-}$), ideally providing pathways for the organic compounds to complete mineralization to CO_2 , H_2O and inorganic ions or acids [8].

Commonly applied photochemical technologies (e.g. UV, UV/ H_2O_2) and increasingly popular photocatalytic oxidation (e.g. UV/ TiO_2) processes both aiming at pollutant abatement, mineralization and improvement of biodegradability, have been actively investigated for water treatment to remove pharmaceuticals. Direct and indirect photochemical degradation protocols have been reported to be efficient to degrade various APIs [9]. The ability of most APIs to undergo direct photolysis may be limited by the poor light absorption by the target compound. Under such circumstances, indirect photolysis by photocatalysts, which generates reactive species such as singlet oxygen, hydroxyl or peroxy radicals, is employed. Recently, photocatalytic oxidation, in particular with semiconductor titanium dioxide (TiO_2) has found increasing attention in water purification. This process, which offers the advantage to operate at mild (ambient) temperature and pressure as well as permitting the use of sunlight as irradiation source has proven to be efficient in the removal of pharmaceuticals from water.

Despite existing studies highlighting the effectiveness of the ultraviolet mediated TiO_2 oxidation (UV/ TiO_2) approach for pharmaceutical degradation, there remains a major gap in knowledge that needs to be addressed to ensure successful application to water purification in the future. Most of the existing research has concentrated on ultrapure water, although studies are attempting to address this deficiency by using environmentally relevant matrices such as wastewater effluents, hospital wastewater and surface water have increased. Literature dealing with bench scale photochemical degradation and artificially induced light sources, in general, outweigh studies performed on pilot scale with sunlight. Also, many existing studies focus on the photodegradation of a single compound rather than pharmaceutical mixtures which would be required for the work to be applied practically. In terms of kinetics, UV/ TiO_2 oxidative studies have shown that removal and degradation rates of pharmaceuticals relies upon operational parameters such as TiO_2 type and concentration, pH and water constituents, all of which vary depending on the compound itself. Variation of photoreactor designs or experimental setup and different water qualities also contribute to API degradation rates [10].

During the course of UV/ TiO_2 treatment, complete degradation of the parent API may not occur and the formation of innocuous photoproducts is common. In most studies, complete degradation of pharmaceuticals resulted in low mineralization rates [9]. An important reason for this is the formation of stable intermediates and degradation products, compared to the parent compound. The non-selective nature of HO^{\cdot} radicals also contributes to the formation of undesirable degradation

products. Hence, the determination of mineralization degree and identification of degradation products upon UV/TiO₂ oxidation treatment are areas of concern.

TiO₂ nanoparticles present a major technical problem, limiting their application in existing water purification technology [11]. While many studies have demonstrated that UV/TiO₂ oxidation is suitable for remediation of pharmaceutical wastewater, a major deficiency in the optimization of this technique is the recovery of TiO₂. One approach to circumvent this limitation is by using the immobilization to generate integrated photocatalytic adsorbents (IPAs), which enable a 'capture and destroy', may be applied. Titania nanoparticles can be dispersed on inert and high surface area supports such as activated carbon, zeolite, silica or glass. Among the supports utilized so far, there is a paucity in studies based on natural zeolites, a naturally abundant material, which can be readily exploited for the preparation of IPAs to degrade pharmaceuticals.

Systematic investigations of the effects of light (artificial UV light source and sunlight) on the degradation of pharmaceuticals via direct photolysis and TiO₂ photocatalysis of individual API and their mixtures as well as the identification of resulting degradation products is important for future applications of this advanced technology in water treatment. Therefore, the approach taken in this study addresses the current shortcomings previously highlighted by:

- i. systematically comparing photolysis and photocatalysis for two commonly used APIs of high environmental concern, diclofenac (DCF) and naproxen (NPX),
- ii. examining photodegradation of API mixtures in water by considering environmentally relevant conditions (e.g. the presence of anions and water matrix),
- iii. immobilizing TiO₂ nanoparticles and their application to the degradation of the photostable beta-lactam (β -lactam) antibiotic, amoxicillin (AMX).

1.2. Objectives

One major objective of the work presented was to investigate the removal of two non-steroidal anti-inflammatory drugs (NSAIDs), DCF and NPX, individually and their mixtures from water upon photochemical and solar treatment using direct photolysis and TiO₂ photocatalysis. Another main objective of the study was to examine the degradation of AMX with immobilized TiO₂. The specific aims of this work were to:

- i. determine the effects of operational parameters on the degradation kinetics of DCF and NPX individually and mixtures thereof in water by direct photolysis and TiO₂ photocatalysis,

- ii. compare the efficiency of UV light and sunlight to degrade these APIs by direct photolysis and TiO₂ photocatalysis in water by evaluating their degradation kinetics and the degree of mineralization measured as either dissolved organic carbon (DOC) or chemical oxygen demand (COD) in the photochemically treated samples,
- iii. identify main degradation products of DCF, NPX and their mixtures formed during UV/TiO₂ oxidation and
- iv. evaluate the efficiency of synthesized TiO₂/zeolite IPAs and TiO₂-containing alginate beads to degrade AMX.

1.3. Relevance

The key strategy of designing drugs with high stability for the various health issues of humans as well as animals has at the same time provided environmental challenges for mankind. Pharmaceuticals are continuously accumulating in the environment as a result of the excretion in urine and faeces by humans and livestock, but also by other important anthropogenic sources. There is frequent detection of either the parent compound or their metabolites in the aquatic environment, and this signifies a major concern when dealing with these micropollutants. Moreover, pharmaceuticals in general are presently neither regulated nor included in any drinking water quality standards. Regulations and strategies imposed for ecological risk assessment of drugs generally varies among countries, although efforts by the European Union (EU), Canada and the United States (US) are more dominant [12].

As typical conventional wastewater treatment involves high operating costs and energy consumption, is generally inefficient at completely eliminating persistent pollutants, and often produces hazardous by-products and generates large amounts of solid waste, efficient elimination technologies for pharmaceuticals are crucial. AOP techniques provide a viable alternative or an add-on option for removal of pharmaceuticals and water treatment in general. This study applies solar photochemical degradation, a green and energy-efficient treatment method for the degradation of environmentally important classes of pharmaceuticals, namely the NSAIDs and antibiotics. It is envisaged that the use of sunlight as a sustainable energy source will not contribute to climate change. Likewise, waste disposal can be minimized due to conversion of pharmaceuticals to more biodegradable compounds. Degradation with artificial UV light conducted under laboratory conditions allows comparison in terms of efficiency with solar degradation. As pharmaceuticals mostly occur in the environment as mixtures, an understanding of the effects on each other has prompted the degradation of pharmaceutical mixtures in this study.

1.4. Thesis organization

The conceptual framework of the work presented in this thesis is illustrated in Fig.1.1.

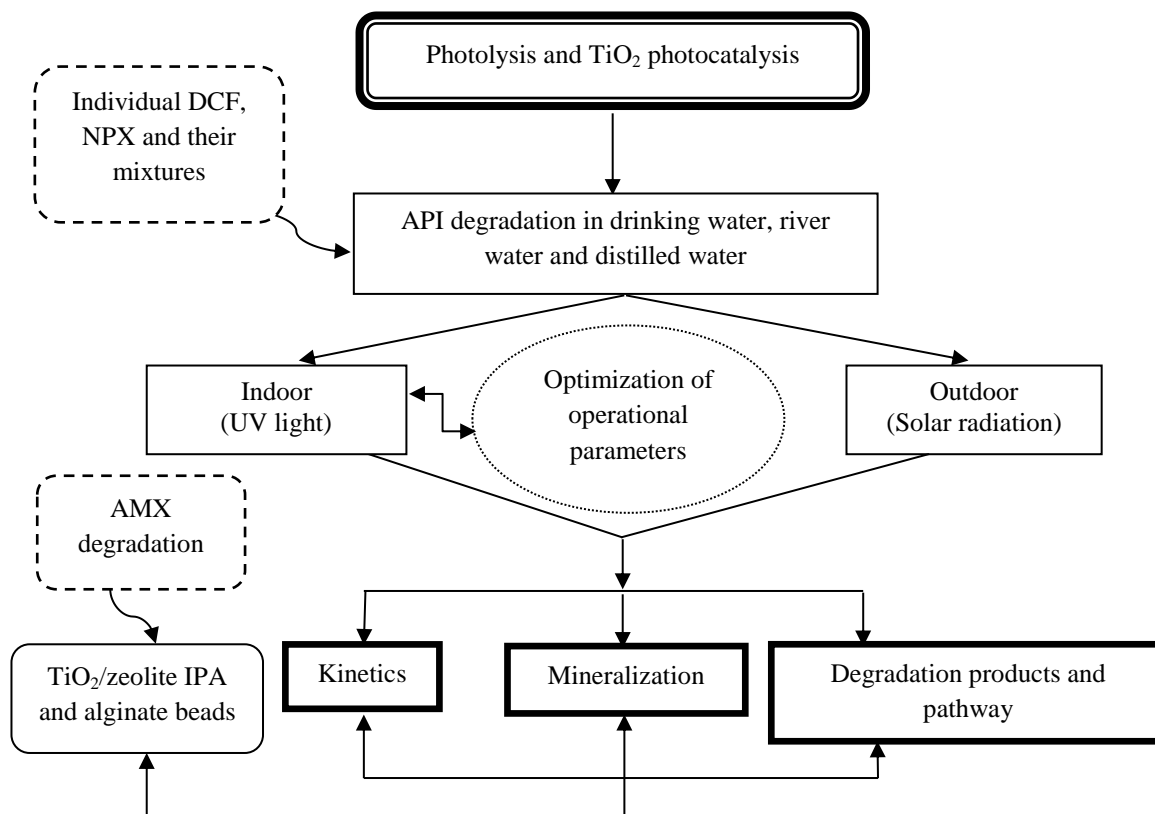


Fig.1.1 Overall framework of work presented in this study

This chapter (*Chapter 1*) provides the statement of problem, objectives, relevance and also the overall framework of this study.

Chapter 2 introduces issues related to pharmaceutical pollution followed by application of different types of AOPs, which can be applied for pharmaceutical water treatment. An overview of direct photolysis and UV/TiO₂ photocatalysis performed on different classes of pharmaceuticals is provided. Likewise, a review of the application of direct photolysis and TiO₂ photocatalytic oxidative systems tailored towards the chosen model compounds, DCF, NPX and AMX is presented.

Chapter 3 describes the materials and methods used to conduct the photochemical degradation experiments of DCF, NPX and their mixtures under either laboratory-based or natural sunlight conditions. Detailed experimental setups and procedures for each photoreactor used are provided. Measurement, analyses and interpretation of the degradation kinetics are also discussed.

Artificial UV photodegradation results for DCF, NPX and their mixtures under different conditions using two different circulating batch reactors are presented in *Chapter 4*.

In *Chapter 5*, findings obtained from solar-mediated degradation of DCF, NPX and their mixtures are discussed.

Chapter 6 details the identification of main degradation products by employing a combination of electrospray ionization, liquid chromatography mass spectrometry (LC-MS) and fourier transform-ion cyclotron resonance-mass spectrometry (FT-ICR-MS) techniques. The identified degradation products and proposed degradation pathways for individual DCF, NPX and their mixtures are presented.

A photocatalytic assessment of TiO₂/zeolite IPA and TiO₂-alginate beads on AMX degradation is shown in *Chapter 7*. The chapter begins with an overview of different immobilization techniques and supports for the TiO₂, followed by preparation procedures, characterization and photocatalytic assessment. The results obtained for AMX degradation with immobilized TiO₂ are discussed. Main degradation products formed during photocatalysis with TiO₂/zeolite IPA were also proposed.

The final chapter, *Chapter 8*, provides the major conclusions drawn from this study and recommendations for future work.

Chapter 2. Literature Review

2.1. Pharmaceutical pollution

Pharmaceuticals and other chemicals with endocrine disrupting properties (EDCs) have gained considerable importance as environmental pollutants, which are reflected through the efforts of several countries and agencies. Recently, the United States Environmental Protection Agency (USEPA) has included three pharmaceuticals on their recent contaminant candidate list (CCL-3) together with eight synthetic hormones and other disinfection by-products and pesticides [1]. Most APIs and EDCs have remained unregulated, although the EU and the USA in particular have demonstrated great interest in combating the presence of pharmaceuticals in the environment [12, 13]. This has been manifested through several directives and frameworks such as the community program of research on endocrine disrupters and environmental hormones (COMPREHEND), ecotoxicological assessments and removal technologies for pharmaceuticals in wastewater (REMPHARMAWATER), environmental risk assessment of veterinary medicines in slurry (ERAVMIS) by the EU and endocrine disruptor screening program (EDSP) by the USEPA [13]. In addition, the Food and Drug Administration (FDA) requires an environmental assessment report for APIs that are anticipated to be released into the environment with concentration $\geq 1 \mu\text{g/L}$ [14]. These efforts clearly indicate that pharmaceuticals can be declared to be environmental threats in the near future and therefore demands attention now.

APIs from human usage are mainly excreted in urine and faeces into receiving waters to different degrees depending on the dose and individual physiology [15]. Elimination from the human body occurs after being partially or completely converted to water-soluble metabolites or, in some cases, without being metabolized via urine and faeces directly into sewage system and eventually to WWTPs. Therefore, urban WWTPs have been recognized as a primary source for the detection of pharmaceuticals in the aquatic environment [16]. Mompelat *et al.* [4] compiled the excretion rate of human and veterinary pharmaceuticals and their metabolites based on therapeutic use. Several metabolites were highlighted in the review such as clofibric acid, major metabolite of lipid regulators and 10, 11-dihydro-10,11-dihydroxycarbamazepine and 10,11-dihydro-10,11-epoxycarbamazepine, two major metabolites of carbamazepine, have already been detected in the environment, raising considerable concern. Other important sources associated for pharmaceutical detection in water bodies include inappropriate disposal of medications by households, pharmaceutical manufacturers, hospitals and pharmacies [17] (Fig.2.1). In addition, a significant contribution of pharmaceuticals due to animal farming takes place directly through aquaculture, agricultural runoff and leaching [2].

Therapeutic or veterinary drugs with different physico-chemical properties, physiological activity and resistance to biological degradation by specific metabolic pathways translate into their persistent characteristics and pharmacokinetic behaviour when released into water bodies [18]. When pharmaceuticals enter WWTPs, they can be degraded and adsorbed in the sewage sludge, depending on their physico-chemical properties and other operating conditions of the treatment facilities such as sludge retention time, hydraulic retention time, temperature and seasonal conditions [19]. Unremoved APIs and their metabolites will be released into surface waters, groundwater and eventually into the aquatic environment. As a result, a wide range of pharmaceuticals, including anti-inflammatories, analgesics, antibiotics, β -blockers, lipid regulators, antiepileptics, psychiatric drugs and hormones have frequently been detected in various compartments of the environment.

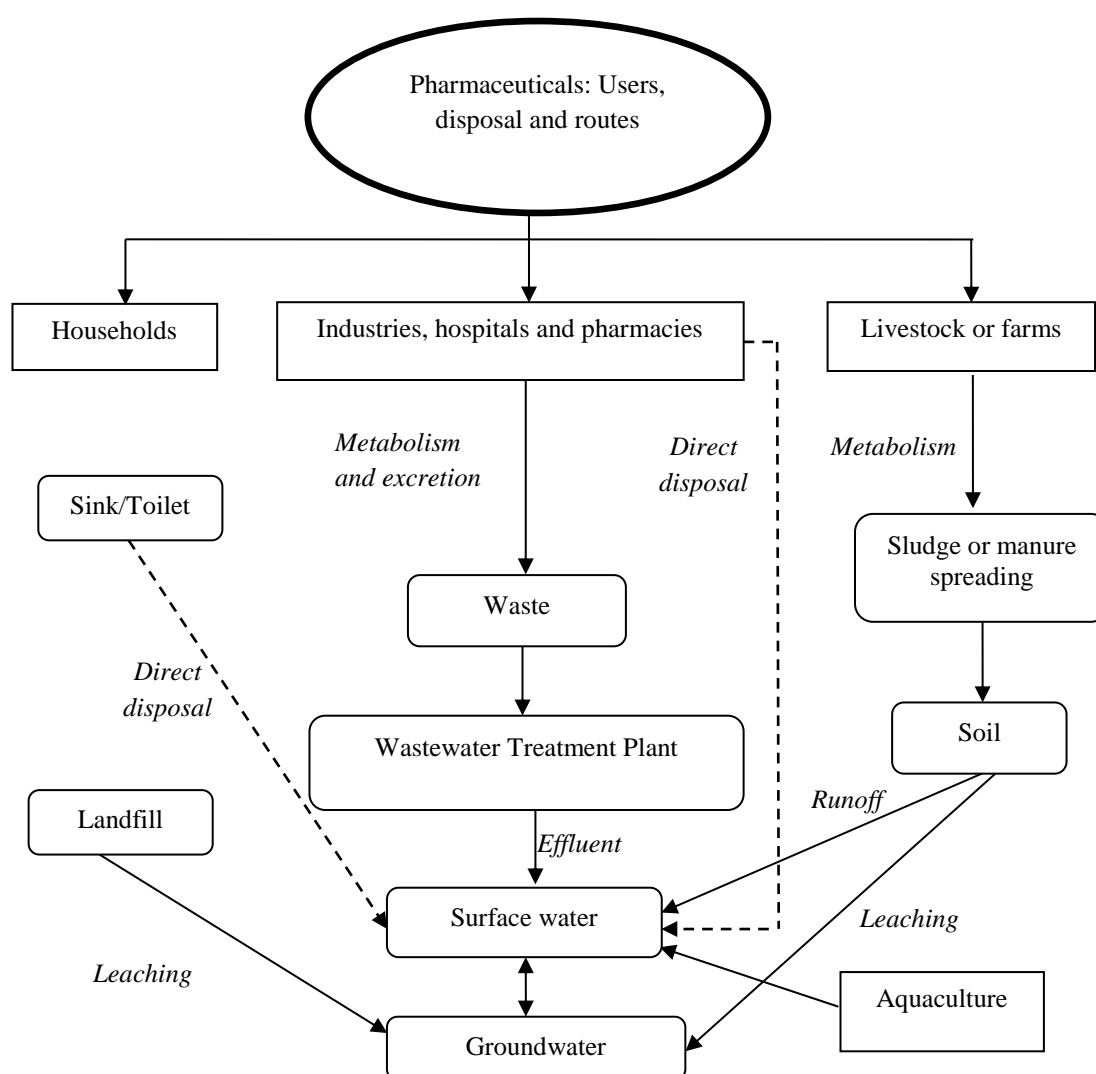


Fig.2.1 Sources and routes of pharmaceuticals in the environment (modified from Nikolaou *et al.* [14] and Mompelat *et al.* [4])

Typically, the existence of APIs in surface water, groundwater and drinking water occurs in trace levels ranging from ppt to ppb (ng/L to $\mu\text{g/L}$) [20]. Investigations on the occurrence of APIs in surface waters [21, 22], groundwater [23, 24] and sewage influents and effluents [25-28] have been reported on and this includes studies specific to certain countries. Studies have been undertaken in the USA, European countries, United Kingdom, Canada and in a few Asian countries (Fig.2.2). However, monitoring studies on the Australian water environment have been limited [29-33]. A study by Watkinson *et al.* [32] confirmed the presence of amoxicillin and cephalexin in WWTP influent and surface water (ng/L); this study monitored 28 antibiotics in watersheds of south-east Queensland. The occurrence and fate of pharmaceuticals has been reviewed [4, 5, 34]. Also, reviews are available based on therapeutic drug classes such as anti-inflammatory and analgesic [17], antibiotic [35, 36] and psychiatric drugs [37], signifying the special attention given to these classes, based on their use and threat to the environment.

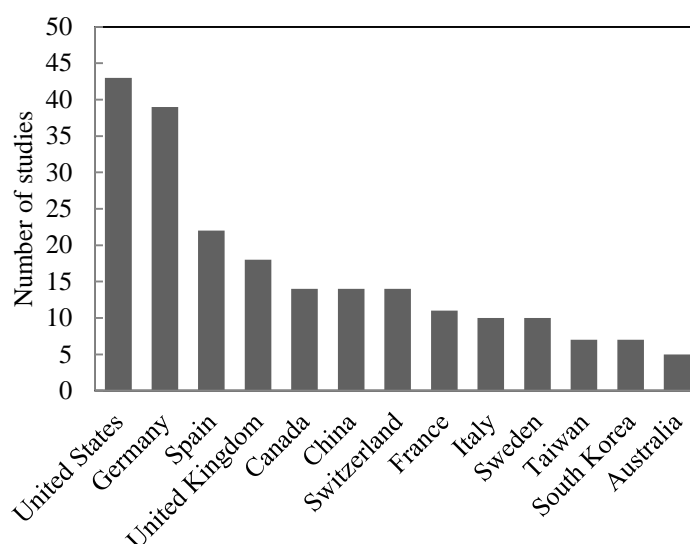


Fig.2.2 Statistics of publications based on country occurrence of pharmaceuticals in the environment (Scopus database for search “Occurrence of pharmaceuticals AND environment” in all subject areas)

The presence of pharmaceuticals in trace quantities has subsequently resulted in reported adverse effects in aquatic and terrestrial organisms [38, 39] as well as probable toxicological effects [7, 18]. Impacts arising from mixtures of pharmaceuticals are also increasing, rather than the focus being on the biological effects of single compound. Recently, a study by Brodin *et al.* [40] revealed that the concentration of the psychotherapeutic drug oxazepam was significantly higher in the muscle tissue of European perch (*Perca fluviatilis*) from River Fyris (Sweden) than in the river water itself as a consequence of bioaccumulation. The study also reported behavioural changes in terms of feeding,

sociality and accumulation in the juvenile fish tested under laboratory conditions on environmentally relevant concentrations ($\mu\text{g/L}$ levels). In addition, the emergence of antibiotic resistance genes and chronic toxicity due to high usage of antibiotics has also been reported [36, 41].

The presence of APIs in drinking water [42-44] and groundwater [45], which are the source of potable water appears to be of concern as there is a lack of evidence of the direct link to human health. Recycling potable water has also raised human health concerns. For example, in some areas of the USA such as California and Florida where they are undertaking such recycling programs, humans may consume water potentially containing active metabolites and degradants [46].

Another important aspect of pharmaceuticals, which is not fully understood, is the fate of parent compounds and their metabolites. Although biotic and abiotic related processes have been identified as common fates for pharmaceuticals, abiotic processes are considered to be more important [47]. Biological degradation, which is an elimination process driven by the metabolic activity of living organisms such as bacteria and fungi [48], has minimal effects on pharmaceuticals, as one of their key characteristics is biopersistence [9]. However, the role of biodegradation remains unclear due to contradictory evidence in the literature. For example, Heberer *et al.* [42] reported that biodegradation contributed 99% to the removal of caffeine but only 8% and 17% for carbamazepine and diclofenac, respectively from sewage treatment plants in Berlin, while Yamamoto *et al.* [49] reported that all tested pharmaceuticals were resistant to biodegradation in river water under laboratory conditions. In another example, carbamazepine has been reported to be resistant to biodegradation and thus, its degradation from surface water is assumed to occur via photodegradation [50]. One possible explanation for the differences in the fate of APIs could be due to the nature of the compound and other factors such as water flow, season, natural environment and simulated conditions in the laboratory.

Concentrations of pharmaceutical compounds are generally higher in sewage effluents compared to freshwater bodies or receiving waters. This is attributed to natural dilution effects and other natural elimination pathways such as hydrolysis, sorption (or adsorption) and photolysis by natural sunlight [34]. Dilution effects, which determine the concentration of pharmaceuticals in the receiving waters, are governed by the wastewater flow from the WWTPs coupled with water flow in the receiving water [51]. Removal of pharmaceuticals via hydrolysis also appears to be minimal [17], as they are designed for oral intake [26]. On the other hand, adsorption of pharmaceuticals onto suspended solids, sediments and sludge is an important physical process which dictates their fate in such materials. Various factors contribute to the adsorption capacity and are related to soil or sediment and have been identified, such as soil type, organic matter content, clay content and ion-exchange capacity [52]. Physico-chemical properties of the API such as solubility in water, octanol-water

partition coefficient ($\log K_{ow}$) and soil-water distribution coefficient ($\log K_d$) are important factors in determining the degree of adsorption [52]. Typical characteristics of pharmaceuticals such as being polar, hydrophilic and possessing a low $\log K_{ow}$ suggest a low binding capacity to the soil, sludge or sediment [51].

Adsorption on activated sludge is one of the main mechanisms employed in WWTPs. Low adsorption of APIs on activated sludge implies that there will be a higher probability of detection in the effluent. There is a general consensus that currently applied technologies in WWTPs are inefficient to completely remove APIs. A recent comprehensive review by Verlicchi *et al.* [19] analysed the removal efficiencies of 118 pharmaceutical compounds, belonging to 17 different therapeutic classes by conventional activated sludge systems and membrane biological reactors. The major highlight of this review was that WWTPs are unable to remove most of the surveyed APIs, while removal efficiencies vary significantly even for similar compounds among WWTPs. There is poor or insignificant correlation between the physico-chemical properties of compounds of a similar therapeutic class with the removal efficiency during treatment. Comparison of removal efficiencies among WWTPs in different countries also varied due to the nature of compounds, geography, climate [27] and operating conditions [17].

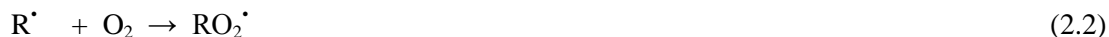
Photolysis, the other important abiotic process, plays an integral part in degradation of pharmaceuticals when exposed to direct sunlight in the natural environment [53, 54].

As water and wastewater containing pharmaceuticals are becoming a potential threat to the ecosystem and also due to lack of facts on the effects and toxicity, destructive methods based on oxidation AOPs may be used for the elimination of pharmaceuticals.

2.2. Overview of advanced oxidation processes (AOPs)

Reactive oxygen or free radical species represent strong oxidants that can initiate AOPs in order to mineralize pollutants to simpler and nontoxic molecules. Free radical species are atoms or molecules containing one or more unpaired electrons such as the hydroxyl radical (HO^\bullet), superoxide anion radical ($O_2^{\bullet-}$), hydroperoxyl radical (HO_2^\bullet) or alkoxy radical (RO^\bullet), with the HO^\bullet radical having attracted the most attention. The characteristic features of HO^\bullet radicals are their non-selective nature, high reactivity and powerful oxidizing species ($E^0 = +2.80V$) [55]. They are ranked second to fluorine (3.03 V) and are able to attack a wide range of organic contaminants with rate constants normally in the order of 10^6 - $10^9 M^{-1} s^{-1}$ [55, 56]. Reactions of HO^\bullet radicals with organic molecules can be either by hydrogen abstraction (Eq. 2.1) from C-H, N-H, or O-H bonds, radical-radical interactions. For example, the addition of molecular O_2 leading to the formation of peroxy radical (Eq. 2.2), or

through direct electron transfer (Eq. 2.3) yielding oxidized intermediates or, in the case of complete mineralization, produced CO₂, H₂O and inorganic acids [56].



Despite the high oxidation potential, kinetic rates of interactions between HO[•] radicals and organic compounds depend on the affinity of these compounds towards the oxidant.

Considerable amounts of work have been published pertaining to the investigation of potential AOPs for the abatement of pharmaceuticals in water. Applications of AOPs for wastewater treatment in general have been reviewed [57, 58] including specific applications of AOPs to pharmaceutical treatment [8, 9]. Recent representative studies carried out in this area for the degradation of pharmaceuticals are presented in Table 2.1. Klavarioti *et al.* [9] summarized and highlighted selected works of different AOPs treatment on pharmaceuticals from 1997-2008. Based on Table 2.1, AOPs commonly applied for pharmaceutical wastewater treatment includes three types: photochemical processes, non-photochemical processes and hybrid processes (Fig.2.3).

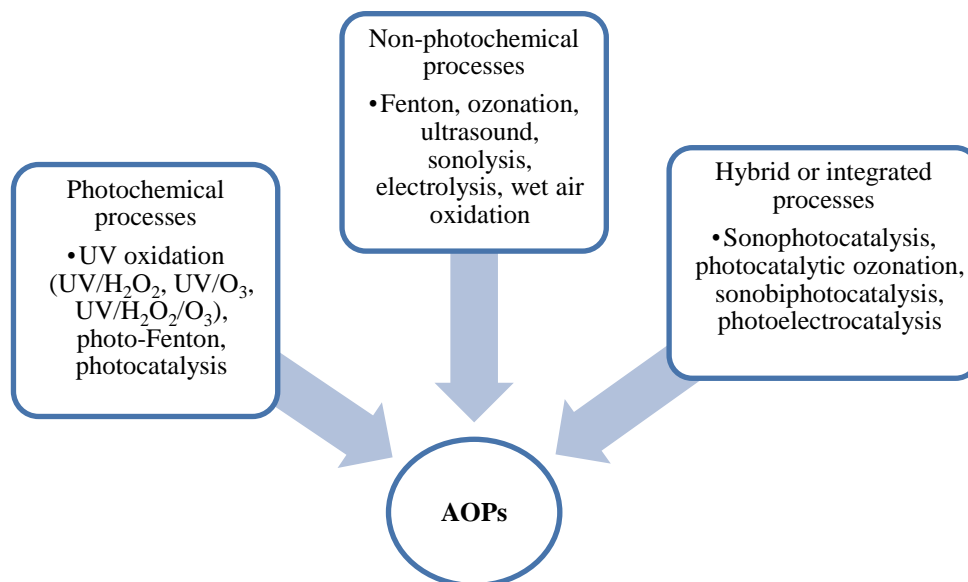


Fig.2.3 Types of AOPs for pharmaceutical wastewater treatment

Table 2.1 Application of different types of AOPs on pharmaceuticals degradation

AOPs applied	Pharmaceuticals	Water matrix	Significant findings	Reference
Single AOP				
Ozonation				
	Propranolol	Milli-Q water	Complete removal of propranolol was achieved in 8 min. Total organic carbon (TOC) removal did not increase above 5% despite increased contact time of 60 min. Low dosage of ozone inefficient to improve biodegradability of ozonated samples.	[59]
	Tetracycline	Deionized water	Direct ozonation showed complete degradation of tetracycline as H ₂ O ₂ concentrations and <i>tert</i> butyl alcohol (HO [•] radical scavenger) showed no effects on the degradation rate. Only 35% of COD removal was attained after 90 min ozonation.	[60]
Fenton and photo-Fenton				
Fenton	Amoxicillin	Milli-Q water	Degradation of amoxicillin with Fenton's reagent using Box-Behnken statistical experimental design revealed that the optimum hydrogen peroxide/Fe (II) dose /amoxicillin ratio of 255/25/105 mg/L led to complete degradation within 2.5 min.	[61]
Photo-Fenton	Amoxicillin	Distilled water	Complete and rapid oxidation was attained for amoxicillin degradation in the presence potassium ferrioxalate complex within 5 min while FeSO ₄ consumed 15 min in experiments conducted using a solar simulator.	[62]
UV and UV/H ₂ O ₂				
UV	Marbofloxacin and Enrofloxacin	Tap water and river water	Under natural sunlight, tap water and river water spiked with 5 and 50 µg/L marbofloxacin and enrofloxacin was removed in 1 h of exposure following first-order kinetics. Addition of inorganic additives (Ca ²⁺ , Mg ²⁺ and Cl ⁻) in tap water under simulated solar irradiation showed no effects on the degradation rate of both compounds but phosphate affected the degradation rate of enrofloxacin.	[63]
UV/H ₂ O ₂ and UV	Sulfamethoxazole,	Milli-Q water, lake	Photolysis rate of all the bioactive compounds towards low pressure UV	[64]

	sulfamethazine, sulfadiazine, trimethoprim, bisphenol A, and diclofenac	water and wastewater treatment plant effluent	photolysis (254 nm) differ at pHs tested while efficiency of UV/H ₂ O ₂ on the tested bioactive compounds was as follows: diclofenac > sulfamethoxazole > sulfamethazine > sulfadiazine > bisphenol A ≈ trimethoprim.	
UV/H ₂ O ₂ and UV-C	Amoxicillin	Distilled deionized water	Degradation of amoxicillin with direct UV and UV/H ₂ O ₂ with low pressure Hg lamp (254 nm) showed that the degradation of 100 μM of amoxicillin (pH 7, 20°C) followed first-order kinetics and the degradation rate increased with H ₂ O ₂ concentrations. An addition of 10 mM H ₂ O ₂ improved the degradation rate up to six fold when compared to direct UV.	[65]
Sonolysis				
	Ciprofloxacin	Deionized water	Degradation of ciprofloxacin at frequency 544 kHz (pH 7, 25°C) fitted pseudo-first-order degradation with half life time of 102 min. Addition of <i>t</i> -butanol (0.45, 4.5 and 45 mM) slowed down the degradation of ciprofloxacin confirming that <i>t</i> -butanol acts as a radical scavenger and the degradation of ciprofloxacin occurred with HO [•] radical.	[66]
	Diclofenac	Milli-Q water	The optimum conditions initial concentration, pH and frequency ultrasound for DCF degradation was found to be 30 μM, 3.0 and 861 kHz, respectively. Addition of Fe-containing additives improved diclofenac elimination in particular with paramagnetic iron oxide nanoparticles. Mineralization only took place after 60 min of sonolysis in all cases.	[67]
TiO ₂ photocatalysis				
	Benzylparaben	Milli-Q water	Photocatalytic degradation of benzylparaben with high pressure Hg lamp (365 nm) was efficient to eliminate benzylparaben. Optimum load of TiO ₂ P25 Degussa was 2.5 g/L and highest degradation occurred at pH 9.	[68]
	Olanzapine	River water and deionized water	The optimum TiO ₂ concentration was found to be 1.56 g/L. Degradation of olanzapine (C ₀ = 50 μM; 1.56 g/L TiO ₂ Anatase) was more efficient with solar simulated light (250 and 500 W/m ²) compared to monochromatic UV light (254 nm and 366 nm) as complete degradation was achieved within 2 h of irradiation.	[69]

Solar photocatalysis and solar photo-Fenton				
Solar photo-Fenton	Mixtures of 15 emerging contaminants (ECs)	Synthetic water, simulated effluent wastewater, real effluent wastewater	Mild solar photo-Fenton (Fe = 5 mg/L, H ₂ O ₂ = 50 mg/L) efficient to degrade mixtures of 15 ECs (pharmaceuticals, personal care products, pesticides) without any pH adjustments. But, toxicity level increased with the degradation products formed from real effluent wastewater.	[70]
Solar TiO ₂ photocatalysis and solar photo-Fenton (Fe ²⁺ /H ₂ O ₂)	Ranitidine	Distilled water and synthetic municipal wastewater	Complete degradation and mineralization of ranitidine was attained in both systems with a compound parabolic collector but degradation was slower in synthetic effluent than distilled water due to the presence of organic compounds.	[71]
Solar photo-Fenton	Nalidixic acid	Demineralized water, saline water, synthetic industrial effluent, real industrial effluent	Although complete degradation was obtained for nalidixic acid, degradation and mineralization was slower in saline water and synthetic industrial effluent with a compound parabolic collector.	[72]
Electro-photocatalysis				
	Sulfamethoxazole	Milli-Q water	Combination of electro Fenton with boron-doped diamond/carbon cell showed highest sulfamethoxazole removal as well as TOC removal.	[73]
Combined AOPs				
Sonophotocatalysis with TiO ₂ , sonophoto-Fenton and sonobiphotocatalysis with TiO ₂ and Fe ²⁺	Ibuprofen	Milli-Q water	Sonobiphotocatalysis produced highest mineralization rate (DOC removal of 98%) with more efficient consumption of H ₂ O ₂ . Initial degradation rate was 3.50 × 10 ⁻³ mM min ⁻¹ .	[74]
Sonophotocatalytic (TiO ₂ and Fe ³⁺) and single systems (sonolytic, photocatalytic)	Ibuprofen	Milli-Q water	Sonophotocatalysis with TiO ₂ and Fe ³⁺ produced higher removal of ibuprofen compared to single systems. However, Fe ³⁺ sonophotocatalytic system yielded better mineralization than TiO ₂ sonophotocatalytic treatment due to the synergistic effect of Fe ³⁺ photocatalyst.	[75]
Ozone/TiO ₂ /UV-B, UV-B/TiO ₂ , O ₃ /UV-B and single systems (UV, O ₃)	Mixtures of nine pharmaceuticals	Water (not specified)	Ozone/TiO ₂ /UV-B (313 nm) yielded the highest TOC removal of 95 % within 120 min for the pharmaceutical mixtures (each 10 ppm).	[76]

AOP classifications are either based on homogeneous oxidation or heterogeneous oxidation processes. Homogeneous oxidation simply means photo-reactions in the gas or liquid phase in the absence of solid. Examples of homogeneous oxidation systems are UV/H₂O₂, UV/O₃, UV/O₃/H₂O₂ and Fe³⁺/H₂O₂. Heterogeneous oxidations employ reaction media consisting of two phases, namely the solid (catalyst) and gas/liquid (reagent).

Chemical oxidation processes, ozonation and combinations of O₃ with H₂O₂ (O₃/H₂O₂), O₃ with UV (O₃/UV) and catalytic ozonation (e.g. O₃/TiO₂) have been applied to treat water containing pharmaceuticals as a single oxidation method or pre-oxidation and/or disinfection step before combination with other treatment [77, 78]. Various parameters such as pH, ozone dose and temperature affect the conversion and mineralization of pharmaceuticals in ozone-based treatments. The short life time of ozone causes this method to be expensive and its high-energy intensity has been identified as a drawback [78]. In addition, ozonation also releases bromate (BrO₃⁻) a suspected carcinogenic disinfection by-product from bromide containing wastewater.

Fenton's reagent is based on the use of a mixture of iron salts (Fe²⁺) and H₂O₂, generating HO[•] radicals under mild acidic conditions (Eq. 2.4). The catalyst can be recovered as shown in Eq. 2.5 or through reaction of Fe³⁺ with other intermediates [79].



Although the Fenton process is not as energy intensive as other AOPs that apply UV and O₃, this advanced technology reaction requires low acidic pH (3-5) [80]. The pH has a great influence on the Fenton reaction. At a pH higher than 3, Fe³⁺ precipitates as Fe(OH)₃ while at even higher pH, the formation of Fe(II) complexes leads to a concentration decline in Fe²⁺. Despite having similar restrictions as the thermal Fenton process, the photo-Fenton reactions can be enhanced by UV-Vis radiation ($\lambda < 580$ nm) to initiate additional HO[•] radicals [55, 56]. Both Fenton and photo-Fenton processes have been found to be effective for the degradation of pharmaceuticals. Solar photo-Fenton has been demonstrated for the treatment of various pharmaceuticals such as antibiotics, anti-inflammatory and analgesic drugs [81, 82]. Trovó *et al.* [82] reported the efficiency of photo-Fenton for the degradation of amoxicillin, bezafibrate and paracetamol in distilled water and in sewage treatment plant effluent under UV-A and solar irradiation. Current research revealed that even low iron and H₂O₂ concentrations have been shown to perform efficiently for a pilot scale solar photo-Fenton conditions [83]. Nevertheless, both Fenton and photo-Fenton face one major disadvantage, requiring an additional separation step in order to remove iron species after treatment [80].

Effectiveness of UV processes for removal of pharmaceuticals depends on the UV energy absorption and quantum yield, Φ , of the pharmaceutical [84]. UV combined with H_2O_2 (UV/ H_2O_2) generally provides better removal efficiency for pharmaceuticals with low UV absorption ability. UV/ H_2O_2 processes are governed by H_2O_2 concentration, rate of HO^\bullet radical formation, UV light intensity, water constituents and also the chemical structure of the pharmaceutical. A study of UV and UV/ H_2O_2 oxidation of 41 pharmaceuticals from a municipal treatment plant was reported on by Kim *et al.* [84]. This study reports that removal efficiencies of UV and UV/ H_2O_2 are highly dependent on the type of pharmaceutical, while H_2O_2 addition during the treatment enhanced API removal up to 90% as well as DOC removal.

Another AOP which has gained popularity as one of the most studied emerging technologies in recent times is ultrasound, also known as sonolysis. This technique is based on the production of HO^\bullet radicals from water pyrolysis due to the high intensity of acoustic cavity bubbles [67]. The efficiency of this AOP to degrade APIs is significantly affected by the power and frequency of the applied ultrasound [85]. Ultrasonic power increases the degradation rate linearly as a result of high number of active cavitation bubbles generating more HO^\bullet radicals [75]. In addition, the sonochemical method has been examined in combination with other AOPs such as ozonation and TiO_2 photocatalysis, with the aim of increasing mineralization of pharmaceuticals which is not readily achieved using sonolysis on its own [74].

Electrochemical-based AOPs also appear as an attractive option for pharmaceutical abatement. A recent review by Sirés and Brillas [86] highlighted research related to this technology, which can be classified as electrochemical separation technologies (such as electrodialysis and electrocoagulation) and degradation technologies (such as anodic oxidation). The combination of electrochemical methods and TiO_2 photocatalysis is known as photoelectrocatalysis and facilitated higher efficiencies over photocatalysis for the removal of tetracycline. This was explained by the suppression of photogenerated electron-hole pairs recombination by the external electric field [87].

Although the treatment of pharmaceuticals typically revolves around single AOP methods, recent developments on AOP hybrid techniques appear to have value and as such, have attracted considerable interest. Hybrid AOPs have been studied in various combinations as shown in Fig.2.3. More efficient removal of pharmaceuticals in such systems compared to the single system is due to increase in the amount of reactive species and has also produced better mineralization efficiencies.

Although it is evident from the aforementioned studies that AOPs are efficient in removing pharmaceuticals and improve biodegradability of wastewater, all AOPs are labelled as expensive methods. To overcome this drawback, the coupling of advanced oxidation treatment with existing

water treatment methods appears to be cost-effective and also enhances the efficiency of the process [48].

2.3. UV light and sunlight for degradation of pharmaceuticals

Application of artificial UV radiation plays an integral part in photochemical degradation studies of pharmaceuticals. Sunlight has been also employed as a renewable energy resource, for some AOP applications such as TiO₂ photocatalysis and photo-Fenton.

Commonly used monochromatic or polychromatic UV light sources are low pressure Hg vapour lamps and medium pressure Hg vapour lamps, pulsed-UV, excimer lamps, light-emitting diodes (LEDs) and xenon arc lamps [88]. The spectral distributions of these lamps are presented in Fig.2.4.

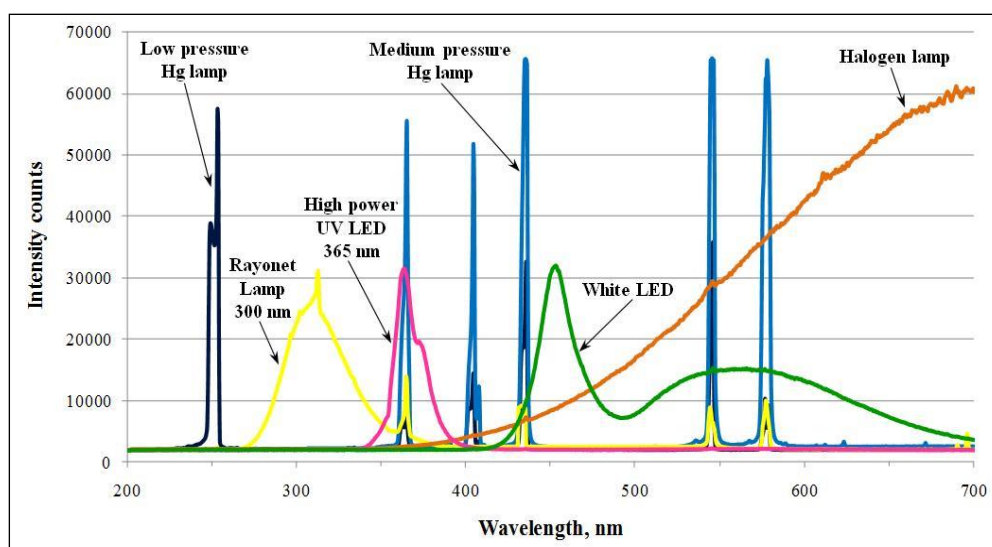


Fig.2.4 Spectral distribution of different lamps [89]

UV and UV-mediated AOPs have proven to be efficient tools for degradation of pharmaceuticals. For example, low pressure Hg arc lamps which emit a quasi single emission line at 253.7 nm (UV-C) (254 nm in 85-90% and 184.9 nm in 7-10%) and are commonly used in UV disinfection, have been assessed for API degradation in various forms such as low pressure-UV photolysis, low pressure-UV/H₂O₂ or low pressure-UV/TiO₂.

Medium pressures Hg lamps emit broad spectra ranging from 185 to 570 nm (185-366 nm in UV region and 405-570 nm in Vis region) and provide photons needed for photodegradation applications and UV disinfection. Medium pressure Hg lamps are regarded as most useful to represent the UV-A part of the sunlight, despite providing a discontinuous output [90]. Medium pressure Hg lamps provide intensive emission lines at 313, 366, 405 and 505 nm. This type of mercury arc lamp is

commonly used in immersion-well type reactors or in compact treatment systems, due to higher UV intensity per lamp than the low pressure systems [91]. Medium pressure Hg lamp driven degradations either as direct photolysis (UV only), indirect photolysis (UV/H₂O₂) or catalyzed oxidation (UV/TiO₂) have been shown to be efficient for the removal of APIs. For example, UV only and UV/H₂O₂ were reported to effectively remove APIs such as ketoprofen, naproxen, carbamazepine, ciprofloxacin, clofibric acid, and iohexol from surface water and laboratory grade water while comparison between medium pressure and low pressure Hg lamps revealed that the former displayed better performance in terms of APIs removal [92].

The choice of a medium pressure or low pressure Hg lamps is determined by the photoreactor setup (glass) and the absorption capacity of the pharmaceutical of interest. However, application of medium pressure Hg lamps with broader emission spectra can be considered more appropriate as there is a greater probability of the spectral emission regions overlapping with that of the absorption of the pharmaceutical.

Excimer lamps, which are also commonly used in AOP-based oxidations, are sources of incoherent UV or vacuum UV (100-200 nm) light. Vacuum UV (V-UV) light, combining 254 and 185 nm, can enhance photolysis of organic compounds owing to their ability to dissociate water molecules into hydrogen atoms, HO[•] and hydrated electrons [93].

Compared to artificial UV light, sunlight constitutes a green solution and sustainable treatment option. Fig.2.5 shows the solar UV spectrum. UV radiation of λ above 300 nm reaching the Earth's surface comprises only 4.5%, while about 43% and 53% of the radiation is in the visible and infrared regions, respectively [88].

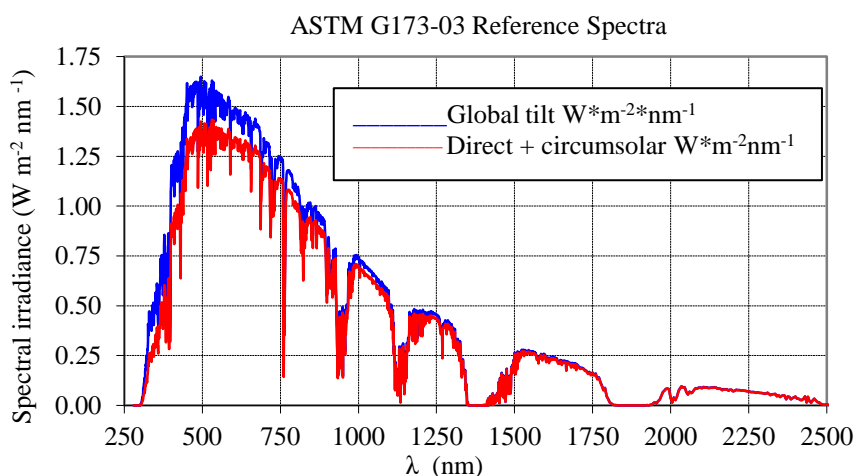


Fig.2.5 Solar spectrum based on data by the American Society for Testing and Materials (ASTM) (<http://www.astm.org/ASTM>)

Typical UV-flux in the range of 300-400 nm near the surface of the Earth has been reported as 20-30W/m² and 0.2-0.3 mol photons/m²/h [94]. Among the various AOPs, heterogeneous TiO₂ photocatalysis and homogeneous photo-Fenton benefit from the application of sunlight as both processes can be driven by solar radiation [95]. Laboratory-scale simulated sunlight employs a solar simulator equipped with Xenon arc lamps.

New developments in photo-initiated photochemical degradation of pharmaceuticals include the application of LEDs and radiation sources in the visible range, such as the black light. LEDs can be used instead of traditional mercury-based lamps. Black light, which emits radiation in the range of 350-390 nm, is of interest to TiO₂ photocatalysis as TiO₂ can be activated by radiation with $\lambda < 380$ nm [96].

Fig.2.6 summarizes the commonly used light sources in pharmaceutical degradation studies.

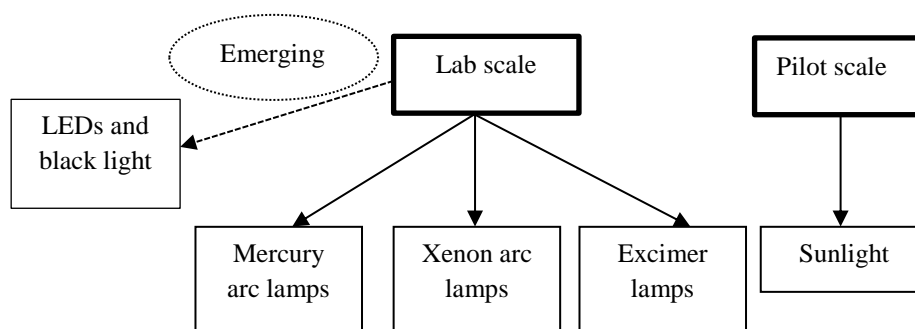


Fig.2.6 Commonly used lamps in pharmaceutical degradation studies

2.4. Photochemical degradation

The International Union of Pure and Applied Chemistry (IUPAC) defines photodegradation as “the photochemical transformation of a molecule into lower molecular weight fragments, usually involving an oxidation process” [97]. The ultimate goal of applying photochemical degradation techniques, which are based on light from either artificial or natural source is to destroy pollutants and ultimately complete mineralization to carbonate species (CO₂, H₂CO₃, HCO₃⁻, CO₃²⁻), water and mineral acids (HX) (Eq. 2.6) [88].



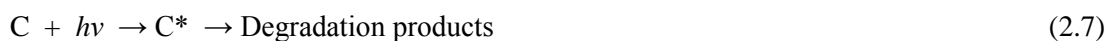
Photochemistry which is the backbone of all photochemical reactions and transformations is governed by two basic principles:

- a. Grotthus-Draper law (First law of photochemistry): Only electromagnetic radiation that is absorbed by a molecule leads to a distinct photochemical change
- b. Stark-Einstein law (Second law of photochemistry): Each molecule that takes part in a photochemical reaction absorbs one quantum of light energy.

Although these two principles are significant in photochemistry, the beginning of photochemistry as a new field of investigation was initiated by Giacomo Ciamician and Paul Silber, who studied the interaction of light with matter between 1900 and 1915 [88].

2.4.1. Homogeneous photodegradation: Photolysis

Photolysis is the interaction of natural or artificial UV radiation with the molecule of interest and can lead to degradation to intermediate products and eventually to total mineralization. This photo-induced process can be either direct or indirect [98]. Direct photolysis takes place when an organic compound, C, absorbs light to form an excited state (C*) which can then decompose as illustrated below (Eq. 2.7) [2]:



UV/H₂O₂ is also a direct method to generate HO[•] radicals through homolytic cleavage of H₂O₂, as shown below (Eq. 2.8):



The quantum yield Φ of the HO[•] radical formed in the Eq. 2.8 is 0.98 and UV/H₂O₂ photolysis can proceed with a low pressure Hg lamp with emission wavelength of 254 nm [99]. The IUPAC definition given for the term quantum yield is the number of defined events occurring per photon absorbed by the system, which strictly applies for monochromatic excitation [97]. The disadvantage of the UV/H₂O₂ process is the small molar extinction coefficient of H₂O₂, 18.6 M⁻¹ cm⁻¹ at 254 nm [56] and the high operating cost of UV-C lamps. In addition, photolysis of aqueous H₂O₂ is also pH-dependent and more favoured under alkaline conditions [55, 56].

Pharmaceuticals can be treated by direct UV photolysis because most of these compounds contain chromophores such as double bonds or conjugated double bonds with delocalised π -electrons [100]. An appropriate light source emitting the required wavelength of radiation should overlap the absorption spectrum of the pharmaceutical. Treatment of pharmaceuticals with direct photolysis also depends on the molar absorption coefficient, ϵ of the compound [101, 102], which depends on the wavelength, solvent and pH. In addition, the quantum yield of the process, the photon flow rate at the

wavelength of excitation, the type of water matrix, the concentration of H₂O₂ and the concentration of dissolved molecular O₂ also contribute significantly to the efficiency of direct photolysis [56].

Photolysis is compound dependent and the absorption of light by pharmaceuticals can be expressed by the Beer-Lambert law. Nevertheless, not all APIs are sensitive to this process. Laboratory-scale photodegradation provides the flexibility to choose the appropriate light source based on the absorption spectrum of the pharmaceutical of interest. Kim and Tanaka [101] highlighted the effectiveness of UV lamps which emit light at a wavelength of 254 nm and a combination of 254 nm and 185 nm on 30 different pharmaceuticals in surface water and sewage treatment plants in Japan.

In surface water and sewage treatment plants, sunlight induced photolysis can play an important role in the degradation of pharmaceuticals [103, 104]. Solar UV-B 280< λ <315 nm and part of UV-A 315< λ <400 nm are known to induce photochemical reactions (direct and indirect) in surface waters, while the visible range is not efficient in initiating direct photolysis of most organic compounds [103, 105]. Pharmaceuticals with chromophores that can absorb light >290 nm in sunlight can possibly undergo direct photolysis. For compounds with absorption <290 nm, indirect photolysis by singlet oxygen (¹O₂), hydroxyl (HO[•]) or alkyl peroxy radicals ([•]OO[•]) can be initiated naturally by photolysis of nitrate, nitrite (NO₃⁻/NO₂⁻), and chromophoric dissolved organic matter (CDOM) present in natural water [5, 106]. The presence of natural CDOM, including humic substances ubiquitously in aquatic environment, are able to produce high ROS such as ¹O₂, superoxide and HO[•] radicals, but can also act as a radical scavenger leading to a decrease in photodegradation of pharmaceuticals. When CDOM absorbs sunlight, a singlet-excited state, ¹CDOM* is formed. The excited state may either return to the ground state or undergo intersystem crossing (ISC) to form an excited-triplet state, ³CDOM*, which is responsible for yielding ROS (Eq. 2.9) [69]. Inhibitory effects of CDOM on the degradation rates as a result of an inner filtering effect have been reported. Likewise, enhancement effects in degradation rates are also known [69, 104].



2.4.2. Heterogeneous photodegradation: Photocatalysis

The IUPAC definition given for photocatalysis is a “change in the rate of a chemical reaction or its initiation under the action of ultraviolet, visible or infrared radiation in the presence of a substance, the photocatalyst that absorbs light quanta and is involved in the chemical transformation of the reaction partners” [97]. While another precise definition is that there should be two simultaneously balanced processes, oxidation from the photogenerated holes and reduction from the photogenerated

electrons. The photocatalyst is (if only momentarily) changed immediately after excitation and is then subsequently regenerated by recombination of the holes with electrons [107].

The goal of the photocatalytic processes is not only the removal of organic pollutants, but at the same time for complete mineralization.

Semiconductors or insulators consist of a valence band (vb) filled by electrons and a conduction band (cb) unoccupied or only partly occupied with electrons. For the semiconductors, electronic transitions between vb and the cb require at least UV/Vis irradiation with equivalent energy to the band-gap energy (E_g) [88]. Semiconductor materials with $E_g > 2$ eV are also referred to as wide band gap semiconductors, due to the energy requirement of near UV radiation or visible light to promote an electron from the vb to the cb. Selected examples of wide band gap semiconductors are presented in Table 2.2. Various semiconductors such as CdS, ZnO, TiO₂, Fe₂O₃ and WO₃, can be activated with minimum wavelength of UV or VIS radiation as shown in Table 2.2.

Table 2.2 Band gap energy and minimum wavelength for selected photocatalysts [108, 109]

Semiconductor	E_g (eV)	λ_{nm}	Radiation type
TiO ₂ (anatase)	3.2	388	UV
TiO ₂ (rutile)	3.0	413	VIS
ZnO	3.2	387	UV
ZnS	3.6	344	UV
Fe ₂ O ₃	2.3	539	VIS
WO ₃	2.7	459	VIS

Among them, TiO₂ is of greater interest for photocatalytic degradations. The properties of TiO₂ accounting for its wide use as a photocatalyst are its high photoreactivity, low cost, low toxicity, chemical stability over a wide pH range, commercial availability and its resistance to photo-corrosion [110]. Besides these advantages, atmospheric O₂ can be used as oxidant and only long wavelength of UV light (UV-A) is required for the photocatalyst activation. In addition, it is possible to drive the process with solar light. TiO₂ suspensions in water cause its surface to be hydroxylated. The hydroxyl groups act as a source of powerful HO[•] radicals, which can oxidize various organic compounds to complete mineralization to CO₂ and other mineral acids [111]. Intermediates formed as a result of partial oxidation of parent compound may possibly impact the reaction rates negatively by competing for adsorption sites on the TiO₂ surface or display a higher toxicity than the parent compound. To evaluate complete mineralization, parameters such as TOC and DOC for evolution of CO₂ are commonly measured.

2.5. Photocatalyst features of titanium dioxide

TiO₂ mainly exists in three crystalline forms namely anatase, rutile and brookite, with the anatase form more commonly used as active photocatalyst than the pure rutile phase. The more frequent application of pure anatase TiO₂ compared to the pure rutile is due to a higher density of superficial hydroxyl groups, which leads to an improved capability of anatase to adsorb oxygen, a larger specific surface area compared to pure rutile samples, and a lower recombination velocity of electron-hole pairs [112].

Combinations of anatase and rutile have also demonstrated better photocatalytic activity, due to the promotion of charge pair separation and inhibition of electron-hole pairs recombination. The superiority of the photocatalytic activity of anatase over rutile or vice versa is still unanswered [113], while their photoreactivity is affected by the origin and the preparation method [108]. In contrast, brookite TiO₂, is known to be rare and difficult to prepare, which contributes to its neglected usage in photocatalysis, although studies have been performed with this form [107]. In fact, a recent study indicated higher photocatalytic activity of brookite compared to anatase and rutile [114].

The extensive use of TiO₂ Degussa P25 (now known as AEROXIDE[®] TiO₂ P25) as a photocatalyst in photocatalytic degradation studies is attributed to its morphology or crystallinities. Being a mixture of 80% anatase and 20% rutile, its high surface area of 50 m²/g and a particle size range of 20-30 nm are the characteristic features responsible for the performance of TiO₂ P25 in photocatalytic applications [88, 110].

The anatase form tends to be the most photoactive and most stable form at temperature <700°C. Anatase and brookite are, however, thermodynamically metastable and can be irreversibly converted to the rutile form, the most stable form at high temperatures [115].

Different TiO₂ materials demonstrate different photocatalytic activity towards similar organic compounds even under identical conditions. Explanations of such differences are differences in morphology, crystal phase, specific surface area, surface charge, particle size distribution, porosity, band gap and surface hydroxyl density control.

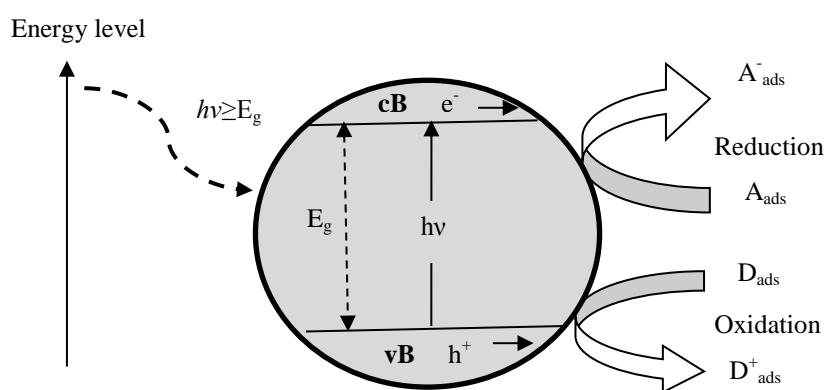
Other commonly used photocatalysts besides TiO₂ P25, include Hombicat UV 100 and Ti (IV) oxide (Aldrich). Table 2.3 displays a comparison of the properties of these common photocatalysts [116, 117].

Table 2.3 Characteristics comparing of TiO₂ P25 to other commercial photocatalysts

Properties	TiO ₂ P25	Hombicat UV 100	Ti (IV) oxide (Aldrich)
Brunauer-Emmett-Teller (BET) surface area, m ² /g	50	>250	190-290
Particle size, nm	21	5	15
Crystal form	75% Anatase: 25% Rutile	100% Anatase (or Anatase>99%)	100% Anatase (or Anatase>99%)

2.5.1 General mechanism of TiO₂ photocatalysis

The most commonly used TiO₂ form, anatase, has a band gap energy of 3.2 eV (Table 2.2). Photon ($h\nu$) illumination ($380 < \lambda < 400$ nm) onto the TiO₂ surface of greater than or equal to the band gap energy results in electron excitation and promotion of the distinct lone electron in the outer orbital from the valence band to the conduction band. This subsequently forms electron-hole pairs (Eq. 2.10), which can undergo rapid recombination either in the bulk or on the surface of the particles, without favouring any reactions. More importantly, the electron-hole pairs can be involved in oxidative and reductive reactions with molecules present at/or near the surface of the semiconductor as shown in Fig.2.7. Mechanistic processes of TiO₂ induced degradations of organic pollutants have been well described in the literature [56, 112, 118, 119].

**Fig.2.7 Photocatalytic processes on TiO₂ semiconductor**

The activated electron reacts with an oxidant (A_{ox}) to yield a reduced product (A^-) and the photogenerated hole reacts with a reductant (D_{red}) to produce an oxidized product (D^+) as shown in Eq. 2.11 and Eq. 2.12:





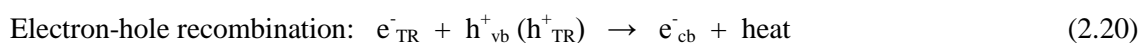
A generated hole (h^+) can react with an adsorbed water molecule, which is an essential process in TiO_2 photocatalysis, or react with OH^- anions to form powerful HO^\bullet radicals (Eq. 2.13 and Eq. 2.14). The HO^\bullet radicals can subsequently oxidize the organic pollutant, P, to complete mineralization (Eq. 2.15). When molecular O_2 is available, it is adsorbed onto the surface of TiO_2 and can scavenge an electron to form the superoxide anion radical ($\text{O}_2^{\bullet-}$) (Eq. 2.16).



Holes can also directly oxidize pollutants P by electron transfer (Eq. 2.17).



The photogenerated electron-hole pairs can undergo rapid recombination within nanoseconds in the absence of electron scavengers, such as O_2 , releasing heat without favouring any reactions (Eq. 2.18-2.20). The e^-_{TR} and h^+_{TR} (Eq. 2.18-2.20) represent the surface trap valence band electron and conduction band hole, respectively.



Hoffmann *et al.* [112] proposed a characteristic time for heterogeneous photocatalysis of TiO_2 on the basis of a laser flash photolysis measurements. The proposed mechanism has been adopted as a mechanism of oxidation for organic pollutants. Nevertheless, investigations of degradation mechanisms of photocatalytic processes remains a challenging task, although it is now generally accepted that the basic steps involve the absorption of photon and HO^\bullet radical formation as the primary oxidant. The degradation mechanisms occur from various reaction pathways as a result of charge separation and also interactions between surface, radicals and organic compounds. Due to the nature of adsorption and desorption phenomena in the heterogeneous photocatalysis, the Langmuir-Hinshelwood (L-H) model has been commonly adopted [118]. This model simplifies to pseudo-first-order model for low initial concentrations and pseudo-zero-order model for high initial concentrations [120]. TiO_2 photocatalytic degradation processes of numerous pharmaceuticals have been reported to fit the L-H kinetic model [120-122].

2.6. Photochemical degradation of pharmaceuticals

Photochemical degradation of pharmaceuticals by means of TiO₂ photocatalysis is undertaken to (i) investigate the kinetics and optimized conditions of the applied process, (ii) determine mineralization of the parent compound and to achieve high biodegradability and (iii) identify possible degradation products formed during HO[•] radical mediated-treatment to ensure the safety of the treated water.

With these three aims, applications of TiO₂ photocatalysis to various APIs have been studied. A few studies have also studied the influence of direct photolysis on the pharmaceutical of interest. Studies conducted to degrade a large number of APIs using UV/TiO₂ catalyzed oxidation based on different therapeutic classes such as NSAIDs and analgesics, antibiotics, anticonvulsants, lipid regulators, β -blockers and psychiatric drugs are summarized in Table 2.4. Important aspects observed in these studies are also summarized in this section.

TiO₂ photocatalysis has demonstrated successful oxidation of a wide variety of drugs treated thus leading to an increasing interest in its application for pharmaceutical removal in water and wastewater. API selection in such studies is either driven by high consumption which correlates with the high probability of detection in the environment, or due to an existing gap or scarcity of available information on these compounds. For example, antibiotics and NSAIDs, such as amoxicillin and ibuprofen, respectively are frequently investigated due to their high consumption, while removal of psychiatric drugs such benzodiazepines represents a knowledge gap despite their wide prescription.

Pharmaceuticals, spiked in distilled water and Milli-Q water, are commonly used in TiO₂ photocatalytic oxidation studies. Nevertheless, real wastewaters such as wastewater effluents, river or lake water and drinking water have also been utilized. Despite a higher removal rates obtained with pure water, lower removal rates can be expected when performing studies with real wastewater samples. The presence of radical scavengers such as carbonate ions, HCO₃⁻ and CO₃²⁻ and natural organic matter in real wastewater typically impacts the degradation efficiencies. Furthermore, studies have shown that filtered or unfiltered wastewater samples influence the degradation rate to different extents both for direct photolysis [91] or UV/TiO₂ photocatalysis.

Researchers predominantly perform laboratory-scale experiments with artificial UV light over pilot scale operations with sunlight, as conditions are easier to control. Often, there is no direct correlation between results from both protocols as shown by De La Cruz [94] for the degradation of propranolol. However, pilot scale studies will be more realistic if scaling-up is required and more practical if

Table 2.4 Photolytic and photocatalytic oxidation of pharmaceuticals

Therapeutic class/compound	Treatment	Water matrix	Experimental conditions	Results	Reference
Antibiotics					
Tetracycline	PC*	Water type not provided	Solar simulator (300-800 nm, Xe lamp, 250 W/m ²)	Irradiation in the presence of catalyst completely removed the solution's antibacterial activity. The catalytic activity indicates that ZnO gives rise to a slightly higher oxidation rates than TiO ₂ .	[123]
Amoxicillin (ampicillin and cloxacillin)	PC	Distilled water	UV lamp (6 W, 365 nm)	Addition of H ₂ O ₂ at pH 5 with TiO ₂ 0.1 g/L led to complete degradation of all antibiotics.	[124]
Oxolinic acid	PC	Milli-Q water	Black lamp (14 W/m ² ; 365 nm)	Experimental conditions of pH 7.5 and 1.0 g/L of TiO ₂ favoured between 80-100% of oxolinic acid degradation. About 20% of oxolinic acid was adsorbed on TiO ₂ under dark conditions.	[121]
Trimethoprim	DP** and PC	Milli-Q water, distilled water and simulated seawater	Solar simulator (1.5 kW Xenon arc lamp) and compound parabolic collector	Trimethoprim demonstrated high stability to direct photolysis and degradation did not follow first-order kinetics. Solar TiO ₂ photocatalysis improved the degradation of trimethoprim with rate constants of 0.22 min ⁻¹ in distilled water and 0.081 min ⁻¹ in simulated seawater.	[125]
Moxifloxacin	PC	Deionized water	UV-A lamp ($\lambda_{\text{max}} = 365 \text{ nm}$)	Maximum degradation rate of moxifloxacin was achieved in the presence of 5 g/L TiO ₂ and air sparging of 60 mL/min. Ambient temperature (298 K) was reported to be sufficient for degradation of this compound.	[122]
NSAIDs and analgesics					
Naproxen	DP and PC	Milli-Q water	Solar simulator (Xe lamp, 1 kW)	Degradation of naproxen mainly caused by photolysis although photocatalysis was more efficient for DOC	[126]

				removal. BOD ₅ /COD ratios were found to be below 0.05 suggesting non-biodegradable products formed during photocatalysis.	
Paracetamol	DP and PC	Milli-Q water	Black light blue UV-A (8 W) and UV-C (15 W)	Rapid paracetamol degradation and mineralization occurred in the presence of TiO ₂ under UV-C irradiation. Also, direct photolysis under UV-C radiation was more effective compared to that of UV-A.	[127]
Ketoprofen and ibuprofen	DP	Milli-Q water	UV (254 nm) and UV/V-UV (254/185 nm)	V-UV irradiation enhanced the degradation rate of ibuprofen while degradation rate of ketoprofen was much higher (40 times) under UV irradiation. Effect of dissolved oxygen (DO) was more dominant in ibuprofen degradation.	[128]
Diclofenac (and amoxicillin)	DP and PC	Milli-Q water	Solar simulator (250-765 W/m ²)	TiO ₂ photocatalysis produced 96% degradation of diclofenac with irradiation level of 400 W/m ² while 80% was achieved with direct photolysis.	[129]
Ketoprofen, diclofenac (and atenolol)	DP	Ultrapure water and secondary effluents (wastewater treatment plant)	Low pressure Hg lamp (254 nm) Medium pressure Hg lamp (150 W; 200-450 nm)	Ketoprofen displayed the highest time and fluence-based rate constants followed by diclofenac and atenolol under medium pressure Hg lamp irradiation in mixture and as a single compound. Unfiltered wastewater resulted in higher photodegradation of ketoprofen and atenolol compared to filtered.	[91]
Anticonvulsants					
Carbamazepine (Clofibric acid, iomeprol, iopromide)	PC	Milli-Q water	Solar simulator Xe short arc lamp (1000 W)	Degradation of carbamazepine was faster with TiO ₂ P25 due to higher adsorption. The first order rate constant increased from 0.0001 min ⁻¹ to 0.36 min ⁻¹ with TiO ₂ P25 concentration from 0.01-1000 mg/L.	[130]
Carbamazepine (clofibric acid, iomeprol)	PC	Milli-Q water	Solar simulator Xe short-arc lamp (1000 W)	Pseudo-first-order degradation rates of carbamazepine for TiO ₂ P25 and UV 100 were 4.7 × 10 ⁻³ and 0.13 × 10 ⁻³ s ⁻¹ , respectively.	[131]
Carbamazepine (and	PC	Milli-Q water and	Solar simulator (1000 W)	Degradation under UV-A irradiation in pure water was	[132]

ibuprofen)		wastewater from WWTP	Phillip Xe lamp) and UV-A lamp (9 W Radium lamp)	sensitive to TiO ₂ P25 loading. Solar and UV-A photocatalysis appear to be efficient for carbamazepine degradation.	
<i>Lipid regulators</i>					
Bezafibrate	PC	Doubly distilled water	Solar simulator (1500 W xenon arc lamp)	Bezafibrate was completely degraded within 200 min following pseudo-first-order kinetics with rate constant, of $2.81 \times 10^{-2} \text{ min}^{-1}$.	[133]
Clofibrac acid	DP	Milli-Q water and secondary effluent from WWTP	Low pressure Hg lamp (10 W; 254 nm)	Temperature greatly influenced the degradation rate of clofibrac acid in filtered wastewater. Photolysis rate, however, decreased compared to in Milli-Q water under investigated temperatures. Humic acid showed negative effect on the degradation.	[134]
<i>β-blockers</i>					
Metoprolol and propranolol	PC	Milli-Q water	Solar simulator (Xe-OP lamp; 1 kW)	Maximum removal of both compounds were achieved with 0.4 g/L TiO ₂ P25. Almost 55% of TOC and COD removal was achieved after 360 min of irradiation.	[135]
Propranolol	DP and PC	Milli-Q water	Solar simulator (Xe-OP lamp; 1 kW) and solar compound parabolic concentrators	Higher pseudo-first-order kinetic constants was obtained in laboratory solar device ($k = 0.0090\text{-}0.01085 \text{ min}^{-1}$) than pilot solar device ($k = 0.00492\text{-}0.00785 \text{ min}^{-1}$).	[94]
<i>Others</i>					
Benzodiazepines (oxazepam, diazepam, lorazepam and alprazolam (psychiatric drug)	DP	Milli-Q water	Solar simulator (Arc Xenon lamp; 1500 W)	Half-life, which was measured for summer sunny days for oxazepam, diazepam, lorazepam and alprazolam were 3.98, 7.3, 0.68 and 228 h, respectively. Direct and indirect photodegradation yielded a similar order of degradation.	[106]
Crotamiton (anti-pruritic drug)	PC	Milli-Q water	UV lamp (0.25-2.0 mW/cm ²)	The studied pH range of 3-9 did not show great influence on the degradation rate. Pseudo-first-order rate constant increased with UV intensity.	[136]

*PC: Photocatalysis

**DP: Direct photolysis

application is extended to real wastewater samples. A compound parabolic collector (CPC) is commonly chosen for solar photocatalytic investigations, as these devices can harvest both non-concentrating and concentrating radiation [95]. TiO₂ photocatalytic studies frequently investigate the effects of operational parameters such as catalyst load, initial concentration, type of photocatalyst, pH of the solution, wavelength and light intensity on the degradation kinetics of the pharmaceutical. The influence of the water quality on reaction kinetics has also been investigated to establish the suitability for real wastewater treatment. However, it is also widely accepted that the design and geometry of the photoreactor dictates the degradation rate of APIs [109, 137]. Differences arising from these parameters among studies even for similar APIs make comparisons difficult.

The degree of mineralization is typically determined to indicate the effectiveness of the treatment. In most cases, complete degradation of the parent pharmaceutical does not correspond directly with the mineralization rate, indicating the formation of more stable compounds during the degradation processes. A non-biodegradable fraction frequently remains in the treated solution. The degree of mineralization is usually reported as DOC and TOC removal or COD and tends to vary based to the nature of the water matrices. Hybrid methods, however, are commonly more effective in improving mineralization as well as biodegradability. For example, sonophotocatalysis on ibuprofen showed a higher TOC removal of up to 92% compared to the single process, sonolysis or TiO₂ photocatalysis, which only achieved 16% and 88%, respectively, after 3 h of irradiation [75].

As shown in Table 2.4, many studies have investigated direct photolysis together with TiO₂ photocatalysis or have exclusively focused on direct photolysis for the chosen APIs. Emphasis has also been directed towards designing photodegradation studies to be environmentally relevant, such as in the presence of humic acids, fulvic acids and ions. Nevertheless, studies have also highlighted that direct photolysis might not be an effective removal pathway for pharmaceuticals. Therefore, TiO₂ photocatalysis is anticipated to be a better option, since TiO₂ generally accelerates (although not exclusively) the degradation process.

Another important point is that the transformation products generated during UV treatment or UV/TiO₂ photocatalyzed oxidation can potentially be more toxic than the parent compound itself. Recent research indicates that photoproducts yielded during UV treatment of carbamazepine were more toxic than the parent API [50]. Likewise, it has been reported that a photoproduct of diclofenac, i.e. 8-chlorocarbazole-1-yl-ethanoic acid, displayed higher toxicity than the parent compound [138]. Therefore, attention must be paid to ensure that there are no more toxic or more persistent products formed compared to the parent pharmaceutical being degraded. Emphasis on this aspect of transformation products identification has been lacking. A few possible reasons identified for this neglect are: (i) difficulties in separating and identifying a large number of transformation products

formed, (ii) lack of or non-existent analytical standards to determine the identity of transformation products and (iii) requirements for more than one analytical technique or sample preparation technique due to their diverse physico-chemical properties [139, 140]. Mass spectrometry methods coupled with chromatographic separations (e.g. GC or HPLC) is most commonly used to identify degradants.

In summary, TiO₂ photocatalysis appears to be a better choice for pharmaceutical degradation in particular when dealing with real wastewater. In contrast, direct photolysis might be restricted to a limited number of compounds. However, the general superiority of direct photolysis over TiO₂ photocatalysis or vice versa for pharmaceutical degradation is not clear and it depends on the compound and the overall experimental conditions.

2.7. Parameters affecting TiO₂ photocatalysis

The efficiency of TiO₂ photocatalysis to degrade pharmaceutical compounds is closely related to several extrinsic parameters that correspond to the photo-oxidation kinetics. These are the initial substrate concentration, TiO₂ concentration, pH of medium, light intensity, light wavelength, temperature and the presence of electron acceptors. Additionally, the intrinsic properties of TiO₂ catalysts such as crystallinity, crystallite size, surface area and other surface related properties [137] are also critical in determining the pharmaceutical degradation rate.

2.7.1. TiO₂ concentration

In TiO₂ photocatalytic treatment, the degradation rate increases with the increase in TiO₂ concentration [141], although this statement has also been disputed. Degradation rate has also been indicated as not always proportional to the catalyst concentration [142]. The choice of an optimal concentration for the photoreactor under investigation is important to establish maximum degradation efficiency. Beyond an optimum concentration, the reaction rate tends to decrease and becomes independent of the TiO₂ concentration. High concentrations of TiO₂ cause turbidity and impede light penetration into the reactor. Thus, the determination of the optimum TiO₂ concentration is critical to guarantee maximum degradation and to avoid sedimentation.

TiO₂ concentration is commonly investigated in TiO₂ photocatalytic studies of various target pharmaceuticals. In most cases, concentrations of TiO₂ Degussa P25 in the range from 0.01-1g/L appear to be satisfactory for pharmaceutical degradation [8]. TiO₂ concentrations vary between studies, even for similar APIs, as they are also dependent on the photoreactor geometry, wavelength and light intensity [95].

2.7.2. Initial substrate concentration

In general, an increase in initial substrate concentration results in a reduction in degradation efficiency. This observation has been linked to three reasons as discussed by Carp *et al.* [110], (i) since adsorption is widely accepted as a prerequisite for TiO₂ photocatalysis, most of the TiO₂ surface is occupied at high initial concentrations thus leading to a decrease in degradation rate; (ii) the formation of intermediates during TiO₂ photocatalysis also affects the degradation rate, where at high initial concentration, high concentrations of adsorbed intermediates can be expected to contribute to the overall rate; and (iii) the generation and migration of generated electron-hole pairs and their reactions with substrate occurs in series where each step becomes rate determining for the overall reaction. In the case of low concentrations, the degradation rate increases linearly with concentration as the process is dominated by migration of photogenerated electron-hole pairs. At higher initial concentrations, as the generation of photogenerated electron-hole pairs become the governing step, the degradation rate increases slowly with concentration and may lead to a constant degradation rate as a function of concentration for a given irradiation period. In addition to these three factors, the nature of compound also typically influences the degradation rate [141].

2.7.3. Solution pH

The solution pH is known to have a significant effect on the ionization of the catalyst surface, the rate of formation of radicals and the size of the aggregates formed by TiO₂ particles [141]. Agglomerates of nano-sized TiO₂ occur due to van der Waals forces, controlled by hydroxylation of the TiO₂ surface, which occurs at pH values below the zero point charge [143]. The zero point charge (pH_{zpc}) is defined as the pH which the surface of an oxide is uncharged [109]. For TiO₂ Degussa P25, pH_{zpc} is reported as 6.25 [112], although it ranges for TiO₂ in general between 4.5 < pH_{zpc} < 7 depending on the production method [109]. The surface of the catalyst is positively charged when pH < pH_{zpc} (protonated form) (Eq. 2.21) and negatively charged when pH ≥ pH_{zpc} (deprotonated form) (Eq. 2.22):



Under highly acidic conditions, agglomeration of TiO₂ reduces the surface area available for photocatalytic reactions. Electron holes (positive holes) are mainly present under acidic conditions, while HO· radicals are dominant at neutral or high pH values. Both species are important for the decomposition of organic compounds [116].

Different states of compounds at different pH values causes complex interaction with the hydrophilic/hydrophobic character of TiO₂, which itself varies with pH [144]. TiO₂ photocatalytic studies of pharmaceuticals have also been conducted at natural pH (i.e. without modifying the pH), which makes this method favourable.

2.7.4. Photon flux

Radiant flux is not a recommended term in photochemistry by the IUPAC although, this term is widely used in photocatalytic related studies. Instead for the purpose of this discussion, the term photon flux is thus used. Photon flux, Φ_p , is defined as the number of photons per time interval [97]. In general, photocatalytic reaction rates are proportional to the photon flux. It is accepted that the reaction rate is directly proportional to the intensity of light with linear variation at low intensities, but beyond a certain level of intensity, which is governed by the reactor conditions, the reaction rate becomes a square root dependence of the light intensity [57, 109]. The energy of a photon is determined by the wavelength while the overall energy input in a photocatalytic process is controlled by the light intensity (Eq. 2.23) [108]. More energetic shorter wavelengths have been reported to be more efficient to promote degradation [57]. Thus, the wavelength of irradiation and intensity has great impact on the photocatalytic performance.

$$E = h\nu = h\frac{c}{\lambda} \quad (2.23)$$

where h is Planck's constant (6.626×10^{-34} Js), c is the speed of light and λ is the wavelength.

2.7.5. Temperature

Photocatalysis is not greatly affected by minor differences in temperature [118]. This is due to the fact that the reaction is initiated by photon absorption and activation [145], which can be realized at room temperature. In addition, as water naturally possesses a high heat capacity, heating can be considered as uneconomical [146].

Nevertheless, studies have correlated the photocatalytic activity with temperature [11]. An operational temperature between 20 and 80°C is considered optimal as it corresponds directly to the apparent activation energy [109, 147]. However, cooling is recommended for temperatures over 80°C to avoid a decrease in rate, as adsorption of compounds becomes unfavourable and tends to be the rate-limiting step [57].

2.7.6. Electron acceptors

Unfavourable electron-hole recombinations in TiO₂ photocatalysis hinder its overall efficiency. Ultrafast recombination of most of the photogenerated electron-hole pairs within femto, pico and nanoseconds after excitation causes low quantum yields (<10%) for TiO₂ photocatalysis [137]. Addition of electron acceptors is thus an important strategy to overcome this limitation. Addition of electron acceptors improves degradation in a number of ways either by (i) capturing trapped electrons, which reduces the recombination phenomena, (ii) producing more radicals and other oxidizing species, (iii) overcoming problems related to deficiency of oxygen concentration and (iv) increasing the oxidation rate of intermediate compounds [107].

In the light of this, molecular O₂ is important for photocatalytic degradation. The role of molecular O₂ is either to generate reactive species such as H₂O₂, O₂^{•-} or ¹O₂ to enhance charge separation inside the TiO₂ surface by capturing electrons or to participate in the reaction [107]. As an acceptor species, O₂ is considered as most economical for this purpose [127]. O₂ absorbs on TiO₂ from the liquid phase following Henry's law. If O₂ is constantly supplied, it can be assumed that its coverage on the TiO₂ surface is constant and can be incorporated into the apparent rate constant [147].

O₂ can react with conduction band electrons to form the superoxide radical anions (Eq. 2.24), which can directly degrade the APIs present on the TiO₂ surface or can undergo further reaction to produce H₂O₂ via two different ways, which in turn acts as a precursor to form HO[•] radicals as shown in Eq.2.25 and Eq. 2.26:



The addition of inorganic oxidants such as H₂O₂ or potassium peroxydisulfate as electron acceptors in UV/TiO₂ photocatalytic studies also accelerates the degradation rate by reacting with conduction band electrons and the superoxide radical anion to yield HO[•] radicals and the hydroxide anion as shown below (Eq. 2.27 and Eq. 2.28).



Dual effects of H₂O₂ include either increasing the formation of additional oxidizing species or suppressing the recombination of electron-hole pairs. At the same time, reactions between H₂O₂ and

photogenerated intermediates cannot be excluded. Studies have suggested that H₂O₂ concentrations, either low or high, can induce significant effects on the degradation rate. Conversely, an excess amount of H₂O₂ may act as an HO[•] radical scavenger or compete with organic compounds for adsorption sites on the TiO₂ surface. Hence, determination of the optimum concentration of H₂O₂ is important to ensure maximum photocatalytic efficiency.

2.7.7. Water composition

The type of water matrix and the presence of ions and natural organic compounds affect the TiO₂ photocatalytic degradation of pharmaceutical to varying extents. Related reviews describing effects of ions on photocatalytic degradations have concluded that ions such as chloride, nitrate, phosphates and sulphates in water may interfere during the photocatalysis, depending on the nature of compound [11, 119]. Ions can either affect the adsorption of the compound, act as HO[•] radicals scavenger or absorb UV light [108].

As a result of the slow reactions between sulphate, phosphate and nitrate ions with the HO[•] radicals, HO[•] scavenging effect can be excluded. Chloride ion is generally considered as an effective HO[•] radical scavenger as this ion can generate less reactive species such as chlorine radicals (Cl[•]) and dichloride anion radicals (Cl₂^{•-}) [88]. Previous studies preferentially study the effects of carbonates and bicarbonates and dissolved organic matter such as humic substances on the photocatalytic degradation of pharmaceuticals [120, 148]. Several reports have evidenced that the presence of carbonate species such as CO₃²⁻ and HCO₃⁻ in a simulated water matrixes or real wastewater competes with pharmaceuticals for the HO[•] radicals thus leading to slower degradation rates [46, 125]. In contrast, enhancement of photodegradation rates have also been reported [120]. Similarly, the effects of humic substances also vary from promotion due to the formation of ROS such as the HO[•] radical, ¹O₂, and superoxide to inhibition as a result of light absorption [104].

Thus, the composition of water plays a significant role in affecting the overall efficiency of UV/TiO₂ for pharmaceutical oxidation.

2.8. NSAID model compound I: Diclofenac

2.8.1. Occurrence of diclofenac

Diclofenac (C₁₄H₁₁Cl₂NO₂) (DCF), 2-[(2,6-dichlorophenyl)-amino]benzeneacetic acid can be easily obtained ‘over-the-counter’ without any prescription, but it is also largely prescribed to treat

inflammation and pain related to rheumatic and non-rheumatic diseases [149]. The global consumption of DCF was estimated to be 940 tons per year with a daily dose of 100 mg [150]. About 15% of DCF is excreted unchanged after human consumption [54]. NSAIDs like DCF with $\log K_{ow}$ greater than three may bioaccumulate in tissues of organisms [151]. This was confirmed when DCF bioaccumulation was found in the liver of rainbow trout with a concentration factor of 2732 [152]. Another study also demonstrated that exposure to environmentally relevant concentrations ranging between 0.5-25 $\mu\text{g/L}$ of DCF caused impairment to the health of rainbow trout [153]. A long-term exposure of the lowest observed concentration of 5 $\mu\text{g/L}$ was also found to cause health impairment in fish, resulting in gill modifications [154]. A major catastrophic effect of DCF was the population decline and high death rate among three species of vultures in India and Pakistan in 2004, due to renal failure from ingesting carcasses polluted with DCF [39].

DCF is also environmentally important due to its frequent detection in water bodies, groundwater aquifers, WWTP influents and effluents. For example, in Germany, 75 tons of DCF are sold annually and monitoring studies recorded 3.02 and 2.51 $\mu\text{g/L}$ in the influents and effluents of WWTPs [155]. Zhang *et al.* [54] reported concentrations of DCF in the range of 0.14-1.48 $\mu\text{g/L}$ in surface water and WWTP effluents. DCF was also detected in several groundwater aquifers (wells) on ng/L levels [156].

The parent DCF and its metabolites have been frequently detected in effluent water because of their resistance towards biodegradation in WWTPs [154]. Removal efficacies of DCF by WWTPs greatly varied from 0-80% depending on the operating conditions of WWTP such as sunlight exposure or the acidic operating conditions, which was observed to be favourable for acidic pharmaceuticals such as DCF [54]. In general, the inability to remove DCF is due to the presence of -Cl and NH- groups in the molecule. Inefficient removal of DCF by WWTPs has been recently confirmed by Salgado *et al.* [157].

Therefore, the effects of DCF on the environment have resulted in a necessity to prevent this API from continuously accumulating in the water cycle.

2.8.2. Photolytic and photocatalytic degradation of diclofenac by UV and sunlight

The degradation of DCF has been investigated by direct photolysis under natural conditions and also by laboratory photolysis. A summary of studies on the degradation of DCF is presented in Table 2.5.

Under natural environmental conditions, DCF can undergo phototransformation when exposed to sunlight. Hence, this mode of degradation has been regarded as an important transformation route in the environment [26, 158]. Seasonal variations such as summer and winter periods, intensity

Table 2.5 Summary of photolytic and TiO₂ photocatalytic studies on DCF

Compounds	Water matrix	Experimental features	HPLC method	Kinetic aspects and removal	Reference
Direct photolysis					
Solar radiation					
	Lake water, distilled water and tap water	Sunlight exposure for 2 h	GC-MS was used	Rapid degradation of DCF in distilled water, tap water and lake water was observed in the range of 2.5-3.7 h ⁻¹ .	[159]
	Milli-Q water and river water	Sunlight (Cork-stopped quartz tubes) (45 °)	Isocratic: ACN: 25 mM KH ₂ PO ₄ buffer (pH 3) (60:40) Monitored λ = 219 nm	DCF was rapidly degraded under sunlight in Milli-Q water ($k = 1.97 \times 10^2 \text{ min}^{-1}$) and river water ($k = 1.97 \times 10^2 \text{ min}^{-1}$). Addition of 1% isopropanol increased the degradation rate to $2.86 \times 10^2 \text{ min}^{-1}$ and $3.32 \times 10^2 \text{ min}^{-1}$ in Milli-Q water and river water, respectively.	[160]
	River water and Milli-Q water	Laboratory exposition under sunlight (on the roof) and field exposure experiment under sunlight in a lake at different depths	Gradient: Solvent A: 8 mmol/L ammonium formate adjusted to pH 4.0 with formic acid and solvent B: MeOH Monitored λ = 254 nm	The half-life of DCF upon laboratory exposition is strongly affected by the solar irradiation. As intensity of solar radiation decreased with increasing depth, DCF degradation took much longer.	[161]
Artificial UV					
	Methanol solution and aqueous phosphate buffer (pH 7)	Medium pressure Hg lamp (125 W)	Isocratic: MeOH:water:acetic acid (60:39:1)	Rapid degradation of DCF under photolytic condition with quantum yield for DCF loss of 0.22 ± 0.08 .	[162]
	Hospital effluent	Medium pressure Hg lamp (125 W)	Isocratic: MeOH:sodium phosphate buffer (70:30)	UV photolysis effective to degrade DCF at pH 5, 7 and 9 after 10 min of irradiation.	[163]

			Monitored $\lambda = 279$ nm		
	Lake water and purified laboratory water	UVA-Vis (315-400-800 nm) and UV-B-UV-A (280-315-400 nm)	GC-MS and ESI-MS	Pseudo-first-order rate constant for the effect of NO_3^- on DCF degradation under UVA-Vis and UVB-UV-A was $1.153 \times 10^{-7} \text{ s}^{-1}$ and $5.083 \times 10^{-5} \text{ s}^{-1}$, respectively.	[105]
	Milli-Q water, filtered and unfiltered treated secondary effluent	Low pressure (254 nm) and medium pressure Hg lamp (200-450 nm)	HPLC	DCF degradation as single compound and in mixture with ketoprofen and atenolol followed pseudo-first-order kinetics. Degradation rate constants of DCF in treated wastewater were lower than in Milli-Q water with $k = 0.01571 \text{ s}^{-1}$ and 0.04181 s^{-1} , respectively, under medium pressure UV.	[91]
	Milli-Q water	Medium pressure Hg lamp	Isocratic: ACN:10 mM NaH_2PO_4 solution (pH 3) (60:40) Monitored $\lambda = 220$ nm	UV photolysis of DCF yielded a rate constant of $0.85 \pm 0.08 \text{ min}^{-1}$, while addition of 25 and 50 mg/L H_2O_2 increased the degradation rates to 0.96 ± 0.07 and $1.00 \pm 0.07 \text{ min}^{-1}$, respectively.	[164]
TiO ₂ photocatalysis					
Artificial UV					
	Milli-Q water	Solar simulator (Xenon arc lamp) (1500 W)	LC-MS Gradient: 0/100-30/70 in 25 min methanol/aqueous ammonium acetate 0.1 mM pH 6.8.	Factorial design was used to investigate the effect of TiO ₂ loading and DCF concentration on reaction rate. The optimum combination of TiO ₂ loading/initial concentration, 0.6 g/L/8.17 mg/L, produced highest degradation rate.	[165]
	Milli-Q water	Solar simulator (1 kW Xe-OP lamp; 290-400 nm)	Isocratic: ACN:10 mM ammonium formate (50:50) Monitored $\lambda = 280$ nm	First-order kinetic model was used to evaluate the degradation of 200 ppm DCF with 0.1 g/L TiO ₂ . The rate constant was reported to be $9.6 \times 10^{-3} \text{ min}^{-1}$.	[142]
	Milli-Q water	125 W black light	UV-Vis spectrometry	Pseudo-first-order fitted well ($R^2 > 0.93$) low DCF	[151]

		fluorescent lamp ($\lambda_{\max} = 350 \text{ nm}$)		concentration (5-40 mg/L), but second-order kinetics fitted better higher concentrations, 40 and 80 mg/L in the presence of high TiO_2 loading (1.6 g/L).	
	Deionized water, groundwater and treated municipal wastewater	UV-A lamp (9W)	UV-Vis spectrometry	TiO_2 Degussa P25 performed best for DCF decomposition, which was affected by water matrix and initial concentration.	[116]
	Milli-Q water	High pressure Hg lamp	Isocratic: MeOH/water (30:70)	Efficiency of TiO_2 photolytic systems ($\text{O}_2/\text{UV-A}/\text{TiO}_2$, $\text{O}_3/\text{UV-A}/\text{TiO}_2$, $\text{UV-A}/\text{TiO}_2$) and single ozonation were compared. DCF was completely removed by photocatalytic process and TOC removed up to 80%, which was higher than single ozonation.	[138]
	Milli-Q water	Medium pressure Hg (near UV-Vis) (366 nm) lamp and low pressure Hg lamp (UV) (254 nm)	Isocratic: 20 mM $\text{NaH}_2\text{PO}_4/\text{H}_3\text{PO}_4$ (pH 4) and MeOH (30:70)	Synthesized anatase (0.5 g/L) under UV irradiation and in the presence of 50% O_2 was found to be optimum condition to yield a first-order rate constant of $0.903 \pm 0.006 \text{ min}^{-1}$.	[149]
Solar irradiation					
	Synthetic freshwater	CPC under sunlight	Isocratic: aqueous of 10 mM ammonium formiate buffer solution:ACN (50:50)	Total decomposition of DCF after around 200 min with 0.2 g/L in standard freshwater, which was much slower compared to photo-Fenton treatment	[166]

differences of the solar radiation and water depth affect the decomposition of DCF in natural surface waters by direct or indirect routes [161]. Direct photolysis of DCF by sunlight in river water and Milli-Q water were comparable and both methods resulted in similar first order constants, $1.97 \times 10^2 \text{ min}^{-1}$, and a half-life of 39 min, due to absorbance of DCF in the solar region [160].

There are some discrepancies in DCF photolysis using artificial UV light. Méndez-Arriaga *et al.* [142], observed up to 75% DCF degradation after 2 h and rationalized this by the overlap of the DCF absorption spectrum with Xe-OP lamp emission spectrum ($>290 \text{ nm}$). Contrary to that, Calza *et al.* [165] reported that there was no significant effect of photolysis with a Xenon arc lamp on DCF after a short irradiation time of 90 min.

A simulated natural environment to examine the effects of dissolved organic matter and nitrate ions on the degradation rate of DCF with UV-A-Vis (315-400-800 nm) and UV-B-UV-A (280-315-400) was also investigated [105]. The presence of dissolved organic matter and NO_3^- decreased the degradation rate of DCF under UV-A-Vis irradiation compared to UV-B-UV-A. Dissolved organic matter acted as a quencher, rather than producing HO^\bullet radicals or other ROS under the conditions tested.

DCF can also be degraded by TiO_2 photocatalysis as demonstrated in numerous studies [116, 129, 149]. Typical parameters, which control the photooxidative behaviour of DCF, include TiO_2 loading, initial concentration, type of photocatalyst, effect of oxidant and water matrices have been thus been studied. Although the TiO_2 -mediated UV photocatalysis process was found to be efficient to degrade DCF, results vary among studies due to the differing experimental conditions. In all cases, TiO_2 photocatalysis led to low degrees of mineralization.

Single AOP approaches have been preferred to investigate removal of DCF. Solar photocatalysis of DCF has also been the focus of several studies [166, 167]. Besides TiO_2 photocatalysis with both UV light and sunlight, another single AOP method which has been used includes ozonation [168], photo-Fenton [81] and sonolysis [169]. Use of combinations of AOPs still remains limited [170].

2.8.3. Degradation pathway of diclofenac

Transformation pathways for DCF photolysis [139, 161, 168, 171] and TiO_2 photocatalysis [149, 165] have been proposed in existing studies. Fig.2.8 summarizes all degradation products that have been identified from two independent studies that investigated direct photolysis of DCF under sunlight and UV irradiation under oxygenated and deaerated conditions. In both cases, DCF degradation was found to follow similar but not entirely identical degradation pathways. Agüera *et al.* [139] reported 13 phototransformation products as shown in Fig.2.8.

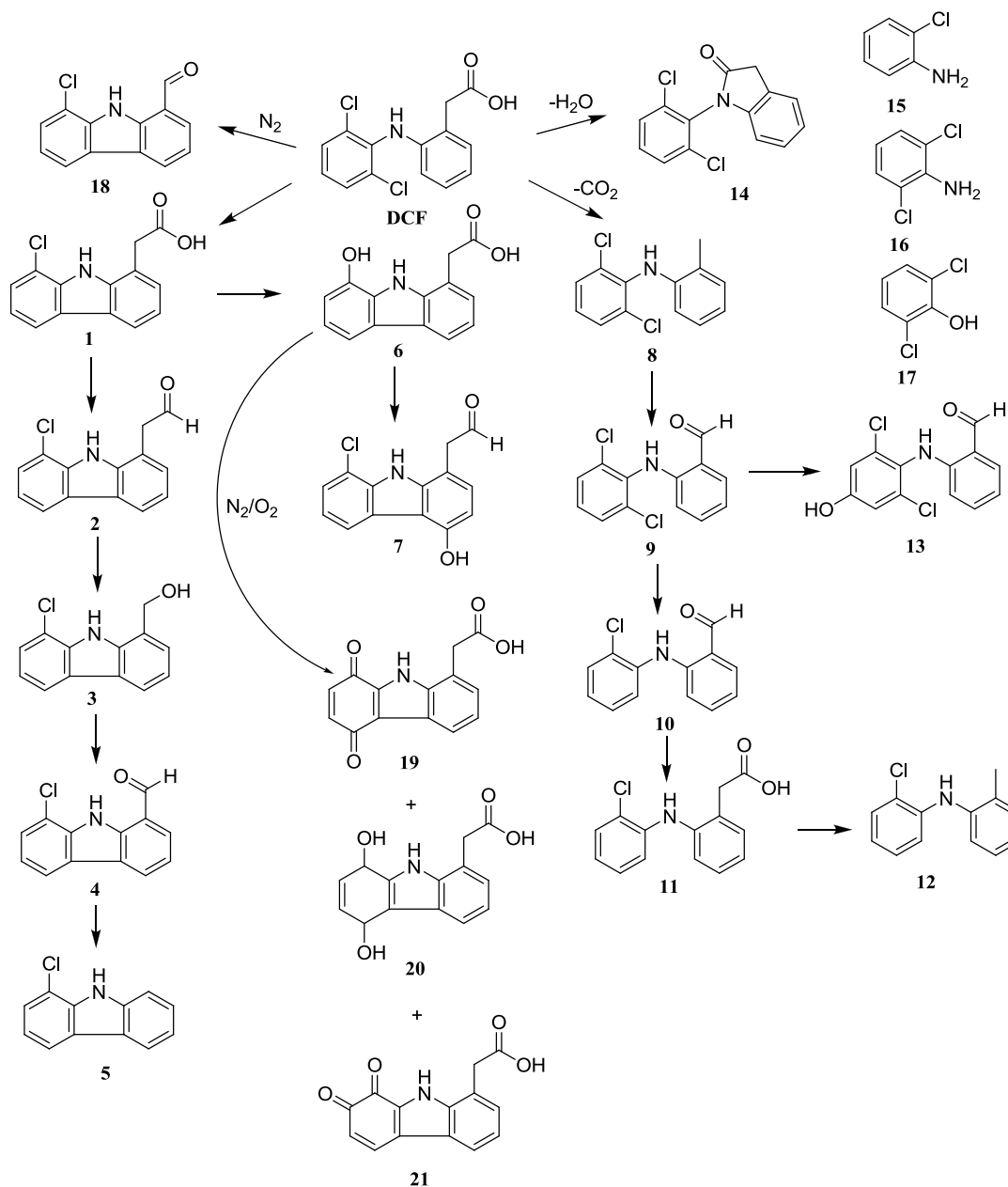


Fig.2.8 Degradation products of direct photolysis of DCF [139, 161, 171]

Compounds **1-13** formed when DCF was exposed to direct sunlight and were identified by LC-TOF-MS and GC-MS. Two initial routes were proposed for direct photolysis of DCF, namely photocyclization to carbazole derivatives and decarboxylation followed by further oxidation of the remaining alkyl-chain. The main photoproduct detected upon direct photolysis of DCF was the 8-chloro-9H-carbazole-1-yl-acetic acid (**1**), a monohalogenated carbazole formed as a result of the photocyclization of DCF. Another study of DCF photolysis under sunlight identified nine photoproducts using GC-MS [160]. Of these, compound **14** was found to be the major product formed. This study also confirmed the presence of compounds **4** and **8-10** as previously identified by

Agüera *et al.* [139]. Three compounds were reported for the first time, 2-chloroaniline (**15**), 2,6-dichlorophenol (**16**) and 2,6-dichloroaniline (**17**), respectively [161]. Deaerated and oxygenated conditions during UV photolysis of DCF solutions also affects the formation of degradation products [171]. Compound **1** was identified as a major degradation product under both deaerated and oxygenated conditions. Aldehyde **18** which was not reported previously was also detected along with compounds **19-21**. Recently, another study used the LC-ESI-MS/MS-QTrap analytical technique to identify the 4'-hydroxy-diclofenac metabolite formed from photolysis of hospital effluent [163]. This compound is known to be persistent to biological treatment but may undergo degradation under solar radiation [163].

In contrast, the TiO₂ photocatalytic degradation pathway of DCF was proposed to occur with hydroxylation, cleavage of the N-H bond, dehalogenation and aromatic ring opening [165]. Martínez *et al.* [149] compared the photoproducts formed from photocatalysis with commercial TiO₂ P25 and synthesized TiO₂ (anatase and rutile) and also composite multi-walled carbon nanotube by using LC-MS. The main photoproduct formed was the monohalogenated carbazole, **1** as a result of the photocyclization of DCF (Fig.2.9). The same major product was identified during DCF photolysis [139]. Other identified routes were decarboxylation and further oxidation of the alkyl-chain and dechlorination of the carbazole structure **1** followed by hydroxyl substitution to **6**. Carbazole compounds formed from during photolysis and TiO₂ photocatalysis have been associated with phototoxicity [149].

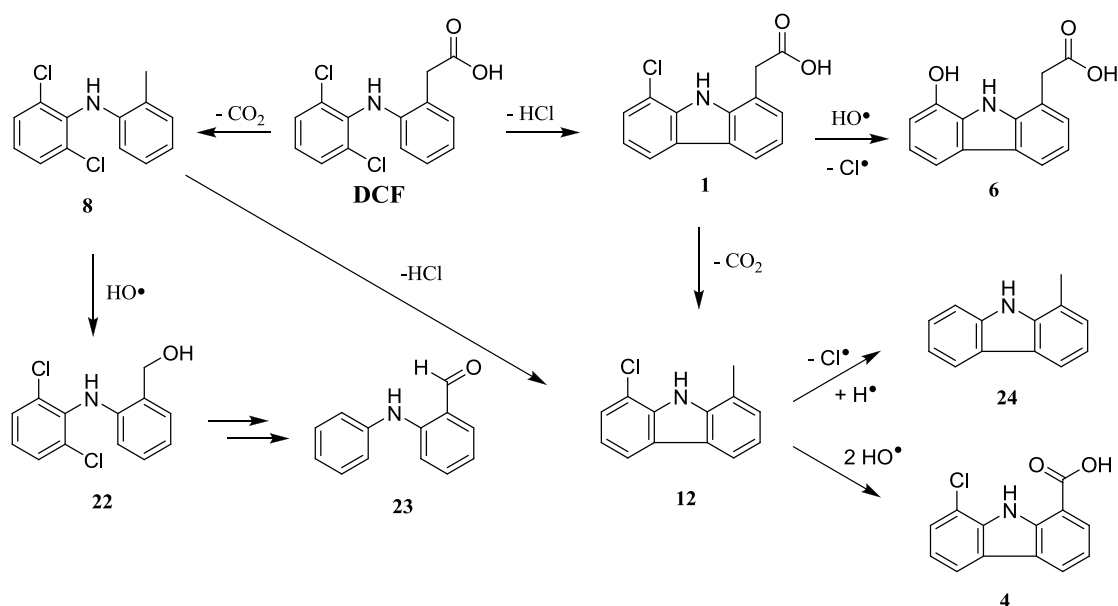


Fig.2.9 TiO₂ photocatalytic degradation pathway of DCF [149]

2.9. NSAID model compound II: Naproxen

2.9.1. Occurrence of naproxen

Naproxen (NPX) ($C_{14}H_{14}O_3$), a 2-arylpropionic acid derivatives, is another commonly used NSAID drug, used for pain relief and treatment related to osteoarthritis and rheumatoid arthritis [172]. NPX has been detected in environmental matrices such as surface water, sewage treatment plant influents and effluents [6, 17, 155]. Despite a high removal rates of NPX (>80%) during wastewater treatment [173], the detection of higher concentrations of NPX in the effluent than WWTP influent has been rationalized based on the presence of high levels of hydrolysable phase-II metabolites [17]. The concentrations of NPX in WWTP effluents have been reported to range between 25 ng/L and 33.9 $\mu\text{g/L}$ [174].

Bioassay tests of NPX have demonstrated higher chronic than acute toxicity [154]. A study by Cleuvers [175] on the toxicity of mixtures containing NPX and three other NSAIDs, ibuprofen, DCF and acetylsalicylic acid on *Daphnia* and algae indicates that the toxicity is more likely to be chronic due to low concentrations of pharmaceuticals in the environment. Thus, the occurrence of environmental problems, anticipated from the presence of NPX has resulted in researchers assessing various AOPs such as photo-Fenton [176], catalytic ozonation [143] and UV/ H_2O_2 [177] for NPX removal.

2.9.2. Photolytic and photocatalytic degradation of naproxen by UV and sunlight

Various aspects related to NPX such as its phototoxicity [178, 179], photodegradation and its photoreactivity [180] have been intensively investigated. Major findings demonstrated that photoproducts of NPX with greater polarity were more toxic than the parent compound [179]. A study by DellaGreca *et al.* [181] also confirmed these findings based on the higher toxicity exhibited on *Daphnia magna* and *Vibrio fischeri* by the photoproducts of NPX, the latter generated from irradiation in drinking water. A further study reported on the toxicity of photomixtures to cultured hepatocytes in the presence of oxygen compared to anaerobic conditions. This was rationalized by the presence of NPX-derived peroxidic products [182].

The removal of NPX from various water samples by means of direct photolysis and TiO_2 photocatalysis is summarized in Table 2.6.

Table 2.6 Summary of photolytic and TiO₂ photocatalytic studies on NPX

Compounds	Water matrix	Experimental features	HPLC method	Kinetic aspects and removal	Reference
Direct photolysis					
Solar radiation					
	Milli-Q water and river water	Natural sunlight and laser flash photolysis	Isocratic: ACN:25 mM KH ₂ PO ₄ buffer (pH 3) (60:40) Monitored $\lambda = 219$ nm	First-order-rate constant showed that degradation of NPX was slower in river water ($2.08 \pm 0.14 \text{ min}^{-1}$) than Milli-Q water ($1.64 \pm 0.54 \text{ min}^{-1}$) under sunlight.	[160]
Artificial UV					
	Laboratory grade water and surface water	Low pressure and medium pressure Hg lamp	HPLC conditions not provided	Addition of 10 mg/L H ₂ O ₂ increased the rate constant from $4.2 \times 10^{-1} \text{ min}^{-1}$ to $29.9 \times 10^{-1} \text{ min}^{-1}$ in laboratory grade water with medium pressure Hg lamp.	[92]
	Distilled water	Medium pressure Hg lamp	Isocratic: ACN:phosphate buffer (60:40) Monitored $\lambda = 220$ nm	First-order degradation rate of NPX in mixture with ibuprofen and DCF with UV treatment was $0.048 \pm 0.006 \text{ min}^{-1}$, while in the presence of H ₂ O ₂ the rate increased to $0.303 \pm 0.0208 \text{ min}^{-1}$.	[183]
	Water (not specified)	Low pressure Hg lamp	Isocratic: aqueous buffer:ACN (60:20) Monitored $\lambda = 220$ nm	In aerated aqueous, NPX was completely removed after 30 min, whereas purging of pure O ₂ did not show any significant change with UV (254 nm).	[174]
	Milli-Q water	Medium pressure Hg lamp	Isocratic: ACN:10 mM NaH ₂ PO ₄ solution (pH 3) (60:40) Monitored $\lambda = 220$ nm	Pseudo-first-order degradation rate of NPX with UV medium pressure Hg lamp was $0.29 \pm 0.04 \text{ min}^{-1}$, while in the presence of 25 and 50 mg/L H ₂ O ₂ (UV/H ₂ O ₂) the degradation rate increased to $0.53 \pm 0.05 \text{ min}^{-1}$ and $0.69 \pm 0.04 \text{ min}^{-1}$, respectively.	[164]

TiO ₂ photocatalysis					
Artificial UV					
	Mili-Q water	Solar simulator (Xe lamp)	Isocratic: ACN:0.05 M ammonium dihydrogen phosphate (80:20) Monitored $\lambda = 254$ nm	Direct photolysis of NPX led to higher degradation (90%) compared to only 40% for photocatalysis. However, a higher DOC removal was attained in the presence of 0.1 g/L TiO ₂ .	[126]
	Milli-Q water	Solar simulator (1 kW Xe-OP lamp; 290-400 nm)	Isocratic: ACN:0.05 M ammonium dihydrogen phosphate (80:20) Monitored $\lambda = 254$ nm	The apparent first-order kinetic constant for NPX degradation was $7.0 \times 10^{-3} \text{ min}^{-1}$ with TiO ₂ loading of 0.1 g/L (30°C).	[142]
<i>Solar radiation</i>					
	Secondary wastewater effluent	CPC and solar simulator	HPLC conditions not provided	Identified concentration of NPX, 2968 ng/L in the real wastewater effluent was degraded under sunlight with 20 mg/L TiO ₂ within 150 min.	[184]

Photodegradation studies by direct photolysis and UV/H₂O₂ have confirmed the feasibility of this mechanism to degrade NPX. A study by Packer *et al.* [160] demonstrated that in the natural environment under sunlight, NPX can be readily photodegraded in short periods of time due to its UV absorption up to 350 nm. Similarly, another study highlighted the importance of phototransformation and biodegradation of NPX in surface water [185]. This has been further confirmed to occur with artificial UV using a medium pressure Hg lamp [164]. Studies using UV/H₂O₂ with a low pressure Hg lamp and a medium pressure Hg lamp can be also found in the literature showing the effectiveness of this degradation technique for NPX [84, 92].

A recent study by Marotta *et al.* [174] proposed simplified reaction schemes for NPX photodegradation under aerated and deaerated conditions with UV-C light of 254 nm. The study concluded that dissolved oxygen greatly influenced the photodegradation rates of NPX, as well as the distribution of major intermediates.

Compared to available reports on direct photolysis of NPX, there have been limited studies on TiO₂ photocatalysis. There is only one study in the literature, which was exclusively dedicated to the photocatalytic degradation aspect of NPX in ultrapure water using a solar simulator [126]. Various factors affecting the degradation, such as TiO₂ loading, temperature, volumetric flow and dissolved oxygen concentration, were the focus of this study, which demonstrated higher NPX removal with direct photolysis compared to TiO₂ photocatalysis. The presence of oxygen greatly influenced the degradation efficiency. DOC removal was, however, observed to be minimal under direct photolysis with only 5% reduction, while a slightly higher removal percentage of 20% was obtained by TiO₂ photocatalysis. The research group also investigated photocatalysis of NPX included two other NSAIDs, DCF and ibuprofen [142]. This study showed that solution temperature exhibited a significant effect on the degradation of NPX at 40°C, when both the degradation of NPX and the TOC increased, whereas an increase in dissolved oxygen concentrations only increased the degradation of NPX.

2.9.3. Degradation pathway of naproxen

Photoproducts generated from direct photolysis of NPX in the presence and absence of oxygen have been identified in various studies [174, 180, 181]. Decarboxylation is the predominant pathway in the photolysis in aqueous solution [180]. Fig.2.10 shows the main degradation pathways of NPX, by photoionization and decarboxylation [158]. Two compounds, 1-ethyl-6-methoxynaphthalene (**25**) and 1-(6-methoxy-2-naphthyl) ethanol (**27**) were observed under anaerobic conditions. Under aerobic conditions, compound **27** or a ketone, **28** (2-acetyl-6-methoxynaphthalene) were formed from

the unstable hydroperoxide intermediate, **26**. Further, studies also reported that some major products of NPX photolysis are sources of singlet oxygen.

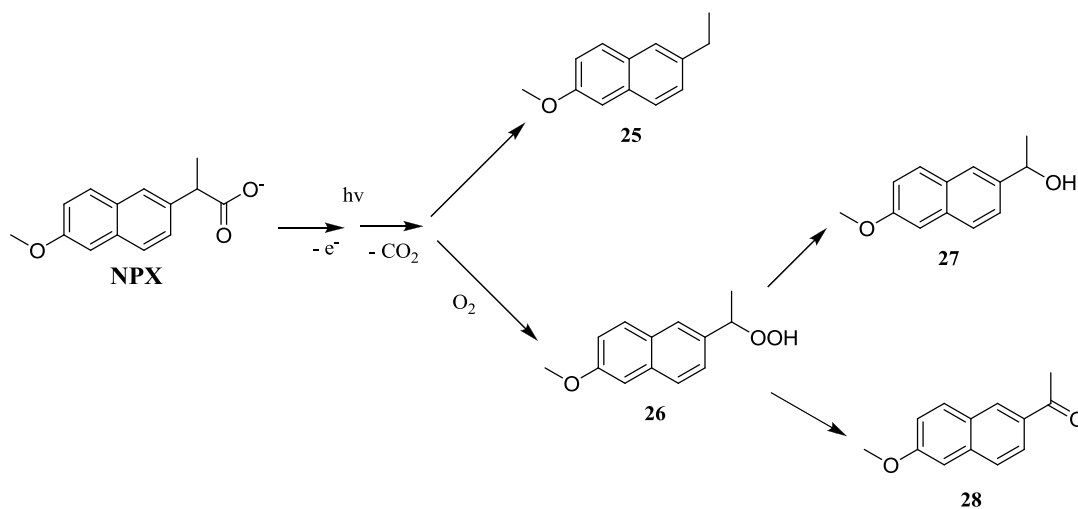


Fig.2.10 Photolysis degradation products of NPX

A detailed study on the TiO_2 photocatalytic products of NPX in the presence of O_2 has been performed by Méndez-Arriaga *et al.* [126] using LC-TOF-MS (Fig.2.11).

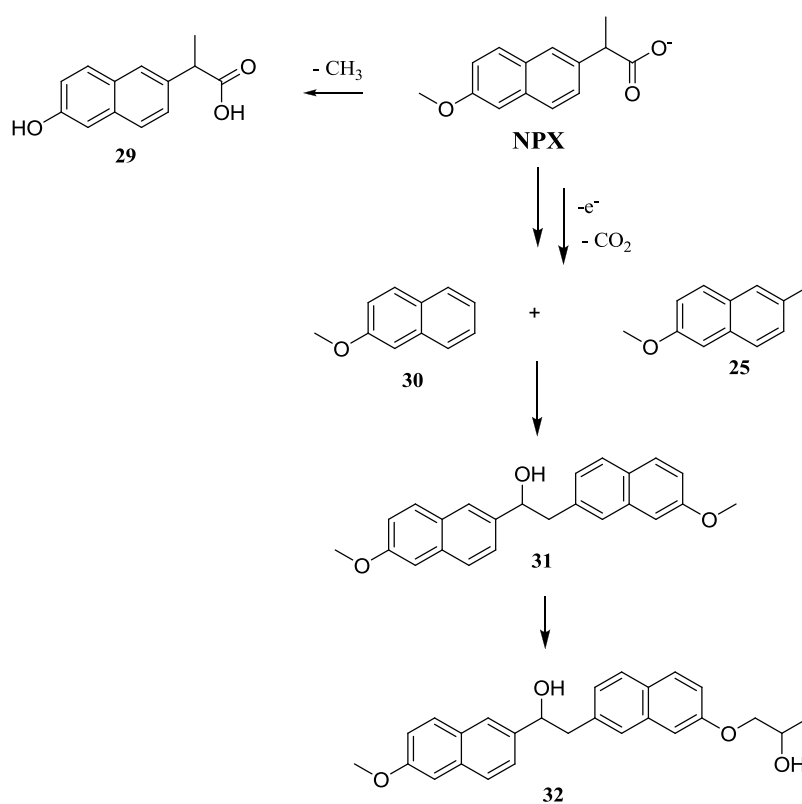


Fig.2.11 TiO_2 photocatalytic degradation products of NPX [126]

Two major pathways, demethylation and decarboxylation, were suggested. Photolytic degradation products were also formed during the photocatalytic process. In the first step, demethylation of NPX led to the formation of 2-(6-hydroxynaphthalen-2-yl)propanoic acid (**29**). The second step, which was initiated by decarboxylation of NPX leads to the formation of dimer **31**. Compound **32** was proposed to be generated from reaction with a $\text{CH}_3\text{OHCH}_2^\cdot$ radical, which formed from the demethylation pathway with dimer **31**.

2.10. Antibiotic model compound: Amoxicillin

In recent years, there have been numerous studies published on antibiotics due to their extensive uses in both humans and animals to prevent and treat microbial infections. The polar and non-volatile nature of antibiotics contributes significantly to their persistent accumulation in the environment either as the parent compound or as metabolites after conventional water treatment [98]. A recent comprehensive review highlighted that urban WWTPs are one of the main reasons why antibiotics are continuously released into the environment [36]. The emergence of antibiotic resistant strains of bacteria as a result of continuous accumulation is also of great concern [41]. Accumulation of small quantities of antibiotics in the long-term may result in adverse effects in both humans and animals.

In this study, amoxicillin (AMX), a β -lactam antibiotic which is widely used in human and veterinary medicines [186], was chosen. Oral administration of 500 mg of AMX in humans resulted in about $86 \pm 8\%$ detected in the urine within two hours of consumption [145]. Excretion of unchanged AMX, due to a slow rate of metabolism in humans has led to its direct discharge into the environment. In Australia, AMX has emerged as one of the most frequently prescribed medicines and has been reported to be present in river water and hospital effluents in ng/L levels [32]. Only partial removal of antibiotics is achieved in general by conventional urban WWTPs, making this class of drugs potentially important pollutants.

2.10.1. Photolytic and photocatalytic degradation of amoxicillin

The removal of AMX by direct photolysis and TiO_2 photocatalysis is summarized in Table 2.7.

Direct photolysis of AMX has rarely been investigated as a method of degradation. Jung *et al.* [65] studied the degradation of AMX by applying UV/ H_2O_2 and direct UV-C. It was noted that increasing concentrations of H_2O_2 resulted in enhanced pseudo-first-order rate constants compared to that of direct photolysis in the absence of H_2O_2 . Study by Xu *et al.* (2011) [187] systematically investigated the effect of hydrolysis, direct and indirect photolysis on AMX. The study concluded that indirect photolysis of AMX in aqueous solution in the presence of DOM in particular excited state DOM*

Table 2.7 Summary of photolytic and TiO₂ photocatalytic studies on AMX

Compounds	Water matrix	Experimental features	HPLC method	Kinetic aspects and removal	Reference
Direct photolysis					
Artificial UV					
	Distilled deionized water	Low pressure Hg lamp	Isocratic: 1% acetic acid and ACN (70:30) λ monitored = 254 nm	Direct UV photolysis and UV/H ₂ O ₂ on AMX both followed pseudo-first-order kinetics. Rate constant was enhanced in the presence of 10 mM H ₂ O ₂ . Likewise, TOC was removed by 50% when 10 mM H ₂ O ₂ was added compared to only <10% with direct photolysis.	[65]
	Milli-Q water	Solar simulator (300 W ceramic Xenon lamp)	Isocratic: 10 mM phosphate buffer (pH 3):MeOH (85:15) λ monitored = 230 nm	The reaction of AMX with singlet oxygen, HO [•] radicals and ³ DOM* was investigated under simulated sunlight. Among these, only ³ DOM* was concluded to contribute significantly to AMX degradation in the aquatic environment.	[187]
TiO ₂ photocatalysis					
Artificial UV					
Amoxicillin (ampicillin and cloxacillin)	Distilled water	UV lamp (6 W, 365 nm)	Isocratic: 0.025 M KH ₂ PO ₄ :ACN (55:45) λ monitored = 204 nm	All treatments degraded the antibiotics and also improved biodegradability except for UV/ZnO which did not show any effect on the latter. Photo-Fenton showed highest rate constant (0.029 min ⁻¹).	[188]
	Hospital wastewater	Medium pressure Hg lamp (125 W; intensity: 401 W/m ²)	Isocratic: MeOH:water:0.01 M KH ₂ PO ₄ (20:70:10) λ monitored = 238 nm	Response surface methodology was used to study the combined effect of pH and TiO ₂ loading on COD reduction and AMX photocatalysis. Maximum COD removal was achieved with 800 mg/L TiO ₂ and pH 3. Toxicity inhibition of 46.3% was obtained.	[145]
Amoxicillin (ampicillin and cloxacillin)	Distilled water	UV lamp (6 W, 365 nm)	Isocratic: 0.025 M KH ₂ PO ₄ :ACN (60:40)	Addition of H ₂ O ₂ at pH 5 with TiO ₂ 0.1 g/L led to complete degradation of all antibiotics. Degradation followed pseudo-first-order kinetic with a rate constant	[124]

			λ monitored = 204 nm	of 0.007 min^{-1} .	
Amoxicillin (ampicillin and cloxacillin)	Distilled water	UV lamp (6 W, 365 nm)	Isocratic: 0.025 M KH_2PO_4 :ACN (55:45) λ monitored = 204 nm	Degradation of AMX followed the pseudo-first-order kinetic with a rate constant of 0.018 min^{-1} at the optimum condition of 0.5 g/L ZnO at pH 11.	[189]
	Ultrapure water and treated wastewater (secondary effluent)	9 W Radium Ralutec	Isocratic: 0.025 M KH_2PO_4 buffer:ACN (70:30)	Complete AMX degradation was achieved after 25 min for 10 mg/L AMX in the presence of 250 mg/L TiO_2 P25 Degradation order shifted from first to zero as the initial concentrations of AMX increased from 2.5 to 5 mg/L and above.	[117]
Solar radiation					
	Water type not provided	Sunlight	Gradient: Water/0.1% formic acid: ACN/0.1% formic acid	Carbon and iron doped titania and Degussa P25 was tested for AMX degradation under artificial visible light and solar radiation. 2 h solar exposure in an evaporation dish reactor yielded a 80% AMX conversion in the presence of 1 g/L TiO_2 P25.	[190]
	Milli-Q water	CPC reactor	Gradient: ACN:MeOH:0.01 M oxalic acid λ monitored = 231 nm	TiO_2 solar photocatalysis degraded the AMX solution from 40 to 3.1 mg/L in the presence of 0.5 g/L TiO_2 after 4.6 kJ of accumulated energy per litre of solution. DOC was removed by 44% under similar conditions.	[191]

significantly contributes to its photodegradation. A study by Andreozzi *et al.* [186] investigated the effect of nitrate ions and humic acids on the degradation of AMX under sunlight at pH 5.5 and pH 7.5. The study concluded that nitrate ions had no effect on the degradation rate as a result of its ability to absorb sunlight, thus reducing the production of HO[•] radicals. However, humic acids were observed to enhance the degradation rate at both pHs.

Only a few studies on the applications of AOPs to the degradation of AMX currently exist and most of these studies applied Fenton, photo-Fenton or ozonation [82, 192], resulting in an opportunity for the TiO₂ photocatalytic oxidation of AMX to be investigated. There are some scholarly disagreements over the performance of the TiO₂ photocatalysis of AMX. Elmolla and Chaudhuri [188] evaluated three different types of AOPs, namely Fenton/photo-Fenton, TiO₂ photocatalytic (UV/TiO₂ and UV/TiO₂/H₂O₂) and ZnO photocatalytic (UV/ZnO) processes in terms of their efficiency and cost for the treatment of AMX and two other antibiotics, ampicillin and cloxacillin, in aqueous solution. The study revealed that photo-Fenton performed better and was the most cost-effective process. Contrary to this, Martins *et al.* [145] reported that TiO₂ photocatalysis yielded 100% AMX degradation in hospital wastewater samples after 30 min of treatment, with a benchscale photoreactor equipped with a medium pressure Hg lamp, while only 85% degradation was achieved using the photo-Fenton process.

The research group of Elmolla and Chaudhuri also conducted two studies on AMX in combination with ampicillin and cloxacillin. Comparing the performance between UV/TiO₂ and UV/H₂O₂/TiO₂ on AMX degradation with UV-A irradiation (365 nm) was the focus of their study [124]. A further study evaluated the effect of UV/ZnO photocatalysis of AMX [189]. Conclusions drawn from these studies were that both UV/H₂O₂/TiO₂ and UV/ZnO performed effectively to remove AMX from aqueous solutions. A study by Dimitrakopoulou *et al.* [117] concluded that photocatalyst TiO₂ P25 efficiently eliminated AMX after 25 min of irradiation in ultrapure water with 93% mineralization after 90 min compared to other TiO₂ materials studied. However, secondary effluent water impeded the degradation of AMX due to the presence of organic matter, bicarbonates and chlorides.

A study highlighted the efficiency of solar radiation over artificial light for the degradation of AMX. It was reported that sunlight produced rapid degradation which was three times faster than that of the artificial UV [190]. A recent study also confirmed the high efficiency of sunlight-driven TiO₂ photocatalytic degradation for the removal of 20 mg/L AMX and DOC compared to the inefficient photolytic process [191].

It can be concluded that artificial UV and solar photocatalysis with TiO₂ allowed for efficient AMX degradation. ZnO proved to be also effective, even though only one of the reviewed studies as mentioned above used this photocatalyst. As a result, more research is needed to evaluate the

potential of ZnO to facilitate AMX degradation by optimizing the parameters influencing its degradation. Since TiO₂ photocatalysis of AMX has only been reported to a limited extent, this photocatalyst also needs to be further explored.

2.10.2. Degradation pathway of amoxicillin

Fig.2.12 shows the proposed pathways for AMX photocatalytic degradation under different concentrations and conditions which was detected by using LC-QTOF-MS [190]. AMX is cleaved at the secondary peptide bond forming *p*-hydroxybenzoic acid (**33**) and a bicyclic lactamic compound (**34**).

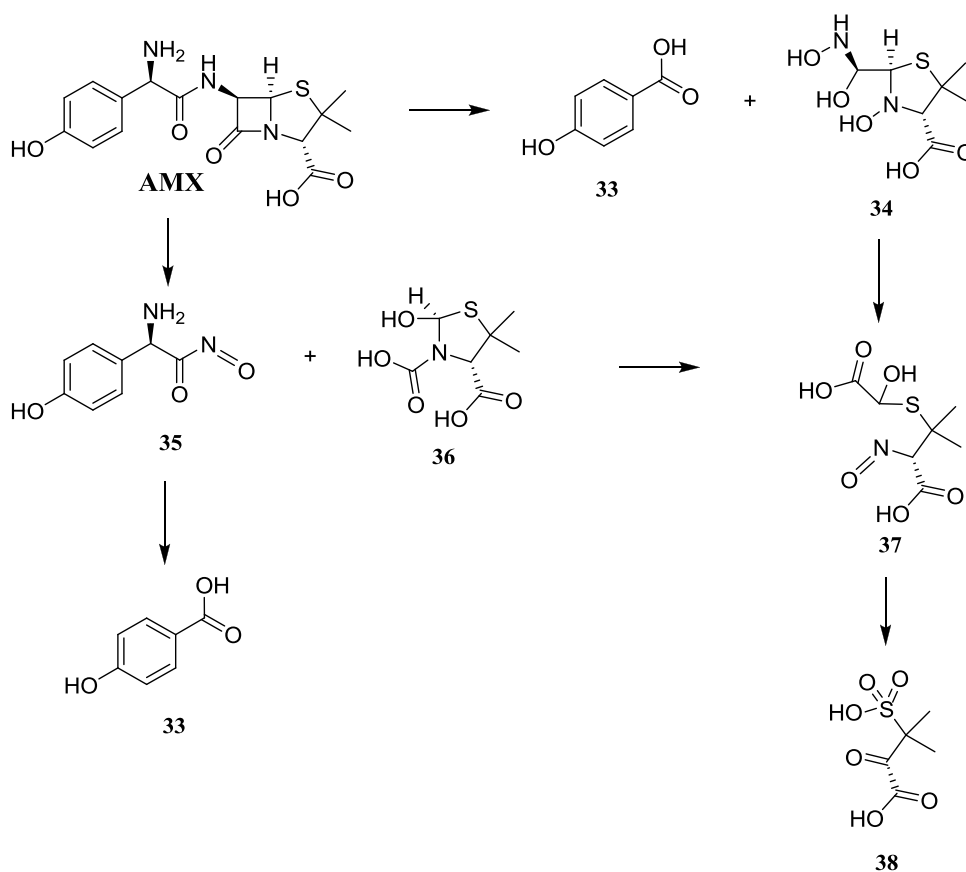


Fig.2.12 Photocatalytic degradation of AMX [190]

Thus far, little attention has been paid to the fate and behaviour of AMX in the aquatic environment. To fill this gap, Pérez-Parada *et al.* [193] studied the transformation products and pathways of AMX in environmental matrices (i.e. river water and WWTP wastewater) using LC-QTOF-MS/MS. The opening of the four-membered β -lactam ring was proposed as the main transformation pathway leading to the formation of compound **39** (Fig.2.13). Decarboxylation of compound **39** leads to the

formation of the stereoisomeric compounds **40** and **41**. Alternatively, compound **39** can act as an intermediate to generate the stable stereoisomeric diketopiperazine **42** and **43** (Fig.2.13).

A study performed by Nägele and Moritz [194] reported similar degradation products obtained under acidic conditions. This study also identified another degradation product, compound **44**, which formed as a result of nucleophilic attack on AMX.

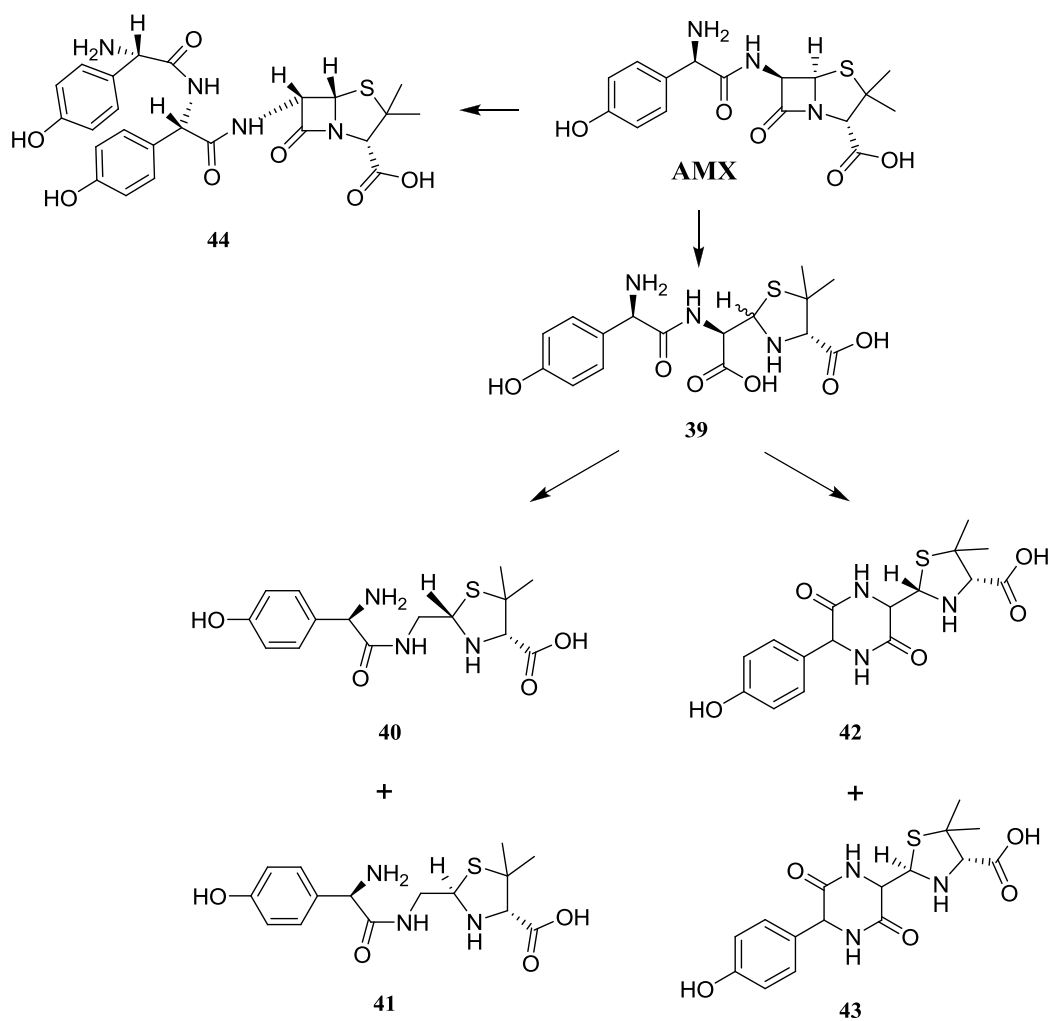


Fig.2.13 Proposed degradation pathway for AMX [193, 194]

Chapter 3. Materials and Methods

3.1. Reagents

Diclofenac sodium salt, naproxen sodium salt and amoxicillin (all of R&D grade) were purchased from Sigma-Aldrich (USA) and were used as received without purification. High performance liquid chromatography (HPLC; Agilent Technologies Australia Pty Ltd, Melbourne, Vic., Australia) and Nuclear Magnetic Resonance (NMR; Varian Oxford 300 with the Varian Software VnmrJ Revision D, Agilent Technologies 55 Australia) analyses showed no impurities. Commercial Aeroxide® TiO₂ P25 (80% anatase and 20% rutile, BET surface area 50 m²/g) was supplied by Evonik industries (Canada). Titanium (IV) oxide, anatase (>99% purity based on trace metal analysis) (45 µm) was purchased from Sigma-Aldrich (USA) and was used as a comparison to Aeroxide® TiO₂ P25. HPLC grade methanol and glacial acetic acid were obtained from RCI Labscan. Potassium chloride (AR grade, BDH Analar), potassium dihydrogen phosphate (AR grade, Univar, Ajax FineChem) and hydrogen peroxide (30%, Univar) were used as supplied.

Stock and standard solutions and mobile phases were prepared using ultrapure water from a Milli-Q system (18.2 MΩcm, Millipore) while laboratory grade distilled water was used for preparing the solutions for the photodegradation experiments.

3.2. River water and drinking water samples

River water was sampled from the Ross River (19°18'59" S, 146°45'7"E) in Townsville between July and November 2012 and was stored at 4°C prior to irradiation and analysis. Unfiltered river water samples were used for the photodegradation studies in order to mimic environmentally relevant conditions. Drinking water was freshly sampled from the laboratory. Table 3.1 displays the average water quality characteristics of drinking water and river water used in this study.

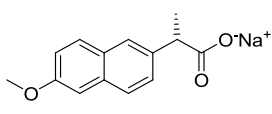
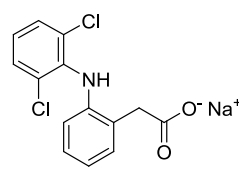
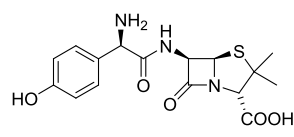
Table 3.1 Water quality characteristics of river water and drinking water

Parameter	Drinking water	River water
Calcium (mg/L)	11.8	31.2
Magnesium (mg/L)	3.0	17.9
Hardness as CaCO ₃ (mg/L)	41.8	151.6
Oxidized N (mg/L)	0.04	<0.01
Sulphate (mg/L)	1.0	5.1
Chloride (mg/L)	16.7	107.3
Dissolved organic carbon (DOC) (mg/L)	2.74	4.39
pH	7.5 ± 0.1	7.8 ± 0.1

3.3. Properties of the active pharmaceutical ingredients

Three APIs, namely DCF, NPX and AMX were chosen for this study due to their frequent detection in the environment and widespread prescription as described in Chapter 2 (sections 2.8-2.10). Table 3.2 presents selected properties of these APIs.

Table 3.2 APIs focused on in this study

Properties	Naproxen sodium	Diclofenac sodium	Amoxicillin
Structure			
Chemical Formula	C ₁₄ H ₁₃ NaO ₃	C ₁₄ H ₁₀ Cl ₂ NO ₂ Na	C ₁₆ H ₁₉ N ₃ O ₅ S
CAS No	26159-34-2	15307-79-6	26787-78-0
Molecular weight (g/mol)	252.24	318.13	365.40
Log k _{ow} *	3.18 [126]	4.51 [195]	0.87 [195]
pK _a *	4.15 [126]	4.15 [54]	2.4, 7.4 and 9.6 [196]
Solubility in water* (mg/L) (25°C)	15.9 [126]	23.7 [54]	15.9

* Data for acid form (HA)

3.4. Adsorption experiments

Adsorption experiments were conducted to evaluate the extent of adsorption of all three API on the TiO₂ surface in the dark. Adsorption experiments were conducted using 100 mL of the API solution and a fixed amount of 0.1 g/L of Aeroxide[®] TiO₂ P25. The API solutions at different initial concentrations (C_{DCF} = 10-70 mg/L; C_{NPX} = 5-60 mg/L; C_{DCF/NPX mixture} = 10-60 mg/L) in the presence of 0.1 g/L TiO₂ were mixed using an orbital shaker (Model Stuart SSL1) at 230 rpm for 24 h to establish an equilibrium between TiO₂ particles, relevant APIs and the aqueous system. Aliquots were collected and filtered through a 0.22 μm syringe filter before measuring the remaining API concentration by HPLC. These steps were repeated at different solution pHs (DCF pH = 3-11; NPX pH = 5-11). Adjustment of pH was carried out with diluted NaOH or HCl.

3.5. Photochemical degradation procedures

Two types of circulating batch photoreactors, an advanced laboratory-scale immersion-well reactor and a novel demonstration-scale loop reactor, were used in this study.

3.5.1. Immersion-well reactor

The smaller immersion-well photoreactor (Heraeus UV-RS-1, Germany, length of 38.4 cm with an optical path <2 cm) is made of pyrex glass (cut-off wavelength ≤ 290 nm) and is shown in Fig.3.1. The reactor was filled with 400 mL of the API solution or suspension of TiO_2/API and irradiated with a medium pressure Hg vapour lamp (TQ 150 Heraeus, Germany, 150 W). A warm-up time of at least 5 min is required to achieve the full intensity of light output.

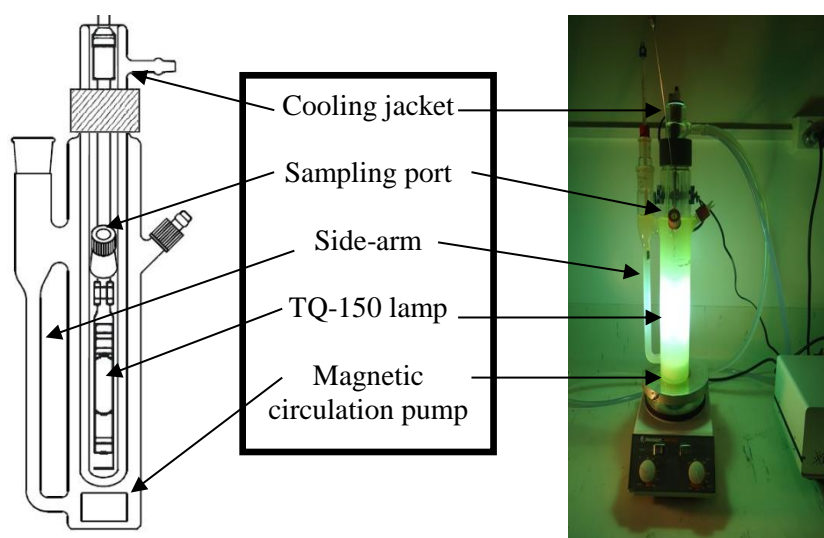


Fig.3.1 Schematic representation and picture of immersion-well photoreactor setup

The reactor was equipped with a powerful magnetic circulation system to circulate the reaction mixture through an attached side-arm. This feature provided very effective circulation and mixing, even under heterogeneous conditions. In contrast, most common batch reactors provide poor mixing, especially those with a narrow gap between the sides of the outer reactor vessel and the inner immersion-well. Chilled water was circulated to prevent the lamp from overheating. Temperature in the reaction vessel during all experiments ranged from 24°C and 29°C. The reaction setup was placed behind a UV-shield and maintained in a dark fume cabinet.

The medium pressure Hg lamp emits polychromatic light across a wide range of wavelengths from UV (UV-C~15-23%, UV-B~6-7%, UV-A~8%) to visible (Vis~15%) [88]. The most prominent emissions were at 254, 313 and 366 nm in the UV region and 405, 436, 546, 578 nm in the visible region, respectively [197] (Fig.3.2). When a pyrex immersion tube was used, the wavelength below 290 nm was filtered out.

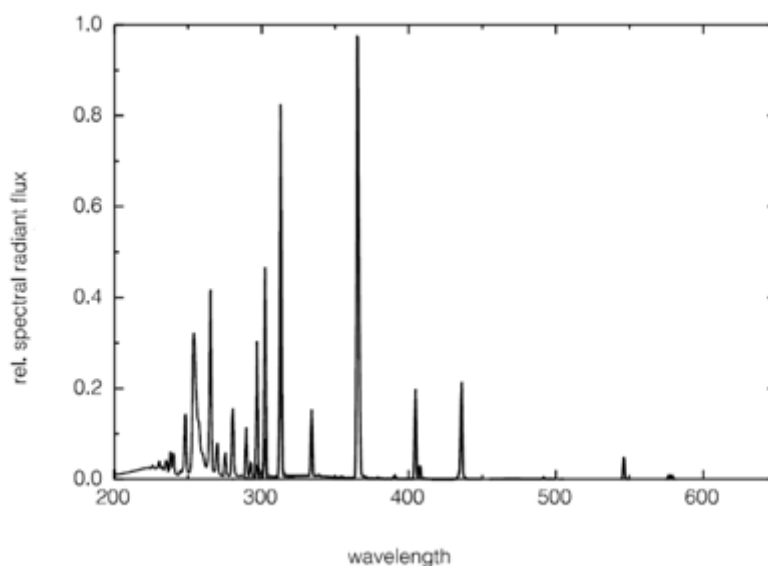


Fig.3.2 Spectral distribution of Heraeus TQ 150 medium pressure Hg lamp (manufacturer data) [198]

To prepare solutions for the degradation experiments, the required amounts of API and TiO_2 were sonicated for 5 min in an aqueous medium. Slightly longer sonication was required for DCF and mixtures of DCF and NPX and TiO_2 in drinking and river water due to their low solubility in these media. The solution with the desired concentration of DCF, NPX or a mixture of DCF and NPX and TiO_2 was stirred at 1000 rpm in the dark for 30 min prior to irradiation to establish an adsorption/desorption equilibrium. The concentration after the adsorption-desorption process was used as C_0 for the degradation kinetics. The same stirring speeds were maintained throughout all experiments. All reactions took place at natural pH except for the pH study. Samples were withdrawn at fixed times and pre-filtered through a 0.22 μm syringe filter before the concentration of the API was determined by HPLC. Direct photolysis experiments were performed using a similar setup, but without the photocatalyst.

In order to optimize the method, four parameters namely initial concentration, TiO_2 P25 loading, pH and water matrix were selected. Details of these studied variables for each APIs are presented in

Table 3.3. For pH adjustment, diluted NaOH or HCl without a buffer solution were used. The pH was measured using a pH-meter prior to the addition of the TiO₂. The pH of each suspension was determined again after TiO₂ addition. Samples were not buffered in order to avoid buffering agent playing a role in the photodegradation process. The effect of H₂O₂ for UV/H₂O₂ and UV/H₂O₂/TiO₂ oxidations was also examined. For this, H₂O₂ was added before the UV irradiation. Photocatalysis with Ti (IV) oxide powder and quartz immersion tube were conducted in addition to compare their effects with the use of TiO₂ P25 and pyrex glass. All photodegradation experiments were performed in triplicate.

Table 3.3 Tested parameters in photodegradation studies of individual APIs and their mixtures in an immersion-well photoreactor with a medium pressure Hg lamp

	API	Parameter	Range or value
Individual API	DCF	Initial concentration	10-70 mg/L
		TiO ₂ loading	0.01-2 g/L
		pH	3-11
		Water matrix	Distilled water, drinking water and river water
		H ₂ O ₂ concentration	250 mg/L
	NPX	Initial concentration	5-60 mg/L
		TiO ₂ loading	0.01-2 g/L
		pH	3-11
		Water matrix	Distilled water, drinking water and river water
		Anions	Chloride and combination of phosphate and chloride
API mixtures	DCF and NPX	Initial concentration	30 mg/L
		Initial concentration ratio	1:1, 1:2 and 2:1
		Water matrix	Distilled water, drinking water and river water
		Anions	Chloride and combination of phosphate and chloride

3.5.2. Demonstration-scale loop reactor

The larger circulating loop reactor (Laboclean[®], Tandem UV, a.c.k. aqua concept GmbH) was fitted with both low pressure (40 W) and medium pressure (500 W) Hg lamps in separate horizontal chambers. The loop reactor has a capacity of 10 L (Fig.3.3). The lamps were housed in quartz mantles, whereas the outer chambers were made of pyrex glass. In this study, only a medium pressure Hg lamp was used to allow comparison with the smaller laboratory-scale immersion-well reactor. The wavelengths of emissions from the medium pressure Hg lamp are as described in section 3.5.1. A 6 L solution was filled into the external reservoir tank and was continuously pumped through the system for 10 min. The liquid streamed tangential through the UV chambers, creating a screw-like flow. This pattern enabled high mass transfer and turbulence to avoid sedimentation of the

photocatalyst. A cooling jacket was placed at the end of the irradiation chambers on top of the reservoir. Measured temperatures of the solution in the reservoir did not exceed 39°C with the circulating reaction medium providing cooling for the lamps. The UV modules were placed behind a large UV-shield and the reactor loop behind a light, well-fitted curtain. Samples were withdrawn prior to commencing irradiations and at selected times throughout the irradiation period. A summary of the studied parameters for each pharmaceutical with this advanced loop reactor is given in Table 3.4.

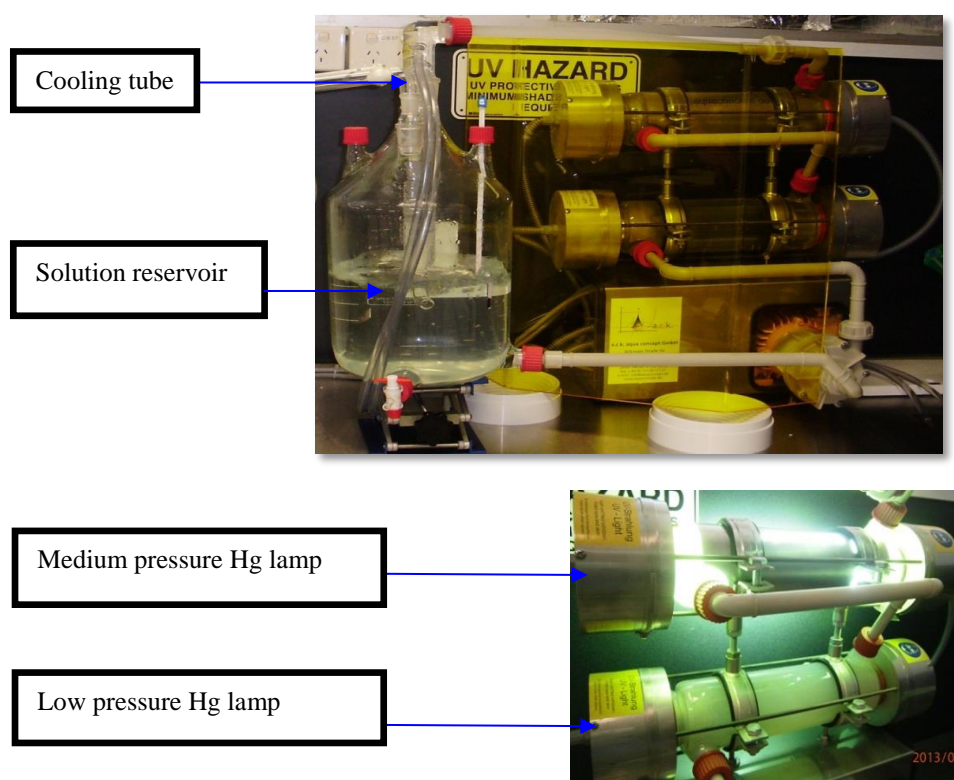


Fig.3.3 Loop reactor (Laboclean®, Tandem UV, a.c.k. aqua concept GmbH)

Table 3.4 Tested parameters in photodegradation studies of individual APIs and their mixtures in a loop reactor (Laboclean®) equipped with a medium pressure Hg lamp

	API	Parameter	Range or value
Individual API	DCF	Initial concentration	30 mg/L
		TiO ₂ loading	0.1 g/L
		Water matrix	Distilled water, drinking water and river water
		H ₂ O ₂ concentration	250 mg/L
	NPX	Initial concentration	30 mg/L
		TiO ₂ loading	0.1 g/L
Water matrix		Distilled water, drinking water and river water	
API mixtures	DCF and NPX	Initial concentration ratio	1:1, 1:2 and 2:1 (C ₀ = 30 mg/L)
		Water matrix	Distilled water, drinking water and river water

3.6. Solar exposures: Immersion-well reactor

For comparative purposes, the immersion-well reactor used in the laboratory was used for solar photochemical degradation studies (Fig.3.4). Solar degradation studies were performed in 2012 on sunny days in July and August and also between October and December. All solar photochemical experiments using an immersion-well reactor were carried out at the James Cook University (latitude 19°19'42" S and longitude 146°45'36" E) campus in Townsville, Australia on different days with different light conditions. Almost all studies were performed from 8 or 9.30 am to 3 or 4 pm.

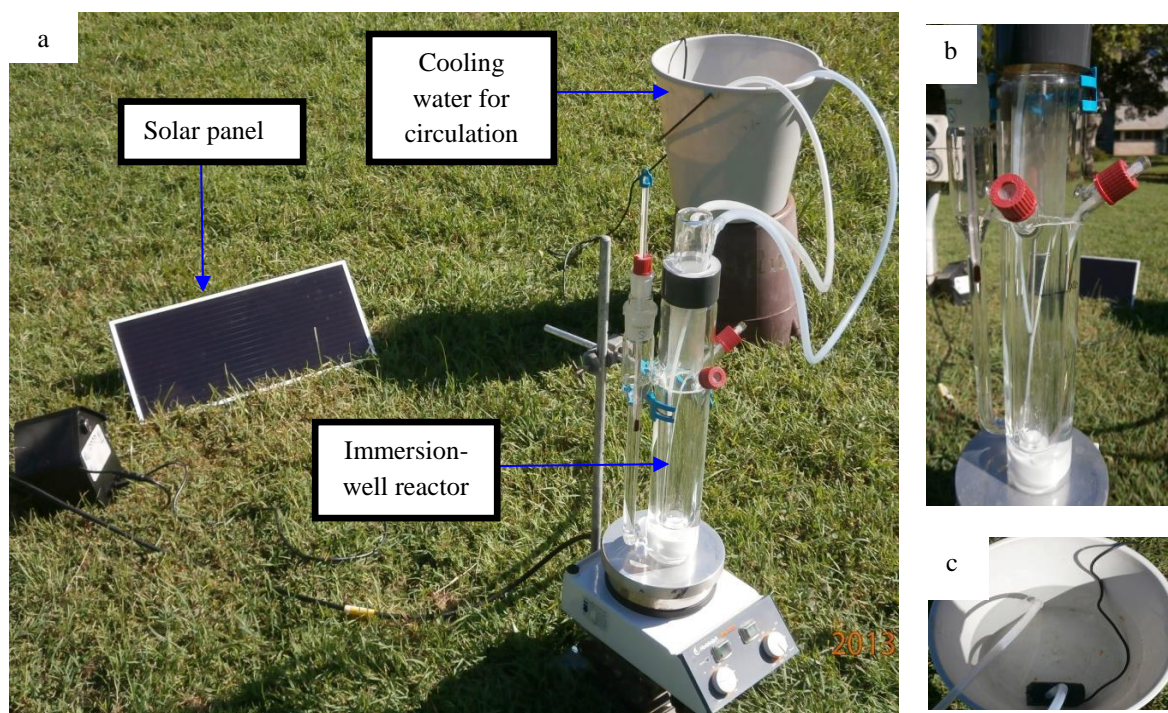


Fig.3.4 (a) Solar degradation experimental setup (b) close-up of photoreactor (c) pump for water circulation

The reaction conditions optimized for the laboratory experiments were applied. All experiments were performed at the natural solution pH. The adsorption-desorption process was allowed to establish in darkness for 15 min before the first sample (t_0) was withdrawn in the laboratory to determine the adsorption. The concentration after the adsorption-desorption process was used for kinetic evaluation. Cooling water was circulated from a reservoir using a pump driven by a solar panel. Samples were withdrawn at regular intervals during the 6 or 7 h of solar exposure. The intensity of solar radiation was recorded using a digital Luxmeter for all solar photodegradation studies. The readings of the recorded solar intensity fluctuated with days and times of the experiments conducted. As the position or elevation where the readings were taken also contributed to the fluctuations, readings were taken from the same position, at the top of the reactor to minimize error. These values

were used as a guideline for discussion of the solar experiments and should be not over interpreted due to the solar radiation fluctuations.

Table 3.5, Table 3.6 and Table 3.7 summarize the parameters recorded during the solar photochemical degradation studies for individual DCF, NPX and their mixtures, respectively. All solar experiments were performed in duplicate.

3.7. Analytical methods

3.7.1. High performance liquid chromatography (HPLC)

The degradation of all APIs was monitored using a Varian 940-LC HPLC equipped with a photo diode array (PDA) detector (Fig.3.5) using a Galaxie™ Chromatography data system software (Version 1.9.302.530) (Varian Inc., Australia).

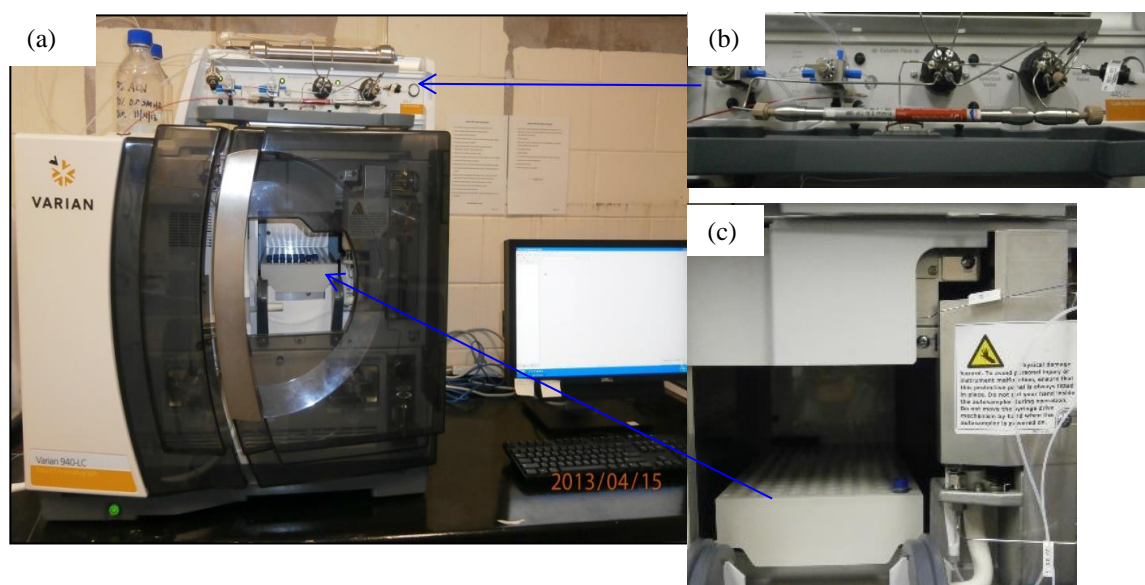


Fig.3.5 (a) HPLC (b) close-up of column unit and (c) close-up of autosampler

The stationary phase was a C-18 Phenomenex column (150×4.6 mm, $2.6 \mu\text{m}$). Separation was accomplished using a flow rate of 0.5 mL/min. Millipore membrane type FH filters with a pore diameter of $0.45 \mu\text{m}$ (Millipore, Ireland) were used to filter the mobile phase. All samples for HPLC analysis were again filtered through $0.22 \mu\text{m}$ (Microscience) syringe filters prior to analysis.

Table 3.5 Selected solar degradation studies of DCF ($C_0 = 30$ mg/L)

Parameter	Exp 1 (8/10/12)	Exp 2 (9/10/12)	Exp 3 (10/10/12)	Exp 4 (15/10/12)	Exp 5 (17/10/12)	Exp 6 (18/10/12)	Exp 7 (19/10/12)	Exp 8 (12/11/12)	Exp 9 (13/11/12)
Treatment	DCF + TiO ₂	DCF only	DCF only	DCF + TiO ₂	DCF + TiO ₂	DCF only	DCF + TiO ₂	DCF + TiO ₂ /H ₂ O ₂	DCF + H ₂ O ₂
Water matrix tested ^a	DW	DW	TW	TW	TW	RW	RW	TW	TW
Concentration of H ₂ O ₂ (mg/L)	Not applicable	Not applicable	Not applicable	Not applicable	Not applicable	Not applicable	Not applicable	250	250
TiO ₂ P25 concentration (g/L)	0.1	Not applicable	Not applicable	0.1	0.1	Not applicable	0.1	0.1	Not applicable
Time of experiment	0915-1515	0930-1530	0920-1520	0900-1500	0925-1525	0930-1530	0945-1545	0915-1515	0920-1520
Solar exposure duration (min)	360	360	360	360	360	360	360	360	360
Temperature (°C) (in the reactor) (min-max)	26-29	26-29	25-28	26-29	25-28	24-28	25-30	26-29	26-29
Lux reading (Lux) (min-max)	280 × 100 - 613 × 100	332 × 100 - 778 × 100	229 × 100 - 953 × 100	261 × 100 - 535 × 100	202 × 100 - 643 × 100	305 × 100 - 659 × 100	207 × 100 - 662 × 100	226 × 100 - 607 × 100	285 × 100 - 589 × 100
UV index ^b	11	11	10	11	11	11	12	11	11

^a Water matrix tested: DW: Distilled water; TW: Drinking water; RW: River water

^b Data from ARPANSA [199]

Table 3.6 Selected solar degradation studies of NPX ($C_0 = 30$ mg/L)

Parameter	Exp 1 (26/7/12)	Exp 2 (3/7/12)	Exp 3 (5/7/12)	Exp 4 (6/7/12)	Exp 5 (18/7/12)	Exp 6 (20/7/12)	Exp 7 (30/11/12)	Exp 8 (25/11/12)	Exp 9 (23/11/12)
Treatment	NPX only	NPX + TiO ₂	NPX only	NPX + TiO ₂	NPX only	NPX + TiO ₂	NPX + TiO ₂ + chloride	NPX + chloride	NPX + TiO ₂ + chloride + phosphate ⁻
Water matrix tested ^a	DW	DW	TW	TW	RW	RW	TW	RW	RW
Concentration of anion (mg/L)	Not applicable	Not applicable	Not applicable	Not applicable	Not applicable	Not applicable	Chloride = 20	Chloride = 20	Phosphate = 20 Chloride = 20
TiO ₂ P25 concentration (g/L)	Not applicable	0.1	Not applicable	0.1	Not applicable	0.1	0.1	Not applicable	0.1
Time of experiment	0850-1450	0935-1535	0930-1530	0920-1520	0925-1625	0905-1605	0900-1500	0920-1520	0800-1500
Solar exposure duration (min)	360	360	360	360	420	420	360	360	420
Temperature (°C) (in the reactor) (min-max)	23-25	22-25	21-25	23-29	24-26	22-26.5	26-30	26-30	28-31
Lux reading (Lux) (min-max)	318 × 100 - 952 × 100	251 × 100 - 685 × 100	184 × 100 - 890 × 100	389 × 10 - 955 × 100	175 × 10 - 653 × 100	362 × 10 - 998 × 100	294 × 100 - 789 × 100	213 × 100 - 736 × 100	198 × 100 - 947 × 100
UV index ^b	7	6	6	6	7	7	No UV index reported	11	10

^a Water matrix tested: DW: Distilled water; TW: Drinking water; RW: River water

^b Data from ARPANSA [199]

Table 3.7 Selected solar degradation studies of DCF and NPX mixtures (DCF:NPX 1:1) ($C_0 = 30$ mg/L)

Parameter	Exp 1 (25/7/12)	Exp 2 (30/7/12)	Exp 3 (30/8/12)	Exp 4 (31/8/12)	Exp 5 (13/8/12)	Exp 6 (28/8/12)	Exp 7 (16/12/12)	Exp 8 (17/12/12)
Treatment	DCF + NPX only	DCF + NPX + TiO ₂	DCF + NPX only	DCF + NPX + TiO ₂	DCF + NPX only	DCF + NPX + TiO ₂	DCF + NPX + TiO ₂ + chloride + phosphate	DCF + NPX + TiO ₂ + chloride
Water matrix tested ^a	DW	DW	TW	TW	RW	RW	TW	TW
Concentration of anion (mg/L)	Not applicable	Not applicable	Not applicable	Not applicable	Not applicable	Not applicable	Phosphate = 20 Chloride = 20	Chloride = 20
TiO ₂ P25 concentration (g/L)	Not applicable	0.1	Not applicable	0.1	Not applicable	0.1	0.1	0.1
Time of experiment	0915-1515	0945-1545	0925-1525	0925-1525	0950-1550	0900-1500	1000-1600	0930-1530
Solar exposure duration (min)	360	360	360	360	360	360	360	360
Temperature (°C) (in the reactor) (min-max)	23-30	24-30	22-27	24-30	22-26	25-29	28-31	28-32
Lux reading (Lux) (min-max)	619 × 100 - 923 × 100	643 × 100 - 996 × 100	1709 × 10 - 935 × 100	188 × 100 - 921 × 100	287 × 100 - 906 × 100	293 × 100 - 985 × 100	191 × 100 - 626 × 100	287 × 100 - 733 × 100
UV index ^b	7	7	9	8	8	8	9	10

^a Water matrix tested: DW: Distilled water; TW: Drinking water; RW: River water

^b Data from ARPANSA [199]

For determination of DCF, a mobile phase 80% MeOH and 20% water (v/v) (pH 3 adjusted with glacial acetic acid) at 274 nm and an injection volume of 20 μL was employed. NPX separation was performed with a mobile phase consisting of 70% (v/v) MeOH and 30% water (1% acetic acid) and a detector wavelength of 230 nm. The HPLC method for the simultaneous determination of DCF and NPX mixture determination used a mobile phase mixture of 70% (v/v) MeOH and 30% (v/v) 10 mM potassium dihydrogen phosphate (KH_2PO_4) (pH 3) buffer. The injection volume was 20 μL . Detection wavelengths of 274 nm and 230 nm were chosen for DCF and NPX respectively, both corresponding to their maximum absorbance.

All standard stock solutions were prepared using Milli-Q water and stored at $5 \pm 3^\circ\text{C}$. Working standard solutions were prepared as needed to construct the calibration curves.

3.7.2. Mass spectrometry

Liquid chromatography mass spectrometry (LC-MS) and fourier transform-ion cyclotron resonance-mass spectrometry (FT-ICR-MS) analyses (Fig.3.6) were performed to identify the degradation products formed during TiO_2 photocatalysis of individual APIs and their mixtures.

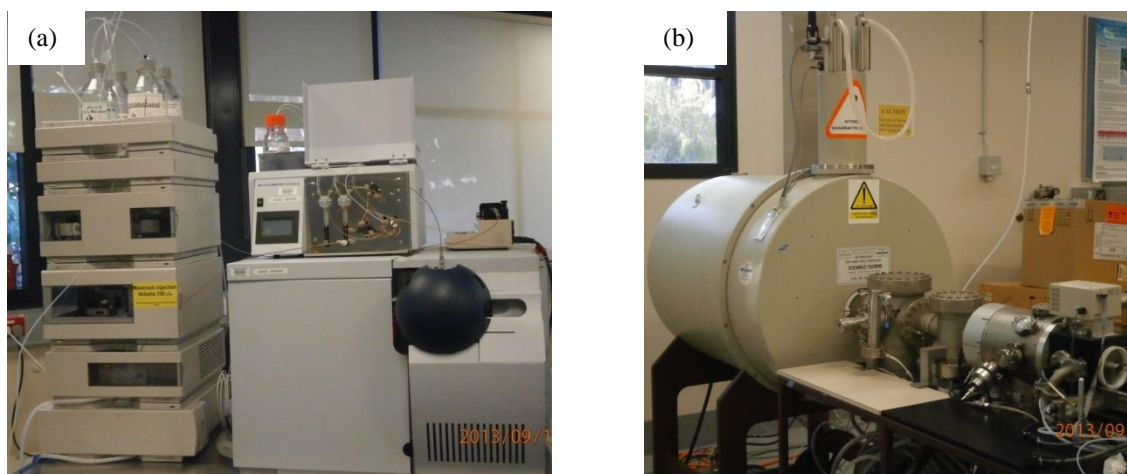


Fig.3.6 (a) LC-MS and (b) FT-ICR-MS

Separation and identification of photoproducts was achieved using an Agilent 1100 HPLC system comprising a degasser, auto injector, binary pump and PDA detector connected to a Bruker Esquire3000 ion trap mass spectrometer with an Apollo electrospray ionization source (ESI) ion source operating in either positive or negative mode. All LC-MS data were collected using Bruker Daltonics Esquire Control v5.3 and Hystar v3.1 operating on Windows XP Professional. The API standard (10 μL) and UV/ TiO_2 irradiated sample (100 μL) were injected onto a C18 Phenomenex

column (150 × 4.6 mm, 2.6 μm) using the same conditions as described in section 3.7.1, monitoring at a wavelength of 220 nm. MS analysis was performed using the following conditions: nebulizer gas 20 psi, drying gas 6.0 L/min and drying temperature 350°C. The presence of the parent and products was determined by monitoring the base peak chromatogram (BPC). High resolution MS data were acquired on a Bruker BioApex 47 FT-ICR-MS with an ESI Analytica of Branford source. Both the API standard and irradiated samples were analysed in either (+/-)-ESI within a mass range of m/z 50-2000 via direct infusion of the diluted LC-MS sample (1:100 methanol) at a flow rate of 1.7 μL/min.

All MS analyses were conducted at the Australian Institute of Marine Sciences (AIMS) in Townsville.

3.7.3. UV-Vis spectroscopy

A UV-Vis spectrophotometer (Model Varian 50 Bio) with Cary® WIN UV Scan software was used to measure the absorbance of aqueous solution and to determine the molar absorption coefficient for each API. A quartz cell with a path length of 1 cm was used. Maximum absorbance was used as the wavelength of detection for monitoring during the degradation studies.

3.7.4. pH

pH was measured using a UB-10 model pH-meter (Denver Instrument). The pH meter was calibrated with buffer solutions of pH 4, 7 and 10.

3.7.5. Dissolved oxygen

A dissolved oxygen meter (YSI Model EcoSense® DO 200) was used to measure the dissolved oxygen (DO) in the samples. Calibration of the instrument was carried out following the water-saturated air calibration method.

3.7.6. Light intensity

The intensity of sunlight was recorded using an auto digital Luxmeter (Model 1010A).

3.7.7. Chloride ion

The concentration of chloride ion was measured using ion chromatography (ICS 2100 Dionex). An anion column (AS 19; 4 × 250 mm) and conductivity detector with suppression was used. The analyses were performed at the Townsville water laboratory.

3.7.8. Determination of mineralization

Two indicators were selected to determine the degree of mineralization by either direct photolysis or TiO₂ photocatalysis, namely dissolved organic carbon (DOC) and chemical oxygen demand (COD). Analyses of DOC were conducted at AIMS (Townsville). The detailed procedures for the determination of DOC and COD are as follows:

3.7.8.1 Dissolved organic carbon

The purpose of measuring DOC is to determine the amount of carbon converted to CO₂ during photochemical treatment. DOC only indicates the fraction of organic carbon present in solution after filtration through a filter with pore diameter of 0.45 μm [88]. To determine DOC, a TOC analyzer (Model Shimadzu 5000 A) equipped with an ASI-5000A autosampler was used. DOC content based on direct injection of filtered samples was established. Potassium hydrogen phthalate was used as a standard for constructing a calibration curve. Non-dispersive infrared detection of CO₂ produced from high temperature combustion (680°C) was performed for each sample and each standard analysis. Sample taken from the loop reactor (20 mL) were withdrawn with a Terumo syringe and connected to a filter holder with 0.45 μm GF/F glass fibre filters. The sample was filtered into a polypropylene screw cap sample tube. Filtered samples were preserved with 200 μL concentrated HCl. For the analysis of DOC samples from the immersion-well reactor, only 5 mL samples were used. In that case, filtered samples were preserved with 50 μL concentrated HCl. Prior to usage, all screw cap sample tubes and Terumo syringes were acid cleaned by soaking in 10% HCl.

3.7.8.2 Chemical oxygen demand

Chemical oxygen demand (COD) measures the oxygen equivalent (mg O₂/L) of the organic (and inorganic) matter present in a water sample, which oxidized using a strong oxidizing agent, potassium dichromate (K₂Cr₂O₇) under acidic conditions in the presence of H₂SO₄, at high temperature [88]. Therefore, COD estimates the amount of organic matter in a water sample based on chemical oxidation. COD was determined using the closed reflux titrimetric method (Standard

Methods for the Examination of Water and Wastewater Method 5220D) [200]. 5 mL of sample were refluxed for 2 h in the presence of 0.250 N $K_2Cr_2O_7$, 0.1 g Ag_2SO_4 , 0.1 g $HgSO_4$, and 20 mL of concentrated H_2SO_4 . The solution was titrated against standardized 0.250 N ferrous ammonium sulphate ($FeSO_4 \cdot (NH_4)_2SO_4$) and ferroin indicator for a colour change from blue-green to a reddish-brown. The reflux procedure was also repeated for blanks. The amount of COD in the sample was calculated using Eq. 3.2:

$$COD = \frac{8000 \times (A - B) \times C}{\text{volume of sample (mL)}} \quad (3.2)$$

where, A = mL of titrant used for sample, B = mL of titrant used for blank and C is the normality of $FeSO_4 \cdot (NH_4)_2SO_4$.

3.8. Kinetic analysis

All experimental data were tested using zero order ($C_t = kt + C_0$), pseudo-first-order ($C_t = C_0 e^{-kt}$) and second-order ($C_t/C_0 (1-C_0) = kt$) kinetic models:

where C_0 is the initial concentration of APIs and C_t is the concentration of API at time t and k is the rate constant.

Chapter 4. Photochemical degradation of diclofenac, naproxen and their mixtures by UV light

4.1. Introduction

This chapter focuses on the photochemical degradation due to exposure of the APIs to artificial UV light emitted from a medium pressure Hg lamp in two circulating laboratory photoreactors (i.e. a small-scale immersion-well and a larger loop reactor). Parameters affecting their degradation and degrees of mineralization such as DOC removal from direct photolysis and TiO₂ photocatalysis were specifically addressed. A powerful analytical technique is important for the detection and quantification of pharmaceuticals, due to their polar nature and chemical stability. For this reason, reverse phase HPLC which is selective and commonly applied to the quantitative determination of pharmaceuticals during degradation studies, was selected. The optimum HPLC analytical conditions and the validation of the proposed method for the quantification and identification of the individual APIs, DCF and NPX, and their simultaneous detection are presented.

4.2. HPLC method

Validation parameters include linearity, accuracy and precision, limit of detection (LOD) and limit of quantification (LOQ). For linearity, a calibration curve was constructed with selected range of concentrations of the API by plotting mean peak areas against known concentrations. The results obtained were fitted using regression statistics in Microsoft Excel 2007. The LOD and LOQ were determined based on the standard deviation of response and slope of the linear curve. The LOD is defined as the smallest quantity of an analyte that can be detected, but not necessarily quantified, whereas LOQ is the lowest amount of analyte in a sample which can be quantitatively determined with appropriate precision and accuracy [201]. The LOD and LOQ were determined to be $3.3d/s$ and $10d/s$, where d is the standard deviation of the y-intercept of the regression line and s is the slope of the regression line [201]. Percentage of relative standard deviation (% RSD) was determined using seven measurements of 100% concentration of standard to express repeatability (precision). Accuracy was assessed by measuring recovery at three concentrations of the calibration curve.

4.2.1. HPLC method for individual compound analysis

The HPLC methods for the individual quantification of DCF and NPX in this study was adapted from the methods reported by Moore *et al.* [162] and Hsu *et al.* [202], respectively. The method was

modified to improve the separation efficiency of the degradation products from the parent compounds. The developed HPLC protocols for DCF and NPX both used isocratic elution. From Table 2.5 and Table 2.6 (Chapter 2) which summarizes the photochemical degradation studies for DCF and NPX, respectively, isocratic elution seems to be preferable in most of the HPLC methods because of its simplicity.

The wavelength chosen for DCF detection in the literature varies between 270-280 nm (Table 2.5), which falls within the range of maximum absorbance of DCF. The wavelength for NPX detection based on Table 2.6 varies from 219-254 nm. For the purpose of this study, the detection wavelength was 274 nm (λ_{max}) for DCF and 230 nm (λ_{max}) for NPX.

The mobile phase composition or solvent strength as well as pH control, when a weakly ionizable compound is involved are important factors in method development [203]. MeOH was chosen over ACN as it is less expensive, strongly polar and protic hence having greater selectivity, and is commonly used in combination with water in reverse phase chromatography. Acetic acid was used to adjust the pH to minimize or correct ion suppression of both DCF and NPX.

In the initial stage, a Pursuit XR_s (250 × 4.6 mm, 5 μm) column was used. Method development for DCF detection commenced with a mobile phase of 80/20 (v/v) MeOH and 1% CH₃COOH composition with a flow rate of 0.8 mL/min. The retention time (t_R) for DCF was 13.5 min accompanied by broad tailing. The composition was modified to 80/20 (v/v) MeOH and water acidified to pH 4 with CH₃COOH. The DCF then eluted at $t_R = 9.82$ min. However, the peak remained broad (Fig.4.1). In order to reduce the tailing, the pH was reduced to 3, which resulted in much improved peak shape.

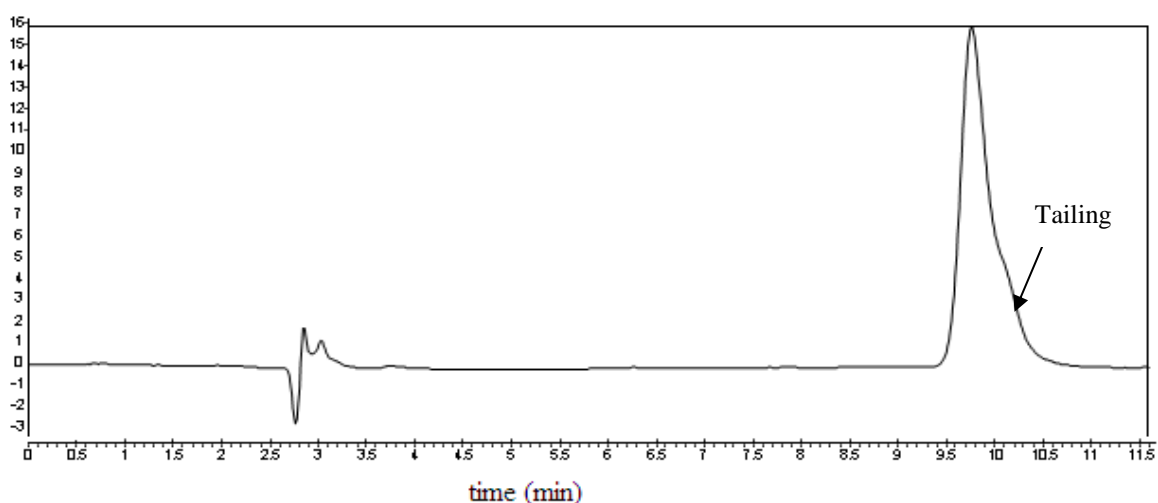


Fig.4.1 DCF chromatogram with 80/20 MeOH/water (pH 4) (20 μL; $\lambda = 274$ nm; 0.8 mL/min, column: C18 Pursuit XR_s (250 × 4.6 mm, 5 μm)

As for DCF, a Pursuit XRs (250×4.6 mm, $5 \mu\text{m}$) column was also used for NPX in the initial stage of the method development. NPX elution was first performed with a mobile phase composition of 60/40 (v/v) MeOH/1% CH_3COOH in water with a flow rate and injection volume of 0.8 mL/min and 20 μL , respectively. These conditions resulted in a broad NPX peak and a t_R of approximately 14 min (Fig.4.2). By increasing the MeOH composition to 80%, NPX t_R was reduced to 7.5 min. However, the peak was broad with tailing. The solvent composition was modified to 70/30 (v/v) MeOH and 1% CH_3COOH (pH~3.01) and a shorter length C18 Phenomenex column (150×4.6 mm) was used.

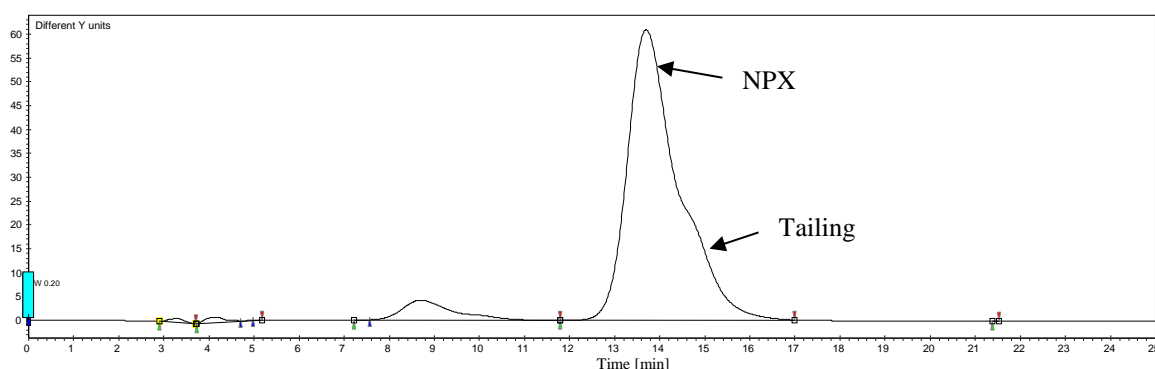


Fig.4.2 NPX (10 mg/L) chromatogram with 60/40 MeOH/1% CH_3COOH (20 μL ; $\lambda = 230$ nm; 0.8 mL/min, column: C18 Pursuit XRs (250×4.6 mm, $5 \mu\text{m}$))

The flow rate for both APIs was maintained at 0.5 mL/min as this was the recommended flow rate for the C18 Phenomenex column, with a higher flow rate, resulting in a high back pressure. A guard column with identical packing (C18, 4.6 mm) and an external standard were used. Table 4.1 lists the conditions used for HPLC detection of individual DCF and NPX in this study.

Table 4.1 HPLC conditions employed for DCF and NPX detection in this study

	DCF	NPX
Mobile phase	80% MeOH and 20% water (pH 3 adjusted with CH_3COOH) (mixture pH~2.9)	70% MeOH and 30% water (1% CH_3COOH) (mixture pH 3.8 ± 0.01)
Detection, λ (nm)	274	230
Sample volume (μL)	20	10
Column	C18 Phenomenex (150×4.6 mm, $2.6 \mu\text{m}$)	
Flow rate	0.5 mL/min @ room temperature ($25^\circ\text{C} \pm 1$)	

The linearity study using seven levels from 10-200% showed an excellent correlation coefficient ($R^2 > 0.9991$) for the range of concentrations investigated for both DCF and NPX (Fig.4.2) (Table 4.2).

Table 4.2 Validated parameters of HPLC methods used for DCF and NPX

Regression Statistics	DCF	NPX
Linear equation	$Y = 38.429x$	$Y = 103.65x$
Linear range (mg/L)	3-60	3-60
R^2	0.9997	0.9991
Standard error	287.7368	0.000688
Observations	7	7
Other parameters		
LOD (mg/L)	1.14	2.06
LOQ (mg/L)	3.78	6.88
% RSD	0.32	0.63
t_R (min) (range)	7.15-7.22	6.29-6.40

The LOD and LOQ for DCF were determined to be 1.14 mg/L and 3.78 mg/L, respectively. For NPX, the values were 2.06 mg/L for LOD and 6.88 mg/L for LOQ, respectively. Percentage RSD for seven determinations at 100% (30 mg/L) concentration was <1% (Table 4.2). The t_R for DCF and NPX was found to be between 7.15-7.22 min and 6.29-6.40 min, respectively.

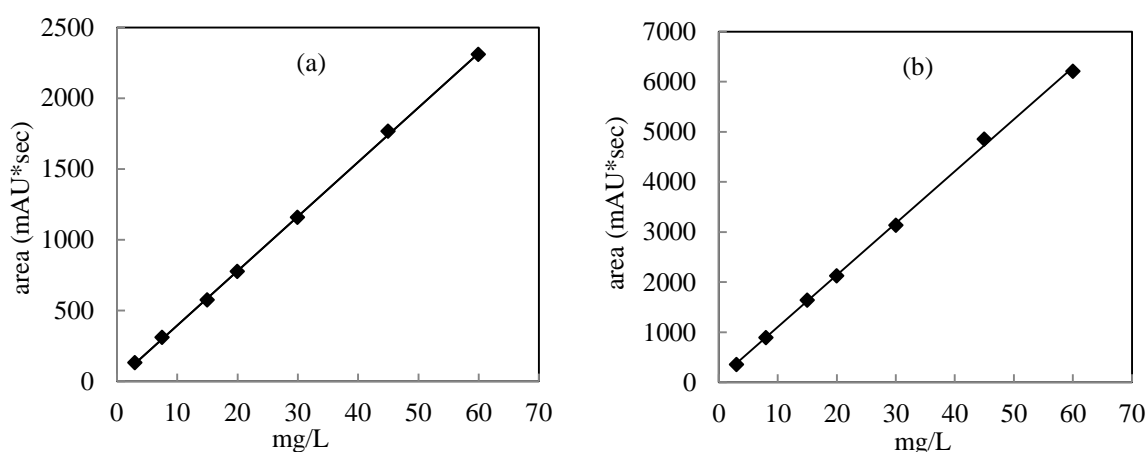


Fig.4.3 Calibration curves for (a) DCF and (b) NPX

The accuracy of the DCF and NPX detection method was evaluated by using the spiked recovery method. Three concentration levels ($n=3$) from the calibration data were chosen. The result of analysis showed excellent recoveries for both DCF and NPX ranging between 94.3%-102.0% and

95.7%-101.0% (Table 4.3). The recovery data, based on the spiked recovery method, suggested good accuracy for the proposed method for each API.

Table 4.3 Results of recovery (\pm standard deviation, SD) for DCF and NPX

Spiked concentration (mg/L)	DCF			NPX		
	Concentration measured (mg/L)	Recovery (%)* (mean \pm SD)	RSD (%)	Concentration measured (mg/L)	Recovery (%)* (mean \pm SD)	RSD (%)
10	9.427	94.27 \pm 0.52	0.58	9.568	95.68 \pm 0.95	1.01
30	28.956	96.52 \pm 0.68	0.63	28.849	96.16 \pm 1.10	0.82
60	61.224	102.04 \pm 1.12	0.032	60.577	101.0 \pm 0.23	0.51

* Average of three determinations

4.2.2. HPLC method for diclofenac and naproxen mixture analysis

A C18 Phenomenex column (150 \times 4.6 mm, 2.6 μ m) was also used for API mixture analyses with a number of mobile phase compositions evaluated for separation of NPX and DCF. Resolution of peaks and sensitivity were the main factors that defined the wavelength selection. Wavelengths of 230 nm and 274 nm, which are the λ_{max} for NPX and DCF, respectively were chosen due to higher sensitivity (response to a given concentration) for both analytes. A combination of 80/20 (v/v) MeOH/0.01 M KH_2PO_4 at pH 3.1 was initially used and the flow rate and injection volume were set to 0.5 mL/min and 20 μ L, respectively. Fig.4.4 shows the chromatogram of NPX and DCF peak at detection wavelength of 230 nm.

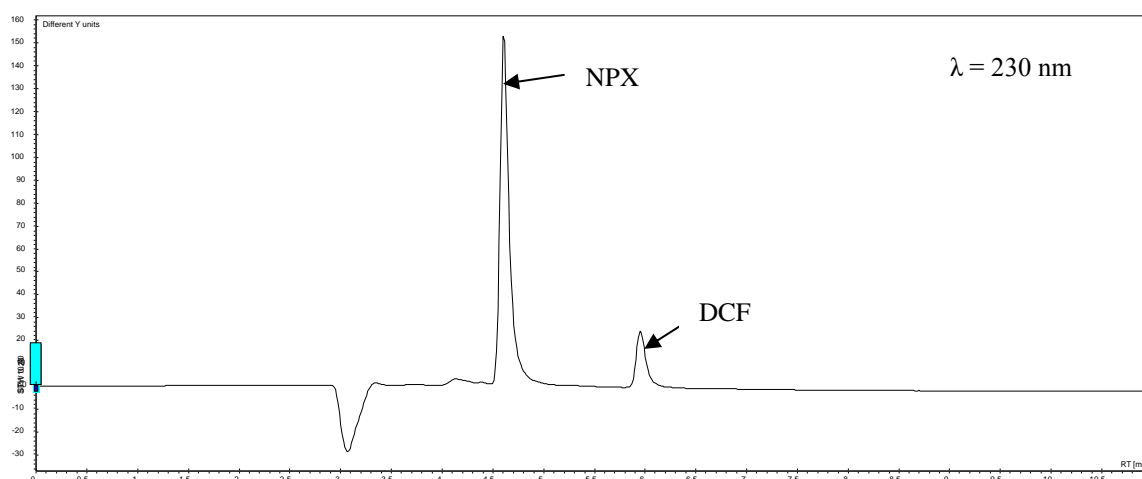


Fig.4.4 HPLC chromatogram of DCF and NPX mixture standard with 80/20 MeOH/0.01 M KH_2PO_4 at pH 3.1 (20 μ L; $\lambda = 230$ nm; column: C18 Phenomenex 150 \times 4.6 mm, 2.6 μ m)

The NPX and DCF peaks eluted at t_R 4.96 min and 5.95 min (Fig.4.4), respectively not allowing sufficient time for the separation of the degradation products. Reduction of the mobile phase solvent strength to 70/30 (v/v) MeOH/0.01 M KH_2PO_4 at pH 3, while maintaining the same flow rate resulted in NPX and DCF being eluted at t_R ~6.6 min and 11.6 min, respectively (Fig.4.5).

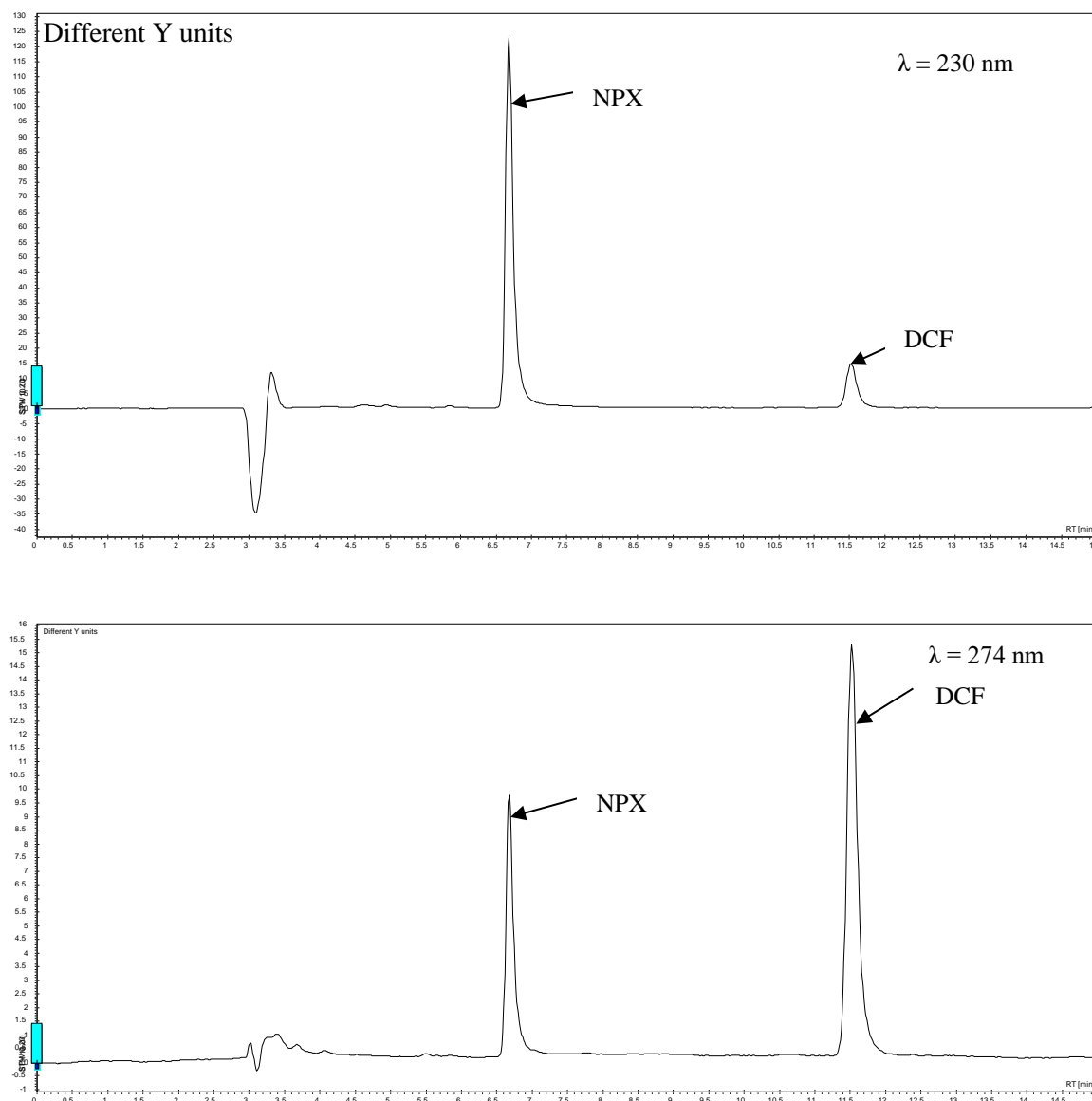


Fig.4.5 HPLC chromatogram of DCF and NPX mixtures with 70/30 MeOH/0.01 M KH_2PO_4 at pH 3 ($\lambda_{\text{DCF}} = 274 \text{ nm}$ and $\lambda_{\text{NPX}} = 230 \text{ nm}$; 20 μL ; column: C18 Phenomenex 150 \times 4.6 mm, 2.6 μm)

The calibration curve was constructed with standard concentrations ranging between 10-60 mg/L (10-200% concentration). Table 4.4 shows the linearity for the proposed analytical method obtained

from this calibration curve. The calculated correlation coefficient, $R^2 > 0.9982$, confirmed the linearity of the analytical response of both APIs (Fig.4.6).

Table 4.4 Results of the linear study for DCF and NPX mixtures

Compound	t_R (min)	Linear equation	R^2	LOD (mg/L)	LOQ (mg/L)
DCF ($\lambda = 274$ nm)	11.6	$Y = 18.441x$	0.99	1.42	4.73
NPX ($\lambda = 230$ nm)	6.6	$Y = 114.94x$	0.99	1.27	4.25

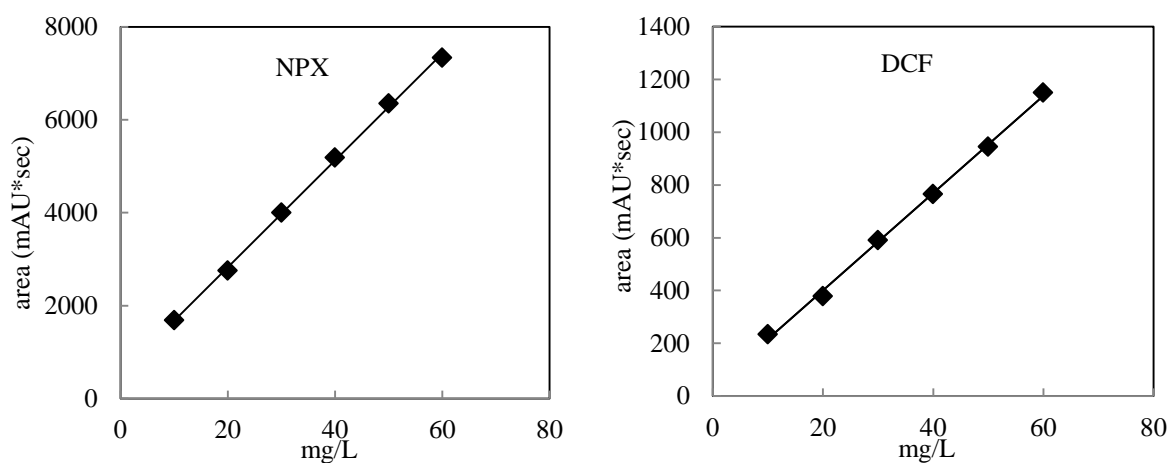


Fig.4.6 Calibration curves of NPX ($\lambda = 230$ nm) and DCF ($\lambda = 274$ nm) in a 1:1 mixture (NPX:DCF)

4.3. Photophysical properties

The molar absorption coefficient (ϵ) is an important physical property of a compound especially in photochemical reactions, as it indicates the ability of a compound to absorb photons of the incident light [102]. The molar absorption coefficient was determined by dividing the measured absorption coefficient (cm^{-1}) at a given wavelength by the molar concentration (M). Absorbance (a) of each API was determined with 1 cm path length (l) quartz cuvette (Eq. 4.1):

$$a = \epsilon \times [\text{API}] \times l \quad (4.1)$$

4.3.1. Diclofenac

Fig.4.7 shows the molar absorption coefficient of DCF at different wavelengths and the main emission lines between 250 and 450 nm of the TQ-150 medium pressure Hg lamp employed in the direct photolysis and photocatalysis studies.

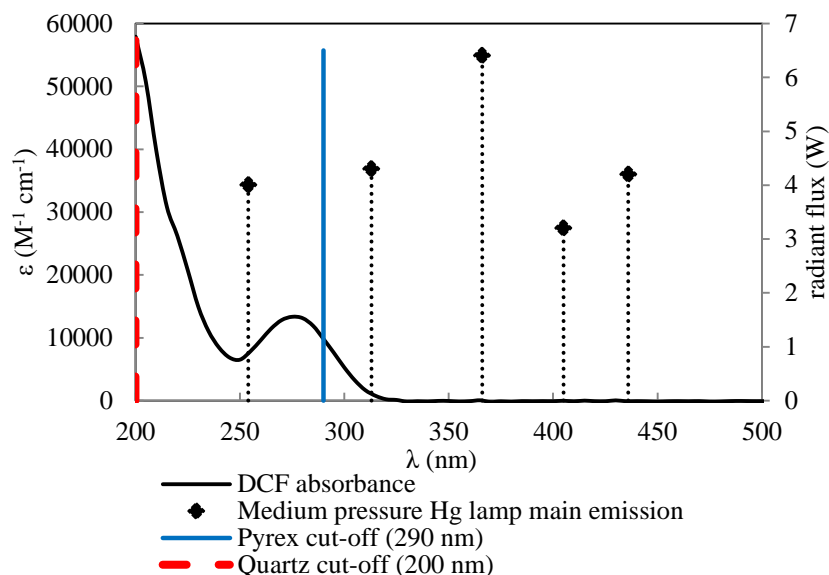


Fig.4.7 Molar absorption coefficients of DCF in water and medium pressure Hg lamp main emission lines (manufacturer data)

DCF exhibits main absorption band at $\lambda_{max} = 274$ nm ($\epsilon_{274nm} = 13340$ $M^{-1}cm^{-1}$). The high molar absorption coefficient suggests high photolability of DCF. DCF shows a shoulder absorbance up to 320 nm (Table 4.5).

Table 4.5 Molar absorption coefficient values of DCF in water at different wavelengths

λ (nm)	ϵ ($M^{-1} cm^{-1}$)	λ (nm)	ϵ ($M^{-1} cm^{-1}$)
245	6864.0	285	11902.1
250	6513.8	290	9854.4
255	7844.3	295	7628.4
260	9652.0	300	5290.4
265	11461.6	305	3249.8
270	12812.7	310	1680.9
275	13340.1	315	758.9
280	13120.2	320	214.0

DCF is therefore susceptible to direct sunlight photolysis, due to the capability to absorb solar radiation $\lambda > 290$ nm. As the immersion-well set-up was fitted with a pyrex glass cooling tube, light

emitted below 290 nm by the medium pressure Hg lamp would be filtered by the glass. Consequently, only the emission at 313 nm would be effective in inducing photolysis. Absorption spectra of DCF at different pHs are shown in Fig.4.8. DCF has a pK_a of 4.15 [54]. At $pH < pK_a$, DCF exists mainly in its molecular form while at $pH > pK_a$, DCF exists as anion.

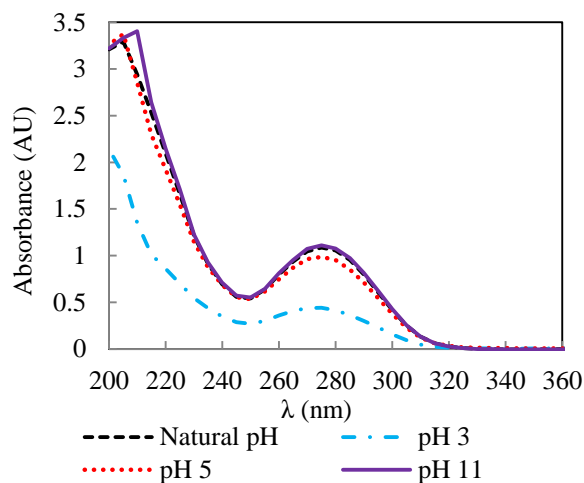


Fig.4.8 Absorption spectra of DCF in water at different pHs

4.3.2. Naproxen

NPX exhibits absorption at 230 nm and at 270 nm (Fig.4.9). The molar absorption coefficient of NPX at $\lambda_{max} = 230$ nm is $96\,693.07\text{ M}^{-1}\text{ cm}^{-1}$ and at $\lambda_{max} = 270$ nm is $6382.44\text{ M}^{-1}\text{ cm}^{-1}$.

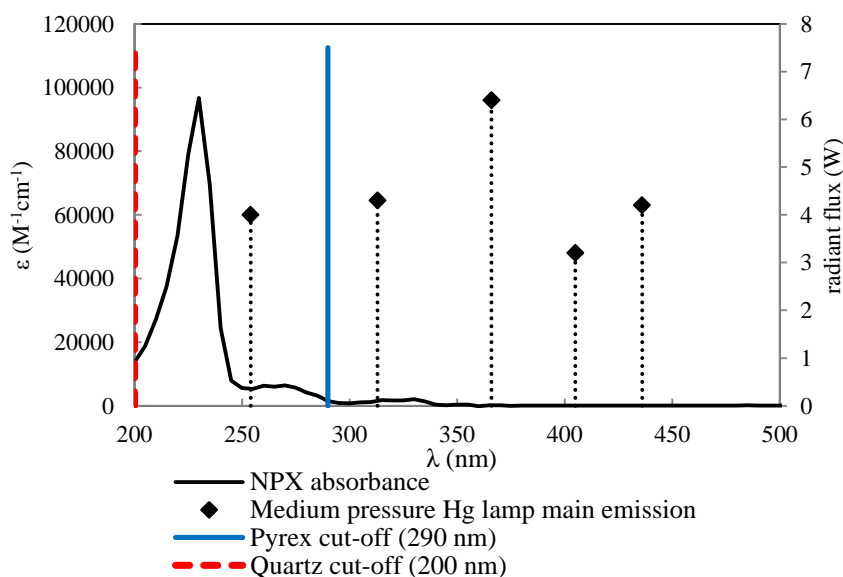


Fig.4.9 Molar absorption coefficients of NPX in water and medium pressure Hg lamp main emission lines (manufacturer data)

The strong absorption was assigned to the $\pi-\pi^*$ transition, due to the transitions involving the conjugated double bonds and that with the lower energy was assigned to the $n-\pi^*$ of the C=O group. NPX can thus undergo direct photolysis, due to its absorption up to 340 nm (Fig.4.9). The emission lines of the medium pressure Hg lamp relevant to the photodegradation of NPX include 238 to 334 nm. However, filters made of either pyrex or quartz determine the range of UV involved in the photochemical oxidation. Molar absorption coefficients at different wavelength are shown in Table 4.6.

Table 4.6 Molar absorption coefficient values of NPX in water at different wavelengths

λ (nm)	ϵ ($M^{-1} cm^{-1}$)	λ (nm)	ϵ ($M^{-1} cm^{-1}$)
245	7948.9	285	3215.4
250	5555.8	290	1490.2
255	5304.6	295	838.5
260	6313.4	300	826.2
265	6055.3	305	1037.0
270	6382.4	310	1182.3
275	5697.8	315	1753.7
280	4223.7	320	1633.7

Fig.4.10 shows the absorption spectra of NPX at different pHs. NPX has a pK_a of 4.15 [126]. Thus, when $pH > pK_a$, NPX exists in its ionic form, whereas at $pH < pK_a$, NPX is found in its unionised molecular form.

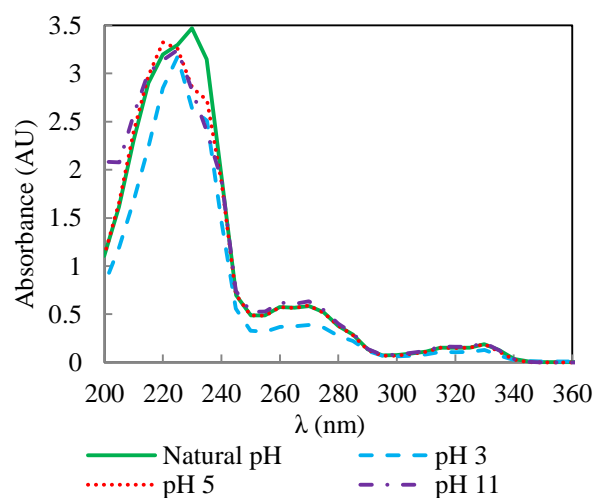


Fig.4.10 Absorption spectra of NPX in water at different pHs

4.3.3. Diclofenac and naproxen mixtures

The absorption spectrum of the 1:1 mixture of DCF and NPX shows the characteristic adsorption bands of NPX and DCF at 230 nm and 274 nm, respectively, with some tailing at 340 nm (Fig.4.11).

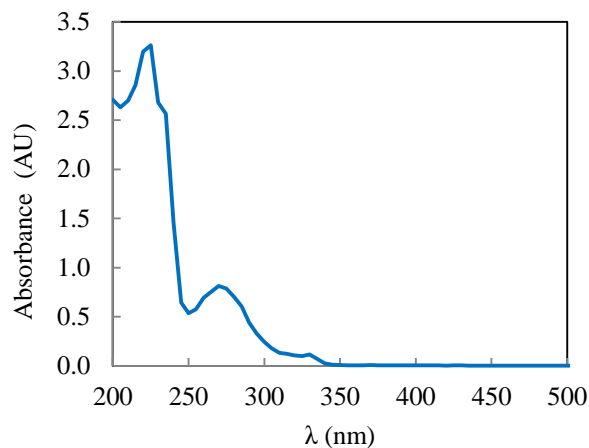


Fig.4.11 DCF and NPX mixture (1:1) ($C_0 = 30$ mg/L) in water

4.4. Direct photolysis

As recommended in the OPPTS 835.2210 *Direct photolysis rate in water by sunlight* guidelines by the USEPA [204], direct photolysis experiments should be carried out for compounds which have absorption maxima below 290 nm and measurable absorption tails at wavelengths over 290 nm. This is in accordance to the Grotthus-Draper law. Accordingly, direct photolysis was investigated.

4.4.1. Direct photolysis using an immersion-well reactor

Direct photolyses of individual DCF and NPX were conducted in the laboratory using a medium pressure UV lamp and two types of immersion-well tubes, pyrex glass and quartz.

Fig.4.12 depicts the degradation kinetics of DCF and NPX in distilled water in both immersion-well tubes. As would be expected, direct photolysis of DCF and NPX was more rapid with the quartz immersion tube, which allows DCF and NPX to absorb light of 254 nm. The molar absorption coefficient of DCF and NPX at 254 nm was $7844 \text{ M}^{-1} \text{ cm}^{-1}$ (Table 4.5) and $5304.6 \text{ M}^{-1} \text{ cm}^{-1}$ (Table 4.6), respectively. With the quartz immersion-well, almost 99% degradation was achieved in 3 min of irradiation for DCF, while a similar level of degradation was achieved in 6 min for NPX. Experiments in the pyrex immersion tube required almost 9 min and 15 min to completely degrade DCF and NPX, respectively.

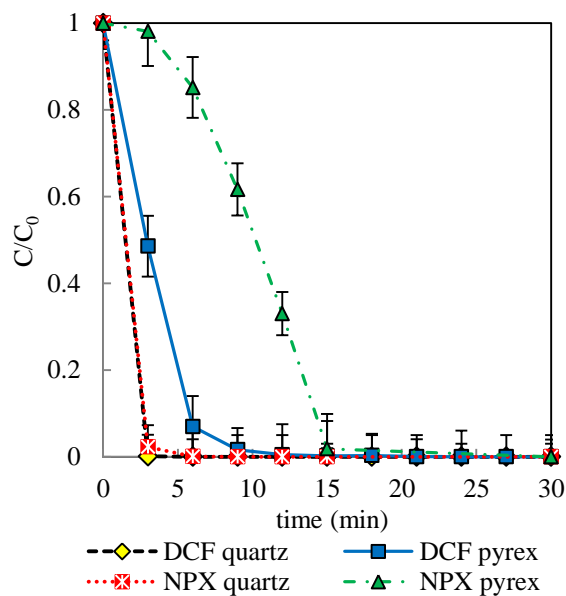


Fig.4.12 Effect of immersion-well tube type on direct photolysis of individual DCF and NPX ($C_0 = 30$ mg/L) in distilled water with time ($n=3$)

In the API mixtures, direct photolysis in a pyrex immersion-well tube, resulted in a faster degradation rate for DCF than NPX (Fig.4.13). A degradation percentage of 98% was achieved after 2 h of irradiation for NPX, while complete removal of DCF was achieved after 30 min of irradiation.

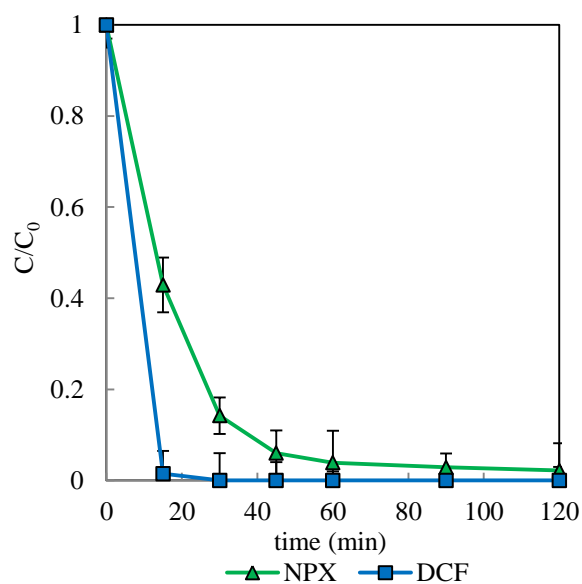


Fig.4.13 Direct photolysis of DCF and NPX in the mixture ($C_0 = 30$ mg/L) with pyrex immersion-well tube in distilled water ($n = 3$)

The determination of kinetic parameters was performed by fitting a pseudo-first-order kinetic model to each result, as demonstrated by Shu *et al.* [164]. In order to compare the degradation rate, for direct photolysis of individual compounds and their mixtures, pseudo-first-order kinetic constants, k (min^{-1}) were obtained from the slope of the plot representing $\ln(C/C_0)$ vs. time as shown in Table 4.7.

Table 4.7 Comparison of direct photolysis on degradation rate constants (k) between individual and API mixtures using different immersion-well tubes ($C_0 = 30 \text{ mg/L}$)

Rate constant, k (min^{-1}) (R^2)					
Distilled water					
Individual API				API mixtures	
DCF		NPX		DCF	NPX
Quartz	Pyrex	Quartz	Pyrex	Pyrex	
1.64 ± 0.08 (0.98)	0.42 ± 0.06 (0.98)	1.16 ± 0.09 (0.99)	0.07 ± 0.004 (0.98)	0.28 ± 0.004 (0.99)	0.06 ± 0.003 (0.98)

Systematic comparison of degradation between individual API and their mixtures with pyrex immersion-well tubes showed that the degradation rate was higher for DCF than the NPX in the mixture, which is consistent with the individual compound degradation studies. This suggests that DCF has a higher photolability than NPX.

Direct UV photolysis appears to be an effective process for DCF degradation as demonstrated by the higher rate constants in comparison with NPX. This result is consistent with findings reported by Shu *et al.* [164], in which DCF was observed to display the highest direct photolysis rate constant ($k = 0.85 \text{ min}^{-1}$) among other target compounds after irradiation with a medium pressure Hg lamp. This was explained by the high quantum yield, which determines the efficiency of photons in photochemical reactions.

The pyrex immersion tube was then chosen over the quartz mantle for further experiments, since it allows a better comparability under sunlight.

Direct photolysis of DCF in pyrex and quartz immersion-well tubes resulted in at least three degradation products after 2 h irradiation. Fig.4.14 shows the HPLC chromatogram of DCF with pyrex immersion tube. The suspected degradation products appeared prior to the DCF peak indicating compounds with higher polarity compared to the parent DCF. The major product at $t_R = 6.51 \text{ min}$ formed during direct photolysis was later identified as carbazole, 8-chloro-9H-carbazole-1yl-acetic acid.

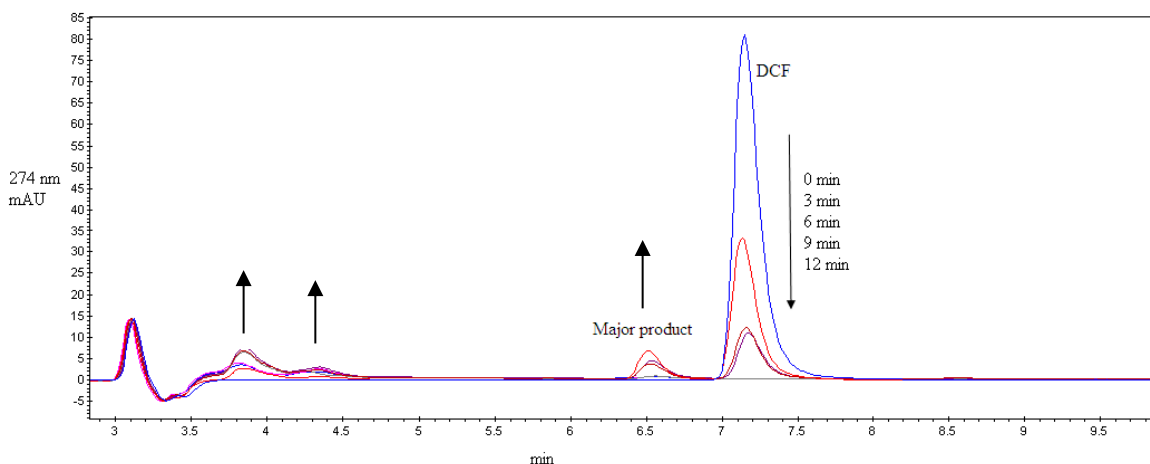


Fig.4.14 HPLC chromatogram of direct photolysis of DCF ($C_0 = 30$ mg/L) using pyrex immersion-well tube

In contrast, four degradation products were observed in the HPLC chromatogram obtained from direct photolysis of NPX in a pyrex immersion-well tube (Fig.4.15). The major degradation product at $t_R = 5.95$ min was 2-methoxy-6-vinylnaphthalene, which has been reported as photolytic product produced under both aerobic and anaerobic conditions [178].

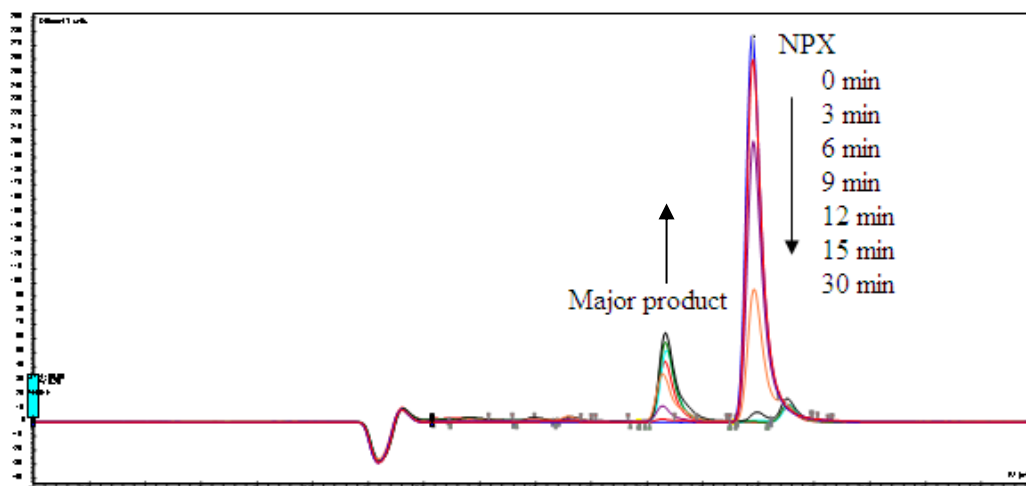


Fig.4.15 HPLC chromatogram of direct photolysis of NPX ($C_0 = 30$ mg/L) using pyrex immersion-well tube

Differences in pH values prior to irradiation ($t = 0$ min) and at the end of irradiation ($t = 2$ h) were also observed. Changes in pH for direct photolysis of NPX with pyrex and quartz immersion-well tubes were 6.85 ± 0.02 - 6.55 ± 0.03 and 6.60 ± 0.01 - 5.60 ± 0.02 , respectively. For DCF, the pH dropped from 6.65 ± 0.01 to 4.25 ± 0.02 , when quartz was used. For pyrex, a decline from

6.35 ± 0.02 to 4.00 ± 0.01 after 2 h of irradiation was observed, with the decrease in pH related to the formation of hydrochloric acids and carboxylic acids. The transparent DCF solution observed at 0 min changed into brown-yellowish colour after 2 h reaction time. The pH of the mixture reaction before irradiation was recorded to be 6.25 ± 0.02 and this value decreased to 5.95 ± 0.02 after 2 h of irradiation. Colour change from a transparent (colourless) solution to a pale brown colour was observed.

Changes in absorption spectra upon direct photolysis of DCF and NPX and their mixtures can be seen in Fig.4.16.

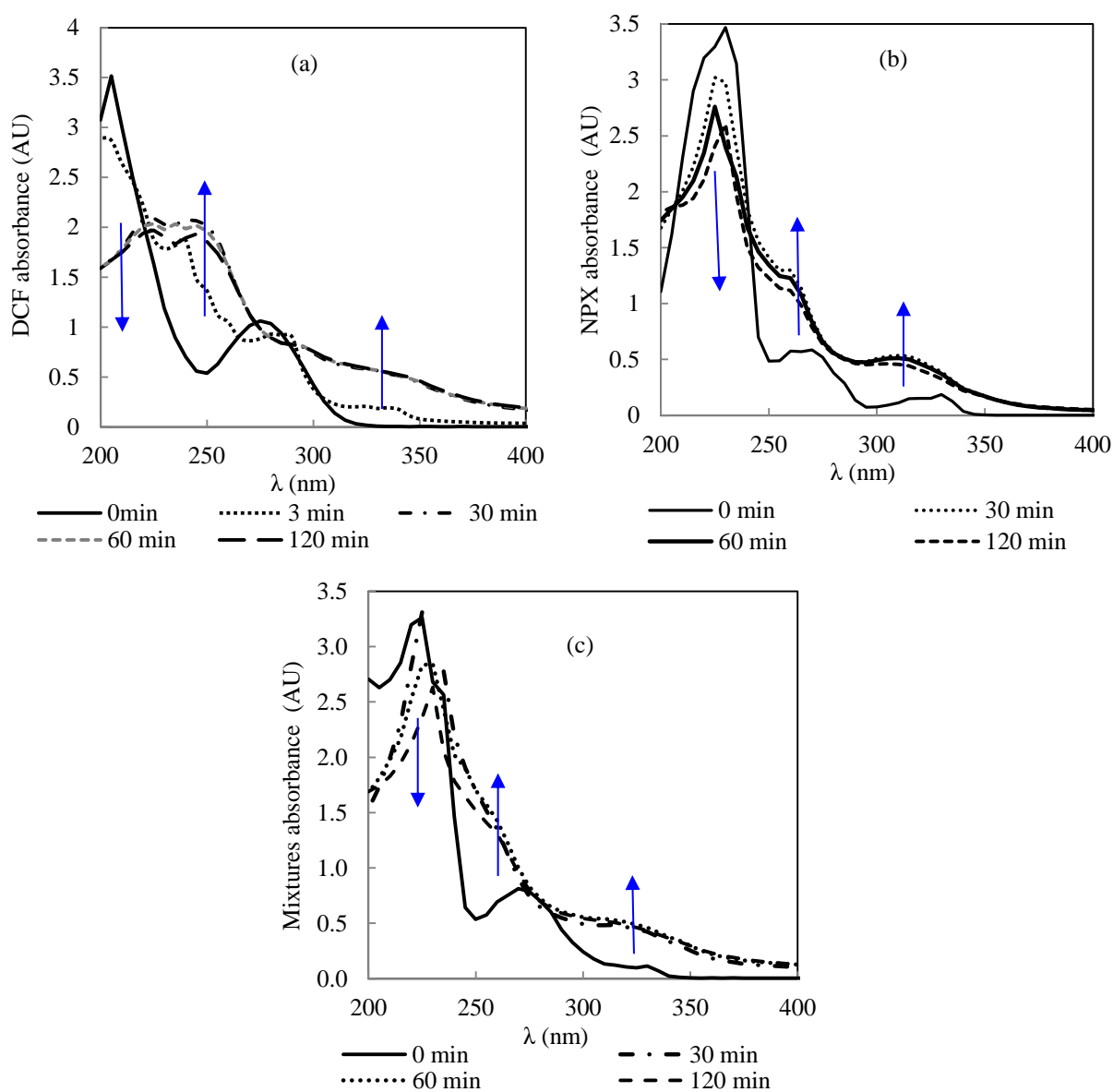


Fig.4.16 UV spectra changes of direct photolysis of individual (a) DCF (b) NPX and (c) DCF and NPX mixtures (1:1) ($C_0 = 30$ mg/L)

For DCF, the characteristic absorption band at 210 nm decreased rapidly over 2 h of irradiation time (Fig.4.16a). New absorption bands in the UV region at 240 nm and >320 nm indicated the formation of new intermediates. Four isosbestic points (215 nm, 265 nm, 288 nm and 305 nm) which formed after 3 min of irradiation, were then altered, suggesting the formation of secondary photodegradation products as suggested by Martínez *et al.* [149].

The characteristic maximum absorption band at 230 nm for NPX decreased from 3.470 AU at 0 min to 2.604 AU at 120 min (Fig.4.16b). The appearance of photoproducts became evident after 30 min of irradiation, where absorbance increased significantly at 260 nm and 310 nm, respectively. In addition, an absorption peak above 340 nm was also formed.

During UV irradiation of the mixed sample, the characteristic absorption band at 225 nm decreased with a slight bathochromic shift (230 nm) (Fig.4.16c). The increase in absorbance at 250 nm and >340 nm signified the formation of transformation products.

4.4.1.2 Water type and initial concentration effects

A comparison of direct photolysis in different water matrices showed that DCF (Fig.4.17a) and NPX (Fig.4.17b) can be easily degraded in distilled water and drinking water. However, degradation of DCF and NPX in river water proceeded rather slowly under direct photolysis, particularly for NPX.

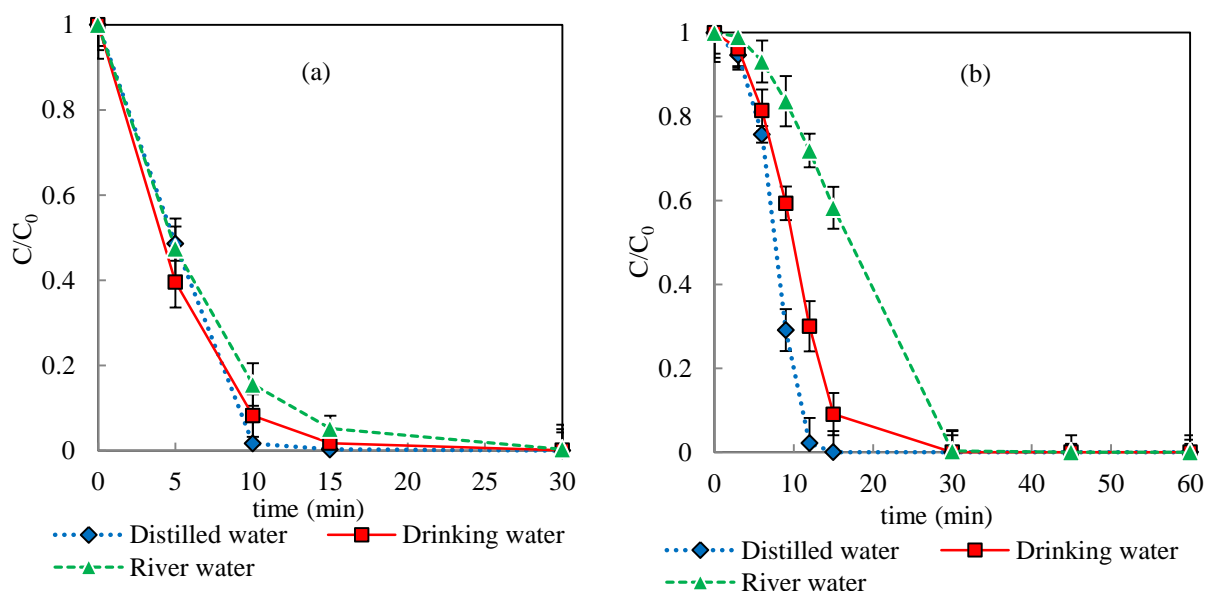


Fig.4.17 Effect of water matrix on direct photolysis of (a) DCF (30 mg/L) (b) NPX (30 mg/L)

Thus, the order of degradation was established as follows: distilled water > drinking water > river water.

Organic matter content has been reported to absorb radiation thus impairing degradation [205]. In this study, the DOC level in the river water (4.39 mg/L) was slightly higher than that of drinking water (2.74 mg/L). The higher DOC level and other organic matter in the unfiltered river water may have slowed down the degradation by absorbing light or acting as inner filters. Study by Benitez *et al.* [205] also reported similar results for NPX and mixtures of amoxicillin, naproxen and phenacetin when degradations were compared for commercial mineral water, groundwater and reservoir water under UV irradiation. The fastest degradation took place in mineral water followed by groundwater and reservoir water with these rates in line with their organic matter content.

The effect of the initial concentrations on the degradation of DCF was also examined by varying the initial concentrations from 10 to 60 mg/L (Fig.4.18a). As expected, UV photolysis resulted in a more rapid DCF degradation at lower concentrations (10 and 30 mg/L) compared to that of at higher concentrations (50 and 60 mg/L). All degradations were accompanied by a decrease in pH from 6 to 3.5. This is attributed to the dechlorination of DCF leading to the formation of chloride ions. Fig.4.19 shows the evolution of chloride ions during direct photolysis of 30 mg/L of DCF (optimal initial concentration studied). The concentration of chloride ions increased up to 30 min and thereafter became constant coinciding directly to the disappearance of DCF and the formation of the degradation products such as carbazole, 2-(8-chloro-9H-carbazol-1-yl)acetic acid.

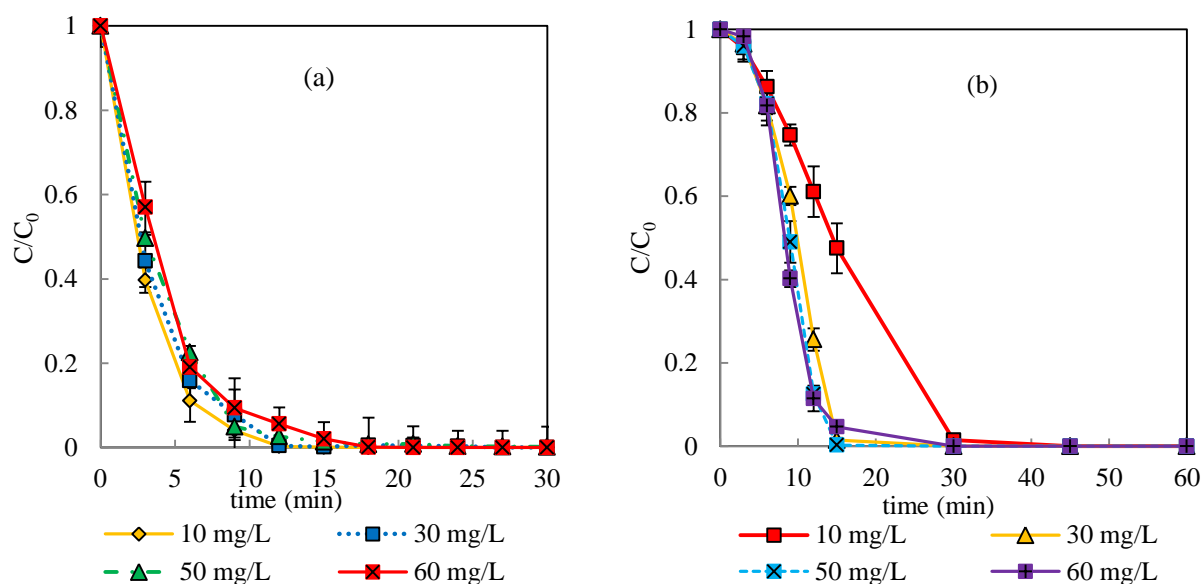


Fig.4.18 Effect of initial concentration on the photolytic degradation of (a) DCF and (b) NPX in distilled water ($n=3$)

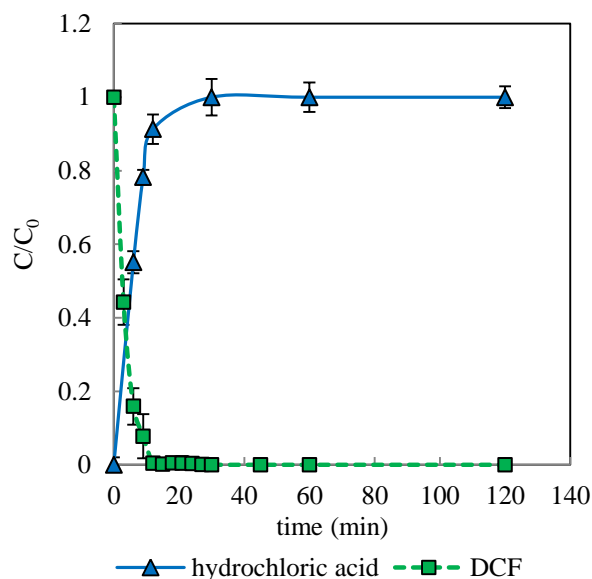


Fig.4.19 Formation of chloride ions during DCF photolysis in distilled water ($C_0 = 30$ mg/L)

In contrast, the degradation of NPX became more rapid with increasing concentration, in particular for concentrations of 30-60 mg/L (Fig.4.18b). This observation is likely due to the effectiveness of UV photon absorption by NPX molecules from the medium pressure Hg lamp source used or due to the formation of photoproducts, which accelerate the degradation. Studies have reported the formation of aromatic ketones such as 2-acetyl-6-methoxynaphthalene during the photodegradation of NPX [178]. These aromatic ketones can potentially act as a photosensitizers as well as photocatalysts and as such increase the photodegradation rate [206]. All concentrations were completely degraded within 60 min of irradiation during direct photolysis.

4.4.2. Direct photolysis using a loop reactor

Direct photolyses of DCF and NPX solutions individually and their mixtures were also performed in the larger loop reactor (Laboclean®) equipped with a medium pressure Hg lamp (500 W) (Fig.4.20) using a similar initial concentration of 30 mg/L.

In the loop reactor, after 60 min of irradiation, DCF was almost completely degraded in distilled water, whereas in drinking water, only 92% of DCF was degraded (Fig.4.20a). No apparent differences were observed for NPX photolysis between distilled water and drinking water implying that the water type had no significant effect on the photolysis (Fig.4.20b). Complete NPX degradation was achieved in the loop reactor within 15 min. In mixture, the degradation was similar to that observed in the immersion-well photoreactor, with DCF degrading more rapidly than NPX

(Fig.4.20c). DCF was rapidly photodegraded within 10 min of irradiation time, while NPX required an additional 5 min to achieve complete degradation.

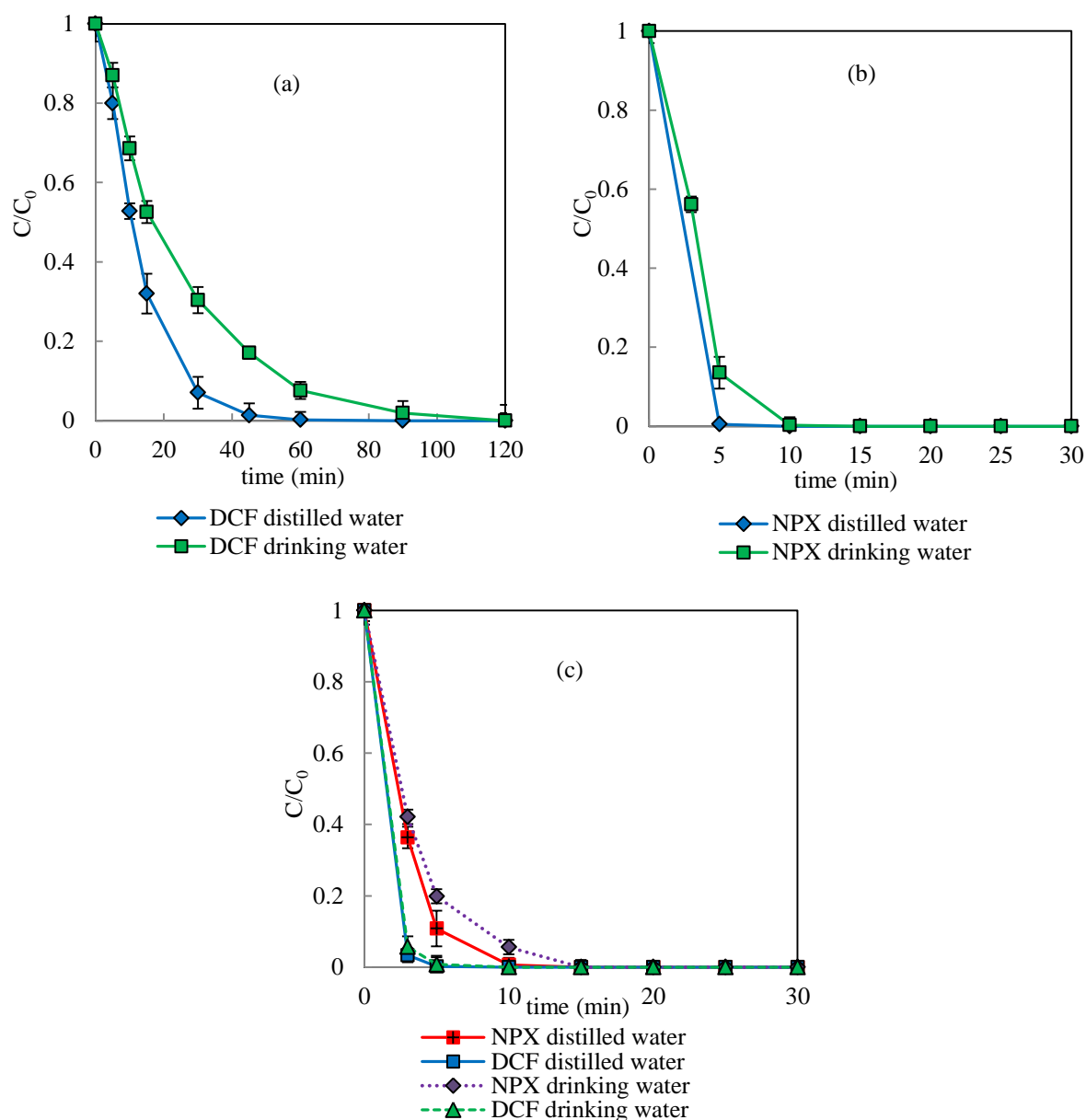


Fig.4.20 Direct photolysis of individual compound (a) DCF ($C_0 = 30$ mg/L), (b) NPX ($C_0 = 30$ mg/L) and (c) DCF:NPX (1:1) mixtures ($C_0 = 30$ mg/L) in the loop reactor (Laboclean®)

Overall, the high efficiency of the loop reactor to degrade individual and the API mixtures can be attributed to the photons emitted at 254 nm and the 500 W power of the medium pressure Hg lamp. The medium pressure Hg lamp was housed in a quartz mantles with the outer chambers made of pyrex glass, allowing strong UV light of 254 nm to participate in the photodegradation process. In

addition, the emitted photons may have been effectively absorbed by the APIs due to their ability to undergo direct photolysis as previously discussed in sections 4.3.1 and 4.3.2 (Chapter 4).

4.5. Photocatalytic degradation of diclofenac using an immersion-well reactor

4.5.1. Adsorption experiments

Dark adsorption experiments for the entire range of 10-60 mg/L in the presence of 0.1 g/L TiO₂ P25 showed that 2.2 ± 0.8 to $10.8 \pm 1.6\%$ of DCF was adsorbed onto the TiO₂ surface. This low adsorption is in accordance to dark adsorption experiments of DCF on TiO₂, as reported by Rizzo *et al.* [151]. Similarly, a study by Méndez-Arriaga *et al.* [142] also concluded that the adsorption DCF does not account for a significant reduction in concentration during photocatalysis.

4.5.2. Effect of initial concentration

Fig.4.21 represent the time-course of DCF degradations in the range of 10-70 mg/L with 0.1 g/L TiO₂ P25. The results obtained showed that, degradation efficiencies decreased as the initial concentration of DCF in solution increased from 10 to 70 mg/L. As a result, the degradation rates also decreased (Table 4.8).

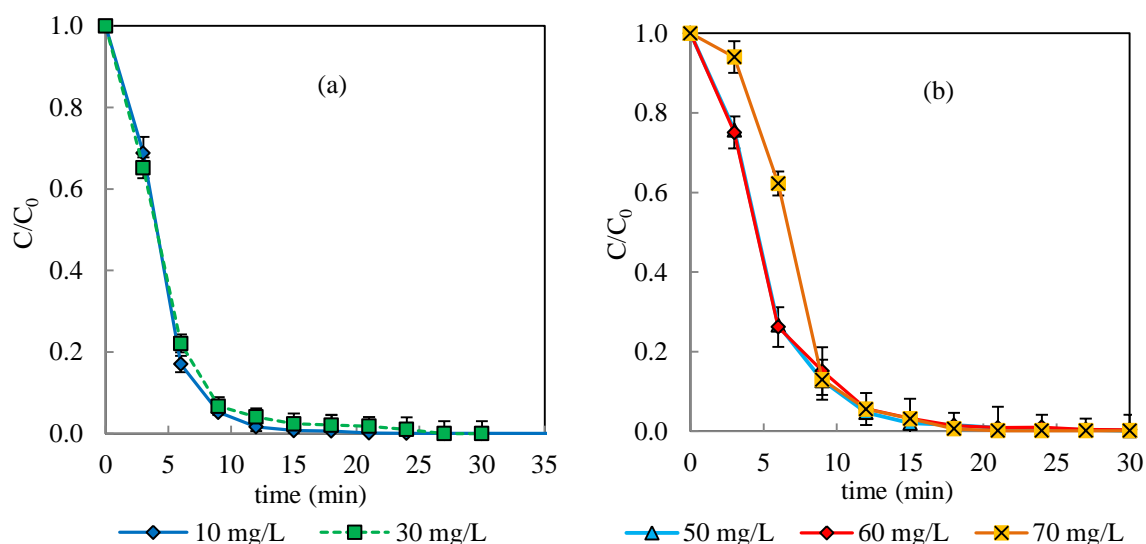


Fig.4.21 Effect of DCF initial concentration (a) 10 and 30 mg/L and (b) 50-70 mg/L on photocatalytic reaction kinetics (0.1 g/L TiO₂ P25, pH = 6, T_{max} 29°C)

Complete degradation was achieved for low range initial concentrations, 10 and 30 mg/L (Fig.4.21a), within 30 min while for higher concentrations, 50 mg/L to 70 mg/L (Fig.4.21b), were similar irradiation times approximately 98-99% of the initial amounts of DCF degraded. The degradation of DCF in the presence of TiO₂ P25 followed pseudo-first-order kinetics. Table 4.8 summarizes the kinetic parameters obtained from TiO₂ photocatalytic degradations of DCF.

The obtained pseudo-first-order rate constant value, k_{app} decreased from 0.30 to 0.14 min⁻¹ over the concentration range studied (Table 4.8). The increase in the initial concentration results in a competition of DCF molecules for available photons and a subsequent decrease in the degradation rate [150]. The initial rate, r_0 , increases with initial concentration of DCF up to 60 mg/L and decreases thereafter. The reaction rate could have attained saturation and thus became independent of the concentration of DCF [207]. A similar phenomenon has been reported for DCF in an earlier study [116]. An increase in DCF concentrations resulted in saturation of active sites of TiO₂, which retarded the generation of HO[•] radicals or other oxidants. As a result of insufficient amounts of reactive species, the degradation efficiency of DCF decreased [127].

Table 4.8 Kinetic parameters for TiO₂ photocatalytic degradation of different initial concentrations of DCF

Initial concentration (mg/L)	k_{app} (min ⁻¹)	R ²	r_0 (mg/L/min)
10	0.30 ± 0.06	0.98	3.0
30	0.25 ± 0.08	0.99	7.5
50	0.22 ± 0.10	0.99	11.0
60	0.20 ± 0.06	0.99	12.0
70	0.14 ± 0.04	0.99	9.8

4.5.3. Effect of TiO₂ concentration

TiO₂ concentrations ranging between 0.01-2 g/L were examined for a fixed 30 mg/L DCF solution (Fig.4.22). Photocatalytic degradation rates were determined after 30 min of pre-adsorption in the dark. A dark experiment was also conducted for comparison. In the absence of light, no noticeable degradation took place indicating the requirement of external light to initiate the degradation process. Negligible degradation of DCF in the dark was also reported by Zhang *et al.* [150].

Low concentrations of 0.01 and 0.1 g/L of TiO₂ led to complete degradation of DCF within 30 min of irradiation, while higher loadings of 1 and 2 g/L resulted in almost complete degradation only after 60 min of photocatalysis (Fig.4.22). The experimental data fitted pseudo-first-order kinetics

($R^2 > 0.96$) (Table 4.9). In the present study, the addition of 0.01 g/L of TiO₂ P25 produced the lowest remaining DCF concentration followed by a concentration of 0.1 g/L TiO₂, which resulted in the same degradation within 15 min of irradiation. In contrast, higher loadings of TiO₂ clearly slowed down the degradation rate, likely due to scattering of light and agglomeration of TiO₂ [141].

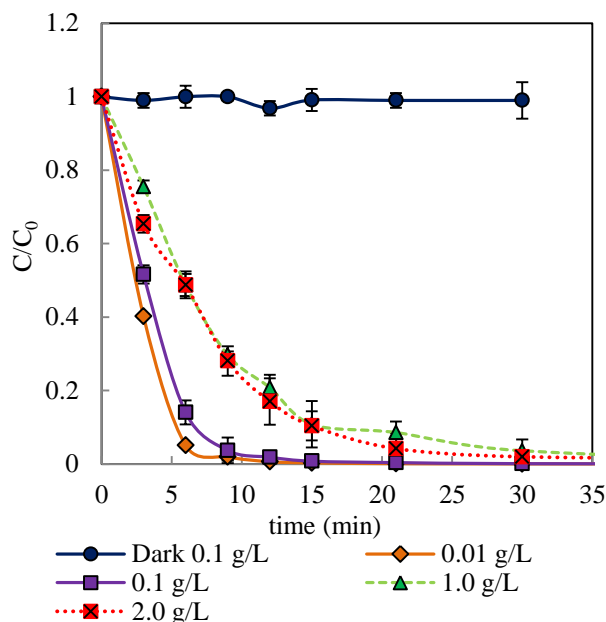


Fig.4.22 Effect of TiO₂ concentrations (0.01-2 g/L) on DCF photocatalytic degradation ($C_0 = 30$ mg/L) in distilled water with a medium pressure Hg lamp

Table 4.9 Pseudo-first-order rate constant for photocatalytic degradation of DCF with different TiO₂ concentrations

TiO ₂ P25 (g/L)	k_{app} (min ⁻¹)	R^2
0.01	0.36 ± 0.02	0.97
0.1	0.25 ± 0.06	0.97
1.0	0.21 ± 0.04	0.99
2.0	0.15 ± 0.05	0.99

Although the highest photocatalytic efficiency was achieved with 0.01 g/L, further experiments were carried out at 0.1 g/L. This concentration has been reported previously as optimal for TiO₂ P25, which generally varies from 0.1 to 5.0 g/L [122]. A loading above 1.0 g/L was not considered as optimal due to the lower degradation rate (Table 4.9) caused by increased sedimentation, which could not be avoided even when stirring at 1,000 rpm and with insufficient absorption of light by the reaction mixture. The optimum dose of photocatalyst represents a critical parameter in the photocatalytic degradation process. Above the optimal loading, degradation rates decreased with

higher catalyst concentrations [122]. Similar findings were reported for the antibiotic, oxolinic acid, where an increase above 1 g/L led to a decrease in API removal [121].

Thus far, the optimal loading published for DCF photocatalysis was 1 g/L [149], 0.624 g/L [165], and 0.25 g/L [116], respectively, which is significantly higher than in this study. The much lower TiO_2 loading determined in this study can be attributed to the effective circulation in the advanced immersion-well setup chosen, which ensured efficient distribution of photocatalyst particles throughout the entire reaction mixture.

4.5.4. Effect of air bubbling

Photocatalytic degradation experiments in the presence of dissolved oxygen (DO) in the form of air were performed to compare the degradation rate in its absence. Air was bubbled into the system at a flow rate of 55.5 mL/min. The degradation profile showed that complete degradation of DCF was achieved after 30 min under both conditions (Fig.4.23).

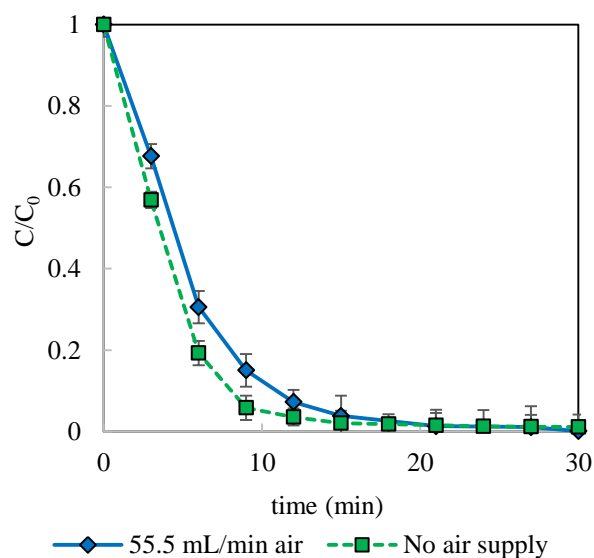


Fig.4.23 Photocatalytic degradation of DCF with TiO_2 P25 and TiO_2 P25/DO ($C_0 = 30$ mg/L, $\text{TiO}_2 = 0.1$ g/L, air flow rate = 55.5 mL/min)

The initial 15 min of the degradation phase showed slightly faster DCF degradation in the absence of air. This result appears to be in contrast to the expected improvement in degradation efficiency in the presence of air as addition of DO has been reported to increase the production of HO^\bullet radicals in TiO_2 photocatalysis [112]. Two conclusions can be drawn from this observation. First, the amount air flow introduced into the reaction may have been insufficient to increase the degradation rate. Second,

the effective stirring maintained in the reaction solution may have maintained sufficient O₂ levels throughout the course of the reaction period [208]. A similar observation was reported for ibuprofen, where an additional O₂ supply failed to improve the conversion of ibuprofen and instead caused a decrease in its degradation [208]. In contrast, DCF removal was found to be favoured slightly with 200 mL/min O₂/Ar (50% O₂, v/v) [149].

The profile shows that DO levels constantly decreased during the reaction, for 90 min and remained almost constant thereafter (Fig.4.24). It can be assumed that the supplied air was not effectively consumed to scavenge electron-hole pair recombination, as no improvement was observed in the degradation profile (Fig.4.24). Photolytic transformations of DCF have been reported to be affected by O₂ [171] while in the TiO₂ photocatalytic studies it was suggested that O₂ did not participate in the mechanism, but resulted in differences in the concentration of photoproducts in the presence and absence of O₂ [149].

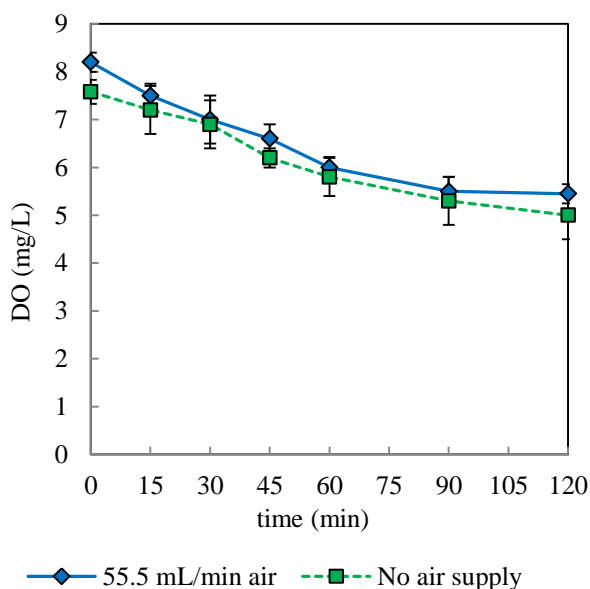


Fig.4.24 Dissolved oxygen profile for the photocatalytic degradation of DCF($C_0 = 30$ mg/L; $TiO_2 = 0.1$ g/L; air flow rate = 55.5 mL/min)

4.5.5. Effect of solution pH

The complex electrostatic interaction between semiconductor, solvent, substrate and charged radicals formed during the treatment make pH an important reaction parameter. pH studies were thus conducted to determine the extent of degradation based on the ionization state of the photocatalysts and DCF. The adsorption of compounds is determined by the electric charge of both the catalysts and substrate. The surface of TiO₂ is amphoteric and thus adsorption is affected by pH. The zero point

charge (pH_{zpc}) of TiO_2 of 6.25 results in a positive surface charge below the pH_{zpc} ($\text{pH} < \text{pH}_{\text{zpc}}$) and a negative surface charge above the pH_{zpc} ($\text{pH} > \text{pH}_{\text{zpc}}$) [112]. The pK_a value of DCF (carboxyl group) is known to be 4.15 (at 25°C) [166]. At a $\text{pH} < \text{pK}_a$, DCF is present in its neutral or protonated form, whereas at a $\text{pH} > \text{pK}_a$ it predominantly exists in its deprotonated form (i.e. as a negatively charged carboxylate).

The initial pH values of the solutions were adjusted to 3.0, 4.9, 5.6, 7.8 and 10.8, respectively, to represent three conditions: strongly acidic, neutral and strongly basic. The degradation profile and rate constants (k_{app}) at the tested initial pH values as a function of irradiation time are illustrated in Fig.4.25 and Fig.4.26, respectively. The DCF experiment performed at pH 3 did not result in any degradation (result not shown). This could be due to the insolubility of DCF and the fact that API becomes practically insoluble (precipitates) below pH 4 ($\text{pK}_a = 4.15$) [166]. This result is in agreement with other DCF degradation studies conducted with other AOPs such as photo-Fenton and ozonation and acidic conditions of pH 5.0-6.0 are utilized due to the reduced solubility of DCF at $\text{pH} < 4$ [81, 168].

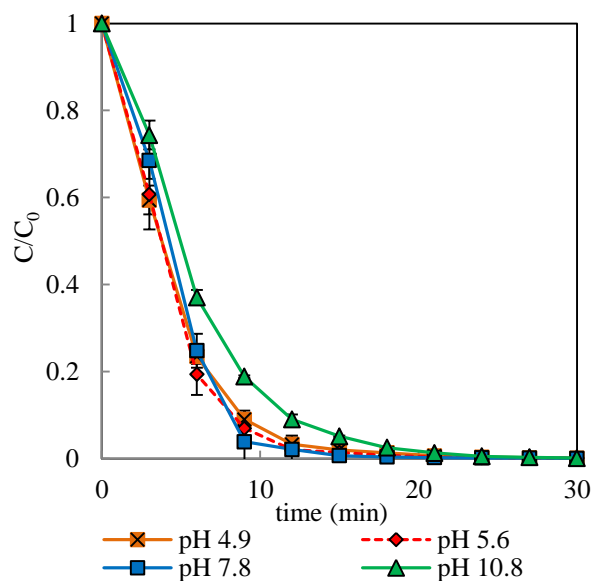


Fig.4.25 Effect of initial solution pH on DCF photocatalytic degradation

The adsorption decreased to 20.2% at pH 5 and then to 6.5% at pH 11, due to the electrostatic repulsion effects of the negatively charged DCF and the TiO_2 surface. DCF degradation is not significantly affected by pH as the degradation reached 100% after 30 min under all conditions. Comparison of the degradation rate at the pHs investigated showed that an increase in pH from acidic to strongly alkaline, caused a decrease in the degradation rate (Fig.4.26). An initial pH below 5.6 inhibited the degradation rate, whereas pHs of 5.6 and 7.8 resulted in the highest initial rates of 0.26 min^{-1} and 0.25 min^{-1} , respectively. These results demonstrate that a pH adjustment is not

necessary prior to the photocatalytic degradation of DCF. At natural pH (~6.2), a slightly higher rate of 0.30 min^{-1} compared to that at other pHs was obtained. Photocatalytic degradation of oxytetracycline was also reported to be most effective in solution without pH modification [209].

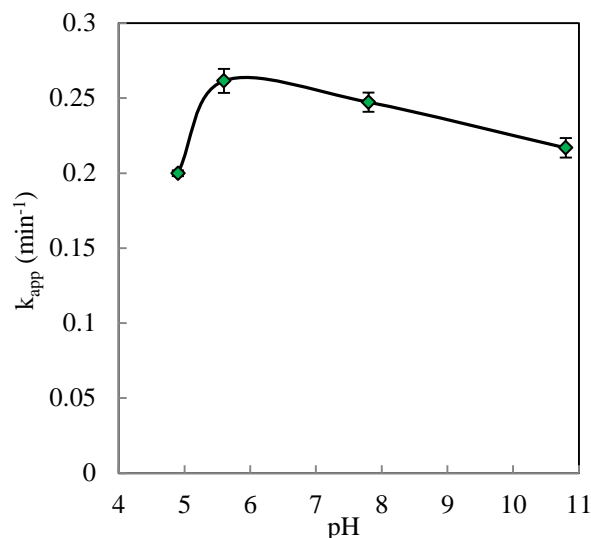


Fig.4.26 Effect of initial solution pH on rate constant (k_{app}) of DCF photocatalysis

The change in pH was monitored throughout the course of the reaction. The pH values after 2 h of irradiation changed to $\text{pH} < 4$ for the acidic and neutral conditions tested, while for the basic conditions, a $\text{pH} < 6$ was recorded. These reductions in pH were observed as a result of the formation of hydrochloric acid and other mineral acids, such as formic acids and carboxylic acids.

4.5.6. Effect of water matrix

A comparison of TiO_2 photocatalysis between drinking water and river water revealed that this oxidation system effectively degraded DCF in both water matrices (Fig.4.27). TiO_2 photocatalysis was able to degrade 99.4% of DCF in drinking water after 30 min, while 98.2% of degradation took place in river water over the same period. After 45 min, a total disappearance of DCF from drinking water and river water was observed. A comparison of degradation rates showed that degradation in the river water was slightly slower with a rate of 0.14 min^{-1} ($R^2=0.99$), compared to 0.17 min^{-1} ($R^2=0.99$) in drinking water (Fig.4.28). The presence of higher DOC could have potentially caused this lower degradation rate in unfiltered river water and a similar trend was observed when the effect of water matrix was studied by direct photolysis (section 4.4.1.2 in Chapter 4).

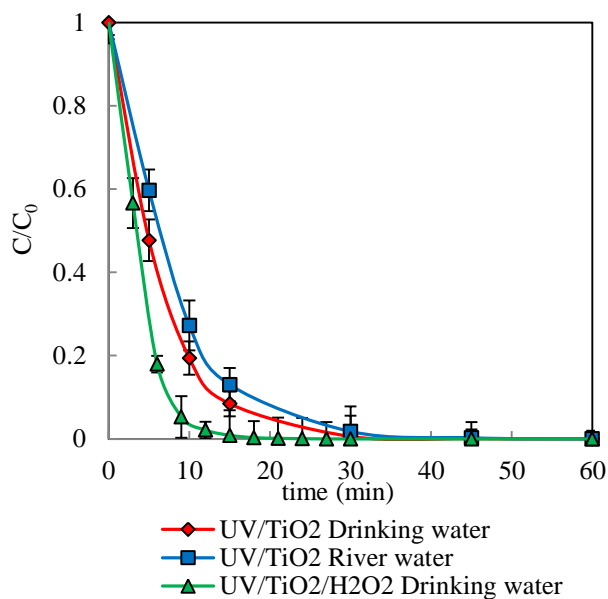


Fig.4.27 Effect of water matrix on DCF degradation by UV/TiO₂ and UV/TiO₂/H₂O₂ (C₀ = 30 mg/L; TiO₂ = 0.1 g/L; H₂O₂ = 250 mg/L)

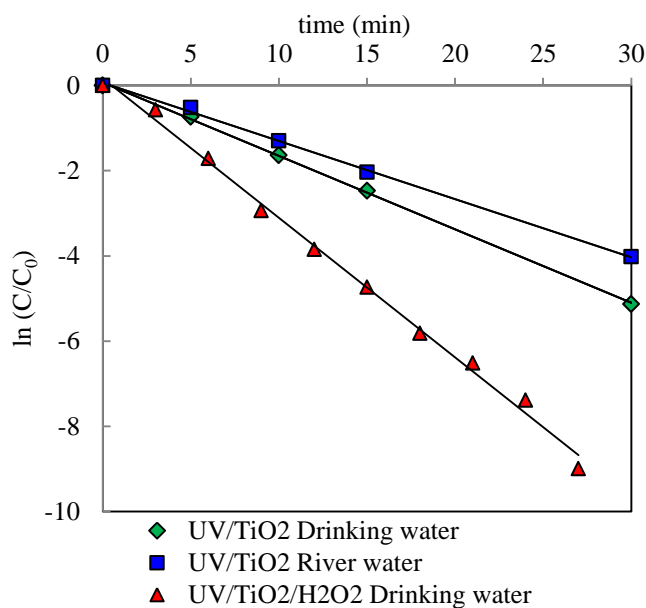


Fig.4.28 Kinetics of DCF degradation by UV/TiO₂ and UV/TiO₂/H₂O₂ oxidation in different water matrices

The influence of 250 mg/L H₂O₂ on the degradation efficiency was also tested in drinking water. The addition of H₂O₂ promoted the degradation efficiency and resulted in a slightly higher degradation of 99% in 15 min, compared to 92% in the absence of H₂O₂ (Fig.4.27). The addition of H₂O₂ into the UV/TiO₂ system shortened the complete degradation time to 18 min compared to 45 min in the pure

UV/TiO₂ photocatalysis. Likewise, the degradation rate constant for DCF in drinking water also increased from 0.17 min⁻¹ (R²=0.99) to 0.33 min⁻¹ (R²=0.99) on an addition of H₂O₂ (Fig.4.28).

These observations are in accordance with those reported by Achilleos *et al.* [116] for DCF degradation in the presence of H₂O₂. Degradation enhancement occurs due to the ability of H₂O₂ to function as an electron acceptor, thus reducing electron-hole recombination and generating HO[•] radicals and OH⁻ ion. H₂O₂ can react with the superoxide radical anion O₂^{•-} to produce OH⁻ ions and HO[•] radicals as shown in Eq. 4.5 and Eq. 4.6:



In comparison, dark reaction of UV/TiO₂/H₂O₂ in drinking water resulted in no degradation over 2 h (data not shown).

4.5.7. TiO₂ type and immersion-well tube material

The effect of a quartz immersion-well as well as another commercially available titania, Ti (IV) oxide (Aldrich) was compared to that of a pyrex cooling jacket and TiO₂ P25, respectively. As expected, rapid DCF degradation occurred with the quartz immersion-well for both, TiO₂ P25 and Ti (IV) oxide photocatalysts (Fig.4.29).

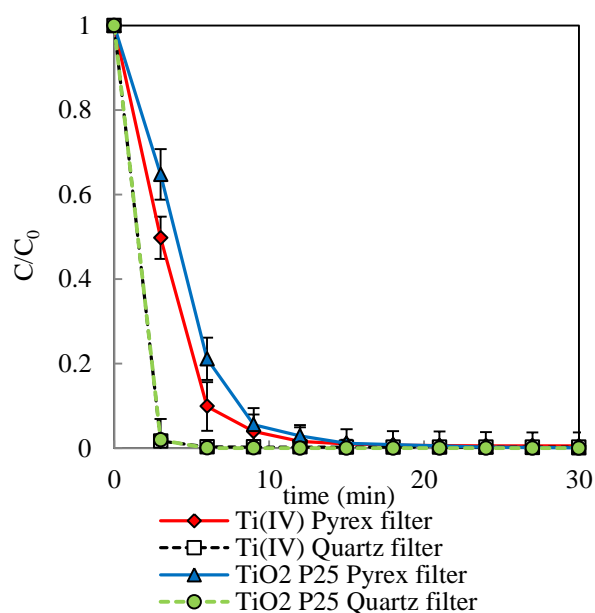


Fig.4.29 Comparison of photocatalytic degradation with different photocatalysts and filters

Since the cut-off wavelength of quartz glass is as low as $\lambda < 200$ nm, the intensive 254 nm emission from the medium pressure Hg lamp provided more energy-rich photons available for direct photolysis (refer to Fig.4.7) [197]. A comparable degradation rate was observed for Ti (IV) oxide ($k = 0.29 \pm 0.12$, $R^2=0.96$) compared to the standard TiO₂ P25 ($k = 0.27 \pm 0.06$, $R^2=0.97$). Initially, 3 min of photolysis with 0.1 g/L Ti (IV) oxide and TiO₂ P25 led to 50% and 35% degradation, respectively. Complete degradation after 30 min of irradiation with both photocatalysts could be attributed to the nature of the photocatalyst [141]. The efficiency to degrade DCF can be explained by the photocatalytic activity of the pure anatase catalyst (Aldrich). Pure anatase TiO₂ has a higher density of superficial hydroxyl groups compared to the pure rutile forms. Combinations of anatase and rutile as in TiO₂ P25 have also demonstrated good photocatalytic activity due to the promotion of charge pair separation and inhibition of electron-hole recombinations [116].

4.6. Photocatalytic degradation of naproxen using an immersion-well reactor

4.6.1. Adsorption experiments

Dark adsorption of NPX for the studied range of 5-60 mg/L showed an adsorption percentage of 4.2 ± 1.2 to $8.3 \pm 1.9\%$. Two individual studies by Méndez-Arriaga *et al.* [126, 142] verified that about 8-9% of NPX adsorbed on TiO₂, which is in accordance with this study.

4.6.2. Effect of initial concentration

Fig.4.30 shows the effect of initial concentration (10-60 mg/L) on the degradation kinetics of NPX. A significant increase in NPX concentrations from 10 to 60 mg/L lowered the degradation rate constants (Table 4.10). Within 30 min, complete degradation of NPX was obtained at initial concentrations of 10 and 30 mg/L, while higher NPX concentrations (50 and 60 mg/L) required considerably longer times of up to 60 min.

The decline in degradation rate at high initial concentrations can be attributed to two reasons as pointed out by Yang *et al.* [127] for paracetamol, where a similar trend in the degradation rate was observed: (i) occupancy on TiO₂ active sites increases with higher concentration of NPX, which impedes the formation of reactive species (HO[•] and O₂^{•-}) and (ii) upon concentration increase, the likelihood of NPX molecules to absorb more photons also increases, which would cause photon deficiency for the activation of TiO₂.

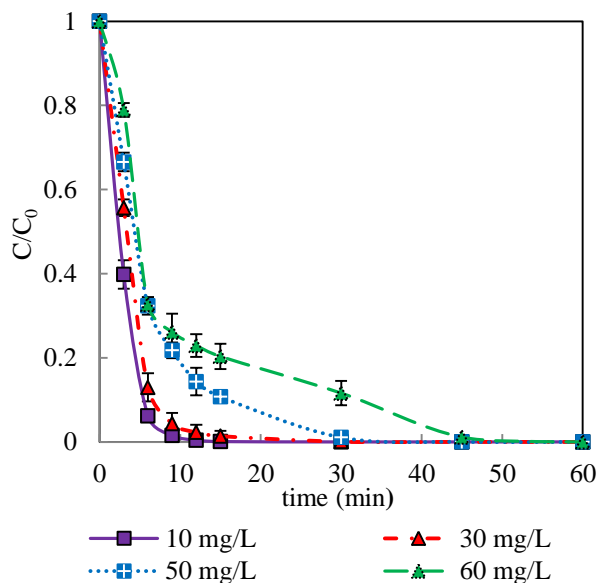


Fig.4.30 Effect of NPX concentrations on TiO₂ photocatalytic degradation

Table 4.10 Kinetic parameters for TiO₂ photocatalytic degradation of different initial concentration of NPX

Initial concentration (mg/L)	k_{app} (min ⁻¹)	R ²	r_0 (mg/L/min)
10	0.48 ± 0.11	0.99	4.8
30	0.30 ± 0.09	0.97	9.0
50	0.15 ± 0.05	0.98	7.5
60	0.11 ± 0.04	0.90	6.6

The initial degradation rate, r_0 , increased until 30 mg/L (Table 4.10) and the values decrease thereafter and became independent of the concentration of NPX. Therefore, a concentration of 30 mg/L was chosen for further investigations.

4.6.3. Effect of TiO₂ concentration

The dependence of the NPX photocatalytic oxidation rate on TiO₂ concentration was examined at a fixed NPX concentration (Fig.4.31). A dark experiment was also conducted for comparison. No degradation took place in the dark, indicating the requirement of external light to initiate the degradation process. A significant improvement in the degradation of NPX was thus observed in the presence of TiO₂.

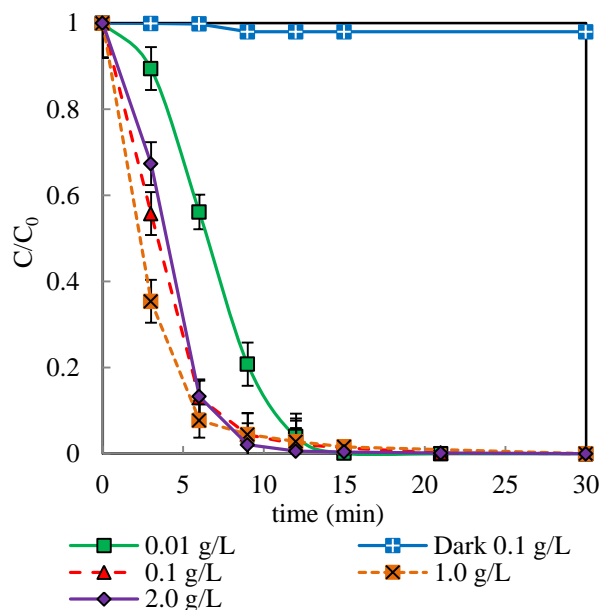


Fig.4.31 Effect of TiO₂ concentration (0.01-2 g/L) on fixed NPX concentration (C₀ = 30 mg/L)

The degradation rate linearly increased from 0.26 min⁻¹ at 0.01 g/L TiO₂ to 0.30 min⁻¹ at 0.1 g/L (Table 4.11; refer to initial concentration = 30 mg/L). However, the addition of a higher loading, 1.0 g/L TiO₂ led to slight decrease in the degradation rate to 0.27 min⁻¹, while at 2.0 g/L degradation increased to 0.41 min⁻¹ (Table 4.11). This clearly demonstrates that there is no linear relationship between the TiO₂ concentration and the degradation rate for 30 mg/L of NPX.

Table 4.11 Extended effect of TiO₂ concentration (0.01-2.0 g/L) on NPX degradation (5 - 50 mg/L)

Initial concentration (mg/L)	TiO ₂ loading (g/L)	Reaction rate, k _{app} (min ⁻¹)	R ²	Degradation (%) (after 15 min)
5	0.01	0.25 ± 0.08	0.99	97.1
	0.1	0.74 ± 0.13	0.96	100.0
	1.0	1.15 ± 0.10	0.99	100.0
	2.0	1.05 ± 0.11	0.99	100.0
10	0.01	0.19 ± 0.03	0.95	93.7
	0.1	0.48 ± 0.09	0.99	99.8
	1.0	0.94 ± 0.15	0.98	100.0
	2.0	1.36 ± 0.20	0.99	100.0
30	0.01	0.26 ± 0.06	0.98	99.8
	0.1	0.30 ± 0.09	0.97	99.3
	1.0	0.27 ± 0.05	0.97	98.4
	2.0	0.41 ± 0.11	0.97	99.7
50	0.01	0.34 ± 0.08	0.96	99.3
	0.1	0.15 ± 0.04	0.98	83.8
	1.0	0.06 ± 0.02	0.96	81.1
	2.0	0.06 ± 0.03	0.95	89.9

A high concentration of TiO_2 can either increase the degradation rate by increasing the overall available catalyst surface area and thus the number of active sites or can decrease the degradation efficiency by limiting light penetration as a result of opacity. As a result of inconsistent effects of higher TiO_2 loading on NPX, further experiments were conducted with 0.1 g/L, which exhibited the best performance.

In order to extend the study of TiO_2 concentration, the effect of this parameter was further investigated with other NPX concentrations. These corresponding degradation rates are summarized in Table 4.11. Degradation rates at lower initial concentrations, 5 and 10 mg/L, increased with TiO_2 concentration with $R^2 > 0.96$ following pseudo-first-order kinetics. For an initial concentration of 50 mg/L, a similar trend was observed as for 30 mg/L of NPX. Fluctuating degradation rates at TiO_2 concentrations > 1.0 g/L indicated a not linear relationship between degradation rate and TiO_2 concentration. These results showed that the rate of reaction is not always proportional to TiO_2 concentration as previously reported [142]. Although the experimental data fitted the employed pseudo-first-order kinetic model with $R^2 > 0.95$, the formation of intermediates and their competition for HO^\bullet radicals with parent NPX may explain these observations. A study on the degradation of sulfamethoxazole by UV-A/ TiO_2 photocatalysis also reported that there was no linear relationship between the reaction rate and TiO_2 concentration due to limitations of photon availability or increasing light scattering at higher TiO_2 concentrations [120].

It is thus suggested that for higher NPX concentrations, 30 mg/L and 50 mg/L, an optimal load of 0.1 g/L of TiO_2 would ensure a maximum degradation rate under the adopted experimental conditions.

4.6.4. Effect of solution pH

The effect of pH on the degradation of NPX during TiO_2 photocatalysis is shown in Fig.4.32. The degradation of NPX appears to be more favoured at acidic and near-neutral pH compared to alkaline pH. Similar observations were made for NPX degradation in aqueous solution by gamma irradiation [210].

The degradation was 99% at pH 5.6 and 6.9 after 15 min of irradiation time. Alkaline solutions of pH 8.0 and 10.8 took a longer irradiation time to completely eliminate NPX from the system. The overall time needed for complete degradation to take place at these pH ranges were 30 and 60 min, respectively.

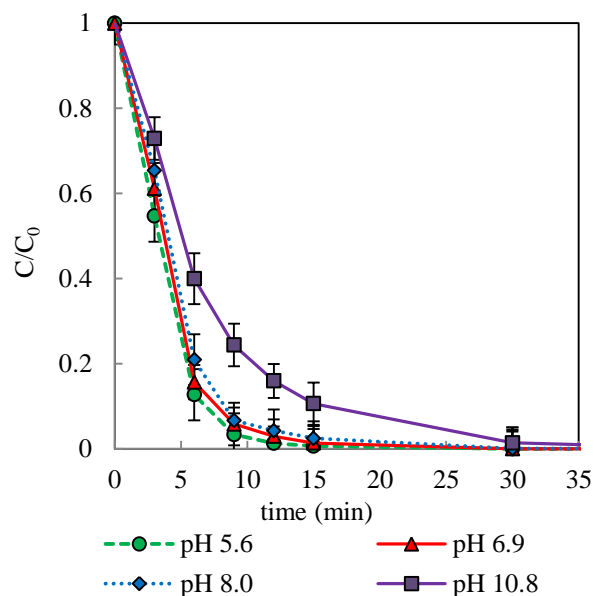


Fig.4.32 Effect of solution pH on NPX degradation ($C_0 = 30 \text{ mg/L}$; $\text{TiO}_2 = 0.1 \text{ g/L}$)

The degradation rates decreased with increasing pH, following a pseudo-first-order kinetics ($R^2 > 0.98$) (Fig.4.33). The degradation rates at pH 5.6, 6.9, 8.0 and 10.8 were $0.36 \pm 0.06 \text{ min}^{-1}$, $0.30 \pm 0.08 \text{ min}^{-1}$, $0.27 \pm 0.08 \text{ min}^{-1}$ and $0.16 \pm 0.04 \text{ min}^{-1}$, respectively. In comparison, degradation at pH ~ 6.25 , without any pH adjustment yielded a degradation rate of 0.30 min^{-1} .

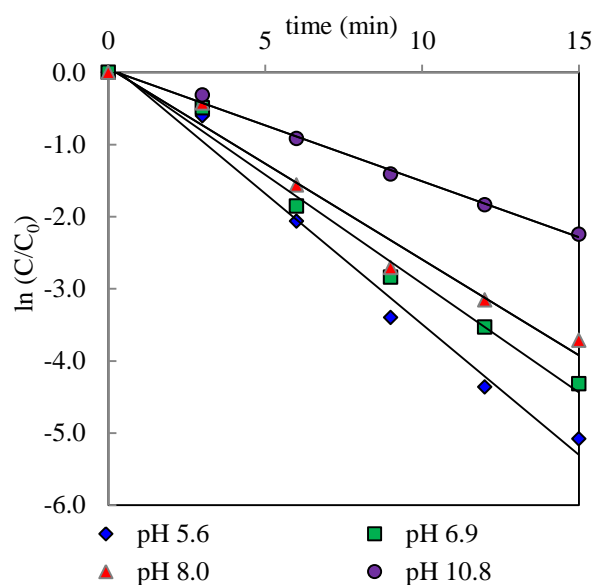


Fig.4.33 Pseudo-first-order kinetics of NPX photocatalytic degradation at different pHs

The superior degradation rate at low pH can be explained based on the NPX adsorption on TiO₂ P25. Acidic pH of 5.6 and near-neutral pH 6.9 showed greater adsorption ranging between 10-15% compared to alkaline pH, which demonstrated the lowest adsorption of 3%. As previously mentioned, the amphoteric nature of TiO₂ causes its surface to be positively charged (TiOH₂⁺) in acidic solution (pH < p*H*_{pzc}), while it is negatively charged (TiO⁻) at alkaline pH (pH > p*H*_{pzc}). NPX shows a p*K*_a value of 4.15 from the presence of carboxyl group at 25°C, which results in NPX typically existing in its neutral or protonated form at pH < p*K*_a, while at pH > p*K*_a the NPX molecule predominantly exists as its anion due to deprotonation of the carboxyl group. The favoured NPX adsorption at lower pH (acidic) above its p*K*_a is thus attributed to the anion attraction to the positively charged TiO₂ surface. Rosal *et al.* [143] observed a similar trend for NPX adsorption onto TiO₂ P25, where the TiO₂ surface was explained to act as an anion exchanger thus favouring high adsorption of NPX at acidic conditions (pH 3). It can therefore be concluded that the degradation rate of NPX at different initial pH values is determined by the amount of adsorption. A study by Yang *et al.* [211] also concluded that the initial pH, which influenced the adsorption, in turn affected the degradation rate of sulfa pharmaceuticals for the studied pH range of 3-11.

Besides affecting the ionization states of TiO₂ and NPX, the solution pH also affects the oxidative power of photogenerated holes and subsequent HO[•] radical generation [212]. Processes by positive holes have been reported to be favoured at acidic conditions [212]. At alkaline pH, HO[•] radicals can be easily scavenged [213] thus limiting the reaction between NPX and HO[•] radicals, which in turn lowers the degradation rate.

4.6.5. Effect of water matrix and anions

To assess the degradation of NPX under environmentally relevant conditions, the effect of anions on the TiO₂ photocatalytic degradation in river water and drinking water were considered. Anions, chloride and phosphate, were chosen as they are present in natural waters. Studies have shown that the presence of anions in water matrices can influence the photocatalytic degradation efficiency. The interpretation of anion effects in a water matrix can be complex due to ability of anions to change the ionic strength of the solution, thereby affecting the overall catalytic activity and photocatalytic degradation [214].

The influence of anions on the UV/TiO₂ photocatalytic degradation of NPX in comparison to UV/TiO₂ oxidation without any anions in river water and drinking water are shown in Fig.4.34a and Fig.4.34b, respectively. The salt added to the water matrices were potassium chloride and sodium dihydrogen phosphate. The anions involved in the degradation process were Cl⁻ and H₂PO₄⁻. For the purpose of discussion, these ions are referred to as chloride and phosphate anions. The natural pH of

both solutions, drinking water and in river water in the presence of anions at which experiments were performed ranged between 7.8 and 8.2, representing alkaline conditions.

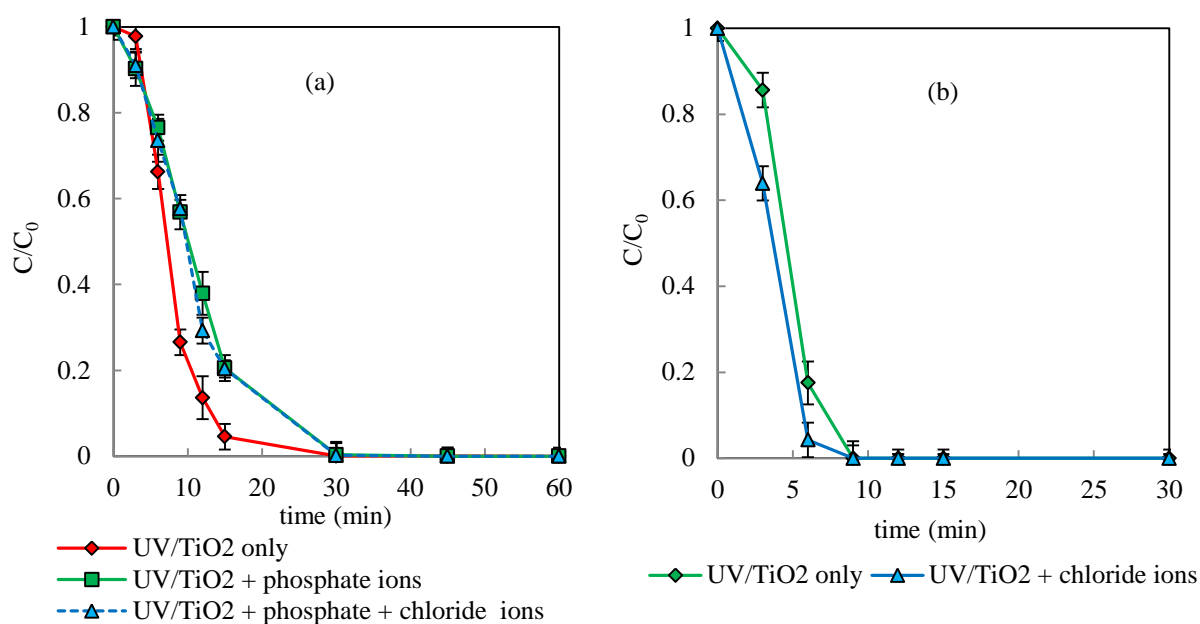


Fig.4.34 Effect of anions on photocatalytic degradation of NPX (30 mg/L, TiO₂ P25 0.1 g/L,) (a) river water (20 mg/L of phosphate and chloride) (b) drinking water (20 mg/L of chloride)

Fig.4.34a shows the effect of single (phosphate) and dual (phosphate and chloride) anions on the UV/TiO₂ photocatalytic degradation of NPX in unfiltered river water. The addition of both anions lowered the degradation rate of NPX when compared to UV/TiO₂ oxidation in their absence. The degradation was well-described by a pseudo-first-order kinetic model. The degradation rate of NPX UV/TiO₂ in river water in the absence of anions was 0.21 min⁻¹ (Table 4.12). Upon addition of either anions, phosphate and chloride in the UV/TiO₂ photocatalytic oxidation, degradation rates markedly decreased to 0.10 min⁻¹ and 0.11 min⁻¹, respectively (Table 4.12). Based on the obtained degradation rates, the effects due to the presence of single and dual ions in river water were rather marginal.

Table 4.12 Rate constants for TiO₂ photocatalytic degradation of NPX in the presence of anions in river water and drinking water

Water type and conditions	k_{app} (min ⁻¹) (R ²)
River water	
UV/TiO ₂ (no anions added)	0.21 ± 0.07 (0.93)
UV/TiO ₂ + phosphate	0.10 ± 0.05 (0.94)
UV/TiO ₂ + phosphate + chloride	0.11 ± 0.05 (0.94)
Drinking water	
UV/TiO ₂ (no anions added)	0.29 ± 0.13 (0.93)
UV/TiO ₂ + chloride	0.50 ± 0.21 (0.95)

In contrast, the addition of 20 mg/L of chloride anions to drinking water promoted the degradation rate of NPX when compared to UV/TiO₂ alone (Fig.4.34b and Table 4.12). Based on the degradation profile, 82.5% and 95.7% degradation was obtained after 6 min of irradiation from UV/TiO₂ oxidation and UV/TiO₂ oxidation in the presence of chloride anions, respectively. Both photocatalytic oxidation systems led to complete degradation after just 9 min of irradiation.

The lowered degradation rate in the presence of phosphate is due to its competition with NPX for adsorption on the TiO₂ surface which in turn deactivates active sites and scavenges HO[•] radicals both at the surface and in solution [215]. Phosphate has an ability to strongly adsorb on the TiO₂ surface over a wide range of pH thus hindering the photoactivity of TiO₂ [216]. In addition, the lowered degradation rate in the presence of anions in the unfiltered river water may be also linked to the naturally occurring organic matter hindering the degradation by filtering radiation required for the TiO₂ activation and competing for reactive sites [215]. The presence of phosphate has been reported to reduce the degradation of oxolinic acid and oxytetracycline as a result of strong adsorption on the TiO₂ surface [217].

The matrix pH has a large impact on the behaviour of chloride anions towards photocatalytic degradation. The observed improved degradation of NPX in the presence of chloride in drinking water can be explained by an ineffective HO[•] radicals scavenging effect of chloride as known for alkaline pH [215]. Chloride anions have been reported to strongly adsorb on the catalyst surface at low pH (e.g. pH 3) and to inhibit degradation. At alkaline pH, repelling effects between chloride and the negatively charged TiO₂ surface (pH_{pzc} = 6.25) do not favour adsorption. Also, chloride radicals have higher affinities for holes than HO[•] radicals, thus preventing the electron-hole pairs recombination and favouring degradations to take place as shown in Eq. 4.7 and Eq. 4.8 [218]:



According to Sirtori *et al.* [219] Cl[•] and Cl₂^{•-} are also strong oxidants ($E^{\circ}_{SHE} Cl^{\bullet}/Cl^- = 2.41 \text{ V}$; $E^{\circ}_{SHE} Cl_2^{\bullet -}/2Cl^- = 2.09 \text{ V}$) and can contribute to the oxidation of organic compounds. This may explain the positive effect of chloride observed on NPX degradation.

A study by Pereira *et al.* [217] also reported, compared to UV/TiO₂ only, a slight improvement in degradation rate for oxolinic acid in the presence of various anions such as chloride and nitrate.

Based on the results obtained in this study, phosphate anions significantly limited the degradation of NPX in river water while phosphate anions in the presence of chloride did not hinder the degradation

of NPX in the river water matrix. The role of chloride anions thus appeared to play an important role in the degradation of NPX.

4.7. Photocatalytic degradation of diclofenac and naproxen mixtures using an immersion-well reactor

To investigate the effect of the UV/TiO₂ oxidation system on a mixture of DCF and NPX, two conditions were considered. Initially, equal concentrations (1:1) of both NSAIDs were subjected to UV/TiO₂ photocatalytic treatment. Subsequently, the effect of non-equivalent API concentrations was investigated (e.g. DCF:NPX 1:2 or DCF:NPX 2:1). As concentrations of pharmaceuticals in the real environment vary, it is essential to consider the effect of varying concentrations of the API mixtures on photocatalytic degradation. In order to stimulate the interfering effects of anions on the TiO₂ photocatalytic degradation of DCF and NPX mixtures, additions of single and dual anion were also investigated.

The DCF degradation was more rapid than that of NPX in distilled water and drinking water in a 1:1 mixture (Fig.4.35). Degradation of NPX was observed to be slowest in drinking water in the presence of DCF with a degradation rate of 0.14 min⁻¹ (Table 4.13).

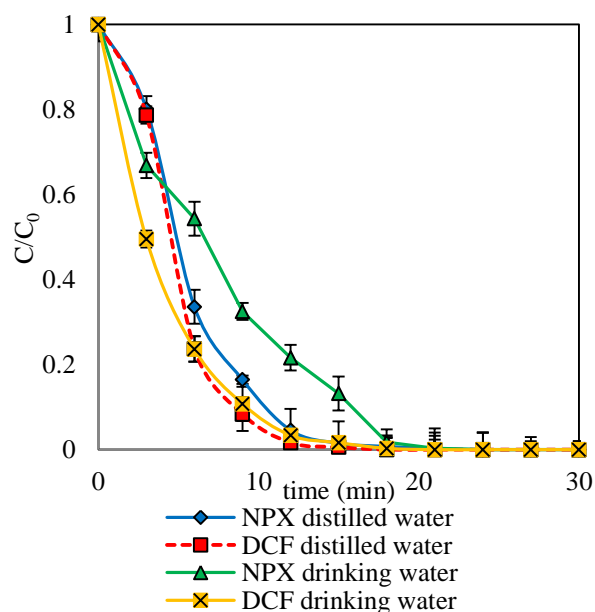


Fig.4.35 Photocatalytic degradation of DCF and NPX mixture (1:1) ($C_0 = 30$ mg/L; TiO₂ P25 0.1 g/L) in distilled water and drinking water

Table 4.13 Rate constants (k_{app}) of UV/TiO₂ degradation of DCF and NPX mixtures ($C_0 = 30$ mg/L) in distilled water and drinking water (UV/TiO₂ and UV/TiO₂ + anions)

DCF:NPX ratio	Water type and conditions	k_{app} (min ⁻¹) (R ²)	
		DCF	NPX
	Distilled water		
1:1	UV/TiO ₂	0.36 ± 0.11 (0.97)	0.30 ± 0.08 (0.98)
2:1	UV/TiO ₂	0.25 ± 0.09 (0.96)	0.13 ± 0.04 (0.99)
1:2	UV/TiO ₂	0.25 ± 0.05 (0.96)	0.22 ± 0.10 (0.99)
	Drinking water		
1:1	UV/TiO ₂	0.31 ± 0.15 (0.98)	0.14 ± 0.02 (0.98)
	UV/TiO ₂ + anions		
	+ chloride (20 mg/L)	0.17 ± 0.06 (0.99)	0.09 ± 0.02 (0.97)
	+ phosphate + chloride (20 mg/L)	0.15 ± 0.05 (0.99)	0.06 ± 0.02 (0.98)
Individual API	Distilled water (UV/TiO ₂)	0.25 ± 0.06 (0.97)	0.30 ± 0.08 (0.97)
	Drinking water (UV/TiO ₂)	0.17 ± 0.05 (0.99)	0.29 ± 0.13 (0.92)

An increase in either DCF or NPX concentration appeared to affect the degradation of NPX as noticed from in the degradation rates. The effect of a higher concentration of DCF versus NPX (DCF:NPX 2:1) was more prominent as the degradation rate of NPX decreased from 0.30 min⁻¹ to 0.13 min⁻¹ (Table 4.13) and required almost 45 min of irradiation to achieve complete degradation compared to only 24 min in the 1:1 ratio system. In contrast, DCF was completely degraded after 15 min although a slight decrease in the degradation rate was observed (Fig.4.36a).

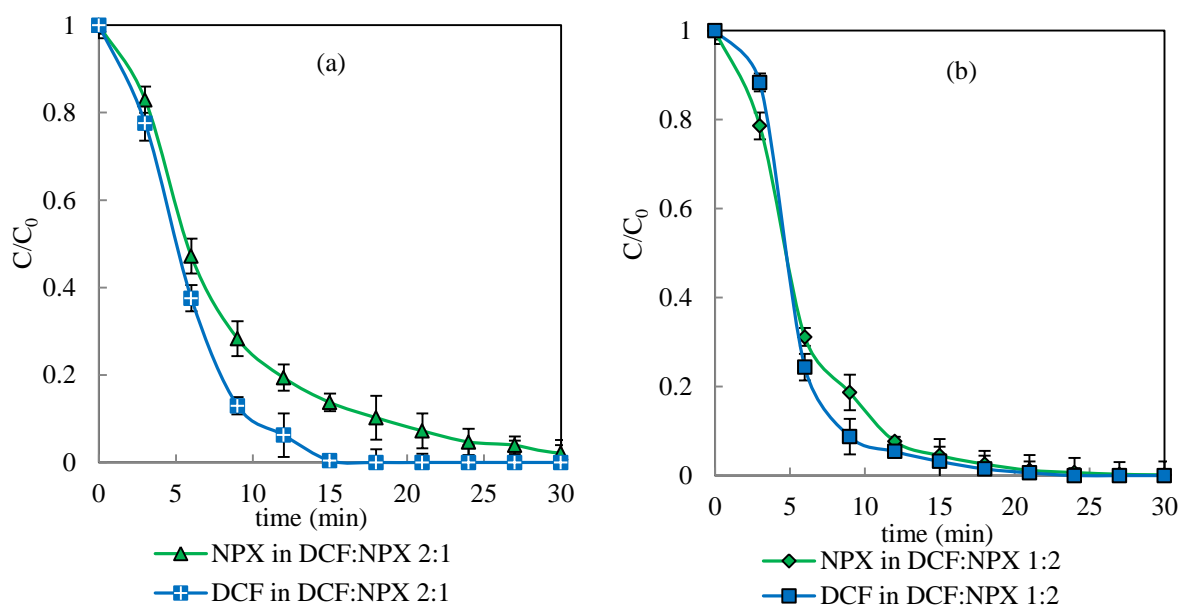


Fig.4.36 Photocatalytic degradation of DCF and NPX mixtures (a) DCF:NPX (2:1) and (b) DCF:NPX (1:2) in distilled water

When the concentration of NPX was increased by two-fold over DCF, no substantial difference in total degradation time for NPX was observed although the degradation rate of NPX increased slightly to 0.22 min^{-1} (Table 4.13). Again, a prolonged irradiation time of at least 30 min was required for NPX while DCF required 21 min to achieve complete degradation (Fig.4.36b).

The degradation rate constants of DCF and NPX decreased when their amounts were not equal. This phenomenon is more likely to be encountered when more than APIs are present during the application of TiO_2 process due to their interactions and competition for the HO^\bullet radicals, which may affect the overall degradation performance.

When compared to the individual APIs, NPX was more readily degraded by UV/ TiO_2 on its own while in mixtures with DCF, DCF was observed to degrade faster. This result implies the different behaviour of APIs when they are present individually in water and in the presence of other APIs.

The effects of anions on the photocatalytic transformation of DCF and NPX mixtures in drinking water are shown in Fig.4.37. The degradation rate of both DCF and NPX were substantially suppressed due to the presence of anions in drinking water, especially when dual anions were present (Table 4.13). As observed for the 1:1 mixture, DCF was reduced significantly faster than NPX in drinking water (Fig.4.37). DCF was completely reduced after 30 min of irradiation even in the presence anions. In comparison, NPX required almost 120 min to achieve complete degradation in both cases.

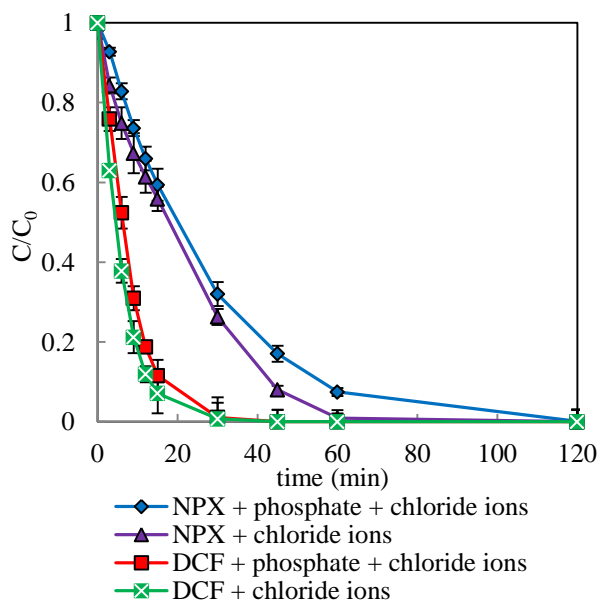


Fig.4.37 Effect of anions on TiO_2 photocatalysis of DCF:NPX (1:1) mixtures in drinking water ($C_0 = 30 \text{ mg/L}$ DCF and NPX; TiO_2 0.1 g/L ; 20 mg/L phosphate and chloride)

The presence of phosphate was more detrimental than chloride for the mixtures. As previously explained this is attributed to the strong binding capacity of phosphate anions on the TiO_2 surface. The ion attaches to the surface of Ti^{4+} by removal of OH groups and this bonding effect is less pronounced for chloride anions [220]. Despite this fact, the interpretation of these results obtained for the mixtures were rather complex due to the presence of two APIs in the solution matrix and their potential interactions with one another in the presence of anions. The competitive surface occupation by these anions with both APIs and other intermediates formed during the photocatalysis needs to be also considered.

4.8. Mineralization in the immersion-well

The degrees of mineralization, as DOC removal, achieved in the immersion-well reactor by direct photolysis and TiO_2 photocatalysis were compared for DCF, NPX and their mixtures. There was no significant DOC removal found for DCF (~3% only) and NPX during direct photolytic treatment in distilled water. Despite reasonable degradations observed for both APIs by direct photolytic treatment, mineralization was not achieved with this degradation method. This simply suggests that most organic degradation products were not susceptible to mineralization by direct photolysis.

In comparison, DOC removal was observed to be more effective by TiO_2 photocatalysis for both DCF and NPX, although it was found to be low compared to the degradation induced by TiO_2 photocatalysis for both APIs together. A maximum DOC removal of 38% and 25% was observed for DCF in distilled water and drinking water, respectively, after 180 min of irradiation (Fig.4.38a).

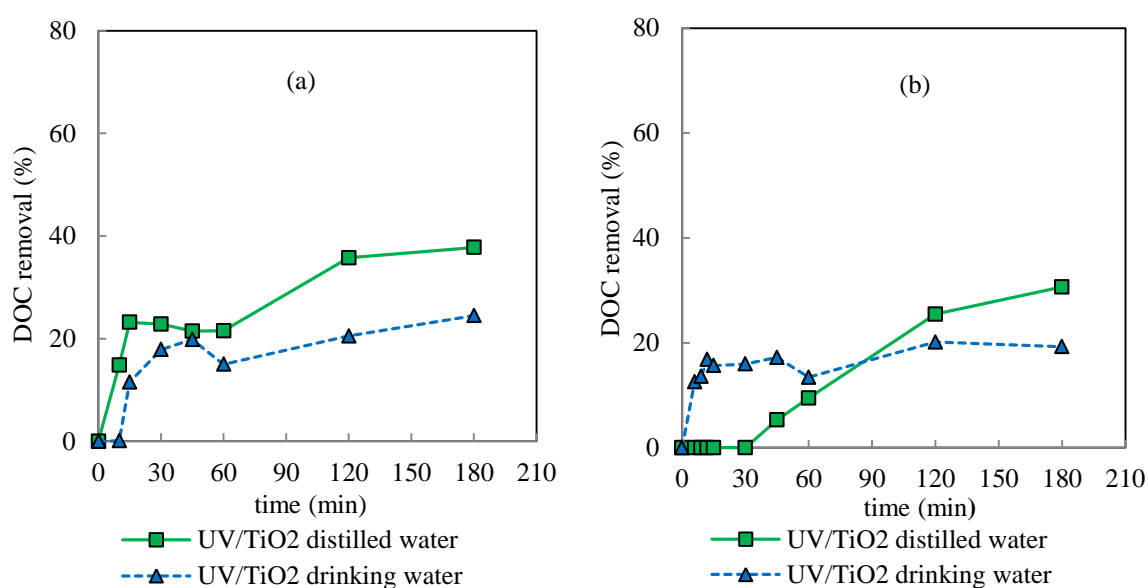


Fig.4.38 DOC removal in the immersion-well during TiO_2 photocatalysis of (a) DCF and (b) NPX in distilled water and drinking water

On the other hand, DOC removal achieved for TiO₂ photocatalysis of NPX after 180 min of treatment was about 30% in distilled water and 19% in drinking water (Fig.4.38b). For both APIs, DOC removal was slightly higher in distilled water than drinking water possibly due to existing DOC content in the drinking water. The DOC removal profiles followed a similar pattern for both DCF and NPX and removal occurred quickly during the initial 30 min, and slowed down thereafter with the exception for DOC removal for NPX in drinking water. A much steeper slope was encountered after 30 min, where the removal increased with the irradiation time.

DOC removal for DCF and NPX mixtures was rather promising as both direct photolysis and TiO₂ photocatalysis demonstrated some degree of DOC removal (Fig.4.39). DOC removal by direct photolysis in the mixtures suggests that besides favouring degradation of parent APIs, this process can also facilitate removal of degradation products. However, the overall low DOC removal observed was due to the multiple stable intermediates from both APIs and also hybrid degradation products as a result of the interactions between both APIs or between the intermediates. The best performance of DOC removal of 48% was produced by TiO₂ photocatalysis for the DCF and NPX mixtures.

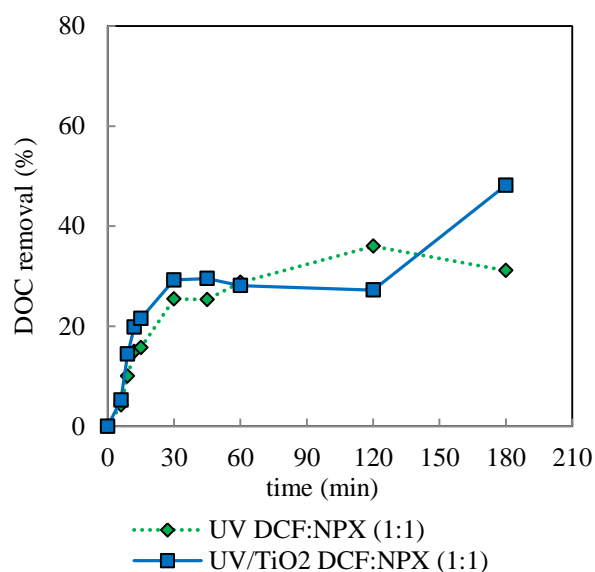


Fig.4.39 DOC removal during direct photolysis and TiO₂ photocatalysis of DCF and NPX mixtures in distilled water

4.9. TiO₂ photocatalytic degradation using a loop reactor

The optimized concentrations and TiO₂ loading from the immersion-well experiments were subsequently applied to degradation studies with the laboratory-scale Laboclean[®] loop reactor of the individual, DCF and NPX and their mixtures.

4.9.1. Diclofenac

Fig.4.40 compares the photocatalytic degradation of DCF in drinking water and distilled water using the laboratory-scale loop reactor. Degradation fitted pseudo-first-order kinetics ($R^2 > 0.98$). After 15 min of irradiation, TiO₂ photocatalysis degraded 97% of DCF in distilled water while 59% of DCF was degraded in drinking water over the same irradiation time. In comparison, UV/TiO₂/H₂O₂ enhanced the degradation of DCF in both water matrices. The addition of 250 mg/L of H₂O₂ enhanced the degradation of DCF to completion and 10 min were required in distilled water. In drinking water, complete degradation occurred within 30 min of irradiation.

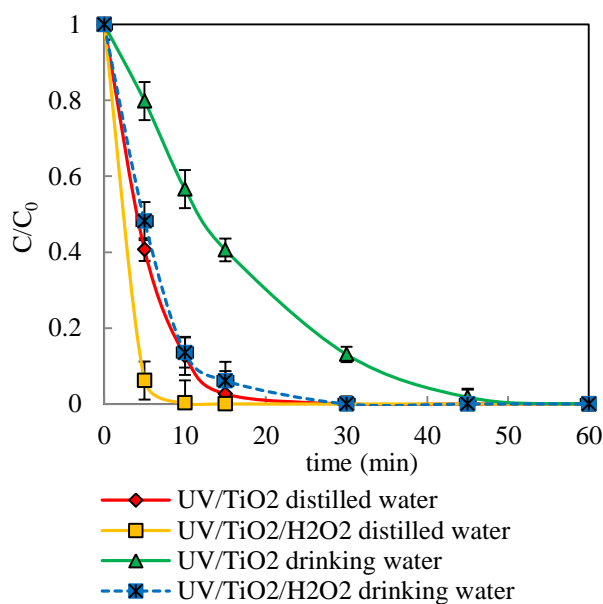


Fig.4.40 Photocatalytic oxidation (UV/TiO₂ and UV/TiO₂/H₂O₂) of DCF in distilled water and drinking water in the loop reactor

The enhanced degradation in the presence of H₂O₂ during the photocatalytic process in both water matrices was attributed to the generation of additional HO[•] radicals (Eq. 4.9) as the reactor material (quartz mantle) does allow direct cleavage of H₂O₂ (UV/H₂O₂). The ability of H₂O₂ to act as an

electron acceptor that inhibits the recombination of electron-hole pairs may have further contributed [221].



Also, larger photon flux of 500 W from the medium pressure Hg lamp in the loop reactor compared to only 150 W lamp in the immersion-well reactor.

4.9.2. Naproxen

NPX was efficiently degraded in the loop reactor (Fig.4.41). Complete degradation of NPX was obtained after 15 min under both conditions, while drinking water required up to 20 min to reach similar degradation levels. The efficient degradation of NPX in this reactor can be explained by efficient photon emission from the 500 W medium pressure Hg lamp and also the efficiency of NPX as strong absorber as a result of its UV absorption up to 340 nm.

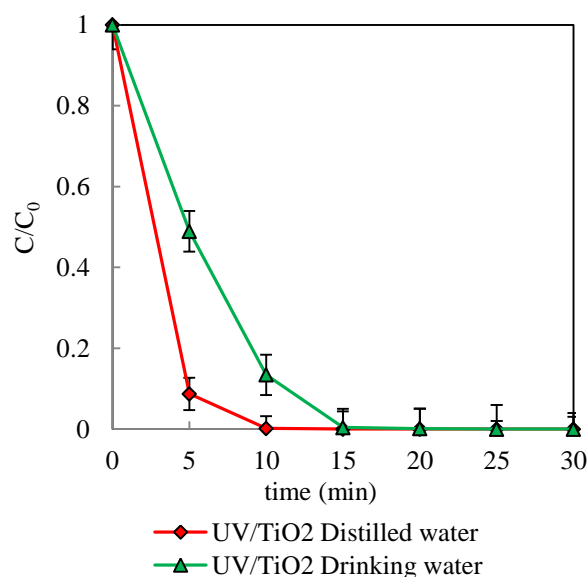


Fig.4.41 TiO₂ photocatalysis of NPX in distilled water and drinking water in the loop reactor (C₀ = 30 mg/L; TiO₂ = 0.1 g/L)

4.9.3. Diclofenac and naproxen mixtures

The degradation of DCF and NPX mixtures in distilled water and drinking water using the loop reactor are shown in Fig.4.42a and Fig.4.42b, respectively. In the mixtures, UV/TiO₂ efficiently degraded DCF within 10 min in both water matrices. DCF degradation also proceeded much faster than NPX in both water matrices. In contrast, NPX in drinking water needed almost 30 min of

irradiation until complete degradation from the mixture was achieved. The efficiency of the loop reactor was once again demonstrated as it efficiently degraded both compounds in the mixture regardless of the water matrix.

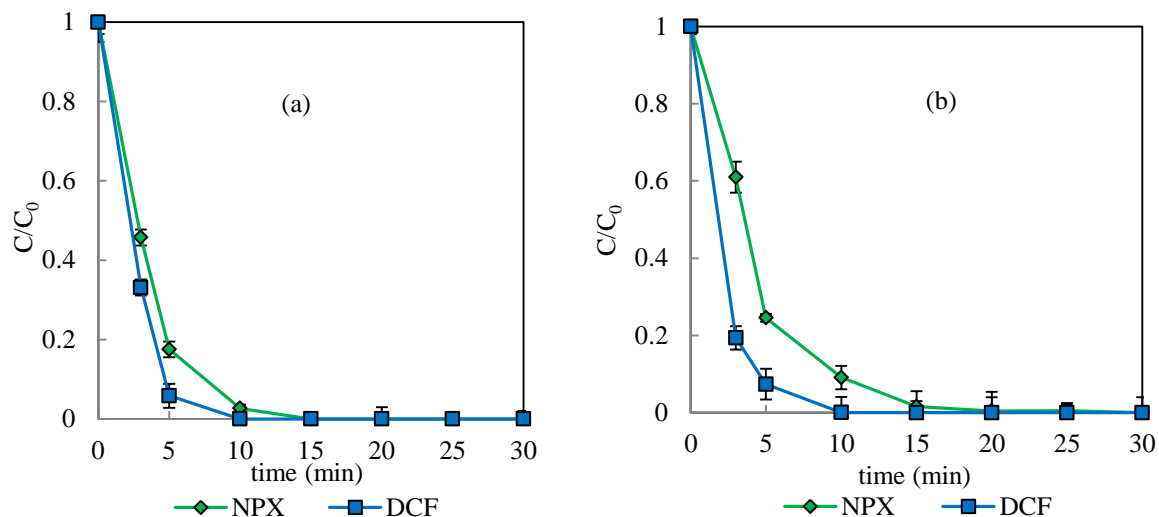


Fig.4.42 TiO₂ photocatalysis of DCF and NPX (1:1) mixtures in the loop reactor (a) distilled water and (b) drinking water ($C_0 = 30$ mg/L; TiO₂= 0.1 g/L)

4.10. Mineralization in the loop reactor

The results from the removal of DOC using the loop reactor for the individual APIs, DCF, NPX, and their mixtures are compiled in Fig.4.43. When compared to the DOC removal in the immersion- well reactor, a much higher removal took place in the loop reactor which coincided with high degradation efficiencies of the individual APIs and their mixtures. The photons emitted at 254 nm and the higher power output of the medium-pressure Hg lamp enhanced the mineralization as well as the degradation of the APIs and their breakdown products.

The DOC removal profiles for the direct photolysis of DCF in drinking water and distilled water were rather similar (Fig.4.43a). Both proceeded at a slow rate and resulted in a maximum removal of 27%. Although direct photolysis was capable of degrading the parent DCF, this oxidation method was less efficient in oxidizing its intermediates and degradation products. This observation is in line with the results obtained using the immersion-well reactor. Within the experimental timeframe of 3 h, TiO₂ photocatalysis contributed to a slightly higher DOC removal both in distilled water and drinking water and increased the removal to 33% and 34%, respectively. The carboxylic acids generated might result in a less significant DOC removal. Carboxylic acids cannot be further oxidized and as a result of this DOC, did not show any significant decrease.

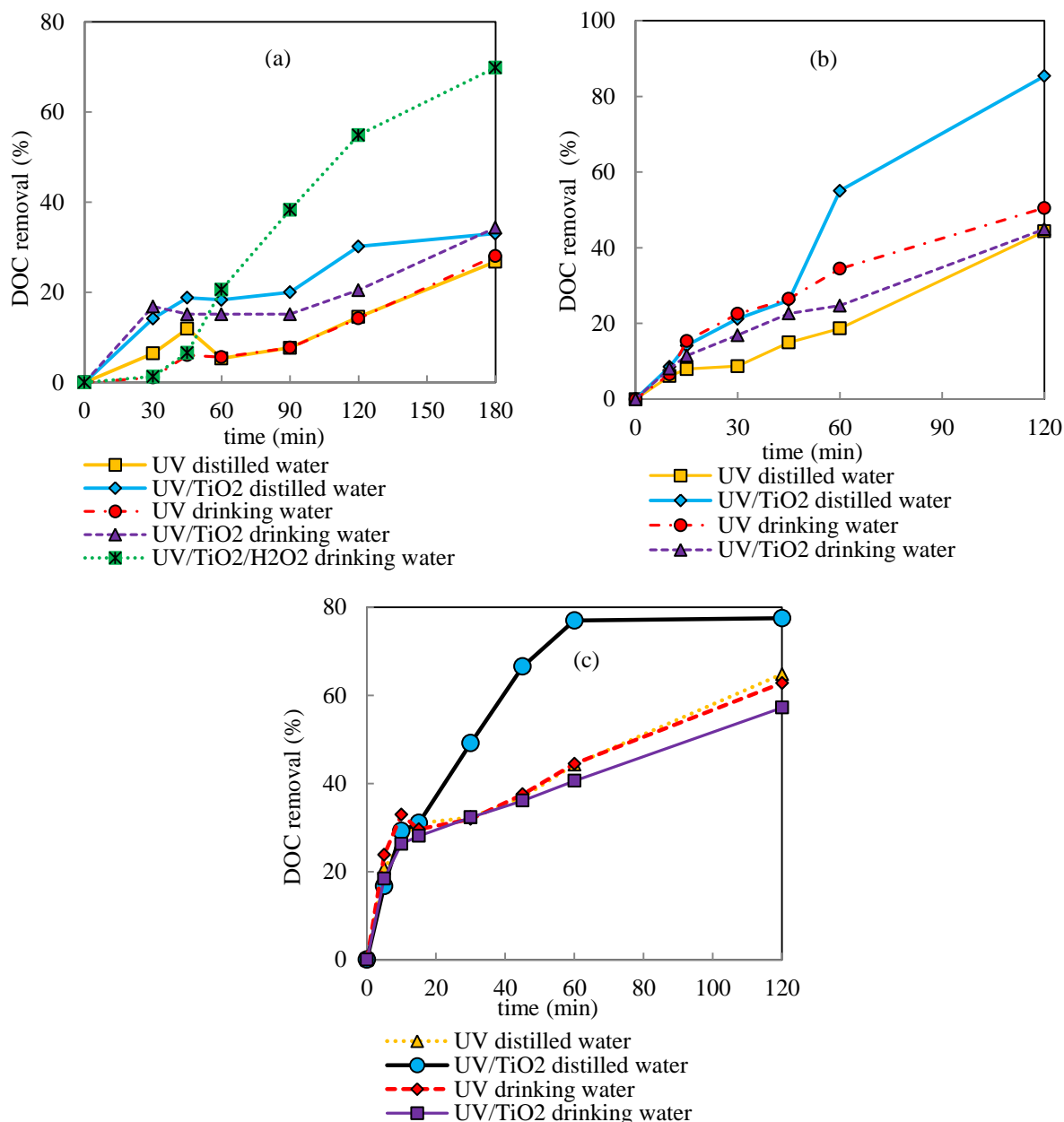


Fig.4.43 DOC removal in the loop reactor for (a) DCF, (b) NPX and (c) DCF and NPX (1:1) mixtures

TiO₂ photocatalytic oxidation in the presence of H₂O₂ corresponded to the highest DOC removal in drinking water with 70% for the same period of irradiation possibly due to additional HO[•] radicals involved in oxidizing the intermediates or formation of other intermediates in the presence of H₂O₂ which could have increased the DOC removal. Thus, H₂O₂ besides efficiently degrading DCF in drinking water, also considerably increased the DOC level.

TiO₂ photocatalytic treatment of NPX in distilled water yielded the highest degradation of 85% (Fig.4.43b). Addition of TiO₂ significantly enhanced the degradation in distilled water compared to

direct photolysis only. In drinking water, direct photolysis displayed a slightly higher DOC removal than TiO₂ photocatalysis with percentages of 51% and 45%, respectively. The somewhat lower DOC removal upon TiO₂ photocatalysis can be attributed to the formation of multiple higher molecular weight products than NPX itself during the degradation process.

As for the DCF and NPX mixture, DOC removal was much more efficient than for the individual APIs as demonstrated by both direct photolytic and TiO₂ photocatalytic operations (Fig.4.43c). The UV/TiO₂ profile for distilled water showed a constant increase up to a DOC removal to 70% over the first 60 min and remained constant thereafter, this is most likely due to the presence of multiple stable intermediates from their synergistic interactions. Again, TiO₂ photocatalysis in drinking water displayed slightly lower DOC removal. There were no substantial differences encountered in the mineralization upon direct photolytic treatment in both water matrices. The DOC removals were 63% in distilled water and 65% in drinking water.

4.11. Conclusions

From this work, it has been demonstrated that DCF, NPX and their mixtures in aqueous solution can be degraded by applying both direct photolysis and TiO₂ photocatalysis. Mineralization measured as DOC was observed to be much slower than the rapid degradation of parent APIs. The DOC indicator reported in this chapter only measured the fraction of organic carbon present in solution after filtration through a filter with pore diameter of 0.45 μm. Thus, organic carbon from degradation products which could have precipitated may have not been measured.

Direct photolysis despite effectively degrading APIs in water matrices was unable to oxidize the intermediates and degradation products. Thus, TiO₂ photocatalysis may offer a better option as it demonstrated better performance for both mineralization and the API degradation. Successful application of TiO₂ photocatalysis however is governed by various operational factors such as TiO₂ concentration, initial concentration of APIs and water matrix was found based on the optimization study performed on the immersion-well reactor. For example, TiO₂ photocatalysis of DCF showed that TiO₂ concentration, DCF concentration, water matrix, solution pH and nature of glass (pyrex or quartz) affects the degradation rate of DCF. Maximum degradation for 30 mg/L of DCF was obtained in the presence of 0.1 g/L TiO₂ P25 at the pH~6.2. Performance of TiO₂ photocatalysis on NPX degradation was observed to be governed by TiO₂ concentration, initial NPX concentration, pH and water matrix and anions. A loading of 0.1 g/L of TiO₂ was found to be optimal for high initial concentrations of NPX, 30 and 50 mg/L as higher TiO₂ loadings did not improve the degradation rates of these concentrations. The degradation rates of DCF and NPX decreased in the mixtures containing non-equivalent ratios of the APIs.

The larger loop reactor efficiently degraded the individual APIs and their mixtures by direct photolysis and TiO₂ photocatalysis and also produced a slightly higher extent of mineralization for all APIs. Its performance can be exclusively associated to the high power of 500 W power medium pressure Hg lamp, which housed in a quartz mantle allowing UV-C irradiation to participate in the degradation process. The performance of this reactor can therefore be considered more effective than the immersion-well reactor for both degradation and mineralization of APIs.

One factor which significantly affects the degradation efficiencies and mineralization in both protocols is the water matrix. The successful application of these protocols needs to be studied with respect to the natural organic matter content present particularly when dealing with raw waters.

Chapter 5. Solar photolytic and TiO₂ photocatalytic degradation of pharmaceuticals

5.1. Introduction

Phototransformations of pharmaceuticals through exposure to direct solar radiation represent important elimination routes in the environment. Sunlight also constitutes a green and economical option for the photochemical degradation of pharmaceutical compounds. The sustainability and cost advantages of activating TiO₂ by solar irradiation makes this a promising approach for the degradation of the selected APIs. Solar radiation varies with geographic latitude, time of the day, time of the year, cloud cover and also atmospheric conditions [125], and can also be diffuse radiation or direct radiation. The location of this study, Townsville, is labelled as Queensland's solar city as it receives more than 300 days of sunshine per year. All solar experiments were performed between July and December 2012 thus representing two distinct seasons, dry and wet. Typically the wet season is known to be hotter than the dry season.

Degradation experiments of DCF and NPX as individual compounds and their mixtures was conducted utilizing direct photolysis and TiO₂ photocatalysis with the same immersion-well photoreactor used for laboratory degradation studies. This approach was sought to permit a reasonable comparison between artificial UV radiation and solar radiation by eliminating differences caused by the geometry of the photoreactor. However, solar exposure requires sunlight to pass through the solar reactor vessel (outside-in) whereas irradiation with artificial light requires light to pass the immersion-well cooler (inside-out). The internal reactor dimensions however, remained the same. The performance of solar radiation for API degradation was evaluated based on degradation kinetics and the degree of mineralization measured by the chemical oxygen demand (COD). COD can be used as an indicator to determine the degree of mineralization [222].

5.2. Solar degradation of diclofenac

Solutions of DCF in distilled water, drinking water and river water were exposed to solar photolysis (solar only and solar/H₂O₂) and solar TiO₂ photocatalysis (solar/TiO₂ and solar/TiO₂/H₂O₂) conditions. Typical operating parameters for DCF solar photodegradation studies are referred to in Table 3.5 (Chapter 3). All DCF solar degradation experiments were conducted during the months of October and November 2012, which corresponds to the spring season in Australia. A summary of all solar degradation studies of DCF is presented in Table 5.1. Experimental degradation data of DCF in

laboratory studies have been reported to follow pseudo-first-order kinetics [149, 164]. All degradation data in this study fitted well to pseudo-first-order kinetics as shown in Table 5.1.

Table 5.1 Summary of solar degradation studies on DCF

Water type	Oxidation system	Mean DCF degradation (%) (after 360 min)	Rate constant k_{app} (min^{-1}) (R^2)	Average solar light intensity (Lux)	Mean COD reduction (%)
Distilled water	Solar photolysis	95.7	0.0089 ± 0.0009 (0.97)	48300	39.0
	Solar/TiO ₂	100.0	0.0233 ± 0.0051 (0.99)	42800	44.1
Drinking water	Solar photolysis	84.0	0.0051 ± 0.0009 (0.99)	54600	19.8
	Solar/H ₂ O ₂	98.9	0.0127 ± 0.0006 (0.99)	43200	46.7
	Solar/TiO ₂	54.1	0.0019 ± 0.0005 (0.97)	60900	43.8
	Solar/TiO ₂ /H ₂ O ₂	100.0	0.0241 ± 0.0033 (0.98)	40600	56.2
River water	Solar photolysis	82.4	0.0051 ± 0.0009 (0.99)	46500	22.2
	Solar/TiO ₂	65.7	0.0028 ± 0.0012 (0.97)	52600	46.5

Fig.5.1(a) and Fig.5.1(b) show the effects of solar photolysis (solar and solar/H₂O₂) and solar TiO₂ photocatalysis (solar/TiO₂ and solar/TiO₂/H₂O₂) on DCF degradation. Solar/TiO₂ photocatalysis of DCF in distilled water (Fig.5.1b) presented a much faster degradation in comparison to solar photolysis (Fig.5.1a). Complete DCF degradation was accomplished after 240 min of illumination under solar/TiO₂ conditions, while solar photolysis resulted in incomplete degradation with 95.7% degradation even after 360 min of solar exposure. This longer time required for the degradation under solar radiation did not correspond to results obtained under laboratory conditions. Using artificial UV light, 99% of DCF elimination by TiO₂ photocatalysis and direct photolysis was achieved with only 15 min and 21 min radiation, respectively, in distilled water. This could be attributed to the fact that only 3-4% of sunlight is in the UV region [88].

COD did not change substantially between the two protocols although COD was decreased by 44% with solar/TiO₂, while solar photolysis caused a slightly lower COD reduction of 39% (Fig.5.2).

In order to assess the effect of the water matrix, drinking water and raw river water spiked with solutions of DCF were also exposed to sunlight. Interestingly, photolysis produced higher degradation than solar/TiO₂ photocatalysis in both the drinking and river water. As previously

indicated, solar/TiO₂ was more efficient at degrading DCF in distilled water compared to solar photolysis.

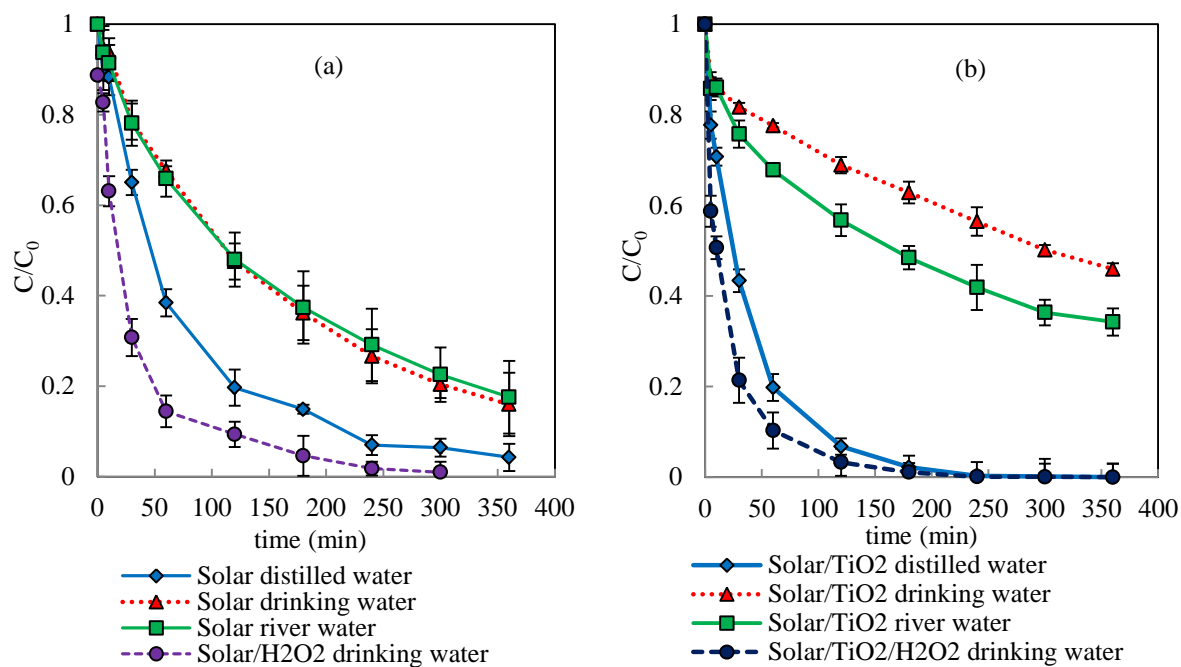


Fig.5.1 Solar degradation of DCF by (a) solar photolysis and (b) solar/TiO₂ photocatalysis (solar/TiO₂ and solar/TiO₂/H₂O₂) in different water matrices at natural pH ($C_0 = 30$ mg/L; TiO₂ = 0.1 g/L; H₂O₂ = 250 mg/L)

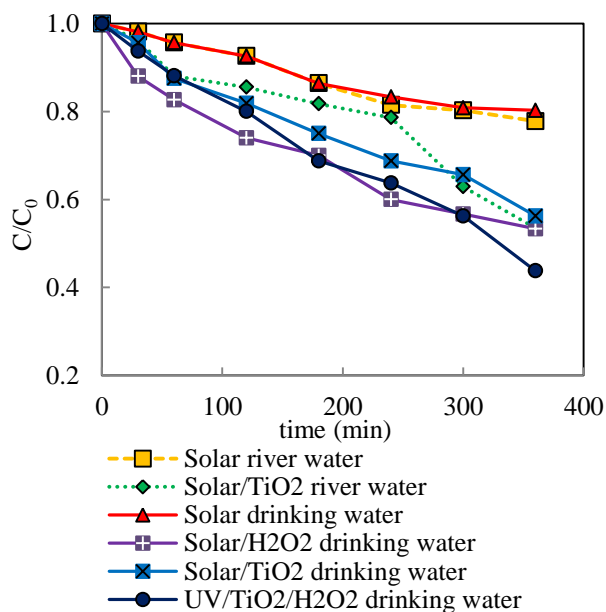


Fig.5.2 COD reduction of DCF during solar photolysis and solar/TiO₂ photocatalysis

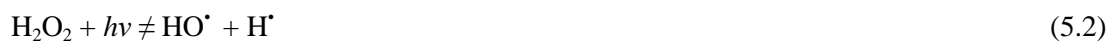
Solar photolysis of DCF in drinking and river water reduced the initial DCF concentration consistently and at the same rate over the entire illumination time (Fig.5.1a). Solar/TiO₂ displayed a higher degradation rate (steeper slope) of DCF in river water as compared to drinking water during the initial exposure period up to 240 min but slowed down afterwards (Fig.5.1b). Comparison of the two solar exposure protocols shows DCF in river water was only degraded by 66% upon solar/TiO₂ treatment, while 82% degradation was achieved under direct sunlight after the same period of time, 360 min. Likewise, a total of 84% and 53% degradation was accomplished with drinking water under direct photolysis and solar/TiO₂, respectively. In contrast, COD was reduced more effectively in drinking water and river water during solar/TiO₂ with 44% and 47%, respectively, after 360 min of exposure (Fig.5.2).

Despite a lower degradation of DCF by solar/TiO₂ (Fig.5.1b), COD reduction in drinking and river water was doubled compared to the percentages obtained from direct solar photolysis, indicating a higher efficiency of this AOP to oxidize degradation intermediates. Nevertheless, incomplete mineralization implies the formation of degradation products originating from DCF and from other organic content in those water matrices [223]. A previous study, which examined the effect of solar photolysis on DCF in both demineralized and synthetically prepared standard freshwater reported a total of 13 degradation products [139], indicating there are a multitude of possible degradation pathways occurring at varying rates.

The solar photolysis results from this study confirm the importance of this degradation route for DCF. A related study with demineralized water and prepared freshwater also highlighted the importance of direct solar illumination for the removal of 50 mg/L DCF. A total degradation of 68% after 32 h and 85% after 62 h for demineralized water and prepared freshwater, respectively, was obtained [166]. Several studies have highlighted the photo-sensitive nature of DCF and that it rapidly undergoes degradation in surface water via direct photolysis [26, 159].

The somewhat lower efficiency of TiO₂ photocatalysis compared to direct photolysis involving DCF was associated with a deficiency in HO[•] radicals and other oxidizing species caused by the presence of naturally occurring organic matter, anions and bicarbonates [224]. The hardness of the sampled river and drinking water measured as CaCO₃, was 151.6 mg/L and 41.8 mg/L, classified as hard and soft, respectively. Inorganic anions such as chloride and sulphate were also detected in the raw water samples (Table 3.1) as they are common anions in natural waters. Radical scavenging due to the presence of such compounds has been linked to a decrease in photocatalytic degradation, in particular when raw water samples from wastewater treatment plants or surface water were used [117, 225].

Another advanced oxidation method, solar/TiO₂/H₂O₂ demonstrated greater degradation efficiency in drinking water than solar/TiO₂ photocatalysis. Upon addition of 250 mg/L of H₂O₂, DCF was completely oxidized after 240 min whereas only 44% degradation was obtained from solar/TiO₂ oxidation after similar solar exposure (Fig.5.1b). The degradation rate also showed an increase from 0.0019 min⁻¹ to 0.0241 min⁻¹ (Table 5.1 and Fig.5.3). The addition of H₂O₂ to TiO₂ also increased COD reduction to 56% compared to only 44% in the absence of H₂O₂ (Fig.5.2). Compared to illumination in the absence of H₂O₂, solar/H₂O₂ direct photolysis also enhanced DCF degradation in drinking water from 84.0% to 99%. Likewise, the COD reduction increased from 20% to 47% in the presence H₂O₂ (Fig.5.3). The results from this study were comparable with those in a report by Méndez-Arriaga *et al.* [226] for ibuprofen. Direct photochemical cleavage of H₂O₂ by solar photon absorption to produce HO[•] radicals or other radical species as shown in Eq. 5.1 and Eq. 5.2 [226] is unlikely, instead H₂O₂ might act as an oxidant for the degradation intermediates.



The promotion of API degradation by H₂O₂ is attributed to the additional supply of HO[•] radicals in the TiO₂ photocatalytic system.

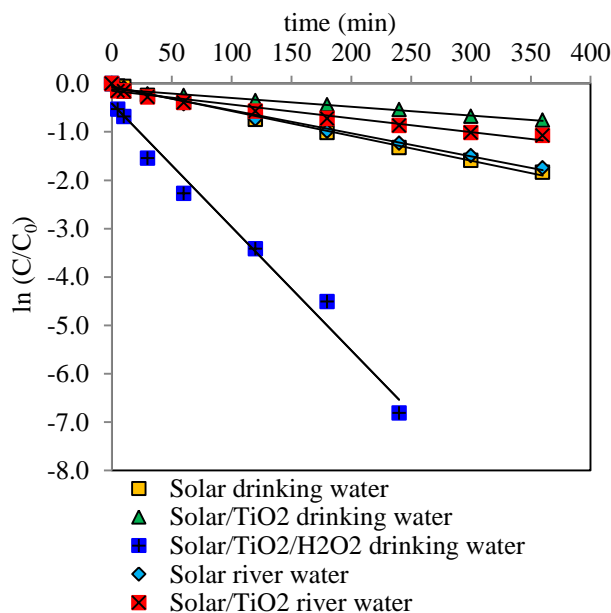


Fig.5.3 Pseudo-first-order kinetics for solar photolysis and TiO₂ photocatalysis (solar/TiO₂ and solar/TiO₂/H₂O₂) of DCF in drinking water and river water

Fig.5.4 shows select examples of solar light intensity (measured in Lux) and temperature variations experienced during the photodegradation studies of DCF in October and November 2012,

respectively. Solar light intensities in experiments fluctuated, with higher intensities recorded for the initial hours of exposure. However, the light intensity did not show a clear correlation to the DCF degradation (Table 5.1). Instead, differences caused by water matrix effects appear to be more dominant. Water matrices or compositions have been identified as important factors in literature, and their effects may vary from inhibition to promotion of oxidation [9].

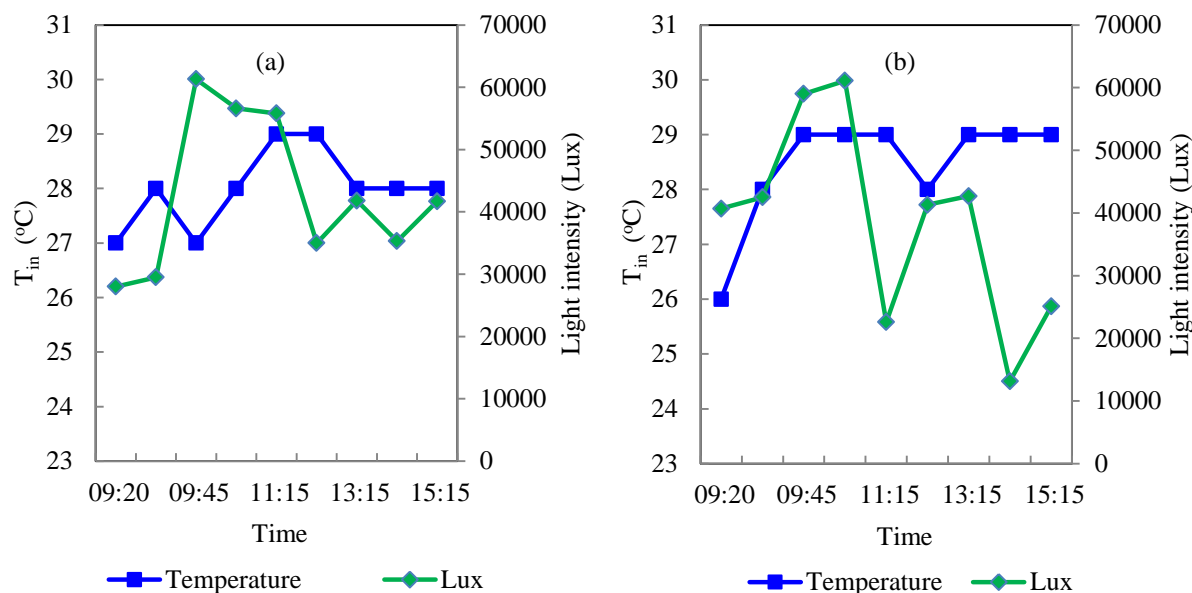


Fig.5.4 Typical variation of lux and temperature in the reactor on (a) 8th October 2012 during TiO_2 photocatalysis (solar/ TiO_2) of DCF in distilled water, and (b) 12th November 2012 (during TiO_2 photocatalysis (solar/ TiO_2/H_2O_2) of DCF in drinking water

Temperatures inside the immersion-well reactor during all solar degradation experiments typically varied from 24–30°C, while ambient temperatures ranged from 26 to 32°C. The temperatures recorded for all solar photodegradation studies increased from morning until about 1 or 2 pm then decreased slowly or remained almost constant until the end of experiment. The variations of up to 6°C within the immersion-well reactor had little to no impact on the overall degradation efficiency. This finding is corroborated by a TiO_2 photocatalysis study on DCF using a solar simulator and temperatures of 20, 30 and 40 C, which showed no effect on the photocatalytic degradation of DCF [142].

With regard to pH evolution, the pH of river water samples was not significantly affected during the course of the illumination, which suggests a buffering capacity of natural freshwater as proposed by Agüera *et al.* [139]. Noticeable pH changes did, however become evident in the solar/ TiO_2/H_2O_2 treatment as compared to solar/ TiO_2 system. A similar behaviour was reported for the solar degradation of ibuprofen by TiO_2 with and without H_2O_2 [226].

5.3. Solar degradation of naproxen

Photodegradations of NPX were also conducted under sunlight to evaluate the efficiency of solar irradiation on the degradation of this API. In addition, the influence of anions (phosphate and chloride) on NPX breakdown was also evaluated. All NPX solar photolysis and solar TiO₂ photocatalysis experiments were conducted in July 2012, which represents the Australian winter season, while experiments investigating anion effects were performed in November 2012 (spring season). A summary of solar photodegradation studies on NPX is presented in Table 5.2. Most degradation data for NPX fitted well with pseudo-first-order kinetics ($R^2 > 0.93$), except for the experimental data of solar TiO₂ photocatalysis in drinking water, which followed second-order kinetics. The profiles of solar photolyses in distilled water and drinking water displayed similar degradation trends (Fig.5.5).

Table 5.2 Summary of solar degradation studies of NPX

Water type	Oxidation system	NPX degradation (%) (after 360 min)	Rate constant k (min ⁻¹) (R ²)	Average solar light intensity (Lux)	Mean COD removal (%)
Distilled water	Solar photolysis	100	0.0302 ± 0.0002 (0.98)	73833	50.4
	Solar TiO ₂	100	0.043 ± 0.010 (0.93)	51778	68.0
Drinking water	Solar photolysis	100	0.0499 ± 0.0013 (0.94)	68722	47.4
	Solar TiO ₂	95.2	0.0016 ± 0.0005 (0.87)*	88878	48.0
	Solar TiO ₂ + chloride	100	0.2431 ± 0.010 (0.98)	46244	56.5
River water	Solar photolysis	93.2	0.0155 ± 0.0023 (0.97)	30716	51.9
	Solar TiO ₂	100	0.0392 ± 0.0015 (0.99)	59816	57.7
	Solar TiO ₂ + chloride + phosphate ⁻	100	0.0357 ± 0.0028 (0.98)	46873	43.8

* Second-order-kinetic model (L/mg.min⁻¹)

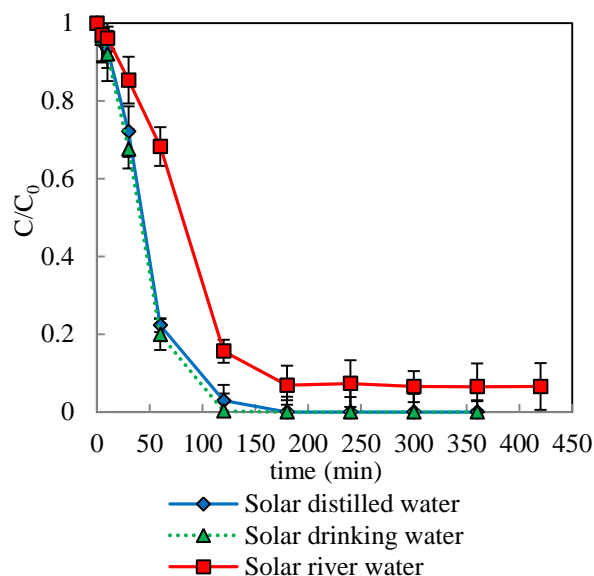


Fig.5.5 Solar photolysis of NPX in different water matrices

Overall, a solar exposure period of 180 min resulted in complete NPX degradation in both water matrices (distilled and drinking water).

However, solar irradiation was only partially effective in the degradation of NPX in the river water. Degradation was incomplete even after 420 min of exposure (Fig.5.5), contrary to results obtained within 30 min of irradiation with a medium pressure Hg lamp under laboratory conditions giving complete degradation. Rapid degradation (93%) of NPX in river water occurred during the first 180 min of exposure and remained almost constant after this point. Compared to complete degradation of NPX in distilled water and drinking water after 180 min, river water was observed to be slightly more resistant towards solar photolysis. A similar result was obtained for river water with direct photolysis under laboratory conditions in an immersion-well reactor. The sunlight intensities recorded for distilled water and drinking water were found to be greater than that for the river water (Fig.5.6) suggesting that the reduced intensity of sunlight impairs NPX degradation in river water. Alternatively, stable intermediates generated during the initial period of exposure may have retarded decomposition. Minor pH changes throughout the course of illumination were noted. The initial pH at 0 min of 7.85 ± 0.01 increased slightly to 7.95 ± 0.01 after 30 min and then remained constant until 360 min. In addition to these factors, a higher organic matter content in river water than drinking water could possibly absorb most of the solar irradiation reaching the reactor thus reducing the amount of photons available for the API [140], NPX. A similar study on solar NPX degradation in river water also reported that degradation proceeded at slightly slower rate with a first-order-rate constant of $1.64 \pm 0.54 \times 10^2 \text{ min}^{-1}$ compared to that in Milli-Q water with $2.08 \pm 0.14 \times 10^2 \text{ min}^{-1}$ [160].

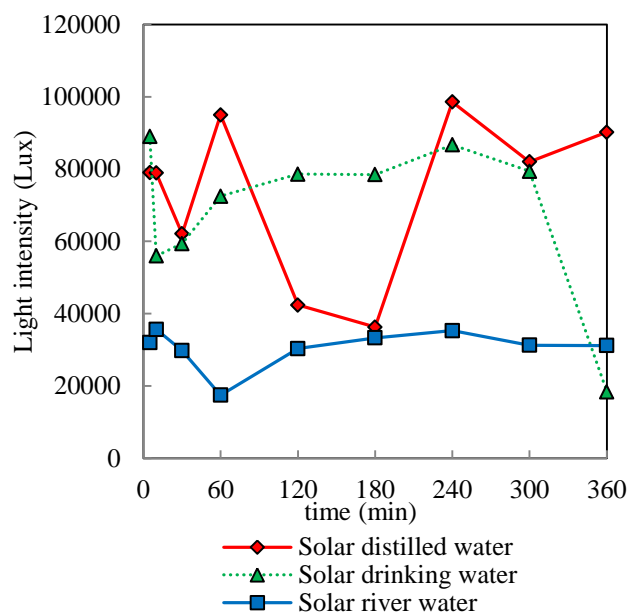


Fig.5.6 Solar light intensity measured during solar photolysis of NPX in different water matrix

This finding has particular implications for the environment, as it suggests that NPX present in surface water can be potentially stable to photodegradation under natural conditions. In reality, photodegradation under environmental conditions in surface waters can be expected to be much more complex due to the presence of other constituents. Surface water contains chromophores such as natural organic matters, able to initiate various photochemical reactions. Natural organic matter is also known to act as a precursor to produce reactive species such as HO[•] radicals and superoxide anions in sunlight, which could lead to faster degradation [9]. At the same time, materials such as humic acids could reduce the photodegradation rate by absorbing light and acting as inner filters [104].

With respect to COD reduction in the solar photolysis experiments, distilled and river water recorded similar reductions of 50% and 52%, respectively, while loss of COD was less so in drinking water with 47% (Fig.5.7). Partial mineralization during solar photolysis of NPX might account for the remaining degradation products. Various photoproducts were identified during the photolytic transformation of NPX in drinking water and distilled water under solar simulator irradiations, including hydroperoxides, ketones, alcohols, olefins, ethyl derivatives and others [181]. Drinking water photodegradation also resulted in dimer formation with a higher molecular weight and toxicity than NPX [181].

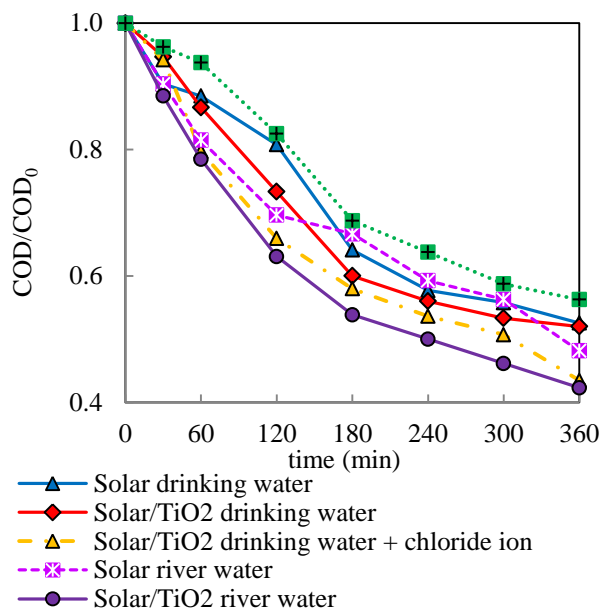


Fig.5.7 COD reduction during solar photolysis and solar TiO₂ photocatalysis of NPX

TiO₂ photocatalytic degradation of NPX in distilled water was completed after 120 min of exposure thus demonstrating the efficiency of TiO₂ (Fig.5.8a). However, while 95% of NPX was degraded in drinking water after 360 min under the same conditions, the degradation did not proceed any further, even after 360 min. In addition, the degradation data did not follow zero, first or second-order kinetic models. The second-order kinetic model showed a fit with $R^2=0.87$ and $k = 0.0016 \text{ L/mg. min}^{-1}$ for the 360 min irradiation data (Fig.5.9b). The degradation data assumed an exponential shape rather than a straight line. This behaviour could have been caused by the formation of degradation products and also the presence of NPX in trace amounts (Fig.5.10). At the same time, oxidation of degradation products may have also influenced the kinetics [225].

The COD results further confirmed this assumption as COD reduction increased constantly until 300 min and thereafter did not increase any further. A total COD reduction of 48% was obtained after 360 min (Fig.5.7). This value was similar to the mineralization degree observed under solar photolysis with 47% COD reduction, indicating a lower extent of mineralization as compared to the degradation of NPX.

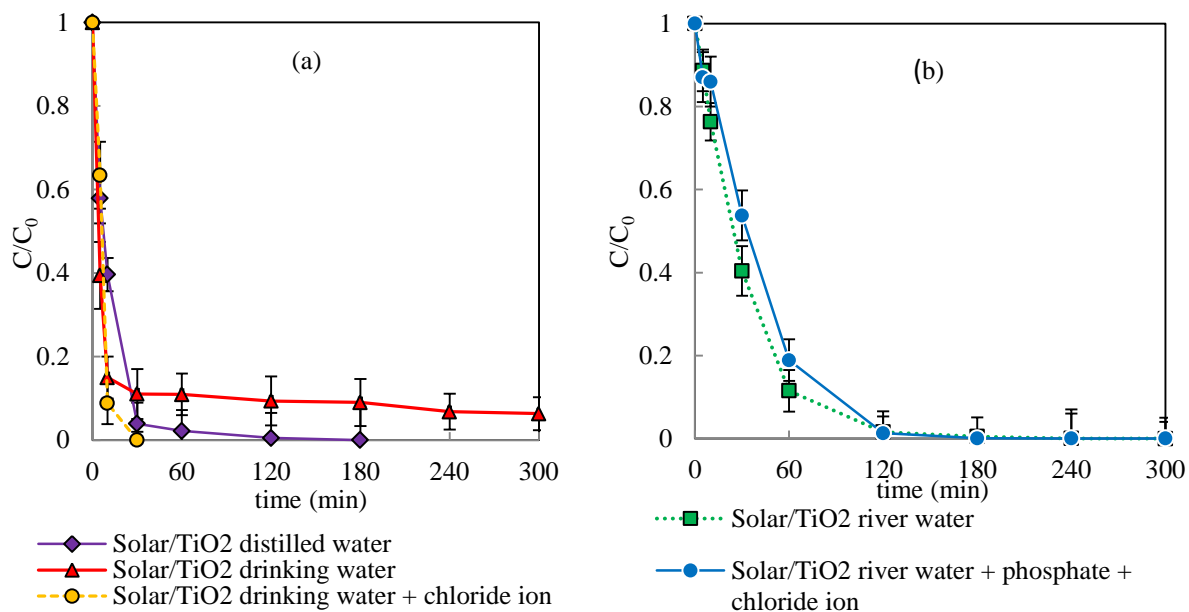


Fig.5.8 Solar TiO₂ photocatalysis of NPX in (a) distilled water and drinking water; (b) river water ($C_0 = 30$ mg/L; TiO₂ = 0.1 g/L; chloride = 20 mg/L; phosphate = 20 mg/L)

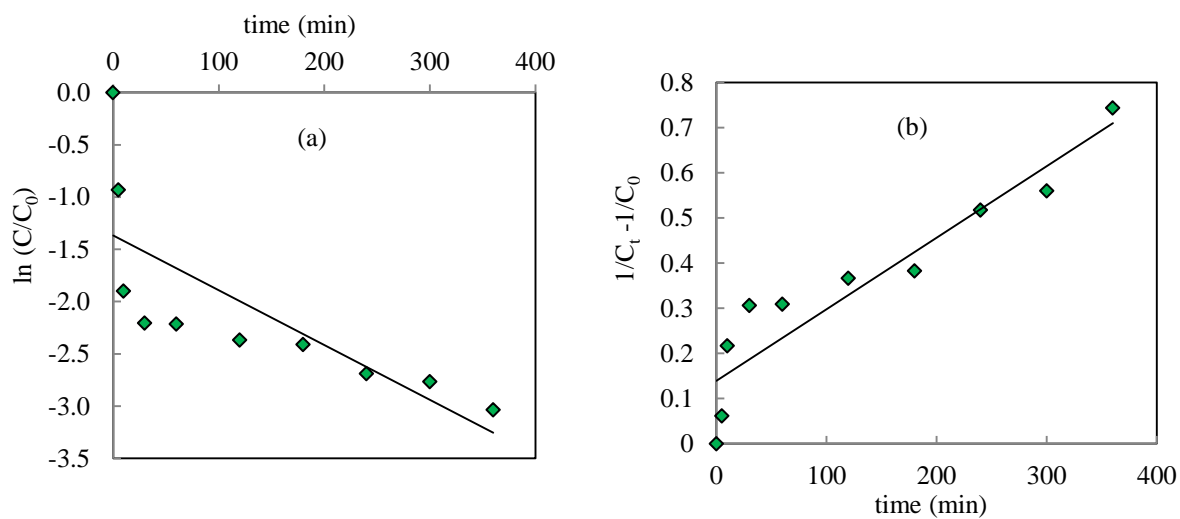


Fig.5.9 Kinetics of solar TiO₂ degradation of NPX in drinking water (a) pseudo-first-order kinetic, and (b) second-order-kinetic

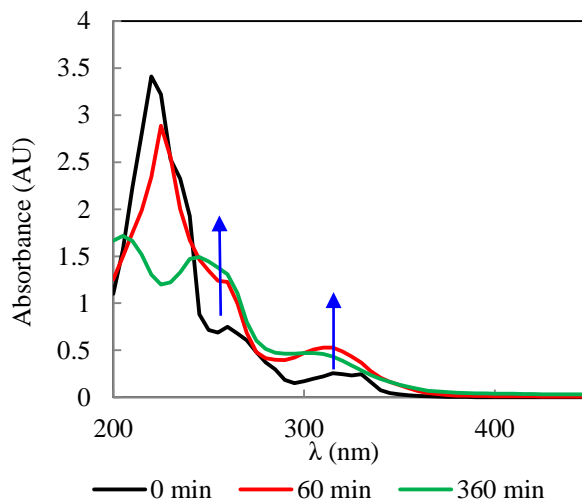


Fig.5.10 UV absorbance changes during solar TiO₂ photocatalysis of NPX in drinking water

In the presence of additional chloride anions in drinking water, complete degradation of NPX occurred rapidly within 30 min of illumination (Fig.5.8a). This result is in accordance with the laboratory-based observation where complete degradation occurred after 9 min of irradiation under UV light. The degradation was accompanied by 57% COD reduction, which was higher than mineralization observed under solar TiO₂ photocatalysis (Fig.5.7). This significant increase in degradation resulting from the addition of chloride could be due to the reasons previously explained in section 4.6.5 (Chapter 4). The effect of chloride addition has been reported to be dependent on the compound or substrate and the irradiation conditions [227]. This study showed that degradation of NPX upon addition of chloride anions was not affected greatly by the irradiation conditions. As a result of rapid degradation in the presence of chloride, experimental data within 30 min followed pseudo-first-order kinetics with $k = 0.2431 \text{ min}^{-1}$ ($R^2=0.98$).

In comparison to direct photolysis of NPX in river water which required a prolonged total irradiation time of over 420 min, TiO₂ photocatalysis appeared more effective for NPX degradation in this water matrix (Fig.5.8b). A similar trend was reported for the degradation of olanzapine in river water, which was performed with a solar simulator and UV lamps emitting monochromatic irradiation [69]. In contrast, the presence of the binary ions, phosphate and chloride in river water did not show any effect on the degradation as exposure times required to achieve complete degradation were almost identical. A total of 180 min of solar exposure was required for complete elimination of NPX in river water regardless of presence or absence of anions (Fig.5.8b). Although the total degradation times for complete elimination were similar, a slightly slower degradation rate of NPX occurred during the initial 60 min of TiO₂ photocatalysis when ions were present. This effect can be explained by competition between NPX (about 20% still present in the suspension), intermediates generated and

anions for TiO₂ surface sites during the initial hour. These events would be less pronounced after complete degradation of NPX. In terms of mineralization, TiO₂ photocatalysis yielded 58% COD reduction, while the value declined slightly to 44% when binary ions were present (Fig.5.7).

The temperature inside the immersion-well reactor ranged between 21-26.5°C during winter and 26-31°C in spring. Ambient temperatures from both seasons varied from 21-31°C. It is unlikely that these differences had any significant impact on the degradations.

5.4. Solar degradation of diclofenac and naproxen mixtures

Investigations of the effect of solar illumination on NSAID mixtures of NPX and DCF were also performed. Photodegradation experiments of these mixtures were conducted between July and September in 2012. Table 5.3 summarizes all solar photodegradation studies of DCF and NPX mixtures. All degradations obeyed pseudo-first-order kinetics, except the experimental data for solar TiO₂ photocatalysis in drinking water which followed a second-order-kinetic model.

Table 5.3 Summary of solar degradation studies of DCF and NPX mixtures

Water type	Oxidation system	Degradation (%) (after 360 min)		Rate constant k (min ⁻¹) (R ²)		Average solar light intensity (Lux)	Mean COD removal (%)
		NPX	DCF	NPX	DCF		
Distilled water	Solar photolysis	95.8	100	0.0092±0.0004 (0.99)	0.0095 ±0.0008 (0.98)	71203	57.6
	Solar TiO ₂	100	100	0.1493±0.0021 (0.99)	0.1392±0.0035 (0.99)	79793	76.0
Drinking water	Solar photolysis	78.7	91.5	0.0044±0.0003 (0.99)	0.0072±0.0006 (0.99)	73005	48.7
	Solar TiO ₂	99.3	100	0.0431±0.0034* (0.98)	0.0218±0.0028 (0.96)	77911	64.7
	Solar TiO ₂ + chloride	96.8	81.0	0.0095±0.0007 (0.99)	0.0044±0.0005 (0.96)	34561	62.1
River water	Solar photolysis	80	90.6	0.0046±0.0005 (0.99)	0.0068±0.0006(0.99)	54600	58.1
	Solar TiO ₂	100	100	0.0296±0.0011 (0.97)	0.0227±0.0023 (0.98)	61161	60.1

*Second-order-kinetic model (L.mg min⁻¹)

Solar photolysis of DCF and NPX mixtures showed a constant but slow progression in the degradation over time in all water matrices (Fig.5.11-Fig.5.13). Also, solar light intensities markedly vary during the solar photolysis studies. Degradations of NPX were incomplete in all water matrices in the presence of DCF, but were more pronounced in drinking water (Fig.5.12) and river water

(Fig.5.13). Similarly, the degradation of DCF was retarded in the presence of NPX in those water matrices and DCF was only completely eliminated in distilled water.

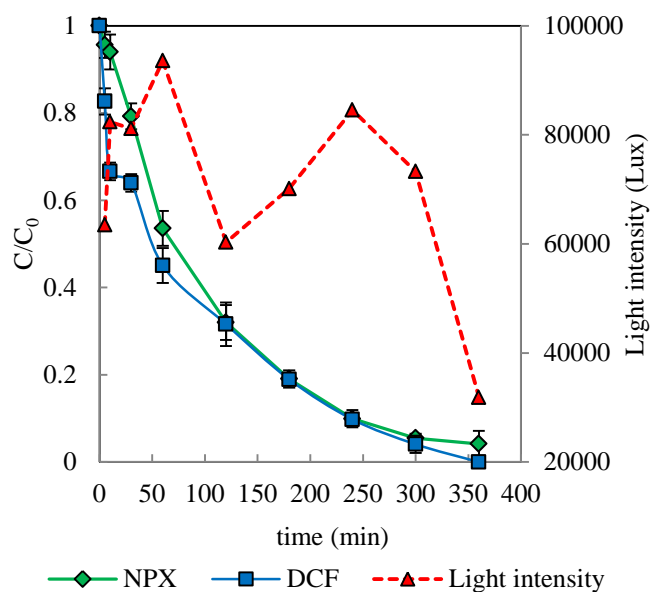


Fig.5.11 Solar photolysis of DCF and NPX mixtures in distilled water

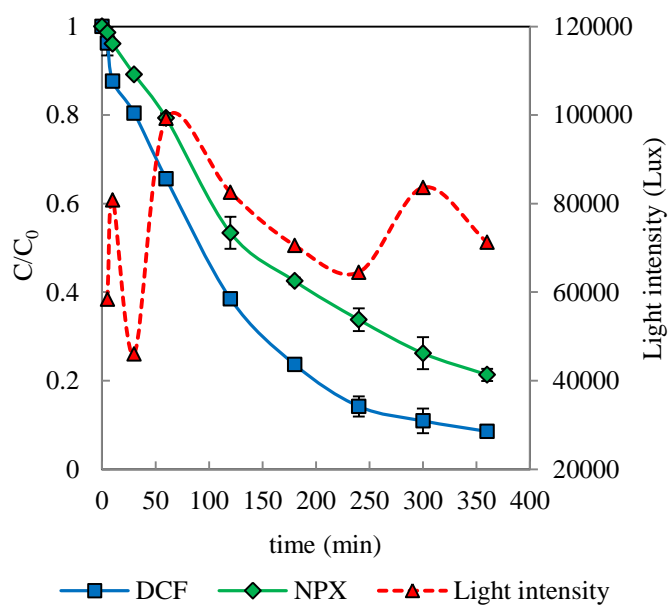


Fig.5.12 Solar photolysis of DCF and NPX mixtures in drinking water

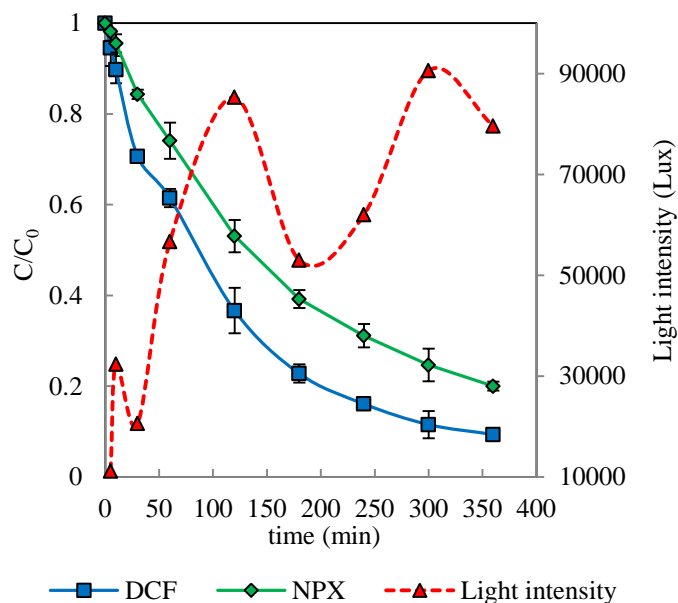


Fig.5.13 Solar photolysis of DCF and NPX mixtures in river water

In a mixture, degradation of NPX ranged from 79-96% with the highest degree of degradation in distilled water, followed by drinking water and river water. A similar order in terms of water type was also observed for DCF degradations, although slightly higher degradation percentages between 91 to 100% were obtained. Under all investigated solar conditions, DCF degraded much faster than NPX. This was somewhat unexpected as NPX absorbance extends deeper into the solar UV spectrum compared to DCF (Fig.5.14).

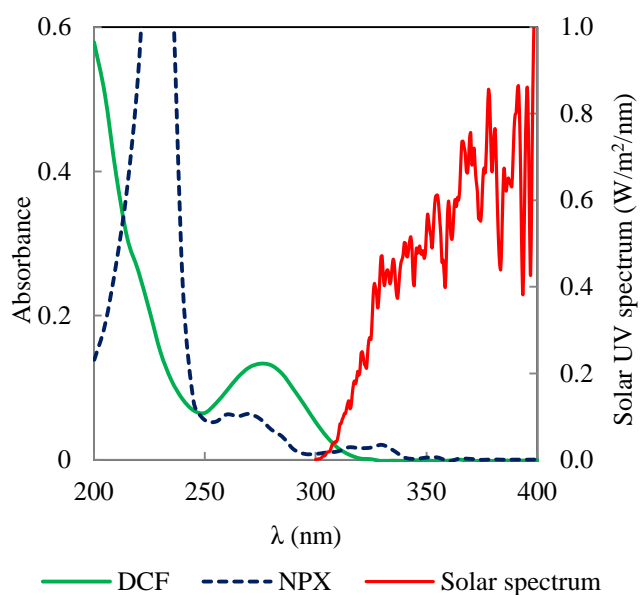


Fig.5.14 Absorbance spectra of DCF, NPX and global solar spectrum (ASTM)

Even though NPX appears to be a better solar photon absorber, other components in the water may have competed for the photons. Photodegradation may thus be dominated by photosensitized reactions and not direct photolysis. DCF also possesses the ability to absorb solar photons, thus resulting in competition between these two APIs. This trend agrees with the results obtained with the medium pressure Hg lamp under laboratory conditions and the fact that DCF showed higher photolability.

In comparison, the degradation levels of DCF alone by solar photolysis were slightly lower than those observed in the presence of NPX with 82-96% degradation. When NPX alone degraded, a higher degradation between 93-100% compared to that in the presence of DCF was accomplished. This inverse trend suggests that the presence of DCF has a greater effect on NPX and vice versa. This observation might explain the smaller extent of NPX degradation under solar photolysis despite its wider wavelength overlap with the solar spectrum.

Degradation profiles of mixtures in drinking water (Fig.5.12) and river water (Fig.5.13) showed similar trends. A steep slope indicating a rapid increase in degradation was observed at the beginning of solar exposure, whereas a smaller slope was observed as the reaction proceeded. In both cases, UV spectra did not show any major differences for the drinking or river water. Fig.5.15 shows the formation of degradation products in comparison to raw drinking water and river water.

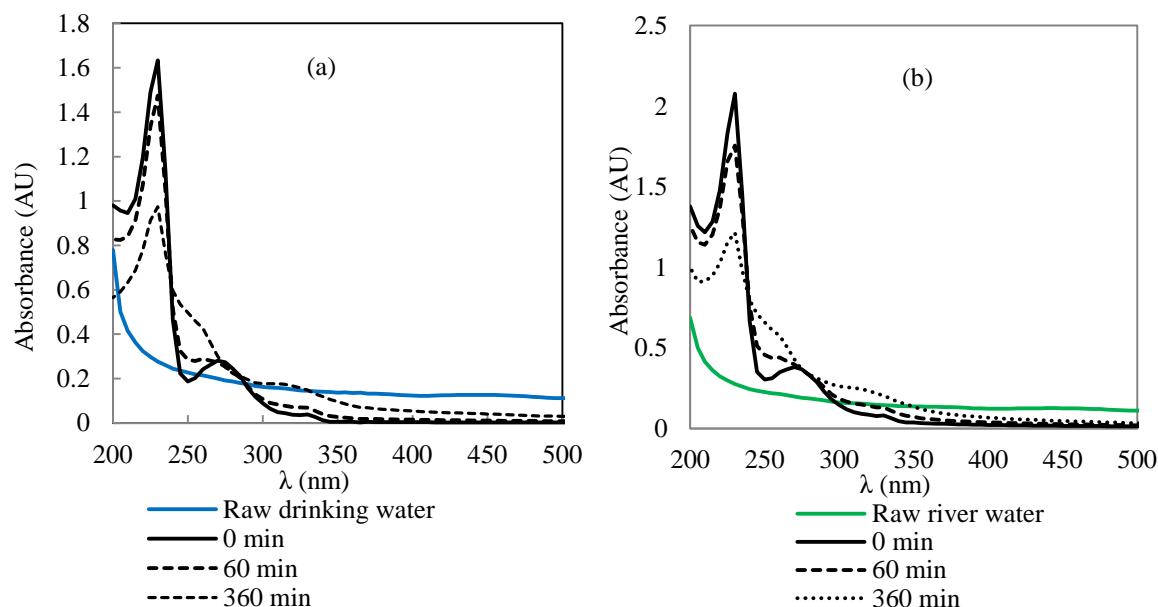


Fig.5.15 UV absorbance changes during solar photolysis of (a) drinking water and (b) river water

The characteristic peak at a wavelength around 280 nm, which represents the aromatic organic fraction [225] of the mixture profile, did not show any major changes during solar exposure in raw

drinking or river water. Changes in degradation efficiencies of the APIs in the mixture suggest a competition between the APIs for solar photon and possible interactions [228]. It is thus likely that in the environment, degradations of mixtures APIs by direct sunlight might be reduced. Although solar photons are generally able to induce photodegradations of substrates these photoalterations are known to be relatively slow [80].

All degradation profiles of the solar TiO₂ photocatalysis showed a rapid, almost linear response to exposure time leading to complete degradation (Fig.5.16a-Fig.5.16c). NPX underwent faster degradation than DCF based on rate constants (Table 5.3).

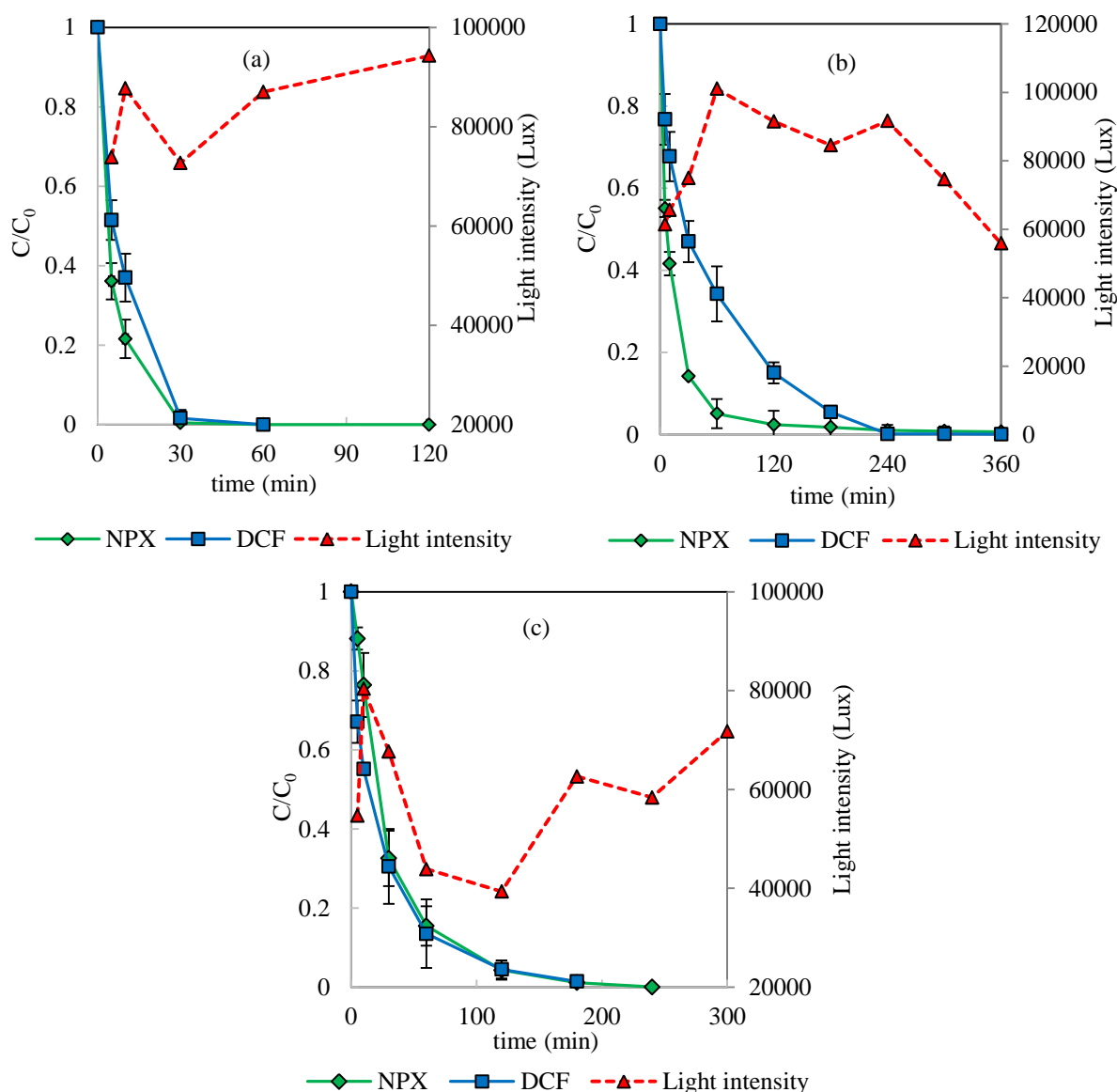


Fig.5.16 Solar TiO₂ photocatalysis degradation of mixtures in (a) distilled water, (b) drinking water and (c) river water

The presence of TiO_2 in the mixture significantly enhanced the degradation rate of both APIs compared to solar photolysis alone (Table 5.3). This confirms the effectiveness of solar TiO_2 photocatalysis to degrade mixtures of both APIs simultaneously in a number of water matrices. Degradation of mixtures by solar photocatalytic oxidation corresponded well to the average amount of solar light intensity recorded during the experiments, which were higher than those recorded for solar photolysis.

A recent study by Pereira *et al.* [217] also reported the effectiveness of the solar photocatalytic process in the concomitant removal of two antibiotics, oxolinic acid and oxytetracycline, from contaminated water. The lower initial rates observed for the aqueous mixture compared to the individual compounds only were attributed to the competition of each compound for holes or HO^\bullet radicals. Although degradation of NPX proceeded at a much faster rate initially, the time period required for complete degradation was similar for both APIs in all water matrices. For example, the initial degradation rate observed for DCF in drinking water was significantly slower, but more consistent, while the majority of NPX degraded more rapidly with the rate slowing at ~95%. Even so, at 240 min both NPX and DCF were completely removed from the solution.

For experiments in the presence of chloride anions in drinking water, 97% degradations of NPX and 81% of DCF occurred after 360 min of solar exposure (Fig.5.17). The presence of chloride anions thus had a negative impact and resulted in slower degradation rates and incomplete removal of the APIs in the mixtures.

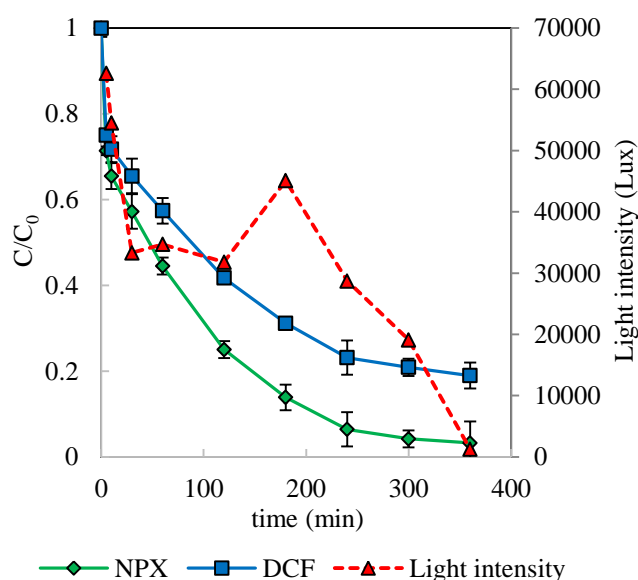


Fig.5.17 Solar TiO_2 photocatalysis degradation of mixtures in drinking water in the presence of chloride anions ($C_0 = 30 \text{ mg/L}$; $\text{TiO}_2 = 0.1 \text{ g/L}$; chloride = 20 mg/L)

The degradation rates of NPX and DCF in the mixtures by solar TiO₂ photocatalysis in the absence of chloride anions were 0.0431 min⁻¹ and 0.0218 min⁻¹. These values decreased to 0.0095 min⁻¹ for NPX and 0.0044 min⁻¹ for DCF in the presence of chloride anions. A similar trend in degradation rates was obtained for the degradation of mixtures in drinking water under laboratory conditions although degradation proceeded to completion after 120 min of irradiation with medium pressure Hg lamp. At natural pH (approximately 7.8) no adsorption of chloride anions is expected on the negatively charged TiO₂ surface (pH > p*H*_{pzc}, p*H*_{pzc} = 6.25) [112]. However, chloride anions can still react with HO[•] radicals to induce a radical scavenging effect, thus decreasing the degradation efficiency and resulting in incomplete removal of DCF and NPX in the mixtures. Therefore, in the mixtures irradiation conditions (UV radiation and solar illumination) contributed to the slight differences in the degradation efficiencies in the presence of chloride anions.

COD monitoring for the aqueous mixtures indicated a higher efficacy of solar TiO₂ photocatalysis (Fig.5.18a), compared to solar photolysis (Fig.5.18b).

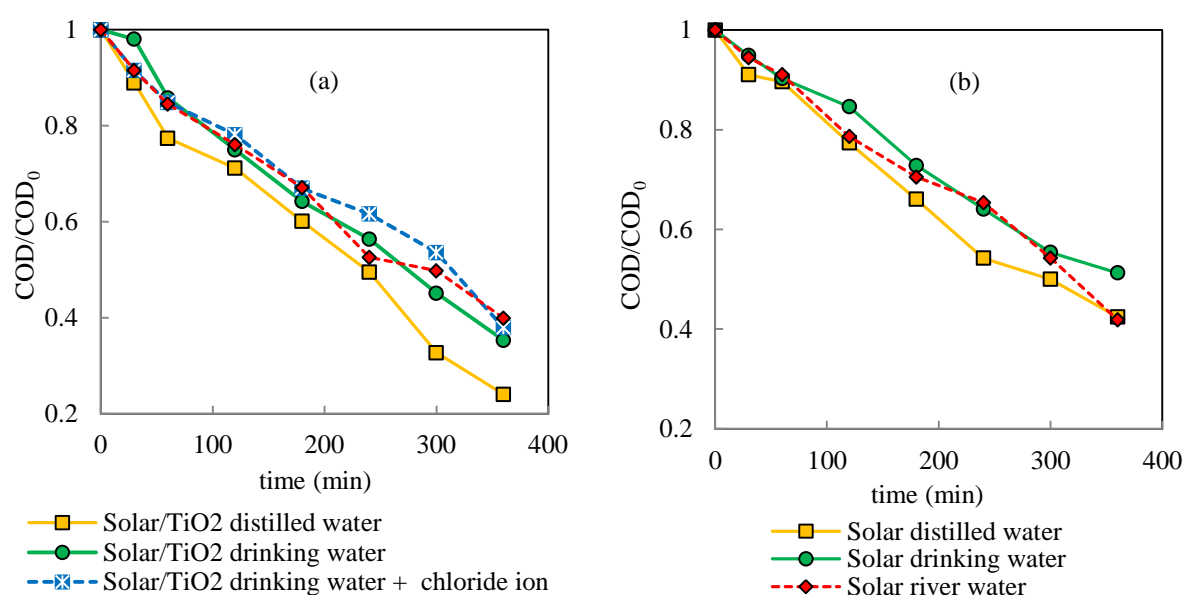


Fig.5.18 COD reduction in the DCF and NPX mixtures by solar (a) TiO₂ photocatalysis and (b) photolysis

COD reduction proceeded slowly when these APIs were degraded simultaneously. Total COD reductions of 76%, 65%, and 60% were achieved by solar TiO₂ photocatalysis for API mixtures in distilled water, drinking water and river water, respectively after 360 min (Fig.5.18a). Mineralization was not influenced by the presence of chloride ions in drinking water. COD reduction in drinking water in the presence of chloride showed a reduction of 62% compared to that in the absence of chloride ions. Degradation initiated by solar photolysis produced only partial reduction of COD for

the mixtures. COD reductions by solar photolyses ranged between 49-58% for all water matrices (Fig.5.18b). Solar photolytic and TiO₂ photocatalytic processes in river water mixture proceeded to similar extents resulting in an overall COD reduction of 58-60%. This slightly poorer performance is most likely the result of the formation of photoproducts with a resistance towards both treatments.

A temperature range between 22-30°C was observed for all the immersion-well mixture experiments. With regard to pH changes, 360 min of solar photolysis caused a decrease in pH of distilled water from 6.2 to 5.4, and a slight increase in drinking water and river water from 7.5 to 8.0 and 7.5 to 7.9, respectively. During TiO₂ photocatalysis in distilled water, the pH at 0 min of 5.95 decreased to 5.90 after 240 min and subsequently increased to 6.20 after 360 min. In river water and drinking water, the initial pHs were recorded to be 8.00 and 7.45, respectively. A slight decline was observed in river water, with the pH decreasing to 7.95 at the end of the exposure. Photocatalytic reactions have been shown to elicit a slight initial drop in pH due to the formation of multiple degradation products with different acidic functional groups [11]. In contrast, the pH in drinking water showed a slight increase to 7.75 possibly due to the nature of degradation products, which have more basic nature than acidic. The pH evolution clearly varied among the different treatments of mixture solutions.

5.5. Conclusions

To allow for appropriate comparison, solar illuminations of NPX and DCF and their mixtures in water were performed using the same setup as was used for the laboratory experiments. Differences between UV lamp and solar driven degradations thus depend mainly on the “photon source”. The medium pressure Hg lamp enables irradiation and a constant supply of photons, while solar irradiation is discontinuous and changes with the time of day. The configurations of light supply also differed between “inside-out” (lamp) and “outside-in” (sun). As solar radiation depends on the time of the day and weather, the amount of UV radiation reaching the immersion-well reactor and thus available for degradation processes can fluctuate significantly.

Individual and aqueous mixtures of APIs showed different behaviours towards solar photolysis and TiO₂ photocatalysis in the water matrices investigated. Solar TiO₂ photocatalysis with the mixtures demonstrated consistent degradation efficiency except when chloride ions were present in drinking water. NPX was also degraded efficiently via solar TiO₂ photocatalysis under almost all conditions even in the presence of anions, except in drinking water when the degradation reached a plateau after 30 min. Degradation of DCF was efficient under solar photolytic conditions, but rendered less efficient under solar TiO₂ photocatalysis in both drinking and river water. Based on solar light intensities, degradations of both individual and mixtures depended mainly on the water matrix.

Effects of anions varied between inhibition and promotion of oxidation of the photocatalysis depending on the API.

Changes in pH and temperature were encountered during all photodegradation experiments. Temperature does not play a significant role in the photocatalytic processes [109, 229]. Changes in pH, however, did provide an indication that acidic degradation products were formed and the degradation was occurring.

COD reduction for mixtures was lower compared to that for individual APIs. Partial mineralization observed for individual APIs and mixtures under both solar photolytic and TiO₂ photocatalytic conditions suggested the formation or release of a wide range of degradation products. COD reduction by means of solar TiO₂ photocatalysis of aqueous mixtures showed greater promise compared to that of individual APIs.

Overall, solar TiO₂ photocatalysis can be considered as an useful and efficient alternative for water purification containing NSAIDs. However, degradations are not easily controllable and their efficiencies greatly varied due to matrix effects and inconsistency in photon supply. This study has shown that artificial light sources, which can be easily controlled, allow for much more straightforward comparisons.

Chapter 6. Identification of photoproducts and elucidation of degradation pathways

6.1. Introduction

The identification of degradation products generated from the parent APIs is necessary in order to predict the risk and impact of photochemical processes, especially as some intermediates have been reported to be more toxic than the parent compound [230]. Researchers have opted for powerful analytical tools such as LC-MS, GC-MS or LC-TOF-MS to identify degradation products, particularly in complex environmental samples such as wastewater [53]. Among these, LC-MS and LC-TOF-MS have found more applicability compared to GC-MS, as degradants are generally non-volatile [231]. In this study, LC-MS was used for the identification of degradation products based on the observed ions and fragment ions. For volatile compounds, LC-MS, which is sensitive, able to separate by polarity and enables the concurrent UV and MS detection of vast numbers of compounds, was the method of choice [53]. Furthermore, data mining enables extracted ion chromatograms (EIC) to be generated in order to identify the products. Additionally, accurate mass detection (FT-ICR-MS) was used to confirm the molecular formulas of the proposed photoproducts.

In this chapter, the main degradation products resulting from TiO₂ photocatalytic treatments of DCF, NPX and their mixtures were identified and degradation pathways proposed for each compound. Standard samples of DCF, NPX and their mixtures were also analysed for possible degradation products for comparison with photochemically treated samples.

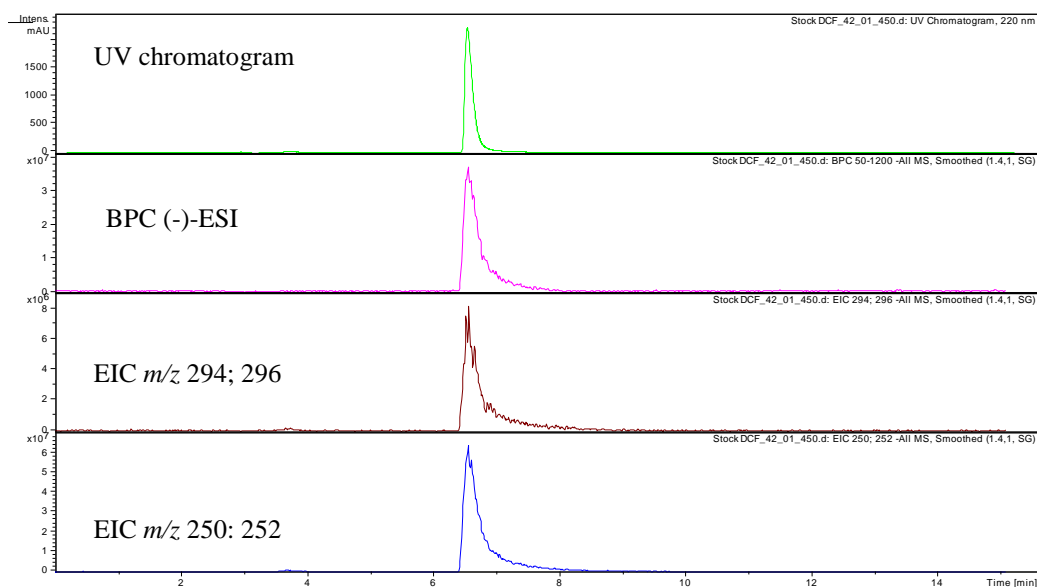
6.2. Degradation products of diclofenac

The initial study with an optimized DCF concentration of 30 mg/L (as in Chapter 4), equivalent to 10⁻⁴ M, which was applied in all photolysis and photocatalytic treatments, did not yield detectable quantities of degradation products. Thus, the initial concentration of DCF was increased to 500 mg/L, corresponding to a level of 10⁻³ M, while the TiO₂ P25 concentration was maintained at 0.1 g/L.

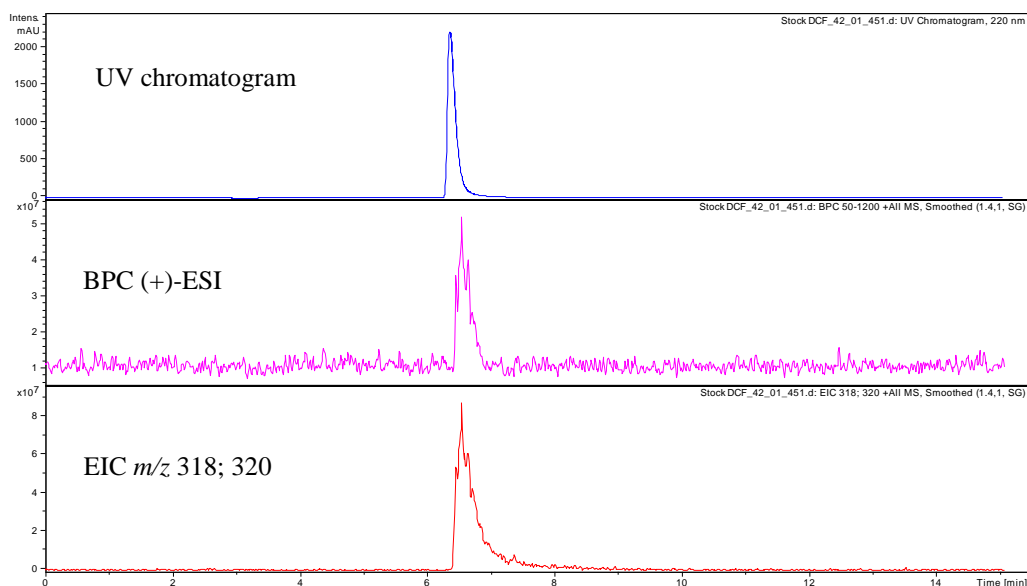
A DCF sample from UV/TiO₂ photocatalytic treatment taken after 120 min of irradiation with a medium pressure Hg lamp was analysed for degradation products by LC-MS. LC-MS analysis was performed by applying a simple isocratic mode which resulted in better resolution of DCF and its photoproducts than the gradient elution commonly applied in other studies [149, 165]. The chromatographic conditions for the separation of DCF and its degradation products were as reported in Chapter 3. In brief, the DCF samples were eluted isocratically and monitored at a wavelength of

274 nm and by both negative and positive MS. The raw LC-MS data was further investigated by viewing the base peak chromatograph (BPC) and the individual ions of interest using EIC.

The DCF standard ($M = C_{14}H_{11}O_2NCl_2$; molecular weight = 295 g/mol; $t_R = 6.5$ min) showed two peaks (m/z 294 $[M - H^+]$ and 250 $[M - H^+ - CO_2]$) in (-)-ESI and one peak (m/z 318 $[M + Na^+]^+$) in (+)-ESI mode. Fig.6.1 shows the LC-MS data of DCF standard.



(a)



(b)

Fig.6.1 LC-MS ions of DCF standard (a) (-)-ESI mode and (b) (+)-ESI mode. The top spectrum in each figure is the UV chromatogram, also shown is the BPC. EICs show the ions formed under ESI conditions

Each of these peaks presented isotopic distributions, representative of a compound containing two chlorines, although at low resolution. FT-ICR-MS analysis enabled both accurate mass determination and confirmation of the isotope distribution (high resolution). The isotope distribution observed in the FT-ICR-MS shows the contribution from the ^{35}Cl (75.77%) and ^{37}Cl (24.23%), with the two highest signals 2 mass units apart, and the intensity of which is determined by the relative abundance of each isotope (Fig.6.2).

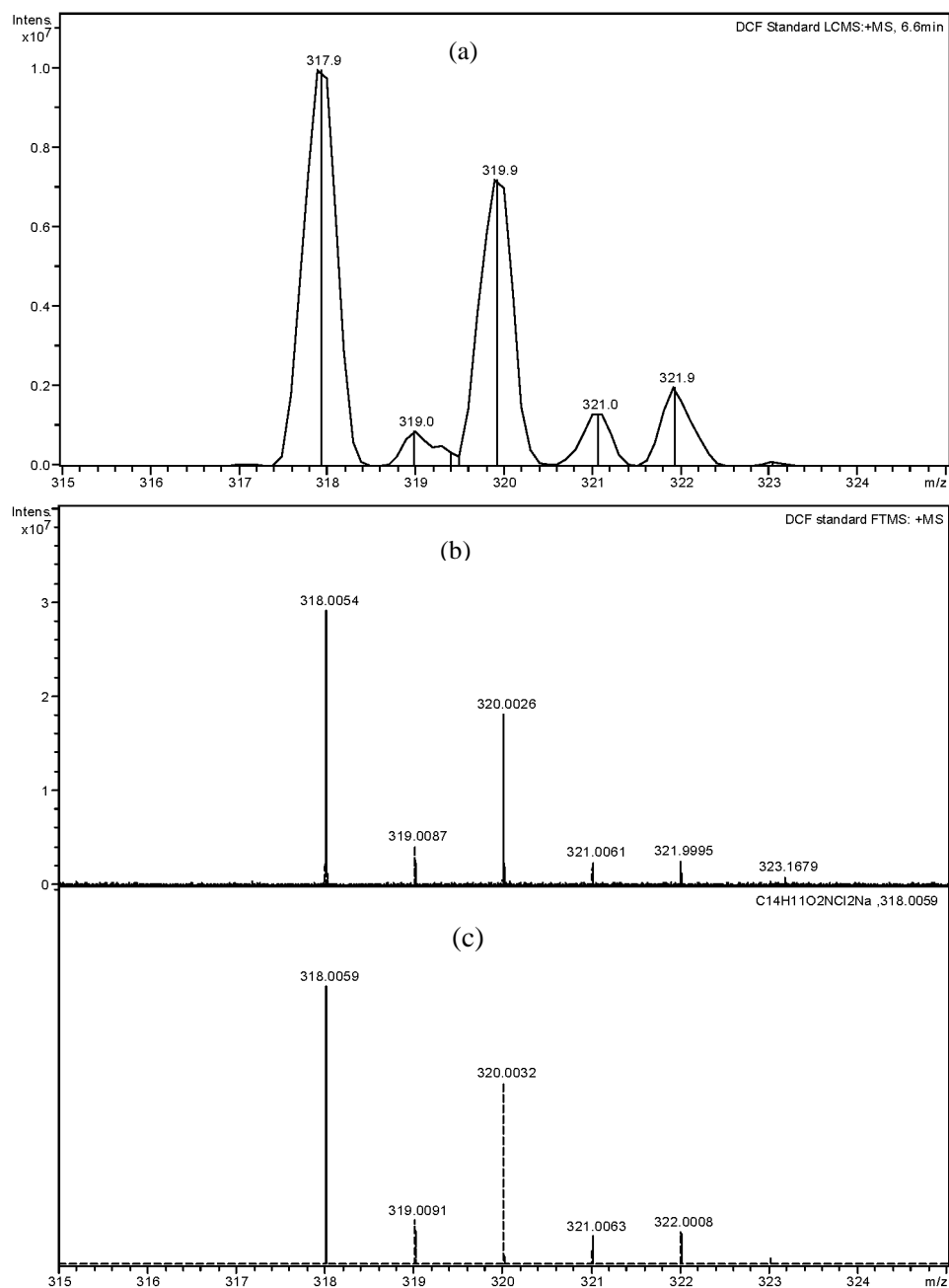


Fig.6.2 Isotopic distribution of the sodiated ion of DCF, $\text{C}_{14}\text{H}_{11}\text{O}_2\text{NCl}_2$, $[\text{M} + \text{Na}^+]^+$ a) observed distribution for $[\text{M} + \text{Na}^+]^+$ by LC-MS b) observed distribution for $[\text{M} + \text{Na}^+]^+$ by FT-ICR-MS and c) theoretical distribution calculated for $[\text{M} + \text{Na}^+]^+$

Table 6.1 shows the six major photoproducts identified during TiO₂ photocatalysis of DCF in distilled water by LC-MS. Subsequent FT-ICR-MS analysis (characteristic isotope distributions and accurate mass determination) confirmed the structures of the degradation products as shown in the proposed degradation pathway. All degradation products identified (Table 6.1 and Fig.6.3), appeared at shorter retention time than the parent DCF peak, confirming the formation of more hydrophilic degradation products. Fig.6.4 shows the LC-MS data comprising UV data, BPC (base peak chromatogram) and EICs of identified degradation products by ESI modes.

Table 6.1 Degradation products of DCF resulting from UV/TiO₂ with a medium pressure Hg lamp identified by a combination of (+/-)-ESI LC-MS and FT-ICR-MS techniques

Compound (ionization mode)	Observed ion	Observed LC-MS EIC (<i>m/z</i>); <i>t_R</i> (min)	Observed FT-ICR-MS (<i>m/z</i>); error Δ ppm	Formula	Molecular weight (g/mol)
1 (ESI+)	[C ₁₄ H ₁₀ O ₂ NCl + Na ⁺] ⁺	282; 6.1	282.0309; 6 ppm	C ₁₄ H ₁₀ O ₂ NCl	259
1 (ESI-)	[C ₁₄ H ₁₀ O ₂ NCl - H ⁺] ⁻	258; 6.1	258.0338; 4 ppm	C ₁₄ H ₁₀ O ₂ NCl	259
6 (ESI+)	[C ₁₄ H ₁₁ O ₃ N + Na ⁺] ⁺	264; 4.4	264.0654; 9 ppm	C ₁₄ H ₁₁ O ₃ N	241
6 (ESI-)	[C ₁₄ H ₁₁ O ₃ N - H ⁺] ⁻	240; 4.4	240.0677; 5 ppm	C ₁₄ H ₁₁ O ₃ N	241
8 (ESI-)	[C ₁₃ H ₁₁ NCl ₂ - H ⁺] ⁻	250; 6.8	250.0206; 4 ppm	C ₁₃ H ₁₁ NCl ₂	251
23 (ESI-)	[C ₁₃ H ₁₁ ON - H ⁺] ⁻	196; 4.4	196.0779; 6 ppm	C ₁₃ H ₁₁ ON	197
12 (ESI-)	[C ₁₃ H ₁₀ NCl - H ⁺] ⁻	214; 6.1	214.0439; 5 ppm	C ₁₃ H ₁₀ NCl	215
24 (ESI-)	[C ₁₃ H ₁₁ N - H ⁺] ⁻	180; 4.9	180.0831; 7 ppm	C ₁₃ H ₁₁ N	181

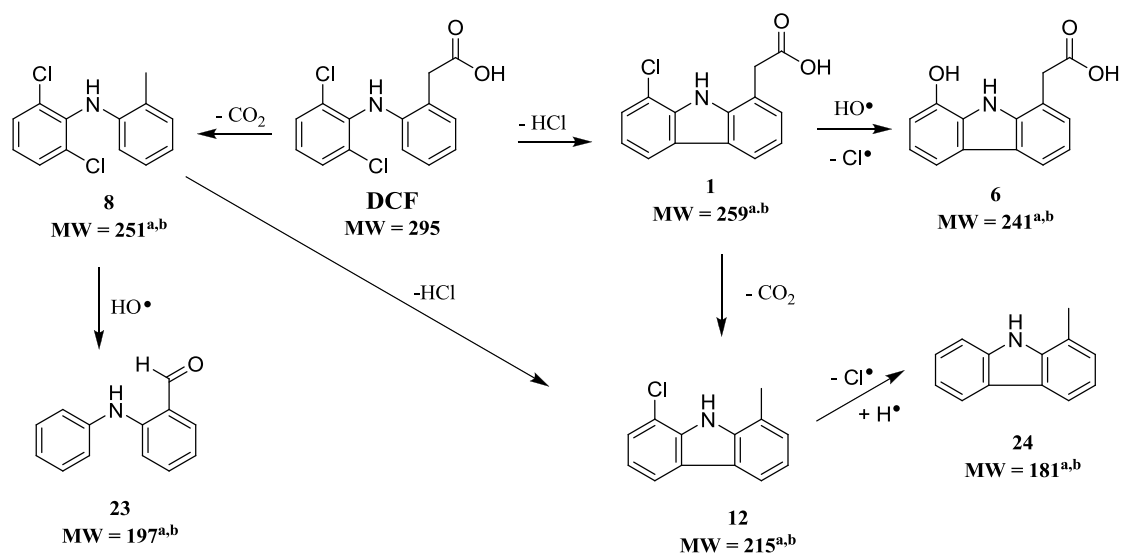
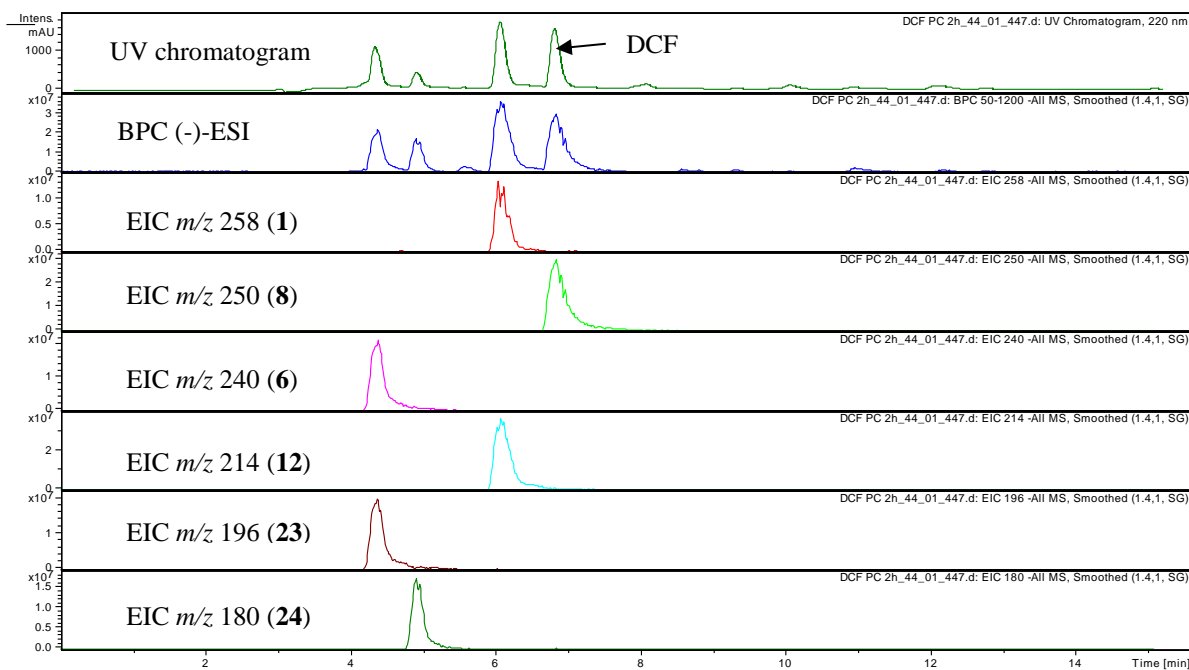
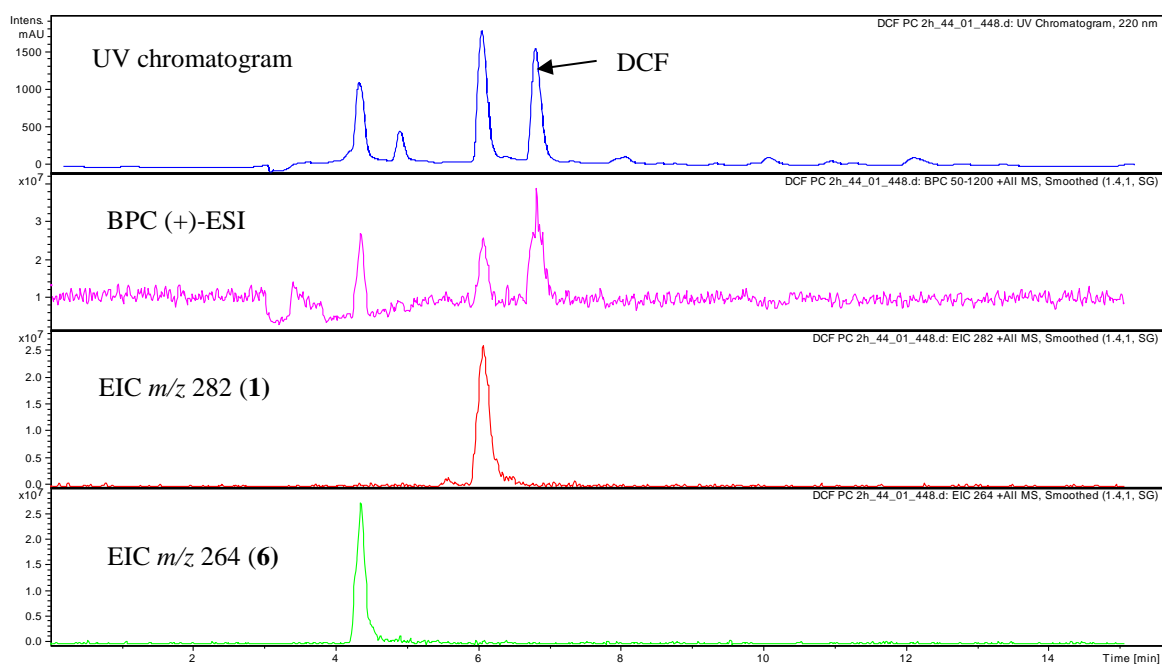


Fig.6.3 TiO₂ photocatalytic degradation pathways of DCF as confirmed by both LC-MS^a and FT-ICR-MS^b



(a)



(b)

Fig.6.4 LC-MS data of TiO₂ photocatalysis of DCF (a) in (-)-ESI mode and (b) (+)-ESI mode. The top spectrum in each figure is the UV chromatogram, also shown is the BPC. EICs show the retention times and masses of the degradation products

Loss of HCl and subsequent photocyclization of DCF resulted in **1** ($t_R = 6.1$ min), a carbazole, 2-(8-chloro-9H-carbazol-1-yl)acetic acid. The degradation proceeded with subsequent photosubstitution

of the remaining chlorine in **1** with a hydroxyl group to produce **6** ($t_R = 4.4$ min), another carbazole, 2-(8-hydroxy-9H-carbazol-1-yl)acetic acid. The presence of intermediates **1** and **6** were confirmed in both negative and positive ESI modes. These carbazole intermediates have also been identified as major products in a photolytic degradation of DCF in water [162] and were linked to an increase in phototoxicity [149]. Decarboxylation of DCF led to the formation of **8**, 2,6-dichloro-N-o-tolylbenzenamine ($t_R = 6.8$ min) which further underwent dechlorination and oxidation to generate intermediate **23**, 2-(phenylamino) benzaldehyde ($t_R = 4.4$ min). Intermediate **8** also underwent loss of HCl to form **12**, 1-chloro-methyl-9H-carbazole ($t_R = 6.1$ min). Intermediate **12** could be alternatively formed as a result of decarboxylation from **1**. The loss of the second Cl from **12** and photoreduction led to the generation of intermediate **24**, 1-methyl-9H-carbazole ($t_R = 4.9$ min). All intermediates found in this study were identical to those reported by Martínez *et al.* [149] except for (2-(2,6-dichlorophenylamino)phenyl)methanol. This compound, proposed as an intermediate in the transformation from **8** to **22**, was not detected, possibly due to its rapid oxidation under the conditions investigated. These intermediates, including the release of HCl and CO₂, also explain the observed decrease in pH: formation of hydrochloric acid (conversion of DCF to **1** and to **12** via **8**).

Chlorine was also detected in the form of chloride ions, as measured by ion chromatography during TiO₂ photocatalysis. Its formation coincided with the disappearance of DCF from the solution (Fig.6.5). Approximately 90% of chloride ions were released into the solution after 30 min, corresponding to a conversion of DCF into dechlorinated degradation products (e.g. DCF to compound **1** to **6**).

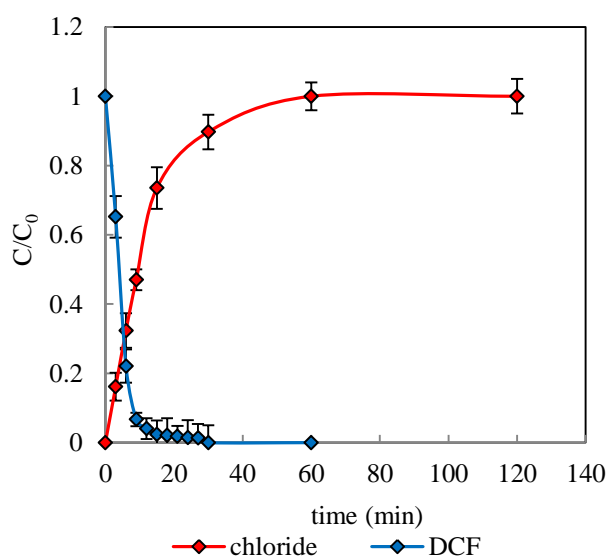


Fig.6.5 Profile of chloride evolution and degradation of DCF by TiO₂ photocatalysis

This result is in accordance with the observation reported by Calza *et al.* [165]; chloride ions reached about 95% of the stoichiometric amount after 1 h of irradiation using their photocatalytic system, which coincided with a decrease and ultimately the complete conversion of chlorinated and dichlorinated derivatives to non-chlorinated products.

Direct photolytic degradation of DCF also occurred via photocyclization and was the most significant pathway [139, 159, 162]. This was proposed to be followed by another pathway involving decarboxylation and dehalogenation (dechlorination) [139]. Degradation products of DCF by direct photolysis were found to be similar to those produced by TiO₂ photocatalysis with the exception of **6** and **23** (Fig.6.6). The major transformation product, **6** (2-(8-chloro-9H-carbazol-1-yl)acetic acid) formed during TiO₂ photocatalysis was also generated under photolytic conditions as the major degradation product.

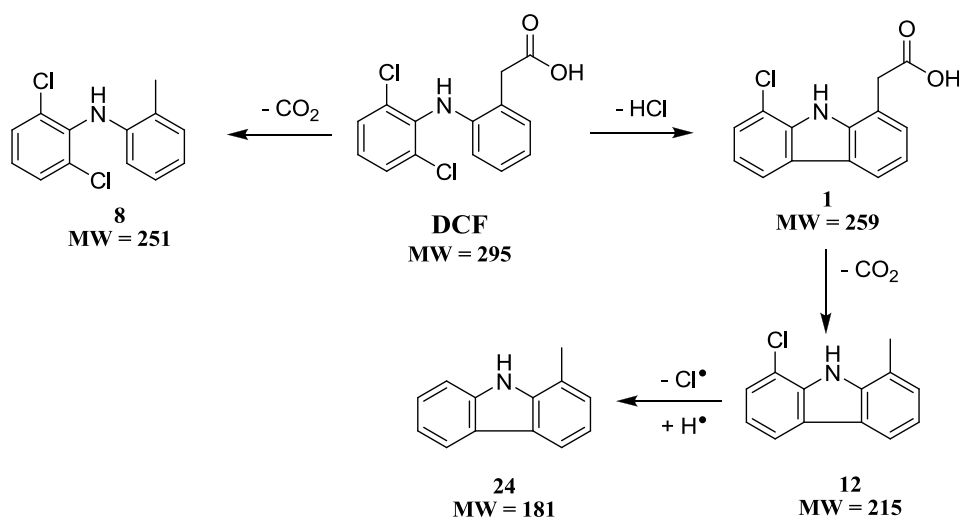
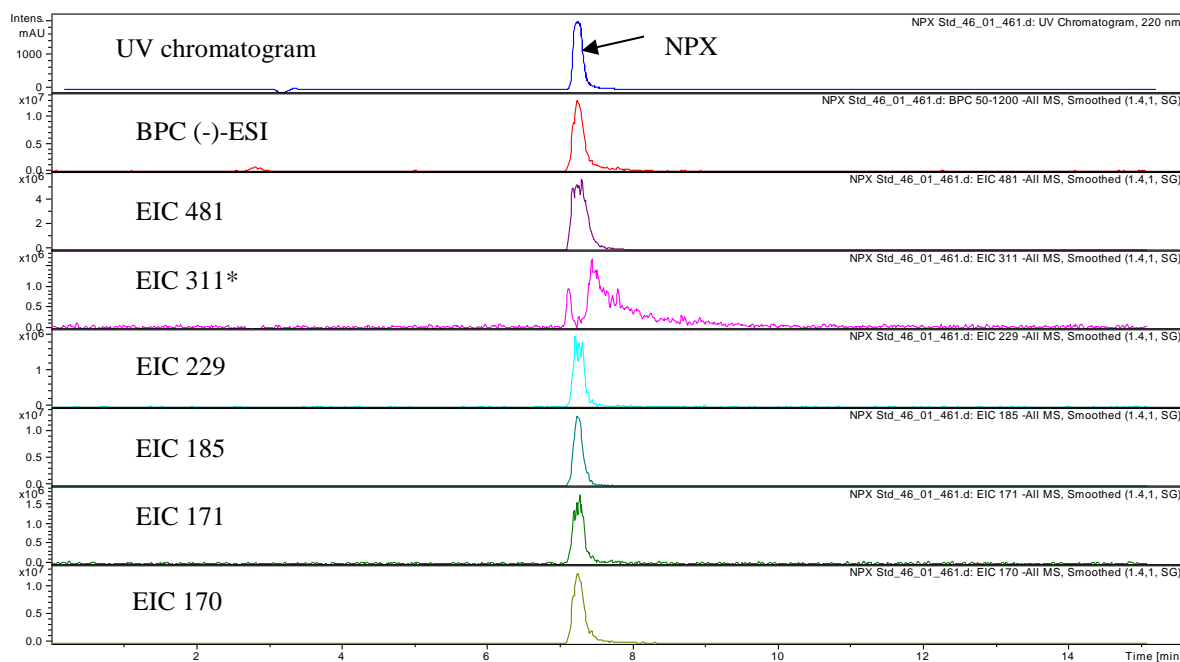


Fig.6.6 Photolytic degradation of DCF in distilled water

6.3. Degradation products of naproxen

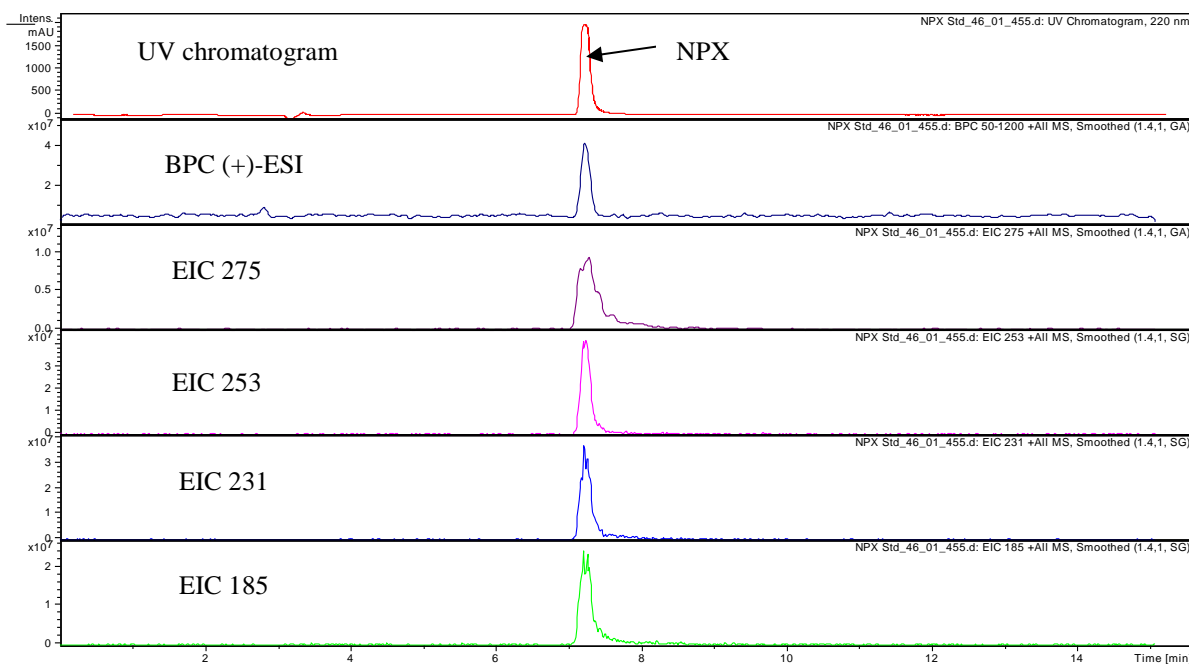
Similar to DCF, the concentration of NPX was also increased to 500 mg/L to obtain detectable amounts of degradants. A NPX sample from UV/TiO₂ photocatalytic treatment taken after 120 min of irradiation with a medium pressure Hg lamp was analysed by LC-MS using both negative and positive modes. Likewise, NPX standard was also analysed for possible ion formation. The chromatographic conditions for the separation of NPX and its degradation products were as reported in Chapter 3. In short, the NPX samples were eluted isocratically and monitored at a wavelength of 230 nm and by both negative and positive MS. A total of six peaks (m/z 481 [2M - 2H⁺ + Na⁺]⁻, 311 [M - H⁺ + C₉H₆ - O₂]⁻, 229 [M - H⁺]⁻, 185 [M - H⁺ - CO₂]⁻, 171 [M - CO₂-CH₃]⁻, 170 [M - H⁺ - CO₂ - CH₃]⁻) in the (-)-ESI and four peaks (m/z 275 [M - H⁺ + 2Na⁺]⁺, 253 [M + Na⁺]⁺, 231 [M + H⁺]⁺ and

185 $[M + H^+ - CH_2O_2]^+$ in (+)-ESI were detected for the NPX standard ($M = C_{14}H_{14}O_3$; molecular weight = 230 g/mol; $t_R = 7.3$ min) as shown in Fig.6.7.



* Note that there is a suppression of m/z 311 that occurs as the concentration of the eluting NPX increases

(a)



(b)

Fig.6.7 LC-MS ions of NPX standard (a) (-)-ESI mode and (b) (+)-ESI mode. The top spectrum in each figure is the UV chromatogram, also shown is the BPC. EICs show the ions formed under ESI conditions

Formulas corresponding to ions at m/z 481, 275, 253, 229 and 185 were confirmed by FT-ICR-MS. TiO₂ photocatalysis of NPX in distilled water generated a total of eight detectable degradation products (Table 6.2). Among these, four corresponding ions at m/z 445, 417, 401 and 215 were confirmed by FT-ICR-MS. Fig.6.8 shows the LC-MS data comprising UV data, BPC and EICs of the identified degradation products by both negative and positive ESI modes.

Table 6.2 Degradation products of NPX from UV/TiO₂ with a medium pressure Hg lamp identified by a combination of (+/-)-ESI LC-MS and FT-ICR-MS techniques

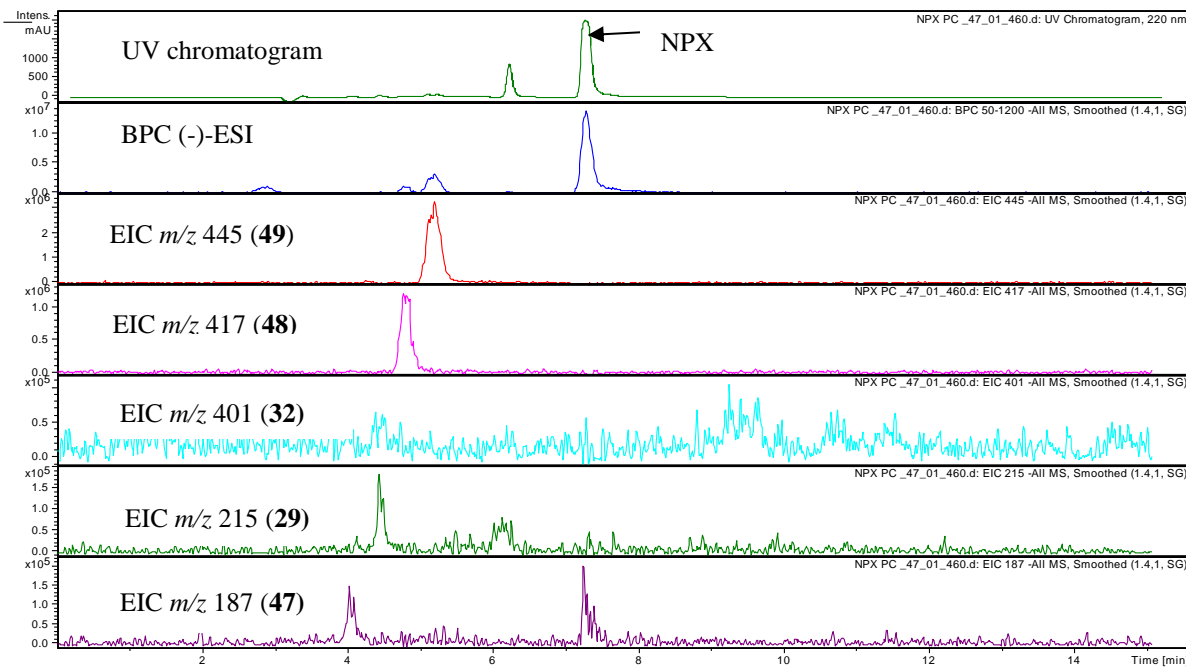
Compound (ionization mode)	Observed ion	Observed LC-MS EIC(m/z); t_R (min)	Observed FT-ICR-MS (m/z); error Δ ppm	Formula	Molecular weight (g/mol)
45* (ESI+)	[C ₁₄ H ₁₄ O ₃ + H ⁺] ⁺	231; 5.2	Not observed	C ₁₄ H ₁₄ O ₃	230
29 (ESI-)	[C ₁₃ H ₁₂ O ₃ - H ⁺] ⁻	215; 6.2	215.0714; 5 ppm	C ₁₃ H ₁₂ O ₃	216
46 (ESI+)	[C ₁₃ H ₁₂ O + H ⁺] ⁺	185; 6.2 and 5.2	Not observed	C ₁₃ H ₁₂ O	184
47 (ESI-)	[C ₁₂ H ₁₂ O ₂ - H ⁺] ⁻	187; 4.0	Not observed	C ₁₂ H ₁₂ O ₂	188
32 (ESI-)	[C ₂₆ H ₂₆ O ₄ - H ⁺] ⁻	401 (weak signal); 4.4	401.1776; 4 ppm	C ₂₆ H ₂₆ O ₄	402
48* (ESI-)	[C ₂₆ H ₂₆ O ₅ - H ⁺] ⁻	417; 4.9	417.1728; 5 ppm	C ₂₆ H ₂₆ O ₅	418
49* (ESI-)	[C ₂₇ H ₂₆ O ₆ - H ⁺] ⁻	445; 5.2	445.1682; 6 ppm	C ₂₇ H ₂₆ O ₆	446
50* (ESI+)	[C ₁₃ H ₁₂ O ₂ + H ⁺] ⁺	201; 7.7	Not observed	C ₁₃ H ₁₂ O ₂	200

* Ions observed but no corresponding structure reported in literature

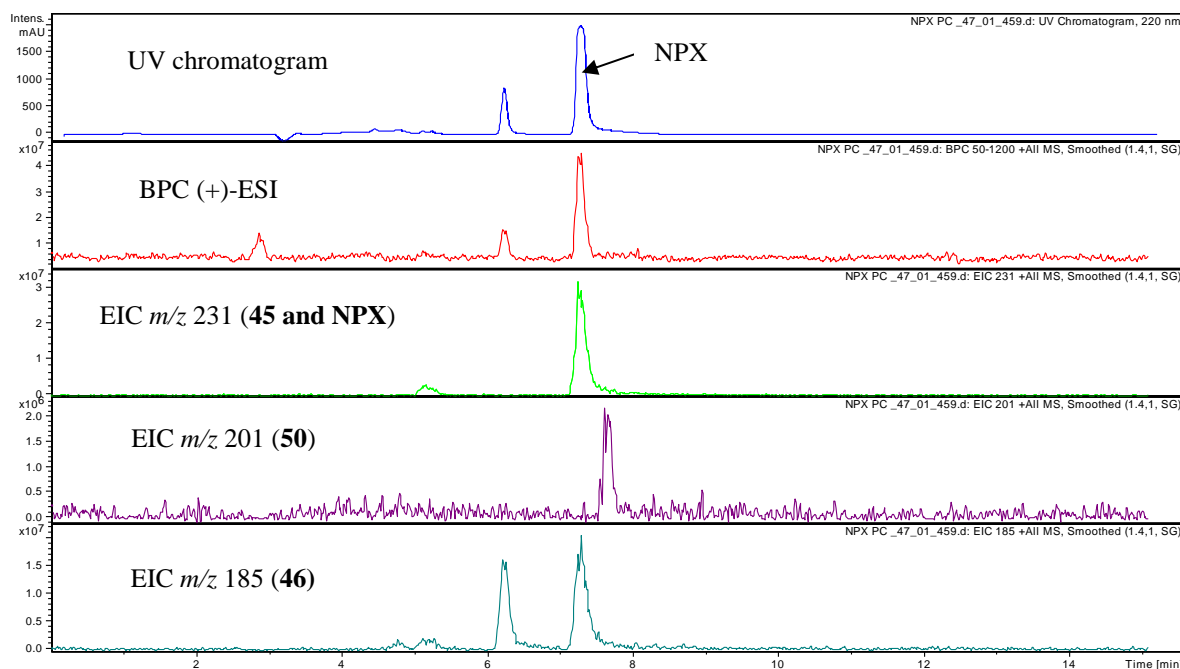
The possible degradation pathways based on the identified degradation products (Table 6.2) are presented in Fig.6.9. Negative ions corresponding to m/z 481, 229, 185, 171 and 170 and positive ions at m/z 275 and 253 were observed in the UV/TiO₂ oxidized NPX sample by LC-MS and FT-ICR-MS.

Thus far, only one study by Méndez-Arriaga *et al.* [126] has proposed a reaction mechanism for TiO₂ photocatalysis of NPX using LC-TOF-MS in negative mode. The study proposed demethylation and decarboxylation as the major degradation pathways involved in the NPX photocatalytic degradation followed by hydrogen abstraction and hydroxylation. Based on the comparison of UV chromatograms and BPCs, major products identified corresponded to m/z 185 (t_R = 5.2 and 6.2 min), m/z 215 (t_R = 6.2 min), m/z 417 (t_R = 4.9 min) and m/z 445 (t_R = 5.2 min). The ion at m/z 215 was reported as the principal peak by Méndez-Arriaga *et al.* [126] together with a compound at m/z 401, the latter of which yielded a weak signal in our study. Both of these peaks were reported to elute after the parent NPX, however in this study both were found to elute prior to NPX (t_R = 7.3 min).

In the first pathway proposed by Méndez-Arriaga *et al.* [126], demethylation of NPX by HO[•] radical attack, leads to a demethylated radical. This can further abstract a hydrogen from water on the surface of TiO₂ to produce **29** (m/z 215) (2-(6-hydroxynaphthalen-2-yl)propanoic acid).

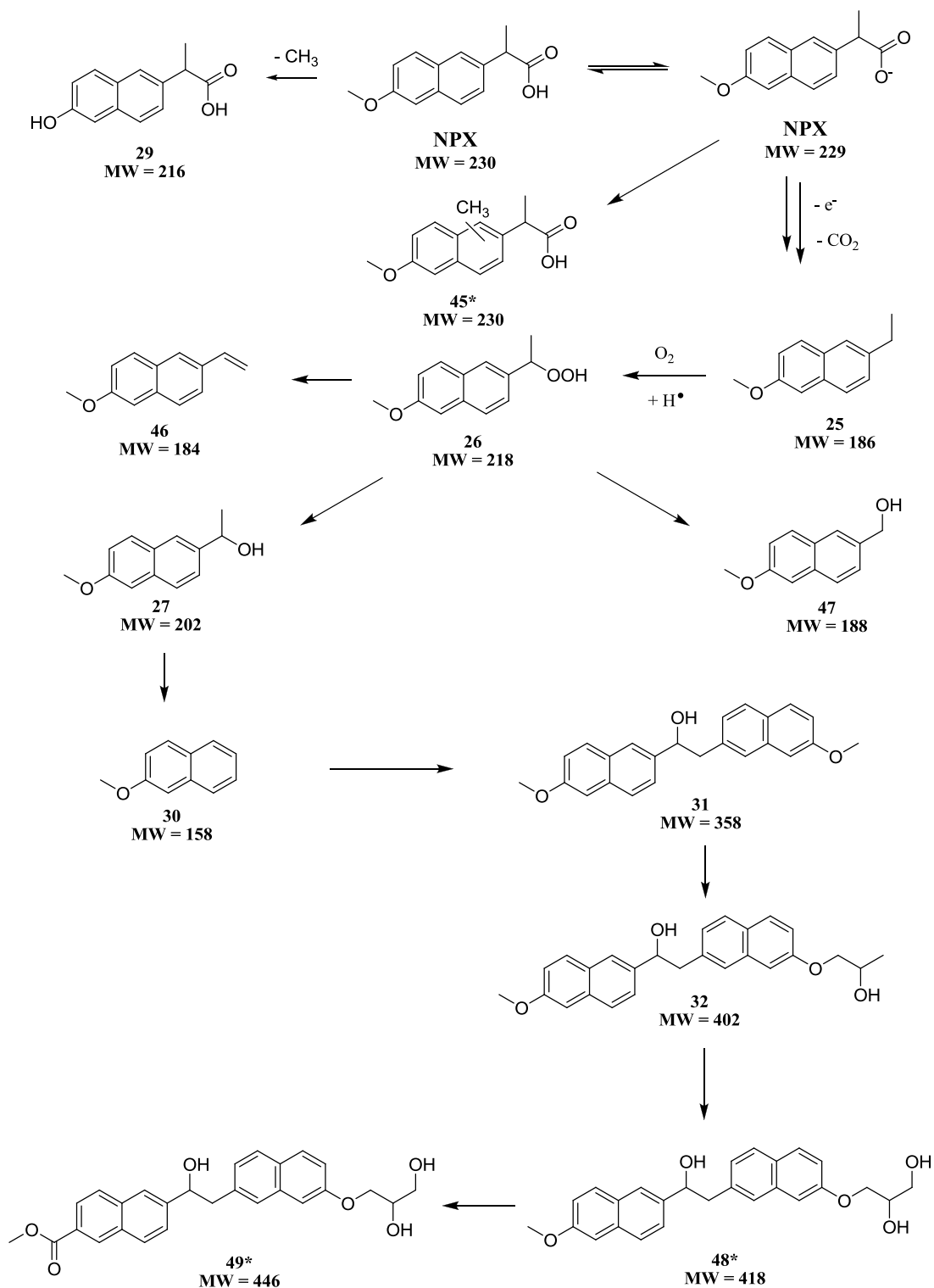


(a)



(b)

Fig.6.8 LC-MS data of TiO_2 photocatalysis of NPX (a) in (-)-ESI and (b) (+)-ESI. The top spectrum in each figure is the UV chromatogram, also shown is the BPC. EICs show the retention times and masses of the degradation products



* These are putative structures and further structural elucidation is required to confirm

Fig.6.9 Proposed TiO₂ photocatalytic degradation pathway of NPX

In another pathway, carboxylate carboxylate NPX, in the form of a Na salt, could be converted to the corresponding carboxyl radical by photoionization (or electron ejection) and subsequent decarboxylation to generate the benzylic radical. Hydrogenation of the benzylic radical yields **25**

with a m/z 185 (1-ethyl-6-methoxynaphthalene). Compound **25** (1-ethyl-6-methoxynaphthalene) has been identified as the main product during direct photolysis under anaerobic conditions [178].

In the presence of oxygen, oxygen trapping by benzylic radicals and subsequent breakdown of these unstable hydroperoxides has been proposed to be responsible for the formation of alcohol **27** and also for the formation of olefin **46** (m/z 185), 2-methoxy-6-vinylnaphthalene [181]. In the present study, compound **27** was not detected. This compound has been reported to be produced under both aerobic and anaerobic conditions [178, 232]. Although oxygen was not supplied during the reaction, dissolved oxygen, generated during stirring could contribute to this pathway. Compound **47** (m/z 187) (6-methoxynaphthalen-2-yl)methanol could be generated from the unstable hydroperoxide (**26**).

Cleavage of the C-C bond of the naphthalene ring in **27** would lead to **30** (2-methoxynaphthalene). Coupling of **27** and **30** would also likely form the dimer **31** (1-(6-methoxynaphthalen-2-yl)-2-(7-methoxynaphthalen-2-yl)ethanol. Compound **31** could react with the hydroxyl alkyl radical, $\text{CH}_3\text{OHCH}_2\cdot$ via an initial demethylation step to compound **32** (m/z 401), which was previously reported during photolytic [181] and TiO_2 photocatalytic processes [126]. The hydroxyl alkyl radical is most likely involved in other pathways leading to the formation of aliphatic acids such as acetic, maleic, succinic and oxalic acids and other compounds such as volatile compounds and low-weight aqueous soluble compounds. Further hydroxylation of compound **32** would lead to **48** (m/z 417) and **49** (m/z 445), respectively. The weak signal obtained for compound **32** compared to **48** suggests that, in the present study, the reaction conditions favour the formation of compounds **48** and **49**, which have not been reported in the literature thus far.

LC-MS also detected the presence of an ion (**45**) with the same formula as the parent NPX, which eluted 2 mins earlier. It is possible that there is a rearrangement occurring by demethylation of the methoxy onto the naphthalene ring.

It has been reported that NPX, which is a commonly prescribed drug for humans, is excreted along with its metabolized form 6-O-desmethylnaproxen [233]. A toxicity study conducted to assess the environmental risk of NPX and its break downproducts showed that compound **31** with m/z 358 exhibited approximately 10 times higher toxicity than the parent NPX [181]. Thus, the formation of yet larger degradation products, as detected in this study, suggests the importance of conducting toxicity assessments on these compounds in the future.

The presence of these degradation products also corresponds to low DOC removal during TiO_2 photocatalysis of NPX in distilled water. DOC reduced by only 19% in the presence of TiO_2 , while direct photolysis did not result in any removal.

6.4. Degradation products of diclofenac and naproxen mixtures

A sample withdrawn from the TiO₂ photocatalysis of a DCF and NPX mixtures (1:1 ratio 250 mg/L each) after 120 min of irradiation with a medium pressure Hg lamp was analysed for degradation products by LC-MS by both negative and positive modes. The chromatographic conditions for the separation of DCF, NPX and its degradation products were as reported in Chapter 3. The standard mixture was also analysed for possible degradation products using LC-MS and FT-ICR-MS.

The ions previously detected in the individual standards of DCF and NPX were all confirmed in the standard mixture (Fig.6.10). Ions of NPX ($t_R = 7.3$ min) (m/z 275, 253, 231 and 185) and DCF ($t_R = 13.3$) (m/z 318) were confirmed to be present in positive mode LC-MS. FT-ICR-MS confirmed the molecular formulas for m/z 275 and 253 in NPX and m/z 318 in DCF. Ions of NPX (m/z 481, 311, 229, 185, 171 and 170) and DCF (m/z 294 and 250) were also confirmed to be present in negative mode LC-MS. Again, formulas corresponding to at m/z 481, 229, 185 and 170 in NPX and m/z 250 in DCF were confirmed by FT-ICR-MS.

To determine the formation of degradation products in the DCF and NPX mixtures, m/z values were compared to those formed by individual APIs. Direct comparison, based on retention time of the degradation products formed after treatment of the mixtures with those formed from NPX or DCF only, was not possible due to the fact that the NPX and DCF samples was undertaken using different mobile phases. Given this, a third mobile phase was used for separation of the NPX and DCF mixtures (section 3.7.1 in Chapter 3) and LC-MS used to identify common degradation products as well as those formed only in the mixtures.

Table 6.3 summarizes all degradation products identified during TiO₂ photocatalysis of DCF and NPX mixtures in distilled water by LC-MS. Subsequent FT-ICR-MS analysis (characteristic isotope distributions and the accurate mass determination) confirmed the structures of the degradation products. Fig.6.11 shows the UV chromatogram followed by BPC in (-)-ESI and (+)-ESI modes.

Several degradation products observed in the individual APIs were confirmed to be present in the photocatalytic degradation of the DCF and NPX mixtures. One example is the degradation product of NPX corresponding to m/z 201, which was also generated in the mixtures of DCF and NPX. This degradation product was identified as 1-(6-methoxy-naphthalen-2-yl)ethanone in the literature [202] and was proposed to be formed under aqueous oxygenated conditions as explained in section 2.10.3 (Chapter 2).

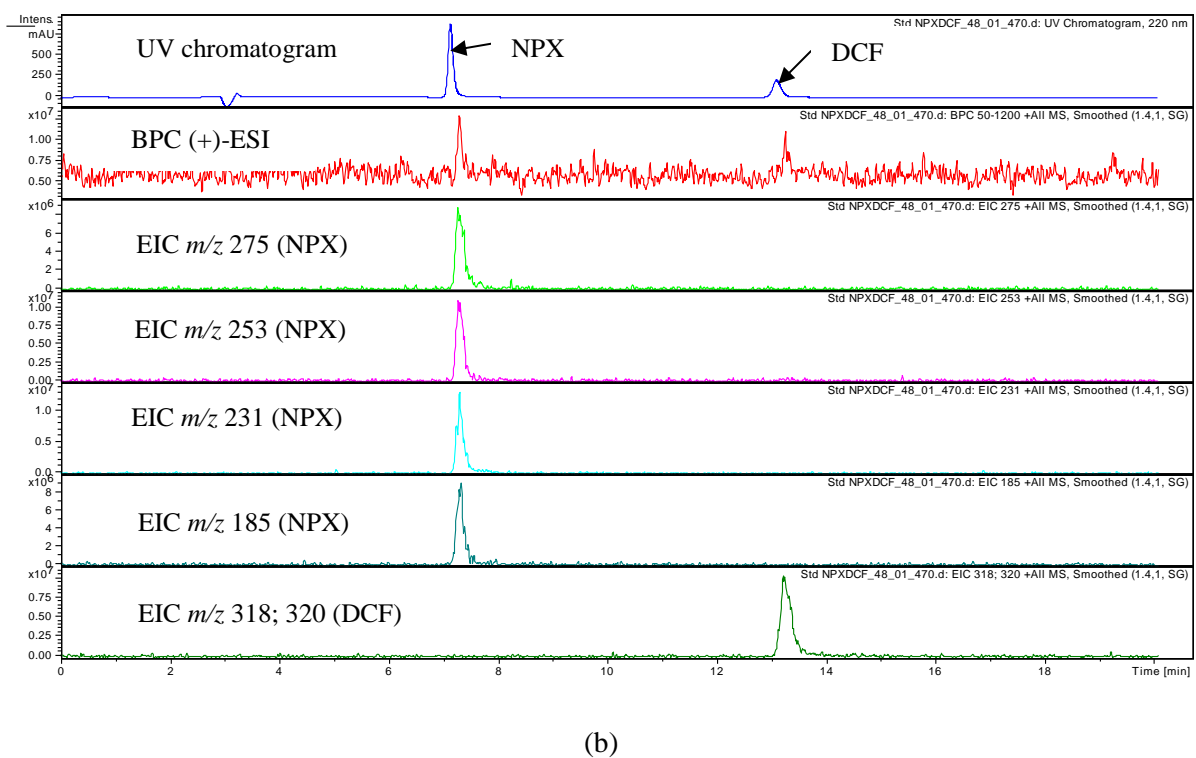
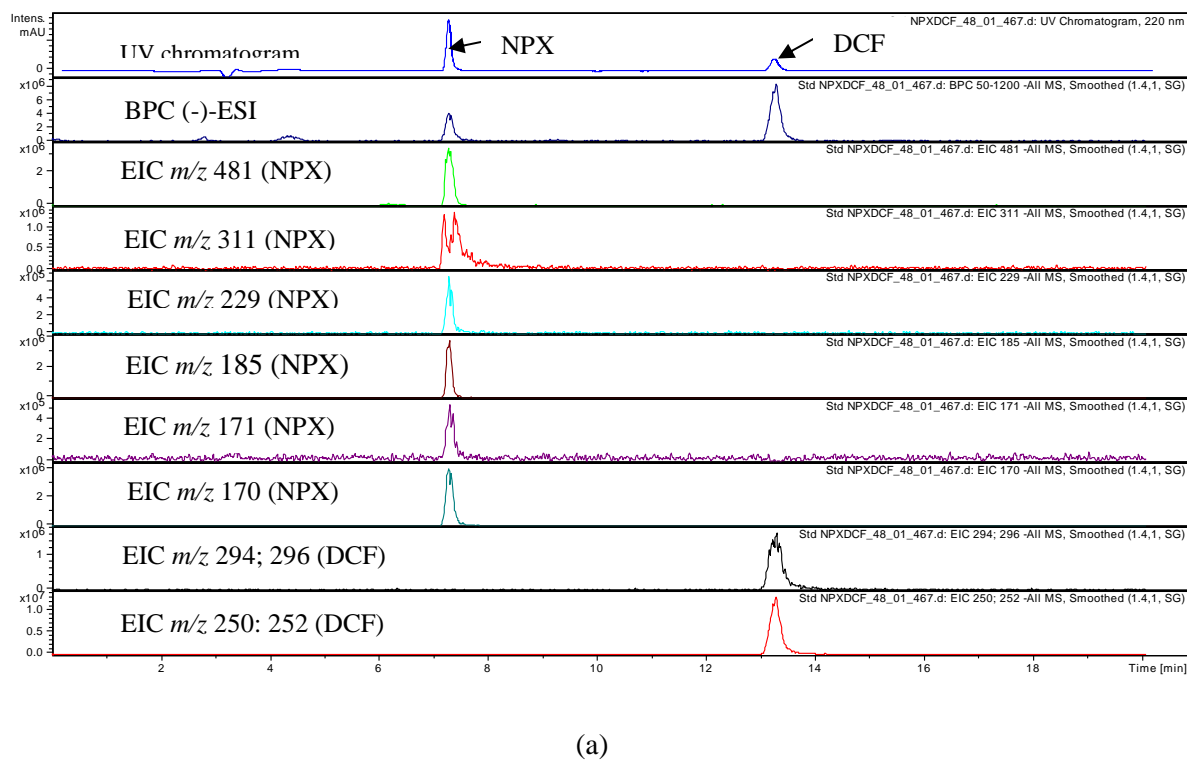


Fig.6.10 LC-MS ion of DCF and NPX mixture standard (a) (-)-ESI mode and (b) (+)-ESI mode. The top spectrum in each figure is the UV chromatogram, also shown is the BPC. EICs show the ions formed under ESI conditions

Table 6.3 Degradation products of DCF and NPX mixtures resulting from UV/TiO₂ with a medium pressure Hg lamp identified by a combination of (+/-)-ESI LC-MS and FT-ICR-MS techniques

Compound (ionization mode)	t _R (min)	Observed ion	Observed LC-MS EIC(m/z)	Observed FT-ICR-MS (m/z); error Δ ppm	Formula	Molecular weight (g/mol)	Ions also observed in treatment of NPX, DCF or mixture only
47 (ESI-)	4.1	[C ₁₂ H ₁₂ O ₂ - H ⁺] ⁻	187	Not observed	C ₁₂ H ₁₂ O	188	NPX
48 (ESI-)	4.9	[C ₂₆ H ₂₆ O ₅ - H ⁺] ⁻	417	417.1712; 1	C ₂₆ H ₂₆ O ₅	418	NPX
45 (ESI+)	5.2	[C ₁₄ H ₁₄ O ₃ + H ⁺] ⁺	231	231.1017; 1	C ₁₄ H ₁₄ O ₃	230	NPX
49 (ESI-)	5.3	[C ₂₇ H ₂₆ O ₆ - H ⁺] ⁻	445	445.1666; 2	C ₂₇ H ₂₆ O ₆	446	NPX
6 (ESI-)	5.5	[C ₁₄ H ₁₁ O ₃ N - H ⁺] ⁻	240	240.0663; 1	C ₁₄ H ₁₁ O ₃ N	241	DCF
23 (ESI-)	5.5	[C ₁₃ H ₁₁ ON - H ⁺] ⁻	196	196.0769; 1	C ₁₃ H ₁₁ ON	197	
6 (ESI+)	5.5	[C ₁₄ H ₁₁ O ₃ N + Na ⁺] ⁺	264	264.0642	C ₁₄ H ₁₁ O ₃ N	241	
29 (ESI-)	6.2	[C ₁₃ H ₁₂ O ₃ - H ⁺] ⁻	215	Not observed	C ₁₃ H ₁₂ O ₃	216	NPX
46 (ESI+)	6.3	[C ₁₃ H ₁₂ O + H ⁺] ⁺	185	185.0964; 0	C ₁₃ H ₁₂ O	184	NPX
24 (ESI-)	6.8	[C ₁₃ H ₁₁ N - H ⁺] ⁻	180	180.0819; 0	C ₁₃ H ₁₁ N	181	DCF
50 (ESI+)	7.7	[C ₁₃ H ₁₂ O ₂ + H ⁺] ⁺	201	201.0913; 1	C ₁₃ H ₁₂ O ₂	200	NPX
1 (ESI-)	10.4	[C ₁₄ H ₁₀ O ₂ NCl - H ⁺] ⁻	258	Not observed	C ₁₄ H ₁₀ O ₂ NCl	259	DCF
12 (ESI-)	10.4	[C ₁₃ H ₁₀ NCl - H ⁺] ⁻	214	214.0429; 0	C ₁₃ H ₁₀ NCl	215	
1 (ESI+)	10.4	[C ₁₄ H ₁₀ O ₂ NCl + Na ⁺] ⁺	282	Not observed	C ₁₄ H ₁₀ O ₂ NCl	259	
1 (ESI-)	10.4	[C ₁₄ H ₁₀ O ₂ NCl + Na ⁺ -2H ⁺] ⁻	280	Not observed	C ₁₄ H ₁₀ O ₂ NCl	259	
(ESI-)*	13.8	[M + H ₂ O - H ⁺] ⁻	424	424.1559		407	Mixture
(ESI+)*	13.8	[M + H ⁺] ⁺	408	408.3081		407	Mixture
(ESI-)*	14.4	[M + H ₂ O - H ⁺] ⁻	424	424.1559		407	Mixture
(ESI+)*	14.4	[M + H ⁺] ⁺	408	408.3081		407	Mixture
(ESI-)*	16.0	[M - H ⁺] ⁻	452	452.1520		453	Mixture
(ESI-)*	17.3	[M - H ⁺] ⁻	452	452.1520		453	Mixture
(ESI+)*	18.6	[M + H ⁺] ⁺	454	454.1395		453	Mixture
(ESI-)*	18.6	[M + H ₂ O - H ⁺] ⁻	424	424.1559		407	Mixture
(ESI+)*	18.6	[M + H ⁺] ⁺	408	408.3081		407	Mixture

*Ions observed but no corresponding structure reported in literature

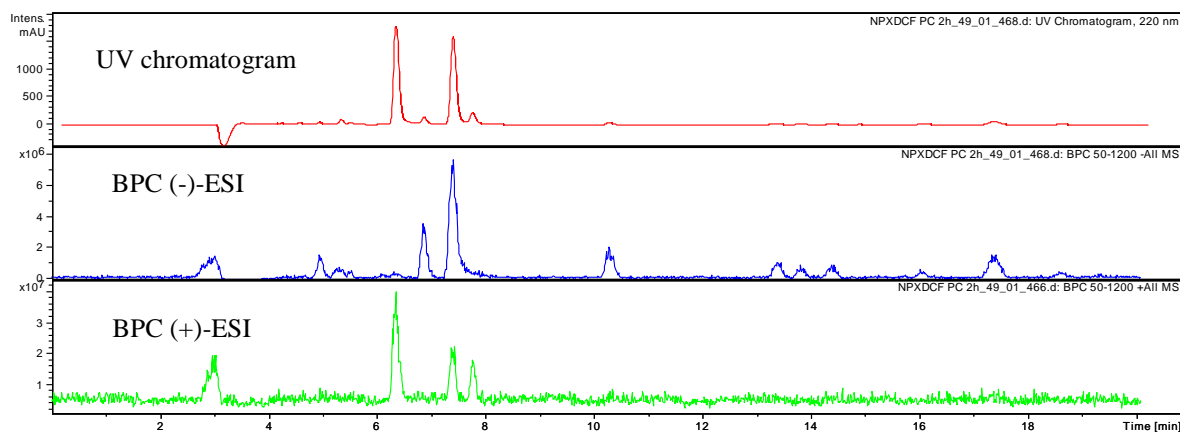
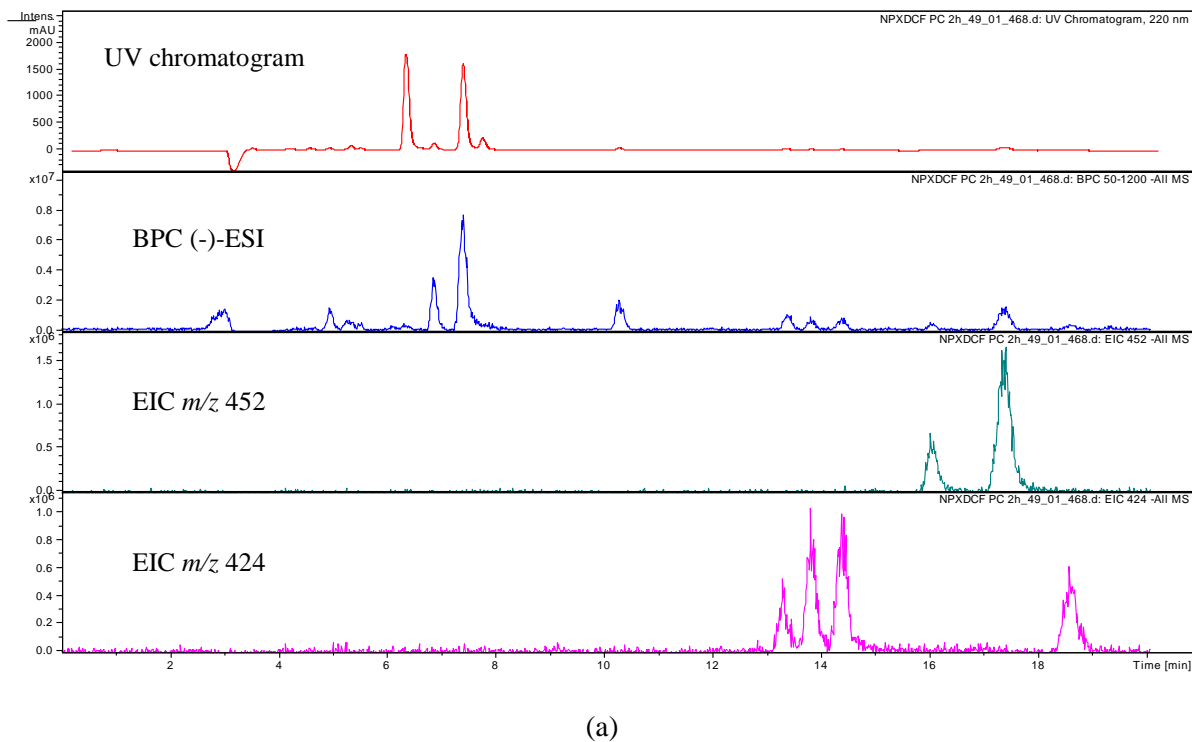


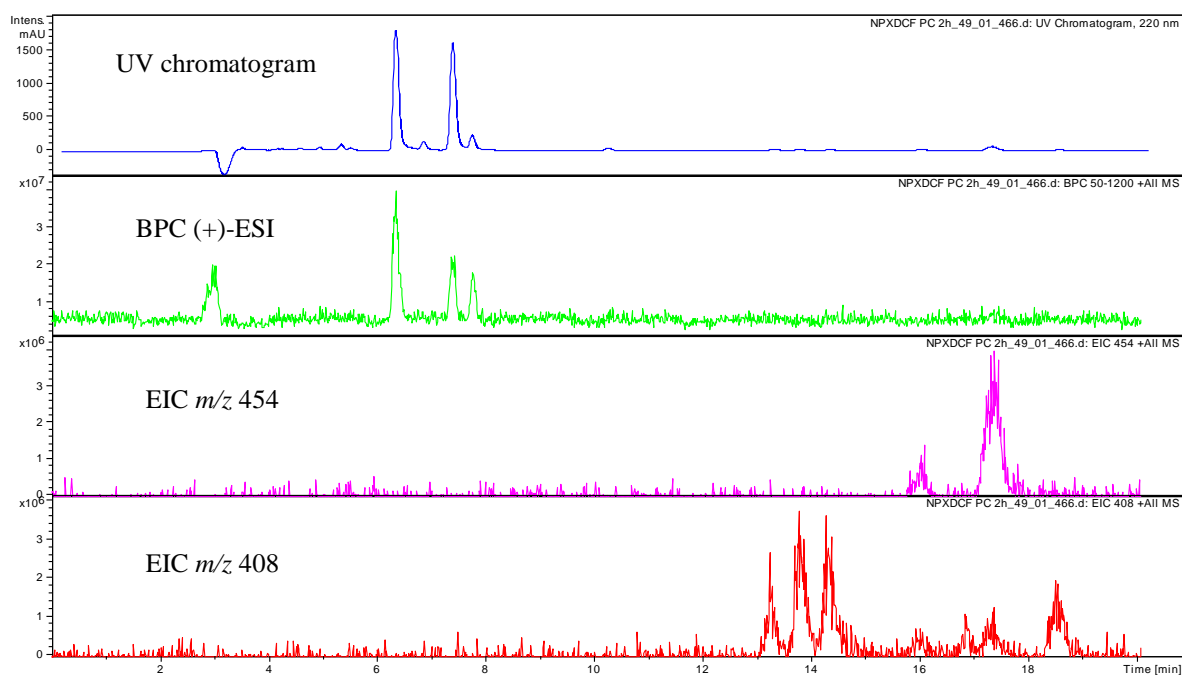
Fig.6.11 UV chromatogram and BPC (-)-ESI and (+)-ESI of DCF and NPX mixtures

Fig.6.12 shows the UV chromatogram, BPCs and the EICs of common ions detected by LC-MS in negative and positive ESI modes in the TiO_2 photocatalysis of DCF and NPX mixtures. Treatment of the DCF and NPX mixtures resulted in the detection of two larger degradation products (putative molecular weight 407 g/mol and 453 g/mol). Neither of these products was formed in the individual treatments. One interesting characteristic of these products was their elution order; they eluted after 13.8 min as compared to starting material NPX ($t_R = 7.4$ min) and DCF ($t_R = 13.3$ min), suggesting generation of hydrophobic degradation products. These two products could possibly result from a hybrid cross-coupling between the two parent APIs, between their intermediates formed during the course of reaction, or between the intermediates and the parent APIs. As a result of these complexities, the assignment of structures is not possible without the application of other techniques e.g. nuclear magnetic resonance (NMR).

Further comparison of the degradation products formed showed that the ions at m/z 250 (corresponding to **8**) and m/z 401 (corresponding to **32**) were not detected in the treated DCF and NPX mixtures indicating that either their degradation pathways were being retarded or that they formed and were immediately converted into other degradation products.



(a)



(b)

Fig.6.12 LC-MS data of common ions in the TiO_2 photocatalysis of DCF and NPX mixtures in (a) (-)-ESI and (b) (+)-ESI. The top spectrum in each figure is the UV chromatogram, also shown is the BPC. EICs show the retention times and masses of the degradation products

6.5. Conclusions

LC-MS analyses allowed the identification of main degradation products during TiO₂ photocatalysis of DCF, NPX and their mixtures. The applied FT-ICR-MS also permitted the confirmation of molecular formulas. A total of six degradation products were identified in the DCF photocatalytic assay while NPX yielded a total of eight degradation products. The major degradation pathways for DCF include photocyclization, decarboxylation and hydroxylation while photocatalytic degradation of NPX proceeds primarily via demethylation and decarboxylation. In the mixtures, two common degradation products were generated in addition to those degradation products formed during the individual photocatalytic treatments. While FT-ICR-MS enabled accurate mass determination, assignment of possible structures for these two compounds would require the isolation of the individual components in larger quantities and undertaking NMR.

The large number of known and new compounds, including those larger molecular weight compounds, detected in the TiO₂ photocatalytic treatment of NPX, DCF and their mixtures thereof, highlights the importance of degradation product identification. Degradation products that exhibit different properties (e.g. polarity), may also possess different levels of toxicity, further highlighting the importance of assessing the potential ecological risk these products may pose to the environment.

Although TiO₂ photocatalysis demonstrated good performance to degrade individual parent APIs and in their mixtures, the indirect generation of degradation products necessitate toxicity assessment of on these products which can be considered in future studies. Also, toxicity data and structural elucidation of these degradation products may provide some indication about the safety or applicability of TiO₂ photocatalysis for wastewater purification.

Chapter 7. Integrated photocatalytic adsorbents for the degradation of amoxicillin

7.1. Introduction

Although application of TiO₂ in a suspension is considered efficient for photocatalytic degradation of pharmaceuticals, such an approach requires a post recovery method at the end of the treatment process. This limits the applications of TiO₂ in real wastewater treatment plants as it is time-consuming and uneconomical due to the high costs involved in catalyst recycling. To overcome the separation of TiO₂ nanoparticles during this process, immobilization of TiO₂ on an adsorbent or an inert support to form integrated photocatalytic adsorbents (IPAs) may offer a viable solution to this problem. By adopting this technique, simultaneous benefits include the: (i) pollutant adsorption capability by the adsorbent and (ii) the decontamination properties by the immobilized TiO₂. Therefore, degradation of pollutants, such as pharmaceuticals can be achieved by adsorption and degradation.

Among the various available adsorbents, natural zeolites were chosen as adsorbents which have been less explored compared to other adsorbents such as activated carbon and synthetic zeolites. IPAs were prepared by combining natural zeolite and TiO₂ which was prepared using the sol-gel method. TiO₂ was also immobilized using the biopolymer, alginate.

This chapter provides an overview of immobilization of TiO₂ on different adsorbents or supports with the main focus on natural zeolite. This is followed by the results for the photocatalytic activity of the synthesized IPAs and TiO₂-gel beads for the degradation of AMX. Another objective of this chapter is to identify the degradation products formed by hydrolysis (during initial adsorption) and photocatalysis by the best performing TiO₂/zeolite IPA materials.

7.2. Optimising titanium dioxide's photocatalytic activity

Studies have shown that some pharmaceutical compounds can undergo direct photolysis [84, 160, 205], although the addition of TiO₂ accelerates this degradation process. Thus far, promising results have been obtained using the TiO₂ photocatalytic degradation processes [121, 142, 184]. Despite this, nanosized TiO₂ has demonstrated a limited photocatalytic activity, which implies that the catalyst needs to undergo some modifications or enhancement. There is a need to improve the photocatalytic efficiencies of nanosized TiO₂ due to several limitations: (i) the low intrinsic photonic yield; (ii) the high band gap energy (3.2 eV; $\lambda < 380$ nm), which requires excitation in the UV region and (iii) the formation of suspensions in wastewater treatment [234, 235]. Thus, metal and non-metal

ion doping, which modifies the band gap and the corresponding excitation wavelength, and solid-supported nanosized TiO₂ to create a hybrid material IPAs are the two common approaches applied to address these limitations.

Doping generates a better adsorption in the visible region and produces higher photonic yields. In return, however, it increases the costs of the photocatalyst due to expensive ion implantation procedures [236]. In contrast, anchoring TiO₂ onto a suitable and inexpensive adsorbent for the creation of “capture and destroy” materials is much more cost effective. However, IPAs may lead to a decrease in photocatalytic efficiency of the catalyst due to a mass transfer limitation as a result of reduction in the specific surface area [237].

7.3. Integrated photocatalytic adsorbents

Numerous studies have been focused on the preparation of IPAs from different adsorbents such as activated carbon [238], zeolite [235], polymers [239], glass [240], clay [241] and fly ash [242]. The choice of the adsorbent is very important and needs to meet multiple criteria. These include: (i) a UV-transparency, (ii) a high specific surface area, (iii) a strong adherence between catalyst and support, (iv) a strong adsorption affinity towards the organic pollutant and (iv) a non-reduction of the catalyst reactivity by the anchoring process [237].

Choosing an adsorbent that addresses all of these criteria represents a challenge. Studies conducted to date have not yet identified the best IPA material for application in real wastewater treatment. Published results displayed variations in photocatalytic activities by different TiO₂ synthesis methods, type of solid supports used, coating methods and model compound chosen for evaluation of the IPAs. Some studies reported complete mineralization of the model compound under investigation but low efficiency of reusability or recovery. According to Malato *et al.* [109], important parameters such as catalyst activity, durability of the IPA and lifetime are insufficiently addressed in many studies. Furthermore, evaluations of IPAs for pharmaceutical degradation are rare and most studies tend to focus on other organic compounds such as phenols [243], salicylic acid [244] and dyes [245].

The sol-gel method is widely used for the preparation of TiO₂ and was also applied in this study. This method is relatively inexpensive, does not require sophisticated equipment and shows a flexible applicability to a wide range of sizes and shapes of substrates. The success of sol-gel preparation is governed by various parameters and conditions, such as type and amount of precursor, solvent used, amount of water, pH and the type of chelating agents used. Several synthetic pathways are available for the preparation of photocatalyst from precursor chemicals such as titanium alkoxides, titanium tetrachloride or titanium halogenide. These precursors are normally calcined at very high

temperatures to obtain both the desired crystal form and strong adhesion to the solid support. Hydroxyl groups (OH) from the catalyst surface and the support can react and upon dehydration, creating an oxygen linkage thus increasing the adherence of the catalyst to the support during calcination [237]. The rate of hydrolysis is difficult to control due to the high affinity of all TiO_2 precursors towards water, thus leading to poor modification of TiO_2 's intrinsic properties, such as the surface structure, its structural properties and porosity. Nitric acid (HNO_3), hydrochloric acid (HCl) and other complex reagents like oxalate and citrate have been commonly applied as additives in the sol-gel synthesis to control the hydrolysis and condensation process.

Zeolite was chosen as the adsorbent in this study. Studies utilizing zeolite as TiO_2 photocatalyst support have been mainly focused on synthetic zeolites such as ZSM-5, HZSM-5, Y zeolites and molecular sieves (e.g. MCM-41). Natural zeolites have not been studied systematically as TiO_2 supports for the degradation of pharmaceuticals. In contrast, applications for the degradation of dyes are common [246-248].

Natural zeolites, which exist naturally in the environment, are available in various forms, for example, modernite and clinoptilolite. Zeolites are hydrated aluminosilicate minerals made of three-dimensional structures of SiO_4 and AlO_4 tetrahedral linked by oxygen atoms to form a cage-structure (Fig.7.1) [249]. They are characterized by good adsorption abilities, uniform channels and regular pores [248].

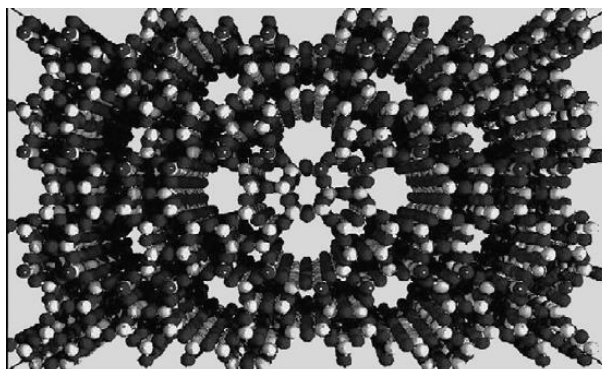


Fig.7.1 Structure of zeolite [250]

TiO_2 can be readily supported in these existing cage-structure or channels in the range of 4-14 Å. Depending on the adsorption site, zeolites can behave as both an electron donor and acceptor [251]. Composition and therefore the physico-chemical properties of natural zeolite vary with geographic location. Due to this variation, pre-treatment of zeolites is commonly applied to enhance their absorption efficiency. Ion exchange with inorganic salts and alkali bases, acid leaching and calcination at high temperature have been applied to modify the surface structure of zeolites [252].

A major challenge when preparing TiO₂ supported zeolite is to retain both the adsorption properties of the zeolite support and the photocatalytic activity of the supported TiO₂ [247].

7.4. Titanium dioxide supported on Ca-alginate

Alginate is a natural biopolymer, which can be extracted from brown seaweed [253]. Alginate is capable of forming stable hydrogels, which can be potentially used as a catalyst support [254]. A study by Albarelli *et al.* [255] investigated TiO₂ immobilization on Ca-alginate beads for the degradation of the methylene blue. Recycling of the TiO₂-gel beads was found to enhance the degradation process which was explained by the increased roughness of the alginate beads upon repeated usage. Although suspended TiO₂ outperformed the TiO₂-gel beads, it was concluded that immobilized TiO₂ offers a more practical approach for wastewater treatment. A recent study furthermore revealed that Ca-alginate polymer fibers demonstrated high efficiency in removing methyl orange from water [254].

Despite very limited application as photocatalyst thus far, alginate represents an interesting option as a support. More studies need to be conducted to explore its ability to degrade other compounds, in particular emerging pollutants such as pharmaceuticals. In this study, several experiments were performed to remove AMX with immobilized TiO₂ on Ca-alginate beads and subsequently to evaluate this material for the degradation of pharmaceuticals.

7.5. Materials and method

7.5.1. Reagents and chemicals

Titanium (IV) isopropoxide (C₁₂H₂₈O₄Ti) (TTiP 95%) (Alfa Aesar, England), absolute ethanol (AR grade from Univar, Australia), nitric acid (AR from BDH Chemical, Australia), hydrochloric acid (AR grade from Ajax Finechem Pty Ltd., Australia), sodium hydroxide (AR grade from Ajax Finechem Pty Ltd, Australia) and amoxicillin (R&D grade from Sigma-Aldrich, USA) were used as received. Commercial Aeroxide[®] TiO₂ P25 (80% anatase and 20% rutile, BET surface area 50 m²/g) was supplied by Evonik Industries (Canada). Natural Australian zeolite (Escott zeolite regular powder, <75 μm) was obtained from Zeolite Australia Pty Limited (NSW, Australia). Alginic acid sodium salt (NaAlg) (Sigma-Aldrich, USA) and calcium chloride dihydrate (AR from Ajax Finechem, Australia) was used for the preparation of Ca-alginate. Milli-Q water was obtained from a Barnstead Nanopure Diamond water ion exchange system (18.2 MΩcm resistivity).

7.5.2. Pre-treatment of natural zeolite

The raw Escott zeolite used in this study consisted of the zeolitic mineral clinoptilolite and other trace levels of mordenite, quartz, clay and mica. The zeolite was analysed for its composition by energy dispersive X-ray spectroscopy (EDS) (Table 7.1). The characterization study of the zeolite supplied revealed SiO₂ and Al₂O₃ as major constituents.

Table 7.1 Composition of Escott natural zeolite

Compound	Mass (wt %)
Na ₂ O	2.29
MgO	1.03
Al ₂ O ₃	11.59
SiO ₂	72.79
SO ₃	4.21
K ₂ O	2.06
CaO	4.15
FeO	1.88

Zeolite (20 g/L) was vigorously stirred in deionized water for 5 h and the suspension was allowed to settle prior to filtration and further washing with deionized water. Two types of treatment were performed on this zeolite sample, (i) an acid activation and (ii) a combination of acid-alkali activation. For the acid activation, the zeolite was treated with 1 M HCl for 24 h under continuous stirring. For the acid-alkali activation, the initial treatment was performed with 1 M HCl and was followed by 1 M NaOH. Contact times of zeolite with each reagent were kept at 5 h under vigorous stirring. The pre-treated zeolite was continuously washed with deionized water and oven dried at 70°C for 24 h in a laboratory oven followed by heat treatment at 300°C in a furnace oven.

7.5.3. Preparation of IPA

Initial TiO₂/zeolite material was prepared using the two-step synthetic method published by Chong *et al.* [241] with titanium (IV) butoxide as Ti precursor. In the first step, 25 mL solution of titanium (IV) butoxide was mixed with 30 mL of absolute ethanol under continuous stirring. According to the published method, the dropwise addition of 60 mL of diluted HNO₃ acid should form a milky white and subsequently transparent homogeneous sol. However, in this study, the addition of 60 mL of diluted HNO₃ acid (0.25 M) failed to result in the formation of a transparent sol. Since the first step could not be reproduced successfully, another approach was followed.

The second synthetic method, modified from Huang *et al.* [248] and Silva [256] as summarized briefly in Fig.7.2 was attempted.

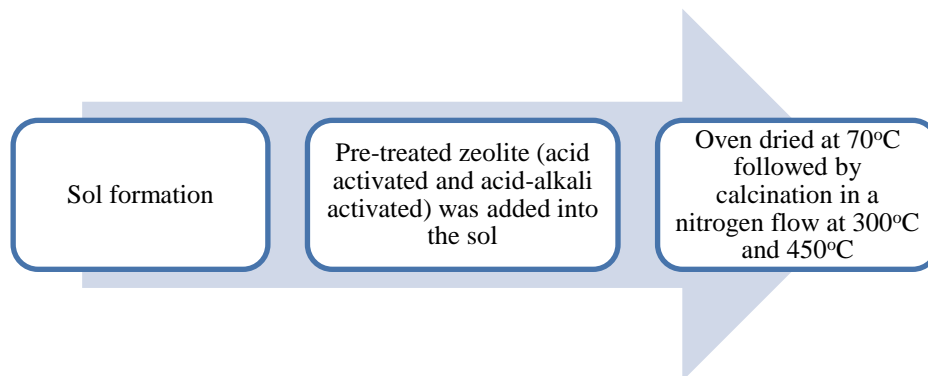


Fig.7.2 TiO₂/zeolite IPA preparation process

0.1 mol of TTiP was dissolved slowly in 100 mL of absolute ethanol. A white sol formed within 10 min of stirring. The sol was left further stirring for 30 min before concentrated HNO₃ was added dropwise (approximately 1.2 mL) until the white precipitate disappeared and a transparent sol formed. The final pH of the transparent solution was checked and adjusted to a pH of 4. HNO₃ acts as a catalyst and also controls the hydrolysis process [248]. A pH that is too low was avoided as it may have caused acid-leaching onto the zeolite which would have damaged its porous crystal structure [234]. Stirring was continued for 6 h at room temperature. A weak, transparent yellow sol was formed. The zeolite was added into the sol in a mass ratio of the 1:5 zeolite:TiO₂. The TiO₂/zeolite was stirred until a gel was formed. The TiO₂/zeolite was aged at room temperature through loose covering for 24 h. Subsequently, it was oven-dried at 70°C for 10 h (Fig.7.3) and ground in a mortar to obtain a homogeneous material. These steps were performed with both acid activated and acid-alkali activated zeolites.



Fig.7.3 Synthesized TiO₂/zeolite from acid-alkali activated zeolites after oven drying (before homogenisation)

The prepared TiO₂/zeolite samples were calcined at 300°C and 450°C in a nitrogen flow with a horizontal split tube furnace (LABEC Model HTFS60/13) for 2 h. For comparison, pure TiO₂ was also prepared following this procedure but without the addition of pre-treated zeolite.

7.5.4. Characterization

Scanning electron microscopy (SEM) images of the raw zeolite and TiO₂/zeolite materials were recorded using a JEOL scanning electron microscope (JSM-5410LV) at an accelerating voltage of 10 kV. The X-ray diffraction (XRD) patterns of the prepared materials were recorded on an X-ray diffractometer (Siemens D5000) using Ni filtered Cu K α radiation ($\lambda = 1.5406$) from $2\theta = 2-65^\circ$. EDS (JEOL JXA-8200) was used to characterize the synthesized IPAs and zeolite materials for composition analysis.

7.5.5. Point of zero charge

The procedure for the point zero charge (pH_{pzc}) determination was taken from Putra *et al.* [196]. Erlenmeyer flasks with 100 mL capacity were filled with 50 mL of 0.01 M NaCl. The pH of each solution was adjusted stepwise from 2 to 12 by adding 0.1 M HCl and 0.1 M NaOH; these solutions represented the initial pH (pH_{initial}). To each flask, a 0.15 g sample of TiO₂/zeolite was added and the mixture was stirred for 24 h. The final pH of the suspension in each flask was subsequently measured (pH_{final}). The point where the curve pH_{final} versus pH_{initial} crossed the line pH_{final} = pH_{initial} represented the pH_{pzc} of the IPA.

7.5.6. Dark adsorption

AMX solutions of various concentrations between 10 mg/L and 50 mg/L were prepared and 100 mL of each solution was transferred into a 150 mL Erlenmeyer flasks. The IPA materials (0.1 g) were added to the AMX solution. The suspension was agitated for 24 h with an orbital shaker. Aliquots were collected and filtered through a 0.22 μ m syringe filter before determining the remaining concentration by HPLC.

7.6. Preparation of Ca-alginate and immobilization of TiO₂

The preparation method was adopted from Kimling *et al.* [253] and Albarelli *et al.* [255] using a 2% NaAlg and 0.1 M CaCl₂ solutions. In order to prepare the TiO₂-gel beads, two methods were

evaluated. In the first approach (method A) (Fig.7.4), TiO₂ P25 was incorporated into the NaAlg solution as follows: 20 mL of 1 g/L TiO₂ P25 was added to 50 mL 2% NaAlg solution under continuous stirring. A 20 mL aliquot of the solution mixture was withdrawn with a luer lock 20 mL syringe. A 23G needle (0.60 × 25 mm) was attached to the syringe and the solution was slowly added into a beaker containing 50 mL 0.1 M CaCl₂ under continuous stirring. The newly prepared Ca-alginate beads were allowed to remain in the Ca²⁺ solution bath for 4 h. The beads were subsequently washed with deionized water and dried at room temperature.

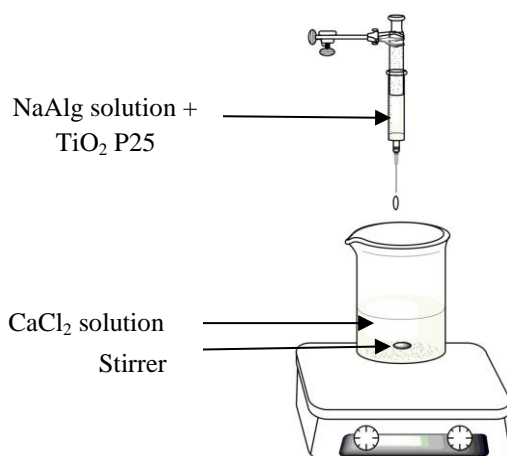


Fig.7.4 Preparation of TiO₂-gel beads based on method A

In the second approach (method B), a 20 mL NaAlg solution was withdrawn with a syringe as mentioned above and was added into 50 mL of 0.1 M CaCl₂. The newly formed Ca-alginate beads were left in the Ca²⁺ solution bath for 3 h under continuous stirring and then washed and soaked in deionized water. After filtration, the gel beads were soaked in 50 mL of either 0.5 wt% and 2 wt% TiO₂ P25 suspension for 4 h under continuous stirring. The gel beads were left in the TiO₂ P25 suspension overnight. Then, the TiO₂-gel beads were filtered, washed with deionized water and dried. TiO₂-gel beads prepared (Fig.7.5) from both approaches were used in the AMX degradation study.



Fig.7.5 Immobilized TiO₂-gel beads

Fig.7.6 shows the differences between method A and method B applied to the preparation of TiO₂-gel beads.

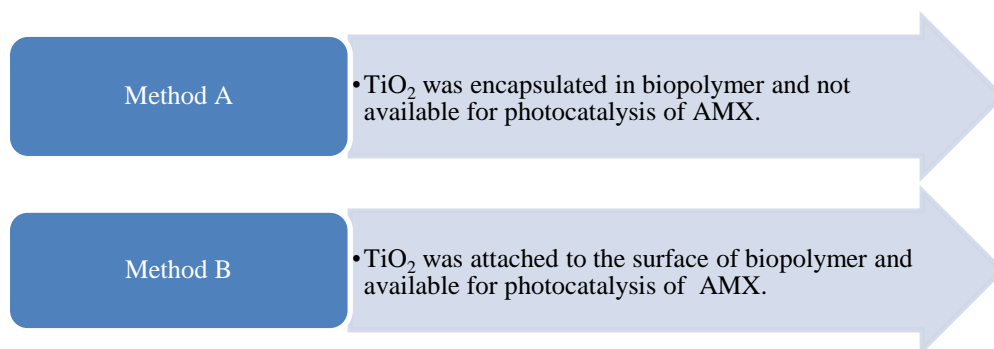


Fig.7.6 Differences between method A and method B applied to the preparation of TiO₂-gel beads

7.7. Photocatalytic assessment on amoxicillin using immobilized TiO₂

The absorption spectra of AMX at λ_{max} at 230 nm and 274 nm is shown in Fig.7.7. The photocatalytic degradation experiments involving AMX were carried out using an immersion-well reactor (optical path: ~0.5 cm) in 250 mL of an aqueous suspension (Fig.7.8).

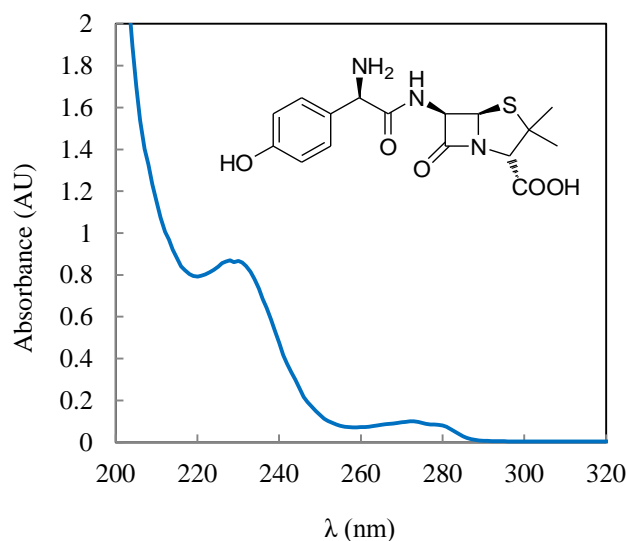


Fig.7.7 Absorbance spectrum of AMX in water

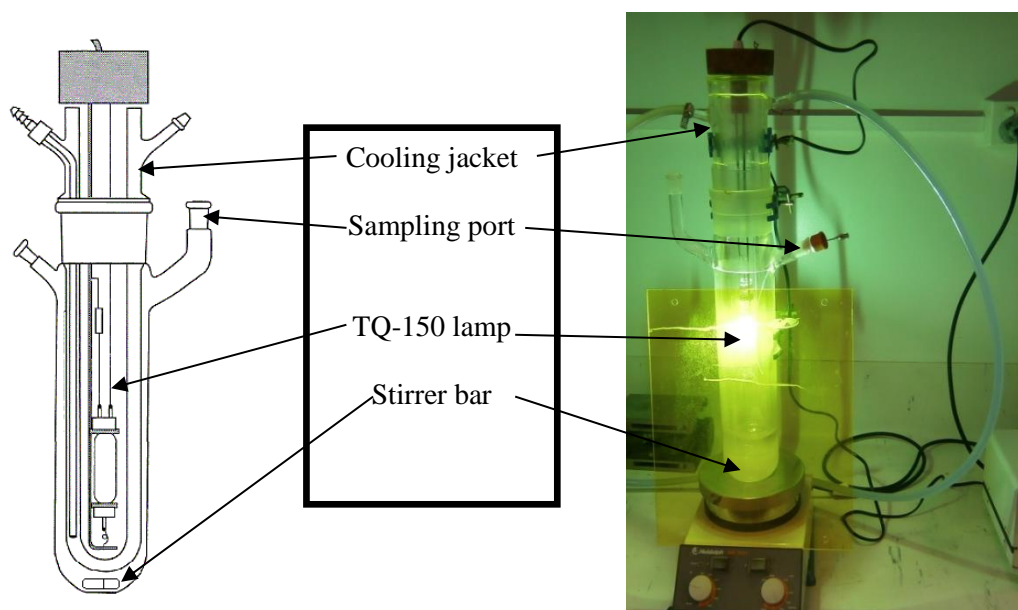


Fig.7.8 Schematic presentation and picture of immersion-well photoreactor setup

A medium pressure Hg lamp (TQ 150) was placed in the centre of the pyrex cooling jacket and a magnetic stirrer was used to provide homogeneous dispersion. The concentration of AMX fixed at 30 mg/L and 2 g/L of TiO₂/zeolite (or TiO₂ P25 or pure TiO₂ for comparison) was used. Prior to irradiations, the reaction mixture was stirred continuously for 30 min to allow adsorption of AMX onto the surface of the IPA. Samples were withdrawn at fixed times after the dark adsorption period and during irradiation and were then centrifuged at 1000 rpm for 15 min (Mini Spin Plus, Eppendoff) to remove suspended particles from the solution prior to analysis with HPLC (LC-940 Varian).

For a recycling study, the TiO₂/zeolite material from the first photocatalysis study was filtered, washed with deionized water and dried in the oven at 70°C for 1 h. These materials were tested for subsequent cycles for its photocatalytic degradation capability using fresh solutions of 30 mg/L of AMX.

A direct photolysis experiment without any photocatalyst present was also performed. For comparison, Aeroxide® TiO₂ P25 in its neat form was also tested. To measure the degree of mineralization during direct photolysis and photocatalysis with TiO₂ P25 and TiO₂/zeolite, DOC analyses were performed using a Shimadzu TOC analyser.

For degradation studies with TiO₂-gel beads, 10% v/v of beads was used for the degradation of a 250 mL of AMX solution. All degradation procedures were as previously described.

7.8. Degradation monitoring and identification of degradation products

AMX concentrations were determined by HPLC using an Agilent 1100 system equipped with a degasser, an auto injector, a binary pump and a PDA detector. Chromatography was achieved isocratically with KH_2PO_4 (pH 4)/MeOH (90/10; v/v) on a reverse-phase Phenomenex XB-C18 150×4.6 mm (2.6 μm) column at 25 °C and a flow rate of 0.5 mL/min. The injection volume was 20 μL and AMX detection was recorded at $\lambda = 230$ nm.

For the detection of degradation products, LC-MS was used but with a different mobile phase due to possible interference of the potassium buffer during ionisation. For LC-MS, the HPLC instrument was operated in gradient mode using the same flow rate, injection volume and column. The mobile phase consisted of water and 0.1% formic acid (mobile phase A) and acetonitrile and 0.1% formic acid (mobile phase B). The gradient elution was as follows: 5 min 95% A/5%B, 15 min 100%B and return to the initial conditions for 5 min.

The HPLC was connected to a Bruker Esquire3000 ion trap mass spectrometer with an Apollo ESI ion source operating in ESI positive mode. All LC-MS data was collected using Bruker Daltonics Esquire Control v5.3 and Hystar v3.1 operating on Windows XP Professional. The operating conditions were as follows: nebulizer gas: 20 psi; drying gas: 6.0 mL/min; drying temperature: 350°C. MS spectra were acquired over 50-2000 m/z .

7.9. Results and discussion

The prepared IPA material was first assessed for its photocatalytic activity by performing degradation experiments with AMX. Based on the results obtained, further experiments were conducted with the IPA, which demonstrated better photocatalytic performance, and this material was further characterized by SEM, EDS and XRD to correlate its performance.

7.9.1. Preliminary degradation of amoxicillin

TiO_2 /zeolite IPAs prepared from acid only and acid-alkali activated zeolites, which were calcined under either an inert nitrogen flow (tube furnace) or ambient atmosphere (muffle furnace, HVS, Analit, Australia) at 300°C were examined for AMX degradation under UV irradiation (Fig.7.9).

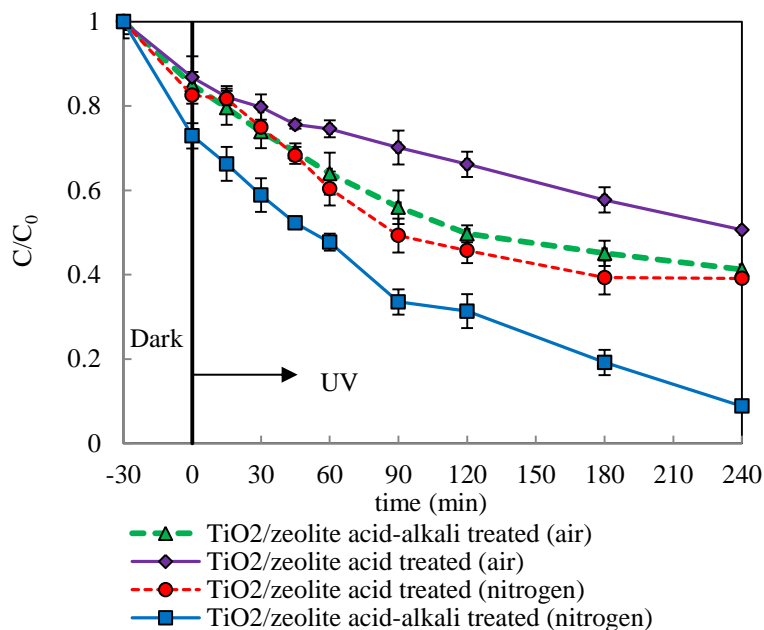


Fig.7.9 Comparison of TiO₂/zeolite calcined under nitrogen and air at 300°C for the degradation performance on AMX

The results revealed that IPAs prepared from pre-treated acid-alkali zeolite calcined under nitrogen demonstrated a better performance in degrading AMX compared to that of acid pre-treated zeolite. The IPAs prepared by acid-alkali pre-treated zeolite performed better than those prepared by acid-treated ones. A similar trend was noted for the acid only and acid-alkali activated zeolites under ambient atmosphere, although calcination in the muffle furnace resulted overall in less degradation. The inert atmosphere, under a nitrogen flow, produced better performing IPA than those exposed to ambient atmosphere regardless of the activation method. These results showed that the calcination conditions clearly influences the photocatalytic activity of the prepared IPA material. However, some studies have argued that the cost of nitrogen purging for calcination can be higher than that of ambient furnace making this approach uneconomical [257].

Studies utilizing natural zeolites have generally used either acid or alkali treatment as the modification method. In contrast, studies combining both acid-alkali activations are rare. The results from this study (Fig.7.9) have shown that IPAs from acid-alkali treated zeolite induced a higher degradation of AMX. This increased efficiency, in combination with nitrogen purging, may make it a more viable economic proposition. Acid activation removes impurities from the pores. Likewise, acid activation also causes elimination of cations, Al³⁺ and Fe²⁺ are further changed into H-form [249]. Ion exchange with H⁺ also improves the effective pore volume, surface area and adsorption capacity of the zeolite material [249]. Subsequent alkali treatment with NaOH could have altered the

porosity and increased the specific surface area. An improvement in reactivity has been also observed when natural zeolite was treated with solutions containing sodium cations [258].

Based on these preliminary results, IPAs prepared from acid-alkali activated zeolite were chosen for all further experiments.

7.9.2. Characterization of integrated photocatalytic adsorbent

The SEM images of natural zeolite indicated a relatively smooth surface (Fig.7.10a). Both acid (Fig.7.10b) and acid-alkali (Fig.7.10c) treatments significantly altered the zeolite surface. The surface of the acid-alkali treated zeolites demonstrated greater irregularity than that of the acid-treated zeolites, appearing pitted. SEM images of TiO₂/zeolite synthesized from acid-alkali and acid treatments showed rough, jagged and uneven surface structures (Fig.7.10d and Fig.7.10e) as a result of TiO₂ being deposited as clusters of irregular shapes.

EDS analyses revealed the presence of a higher TiO₂ contents with approximately 74% in the acid-alkali treated TiO₂/zeolite compared to 52% for the acid-treated TiO₂/zeolite (Table 7.2). Higher composition of TiO₂ correlated with the lower levels of SiO₂ and Al₂O₃ in the samples, indicating that the acid-alkali treatment is more efficient at removing these Si and Al oxides than acid treatment. Acid treatments have been shown to effectively remove Al from the zeolites, thus enhancing its porosity [259]. In this case, a combination of pre-treatments has also increased the surface area and the TiO₂ content.

Table 7.2 Quantitative analysis of IPA with EDS

IPA	Metal oxide (%)		
	TiO ₂	SiO ₂	Al ₂ O ₃
TiO ₂ /zeolite acid-alkali (300°C)	74.2	23.3	2.5
TiO ₂ /zeolite acid (300°C)	52.5	43.5	4.0

The crystal phase of the prepared IPA materials was studied by XRD. The XRD patterns of TiO₂/zeolite samples were compared to that of neat natural zeolite (Fig.7.11). The characteristic peak for the most stable rutile polymorph of TiO₂ is typically found at $2\theta = 27.7^\circ$. However, the natural zeolite also displays a signal at $2\theta = 27.7^\circ$ and thus this characteristic peak could not be used to confirm the presence of the TiO₂ rutile polymorph. Examination of the natural zeolite coincided with the natural zeolite peak. Even so, the XRD results revealed a mixed phase of TiO₂ anatase and rutile polymorphs.

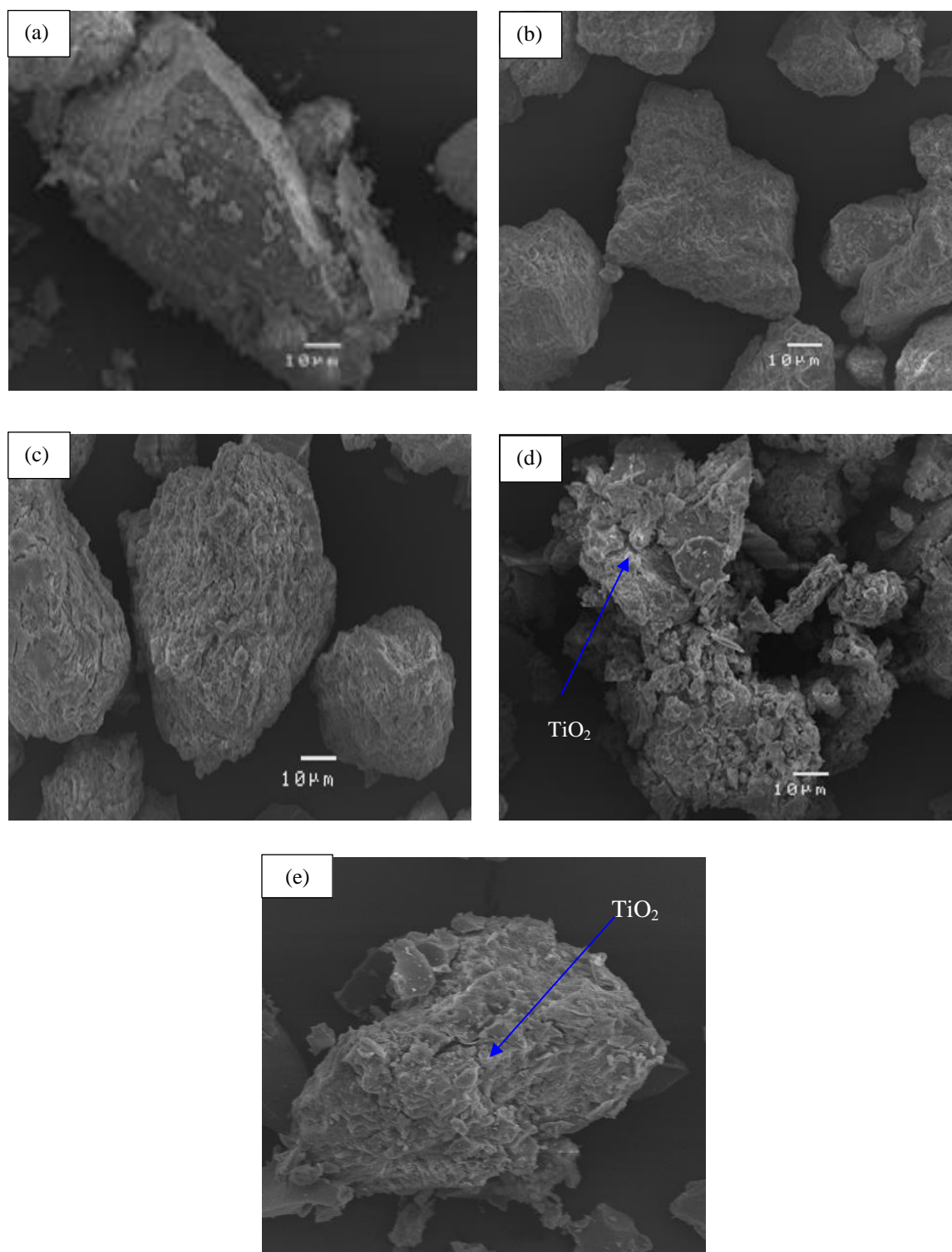


Fig.7.10 SEM images of the materials: (a) natural zeolite, (b) acid-treated zeolite, (c) acid-alkali treated zeolite, (d) TiO₂/zeolite acid-alkali (300°C) and (e) TiO₂/zeolite acid (300°C)

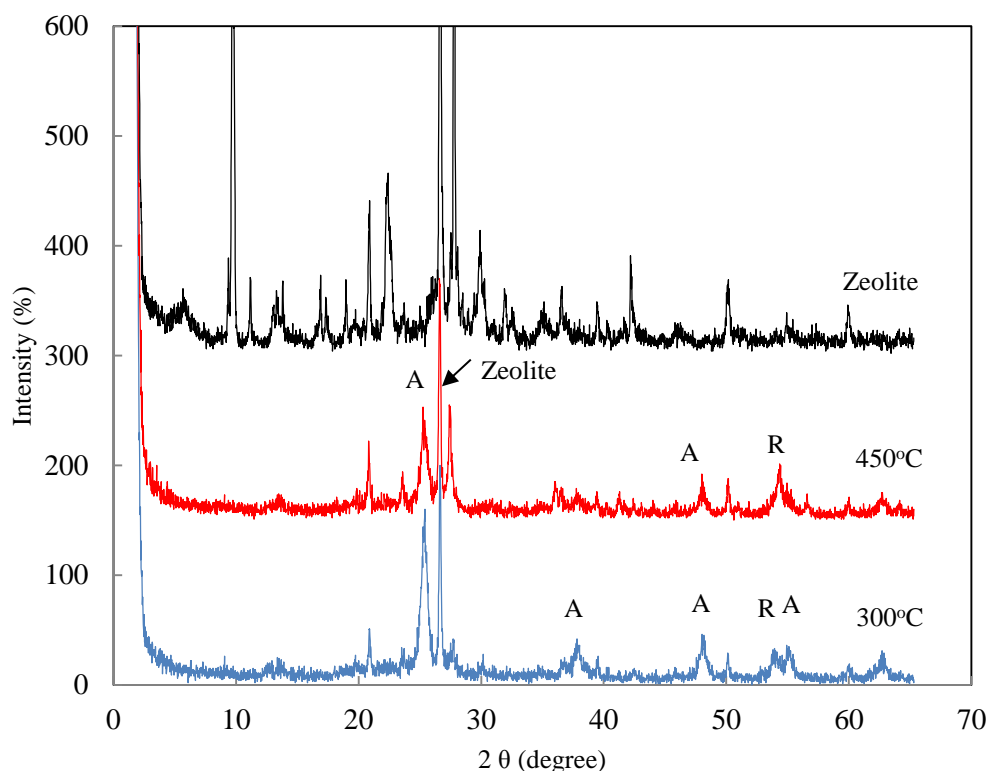


Fig.7.11 XRD pattern of TiO₂/zeolite calcined at 300°C and 450°C and bare zeolite (A = anatase and R = rutile)

Anatase peaks were prominent in the IPA samples calcined at 300°C, however, when the temperature was increased to 450°C, the intensity of the characteristic anatase peaks corresponding to $2\theta = 25.4^\circ$ decreased while the rutile peak at $2\theta = 54.3^\circ$ become stronger and sharper. The main peak of the zeolite (27.7°) remained unchanged regardless of the temperature, suggesting that the frame structure of zeolite remained intact after TiO₂ loading. Similar observations by Huang *et al.* [248] attributed this to the good thermal stabilization properties of structure of natural zeolite.

Impurities, cations or other minerals which may still be present within the structure of the zeolite may have suppressed the growth of the anatase phase, which is the predominant phase and is linked to a higher photocatalytic activity. Another study indicated that minor changes in XRD patterns of TiO₂/zeolite and natural zeolite indicated that the zeolite structure was robust and that there was minimal TiO₂ loading occurring [247].

In general, calcination temperature ranges between 550-800°C have been reported to initiate the conversion of anatase to rutile with factors such as the preparation conditions and the chemical treatments also influencing this process [241]. Conversely, TiO₂/zeolite, which was calcined at the low temperature of 200°C, was found to consist of anatase, rutile and trace amounts of brookite

polymorphs [257]. This study has shown that calcination at intermediate temperatures of 300°C and 450°C also produced a mixture of anatase and rutile polymorphs, but not brookite.

7.9.3. Point of zero charge measurement

The point of zero charge (pH_{pzc}) is defined as the point where $\text{TiO}_2/\text{zeolite}$ has zero potential charge on its surface. Fig.7.12 depicts the point of zero charge determination of $\text{TiO}_2/\text{zeolite}$ IPA. The point of zero charge of the IPA was determined as 5.52. Thus, when the pH of the solution is above the pH_{pzc} , the $\text{TiO}_2/\text{zeolite}$ surface will be deprotonated and therefore negatively charged, when it is below the pH_{pzc} the surface will be protonated and positively charged.

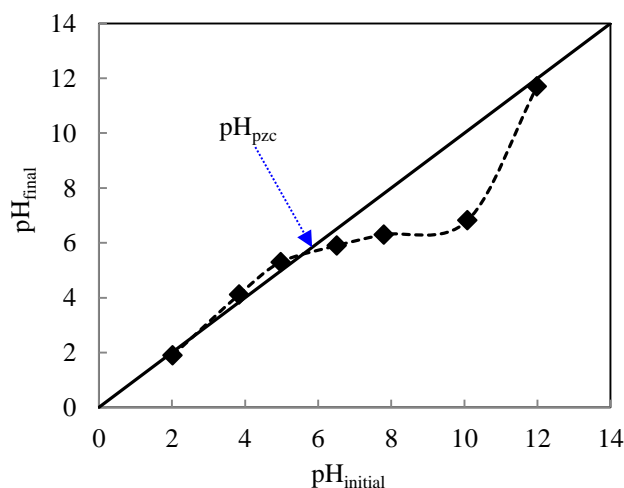


Fig.7.12 Point of zero charge for $\text{TiO}_2/\text{zeolite}$

The determination of pH_{pzc} provides an indication of the adsorption capacity of the $\text{TiO}_2/\text{zeolite}$. The presence of impurities on the $\text{TiO}_2/\text{zeolite}$ surface can influence the final pH_{pzc} value obtained. Furthermore, AMX may display different degrees of adsorption on the $\text{TiO}_2/\text{zeolite}$ owing to its ionisable functional groups, carboxyl ($\text{pK}_a = 2.68$), amine ($\text{pK}_a = 7.49$) and phenolic group ($\text{pK}_a = 9.63$) [196].

7.9.4. Photocatalytic degradation of amoxicillin

Literature studies on the photocatalytic degradation of AMX have utilized various commercially available TiO_2 photocatalysts [117, 124] including doped and undoped titania [190]. A study with a $\text{TiO}_2/\text{activated carbon derived IPA}$ was performed by Basha *et al.* [238]. It demonstrated that 10% TiO_2 IPA produced the highest removal of 87% for a 150 mg/L of AMX solution after 150 min of

irradiation. Recycling of the IPA exhibited stability for up to four cycles. In a separate study, the adsorption of AMX was evaluated on activated carbon and bentonite [196].

The widespread usage of AMX and its frequent detection in the environment signifies the need for its removal. In general, AMX is difficult to degrade and it, along with a number of metabolised by-products can be found in urine and faeces [196]. Due to the lack of studies on its photodegradation, the novel IPA photocatalysts synthesized in this study were employed.

Due to favourable characteristics, most experiments were conducted using $\text{TiO}_2/\text{zeolite}$ IPAs obtained from acid-alkali treatment and calcination at 300°C . Limited experiments were conducted with other IPA materials for comparison purposes.

Adsorption is known to be integral part of heterogeneous photocatalysis. Thus the adsorption of AMX onto the $\text{TiO}_2/\text{zeolite}$ material from acid-alkali treatment and calcined at 300°C was determined. The percentage adsorption for 5 mg/L, 10 mg/L, 30 mg/L and 50 mg/L solutions of AMX were 9%, 10%, 14% and 9%, respectively. This shows that adsorption can somewhat contribute to the removal process of AMX, although partial acid-catalyzed hydrolysis cannot be ruled out. Fig.7.13 shows the degradation of AMX under different conditions investigated.

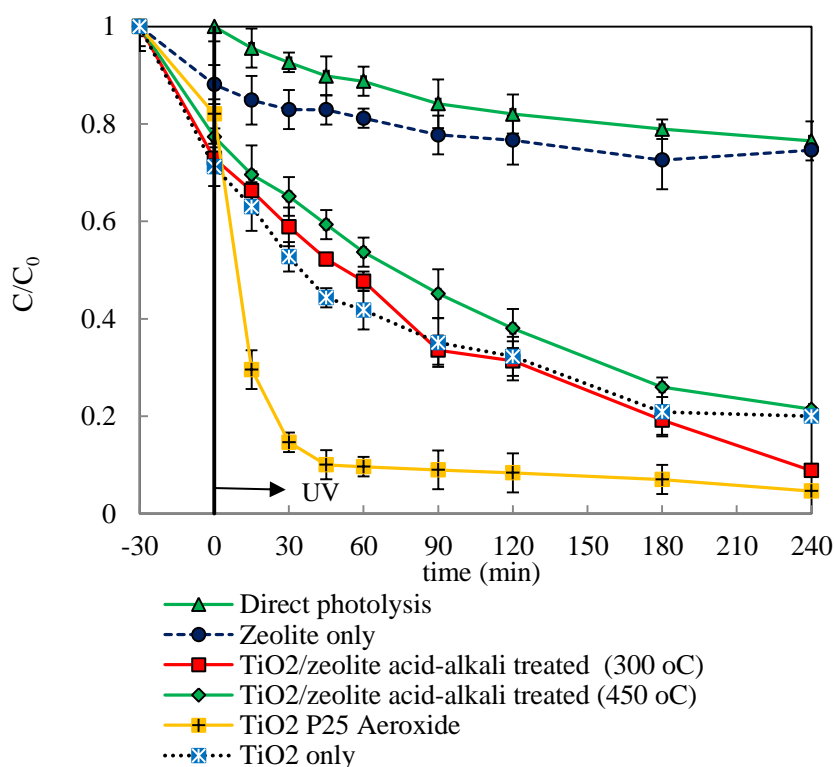


Fig.7.13 Degradation of AMX under different conditions ($C_0 = 30 \text{ mg/L}$; catalyst concentration: 2 g/L)

Although previous studies have demonstrated the photostability of AMX towards direct photolysis [117, 129], this degradation mechanism was included. The results obtained confirmed that direct photolysis contributed only marginally to the degradation process with a 23% reduction in amount of AMX after 240 min of irradiation with light emitted from a UV-lamp.

To prove that zeolite only acts as an adsorbent, exposure of AMX to TiO₂-free zeolite revealed a negligible degradation of only 15% of AMX after 240 min of irradiation. A similar study by Li *et al.* [246] also showed that natural zeolite, modernite, did not participate in the photocatalytic degradation of methyl orange.

Photocatalytic degradations of AMX were performed with TiO₂/zeolite which was subjected to two different calcination temperatures (Fig.7.13). Calcination temperatures below 200°C were not used for the preparation of TiO₂/zeolite because they are known to produce poor quality of TiO₂ crystallinity which consequently affects the photocatalytic activities of TiO₂ in the degradation process [234]. Calcination at 300°C was found to yield a higher degradation than 450°C. The degradation percentages of the 300°C and 450°C materials were 88% and 72%, respectively. An increase in calcination temperature is expected to enhance the photocatalytic performance due to the increased formation of TiO₂ anatase phase [242]. The higher degradation of AMX in this study by TiO₂/zeolite calcined at 300°C can be explained from the SEM image, which showed an increase in the surface roughness. As surface roughness increases, the surface area also increases and provides more active sites for adsorption and degradation to take place. A similar finding has been reported by Shi *et al.* for the removal of phenol [242]. 110°C was compared to 200-500°C found to be the best calcination temperature for Pt modified TiO₂ on natural zeolite [248]. Conglomeration of catalyst particles, which can also take place at elevated calcination temperatures reduces the specific surface area [248].

The TiO₂/zeolite IPA material calcined at 300°C which yielded the best degradation was therefore chosen for all subsequent experiments. In order to compare the photocatalytic activity of the synthesized TiO₂/zeolite materials, pure synthesized TiO₂ was also examined for its photocatalytic activity. Although synthesized TiO₂ performed better during the first 60 min, TiO₂/zeolite calcined at 300°C demonstrated a higher ability to degrade AMX (Fig.7.13). The obtained percentage AMX degradation with TiO₂ was 79%, while the TiO₂/zeolite material gave a slightly improved response at 88%. This also confirms that the photocatalytic activity of TiO₂ did not decline once anchored to zeolite. The same phenomenon was also observed when TiO₂/fly ash was compared with TiO₂ alone for phenol degradation [242]. Also, the higher degradation rate obtained for the TiO₂ supported on zeolite can be attributed to higher adsorption capacity and HO[•] radical availability [260].

However, the degradation of AMX with TiO₂ P25 was found to be somewhat more efficient than the IPA prepared. Although it has been well-documented that pure anatase has the highest photocatalytic activity compared to rutile and brookite, the mixture of anatase and rutile phases in commercial TiO₂ P25 is regarded as the best photocatalyst. An advantage of the synthesized IPA, which is also a mixture phase of anatase and rutile, is that the photocatalyst can be recovered from the solution after irradiation. TiO₂ P25 is a fine powder, making it difficult to separate. In addition, the adsorption capacity of TiO₂/zeolite was comparably higher than that of TiO₂ P25 as can be seen in Fig.7.13 and its acidic nature may have assisted degradation by partial hydrolysis.

7.9.5. Effect of catalyst concentration

To determine the optimum catalyst concentration, the degradation of AMX was performed with four catalyst loadings of the most active TiO₂/zeolite (acid-alkali treatment and calcined at 300°C), 0.5 g/L, 1 g/L, 2 g/L and 4 g/L (Fig.7.14). Degradation increased with the concentration of catalysts up to 2 g/L, but decreased when the concentration was increased to 4 g/L, likely due to a light scattering effect. In addition, adsorption in the dark slightly increased for 2 g/L compared to the lower catalyst loadings. As 2 g/L revealed the highest degradation, this concentration was considered optimal and used for all further experiments.

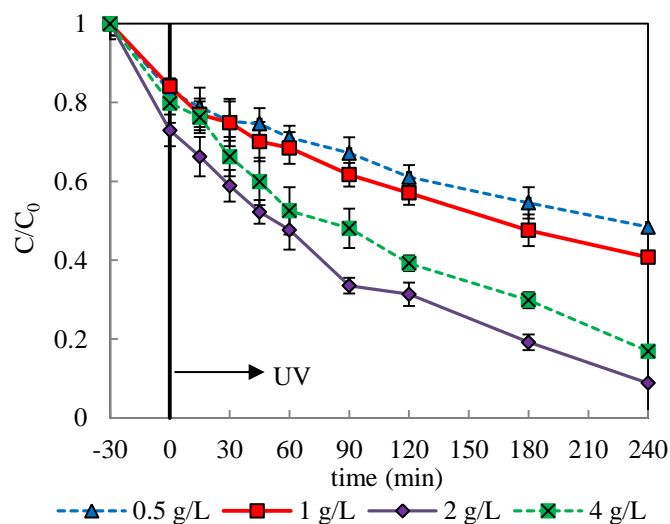


Fig.7.14 Effect of catalysts concentration on the degradation of 30 mg/L AMX

7.9.6. Catalyst recycling

A catalyst recycling study was conducted to determine the stability of the synthesized material over repeated photocatalytic degradation studies. A slight decrease in the photocatalytic activity was

observed upon continuous usage and degradation of 88% obtained during the first cycle (after 240 min) decreased to 83% in the second cycle and eventually to 69% after being used for the third time (Fig.7.15). This loss of photocatalytic activity as observed in the degradation levels can be associated with accumulation of intermediates and degradation products on the surface and in the cavities of the catalysts, thus affecting the adsorption of AMX and the photocatalytic activity of the IPA material [251]. According to Sharma *et al.* [260] high calcination (e.g. 400°C) is able to improve the catalytic activity compared to recycling the catalyst without calcination.

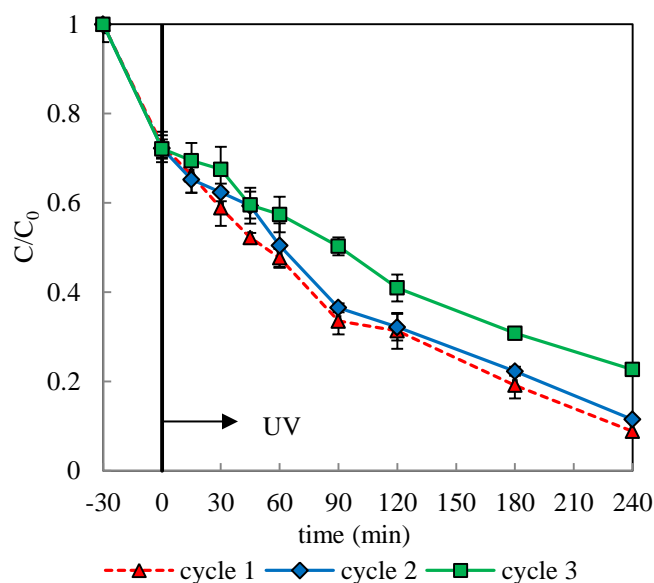


Fig.7.15 Performance of recycled TiO₂/zeolite for AMX degradation

7.9.7. Mineralization

The extent of mineralization was compared for four different conditions over the course of 240 min of irradiation (Fig.7.16). In line with the degradation results, only negligible mineralization (3%) was achieved with direct photolysis. TiO₂ P25, despite inducing high levels of AMX degradation, was unable to effectively eliminate the resulting degradation products via mineralization. DOC was reduced by as much as 36% with TiO₂ P25, while a 25% reduction was achieved with TiO₂/zeolite. Synthesized TiO₂ alone also reduced the DOC by 23% and was in the same range as the TiO₂ supported on zeolite. Intermediates forming during irradiation could have possibly affected the slow degree of mineralization observed.

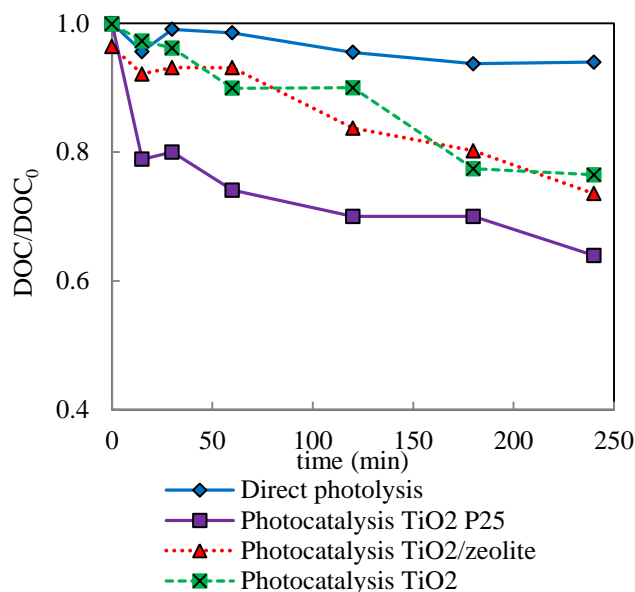


Fig.7.16 DOC removal during direct photolysis and photocatalysis (TiO₂ P25, TiO₂/zeolite and TiO₂ only) on AMX

7.10. Amoxicillin degradation with TiO₂-gel beads

The average size of the prepared TiO₂-gel beads, measured with a micrometer, was 1.98 mm. Fig.7.17 shows the ability of the TiO₂-gel beads prepared from both methods to degrade AMX. The results obtained were not very satisfactory.

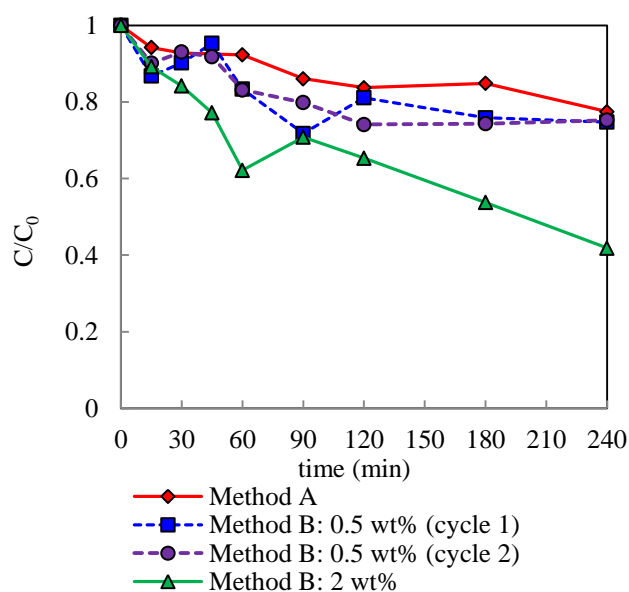


Fig.7.17 Degradation of AMX (30 mg/L) with TiO₂-gel beads (10% v/v) from method A and method B

Beads obtained by method A only led to a decrease of AMX of 23% after 240 min of irradiation. TiO₂-gel beads prepared from method B although displaying a slightly higher degradation, were limited by fluctuations over the irradiation time at both tested loadings of TiO₂ P25 (0.5 wt% and 2 wt% TiO₂ P25). A 25% degradation of AMX was attained with 0.5 wt%. Recycling of the same TiO₂-gel beads, besides demonstrating a similar level of degradation as the first cycle, did not result in any major fluctuations. While an increase of TiO₂ P25 loading to 2 wt% concomitantly increased the degradation level to 58%, it again displayed fluctuations.

The constant decrease with method A material suggests that TiO₂ could have been absorbed into the alginate support prior to the formation of the gel beads themselves and was thus not exposed to photodegradation conditions. The fluctuations observed for method B material could be due to TiO₂ P25 leaching as a result of loose coating or dispersion on the Ca alginate beads. Recycling of the TiO₂-gel beads may have stabilized the immobilization as a greater degree of and more consistent degradation was observed in the second cycle. Another reason for the observed fluctuation in general is that the gel beads which initially functioned as an adsorbent, later released organic matter due to mechanical damage or photochemical depolymerisation [261].

Despite the satisfactory performance of the prepared TiO₂-gel beads with respect to AMX removal, thus validating the proof-of-concept, the differences arising from their preparation methods need to be further evaluated in future studies.

7.11. Degradation products of amoxicillin

The thermal degradation of 30 mg/L AMX generated from TiO₂/zeolite from acid/alkali treatment and calcination at 300°C IPA was analysed by LC-MS under (+)-ESI conditions. Samples withdrawn prior to and after 240 min of irradiation were compared for possible degradation products.

LC-MS analysis of AMX (M = C₁₆H₁₉N₃O₅S; molecular weight = 365 g/mol; t_R = 12.2 min) resulted in the detection of the parent ion and three fragment ions: *m/z* 366 [M + H⁺]⁺, 349 [M + H⁺ - NH₃]⁺, 160 [M + H⁺ - NH₃ - CO - C₉H₇O₂N]⁺ and 114 [M + H⁺ - NH₃ - CO - C₉H₇O₂N - CO₂H₂]⁺ (Fig.7.18).

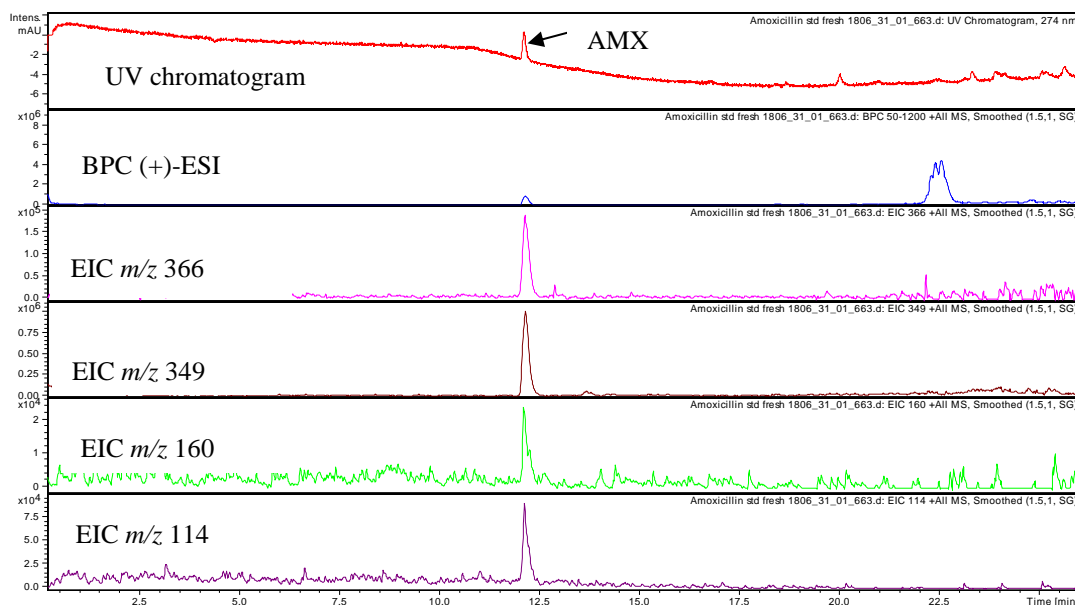


Fig.7.18 LC-MS ion of AMX standard in (+)-ESI mode. The top spectrum in each figure is the UV chromatogram, also shown is the BPC. EICs show the ions formed

After several hours of standing in the dark, AMX was almost completely degraded and numerous new peaks appeared in the LC-MS spectrum (Fig.7.19a). Hydrolysis is known to yield a multitude of smaller break-down products as well as higher oligomers [194, 262]. By comparison with literature spectra, three major degradation products resulting from hydrolysis could be identified (Table 7.3, Fig.7.20). Initial opening of the β -lactam ring of AMX led to the formation of diastereoisomeric amoxicillin penicilloic acids (**39**), which were assigned based on their characteristic fragmentation peaks at m/z of 367. These compounds undergo further decarboxylation to generate a stereoisomeric mixture of amoxicillin penilloic acids (**40/41**) with typical ion fragments of m/z 323. A compound with m/z 189 was assigned to phenol hydroxypyrazine (**51**) and this highly fluorescent degradant dominated the chromatogram upon UV-detection [262]. Additional degradation products were found but their structures could not be determined without further isolation and characterization.

After irradiation for 240 min, almost all thermal degradants had been removed and only small amounts were still detectable by LC-MS (Fig.7.19b). Various hydroxylated products have been reported by Klauson *et al.* for visible light photocatalysis with doped titania [190]. In both cases, low intensity light was applied to allow for the detection and subsequent identification of degradants. The reaction mixtures obtained in this study were screened by LC-MS for the characteristic ions of the reported degradants but their presence could not be confirmed. The harsh UV-light conditions used and the prolonged irradiation time likely caused rapid degradation of all primary and secondary decomposition products. The observed mineralization rate of 25% further confirmed that the degradation process was highly efficient under these conditions.

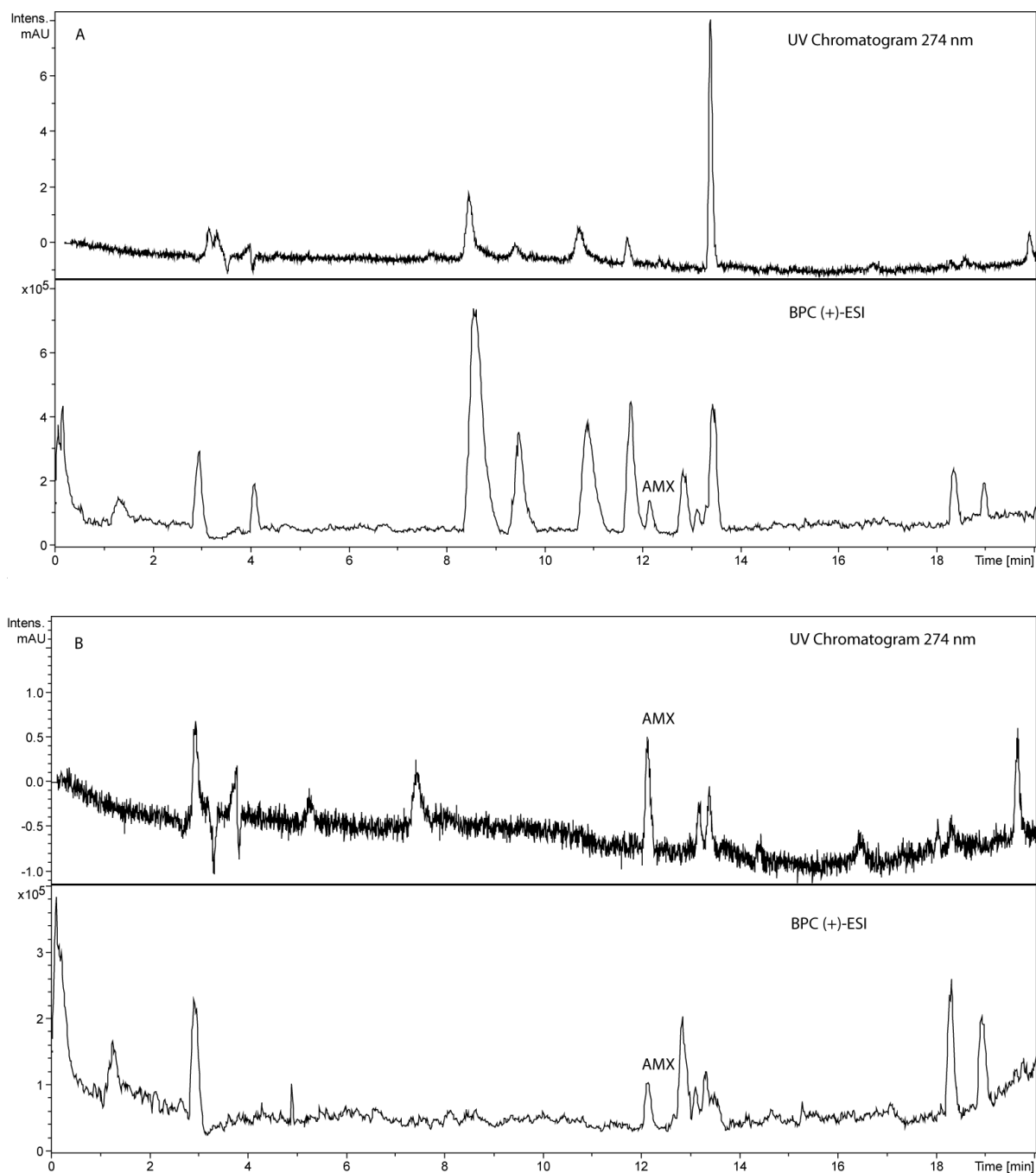


Fig.7.19 UV (274 nm) and BPC (+)-ESI of TiO₂/zeolite photocatalysis of AMX. (A) After hydrolysis and (B) after 240 min of irradiation

Table 7.3 Hydrolysis products of AMX detected by LC-MS in (+)-ESI mode

t_R (min)	Formula	EIC (m/z)	Observed ion
8.5	$C_{16}H_{21}N_3O_6S$ (383 g/mol) 39	384 [M^{+1}]	$[C_{16}H_{21}N_3O_6S + H]^+$
		367	$[C_{16}H_{21}N_3O_6S + H - NH_3]^+$
		349	$[C_{16}H_{21}N_3O_6S + H - NH_3 - H_2O]^+$
		340	$[C_{16}H_{21}N_3O_4S + H - CO_2]^+$
		323	$[C_{16}H_{21}N_3O_6S + H - NH_3 - CO_2]^+$
		295	$[C_{16}H_{21}N_3O_6S + H - NH_3 - CO_2 - CO]^+$
		189	$[C_{16}H_{21}N_3O_6S + H - NH_3 - CO_2 - CO - C_7H_6O]^+$
		160	$[C_6H_{10}NO_2S]^+$
9.5	$C_{15}H_{21}N_3O_4S$ (339 g/mol) 40/41	340 [M^{+1}]	$[C_{15}H_{21}N_3O_4S + H]^+$
		323	$[C_{15}H_{21}N_3O_4S + H - NH_3]^+$
		295	$[C_{15}H_{21}N_3O_4S + H - NH_3 - CO_2]^+$
		277	$[C_{15}H_{21}N_3O_4S + H - NH_3 - CO_2 - H_2O]^+$
		189	$[C_{15}H_{21}N_3O_4S + H - NH_3 - CO - C_7H_6O]^+$
10.8	$C_{16}H_{21}N_3O_6S$ 39	384 [M^{+1}]	$[C_{16}H_{21}N_3O_6S + H]^+$
		367	$[C_{16}H_{21}N_3O_6S + H - NH_3]^+$
		349	$[C_{16}H_{21}N_3O_6S + H - NH_3 - H_2O]^+$
		340	$[C_{16}H_{21}N_3O_4S + H - CO_2]^+$
		323	$[C_{16}H_{21}N_3O_6S + H - NH_3 - CO_2]^+$
		189	$[C_{16}H_{21}N_3O_6S + H - NH_3 - CO_2 - CO - C_7H_6O]^+$
		160	$[C_6H_{10}NO_2S]^+$
		160	$[C_6H_{10}NO_2S]^+$
11.7	$C_{15}H_{21}N_3O_4S$ (339 g/mol) 40/41	340 [M^{+1}]	$[C_{15}H_{21}N_3O_4S + H]^+$
		323	$[C_{15}H_{21}N_3O_4S + H - NH_3]^+$
		295	$[C_{15}H_{21}N_3O_4S + H - NH_3 - CO_2]^+$
		277	$[C_{15}H_{21}N_3O_4S + H - NH_3 - CO_2 - H_2O]^+$
		189	$[C_{15}H_{21}N_3O_4S + H - CO - NH_3 - C_7H_6O]^+$
13.4	$C_{10}H_8N_2O_2$ (188 g/mol) 51*	189	$[C_{10}H_8N_2O_2 + H]^+$
		171	$[C_{10}H_8N_2O_2 + H - H_2O]^+$
		130	

* Ions observed but no corresponding structure reported in literature.

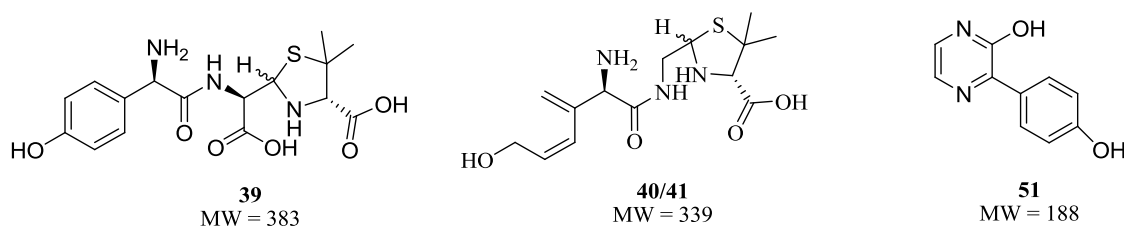


Fig.7.20 Hydrolysis products of AMX confirmed by LC-MS analyses prior to irradiation under TiO_2 /zeolite photocatalytic conditions

7.12. Conclusions

Synthetic TiO₂/zeolite IPA was characterized and evaluated for the degradation of AMX in aqueous solution. The efficient degradation performance was attributed to the adsorption of AMX on the zeolite and also the photocatalytic degradation by TiO₂.

The performance of 2 g/L neat TiO₂ P25 on AMX degradation was more efficient than direct photolysis, however, recycling of the catalyst is not economically viable. The best degradation performance for AMX was achieved with TiO₂/zeolite synthesized from a pre-treated acid-alkali zeolite that was calcined at 300°C in a nitrogen stream. A catalyst loading of 2 g/L was required to produce 88% degradation of AMX after 240 min of irradiation. Recycling studies, however, revealed a decline in its performance over usage, possibly due to the accumulation of degradation products on 1) the surface of zeolite, blocking the available active sites for adsorption, and 2) also passivating the TiO₂ crystals, reducing their reactivity. Both gradually decreased the overall photocatalytic activity of the TiO₂/zeolite. Both photocatalysts, also produced low degrees of mineralization, which will need to be addressed in future studies.

Degradation product analyses suggested that the initial phase of AMX degradation is via β -lactam ring opening. Degradation products resulting from TiO₂/zeolite IPA induced hydrolysis were identified by LC-MS.

The location of TiO₂ loading either on the surface or in the bulk is known to affect the photocatalytic activity [234]. On the basis of SEM, XRD and EDS analyses there was no conclusive evidence to prove the location of the loading sites. The photocatalytic activity of TiO₂ is also influenced by calcination temperatures, and the temperature in turns affects both the surface area and the crystal size. These factors need further investigation.

The adsorption capability of the TiO₂/zeolite, effectively removing the AMX from the solution and anchoring it near the catalyst; the catalytic activity of the TiO₂ crystals, effectively degrading the AMX parent and producing numerous degradation products and the UV-induced degradation of these degradation products, all coupled with the relatively effectiveness of mineralization gives this catalyst a distinct advantage over commercially available TiO₂ P25.

Chapter 8. Conclusions and recommendation for future research

8.1. Summary

Occurrence and the frequent detection of pharmaceuticals in natural and wastewater bodies has attracted much attention because many of them (1) do not readily biodegrade, (2) remain toxic, and (3) produce potentially harmful degradation products, all of which pose on-going health and environmental risks. There are also inherent risks associated with the techniques for its removal from water due to associated potential risk. Destructive methods based on AOPs such as TiO₂ photocatalysis, which utilize the high reactivity of HO[•] radicals to progressively oxidize organic compounds to innocuous products, have been applied as a possible removal method for pharmaceuticals. Current state-of-the-art technique using TiO₂ photocatalysis revealed that, despite its effectiveness in laboratory-based studies, there was limited application of this method on a larger scale and in most cases there was a failure to draw a direct correlation between indoor and outdoor studies.

This dissertation aimed to investigate the potential of two degradation methods, direct photolysis and TiO₂ photocatalysis and to degrade individual APIs, DCF and NPX and their mixtures in water. DCF and NPX were chosen due to their global high use and have been regarded as APIs of environmental concern. Investigation of the resulting mixtures formed during the TiO₂ photocatalytic treatments was necessary since parent compound degradation may generate various intermediates and degradation products with unknown stability and toxicity. Past studies have also indicated that these degradation products can be more toxic than the parent compound. Therefore, for the present study, attention was focussed on the detection and identification of the main degradation products formed during TiO₂ photocatalysis of DCF, NPX and their mixtures.

The factors influencing the degradation of APIs and their mixtures were also examined. Photons sourced from an artificial light source (medium pressure Hg lamp) and a renewable energy source (natural sunlight) were employed in the degradation experiments. Parameters affecting the performance of TiO₂ photocatalytic degradation such as TiO₂ concentration, initial concentrations of APIs and water matrix were explored. In addition, the effect of direct photolysis on the APIs was also investigated due given to previous documentation of their ability to undergo solar degradation, taking into account parameters such as water matrix and initial concentrations.

One major issue limiting the application of the commonly applied commercial nanosized TiO₂ P25 photocatalyst in real water treatment is recovering the catalyst after treatment. Anchoring TiO₂ to an adsorbent was proposed as a viable method to overcome such a problem. Synthesized TiO₂,

combined with natural zeolite was characterized and assessed for its photocatalytic activity against AMX in water. In addition, degradation products produced by hydrolysis and photocatalysis with TiO₂/zeolite from acid-alkali treatment (300°C) were also identified.

8.2. Conclusions

Overall, this study faced a number of challenges dictated by the many factors affecting the degradation process. Supporting explanations provided for the numerous observations obtained in the experimental approach are somewhat speculative rather than providing a definite outcome, mostly due to the complexity inherent in this kind of study. The discrepancies, some of which have been observed in past studies and others which have been highlighted by this study, confirm the difficulties in placing the findings in a commercial or industrial context. Among the various factors studied, water composition, whether untreated or treated, clearly has a greater impact on determining the success of the degradation process.

The main conclusions drawn from this study are summarized in this section relevant to the chapters of this dissertation.

8.2.1. Photochemical degradation of diclofenac, naproxen and their mixtures by UV light

It has been demonstrated that photochemical degradation methods either by direct photolysis or TiO₂ photocatalysis using medium pressure Hg lamps emitted from two batch photoreactors, immersion-well and the loop reactor, were effective in the degradation of individual APIs, DCF and NPX and their mixtures in water.

Applied direct photolysis studies showed that DCF, NPX and their mixtures can be degraded using this method but that its performance is governed heavily by the water matrix. The level of DOC or organic matter in general may act as an inner filter and compete for photons with the APIs, thus reducing the degradation of APIs. For example, degradation of individual DCF and NPX in river water was rather slow with these results being attributed to higher DOC levels in both water matrices. Direct photolysis, although effective in the degradation of these APIs, was ineffective for decreasing the DOC level and suggesting that only partial oxidation was achieved for parent APIs, intermediates, degradation products, or all of the above.

When considering the operational parameters on individual API degradation, it was found that high concentrations of TiO₂ did not favour the degradation of both DCF and NPX. An optimal

concentration of TiO₂ P25 at 0.1 g/L was found to be the most efficient. Degradation of DCF and NPX was observed to be sensitive to solution pH. An increase in pH led to a decrease in the degradation rates of both APIs. When the initial concentrations of APIs increased, the degradation rates of APIs decreased. Addition of the oxidant, H₂O₂ in selected experiments enhanced the degradation rate. For example, addition of H₂O₂ in the degradation of drinking water showed an increase in degradation rate compared to UV/TiO₂ alone. Water matrix, in particular unfiltered river and drinking water, inhibited the degradation rates of NPX and DCF TiO₂ photocatalysis. An addition of dual anions, phosphate and chloride had much more of an effect on the degradation rate of NPX than the presence of single anion in river water. However, in drinking water, addition of chloride anions was found to enhance the degradation rates of NPX.

TiO₂ photocatalytic degradation of aqueous mixtures appears to be more complex due to the presence of the two APIs; the effect of one on the other is not clearly understood. DCF in general degraded much quicker than NPX, under the two different conditions examined when both APIs were present in either equivalent or non-equivalent levels. This observation was linked primarily to its higher photolability. Dual anions, phosphate and chloride had a more significant effect on the degradation of API mixture in the drinking water where the degradation rates decreased for both APIs. The presence of chloride anions alone did not have a major effect on the degradation. Thus, it can be concluded that for the photocatalytic degradation of mixtures the presence of more than one anion in the water matrix (which is likely to be encountered in natural environment), may greatly affect the overall progress of this advanced oxidation process.

While comparisons based on the type of reactor used showed that the larger loop reactor was somewhat more efficient for API degradation, its application may be limited for solar reactions as it has a quartz mantle.

Overall, the high degradation of parent APIs did not correlate with a significant improvement in the decreasing DOC and only partial oxidation was achieved for parent compound.

8.2.2. Solar photolytic and TiO₂ photocatalytic degradation of pharmaceuticals

The application of renewable energy sources, natural sunlight for the degradation of DCF, NPX and their mixtures revealed that this “photon source” can be used to degrade these APIs in water. It should be noted that all experiments were performed under different solar incident radiation (determined by the climatic conditions) and on different days.

Solar degradation of DCF either by solar photolysis or TiO₂ photocatalysis was also governed by the water matrix. For example, degradation of DCF in drinking and river water were slightly slower than

in distilled water under solar TiO₂ photocatalytic conditions most likely due to the deficiency of HO[•] radicals in the presence of organic matter. Degradation of NPX in all water matrices proceeded efficiently and at similar rates by both solar photolysis and TiO₂ photocatalysis. Only the presence of chloride anions in drinking water hindered solar TiO₂ photocatalysis. Solar photolysis of the DCF and NPX mixture, showed some competition in particular in drinking water and river water, as both have the ability to undergo photolysis. Solar TiO₂ photocatalysis effectively degraded DCF and NPX mixtures; however, the addition of chloride anions again slowed down the degradation rate, resulting in incomplete removal. Mostly, the degradation followed the pseudo-first-order kinetic model.

Partial oxidation of individual APIs and mixtures were observed based on the monitored COD indicator. Generation of numerous intermediates and degradation products at different rates during the solar exposure may have led to these results.

Similarities and differences observed among studies conducted under sunlight and laboratory conditions thus inferred that in most cases, direct correlations between those environments are not possible. Laboratory studies where light intensity from the medium pressure Hg lamp is consistent throughout the course of irradiation are far easier to control while studies under sunlight were dependent on various climatic factors such as cloud cover, intensity of light and winds. Solar radiation can also fluctuate depending on the day, time and season.

Sunlight intensities and the water matrix appear to be the main factors influencing the overall performance of the solar photolytic and TiO₂ photocatalytic methods for degradation of APIs.

8.2.3. Identification of photoproducts and elucidation of degradation pathways

Application of photochemical methods ultimately aimed at the complete degradation of APIs into small non-toxic by-products, such as CO₂ and H₂O, often result in the simultaneous generation of other intermediates.

Identification of degradation products formed by the TiO₂ photocatalytic treatment of individual APIs, DCF, NPX and their mixtures by LC-MS and FT-ICR-MS provided some information about their molecular formulas.

For TiO₂ photocatalysis of DCF, much lower molecular weight compounds were formed. Likewise, degradation of NPX (molecular weight of 230 g/mol) using similar protocols formed smaller compounds, however much larger compounds corresponding to 402, 418 and 446 g/mol were also observed. DCF and NPX mixtures, despite forming similar degradation products as observed in the individual treatments, also produced larger molecular weight degradation products (407 and

453 g/mol). In this study, TiO₂ photocatalysis has been shown to be an effective method in degrading APIs in water, while information gained on degradation products (in particular, those previously unknown larger molecular weight compounds) highlights the importance of studying this aspect of treatment.

If the TiO₂ photocatalytic treatment on merely pure water generates multiple degradants, it is highly plausible that the complexity of pharmaceutical contaminated wastewater would lead to the generation of a multitude of degradation products. This study, despite proposing several possible degradation products, was not designed to isolate and provide structural confirmation of the degradation products. The identified degradation products or detected ions may be used as a guideline for future isolation and structural elucidation studies by NMR.

8.2.4. Integrated photocatalytic adsorbent for the degradation of amoxicillin

Preparation of TiO₂/zeolite IPA was achieved by (1) synthesis of TiO₂ employing a simple sol-gel method followed by (2) attachment to natural zeolite pre-treated with either acid activation or acid-alkali activation. TiO₂/zeolite IPA prepared from acid-alkali pre-treated zeolite calcinated at 300°C in nitrogen flow exhibited a better performance with respect to degradation of 30 mg/L of AMX than that prepared from acid pre-treated zeolite. In fact, the higher calcination temperature (450°C) of the IPA materials slowed the degradation of AMX. The TiO₂/zeolite IPA was characterized via XRD, SEM and EDS.

A maximum degradation of 88% was achieved with an optimum loading of 2 g/L TiO₂/zeolite after 240 min of irradiation. The efficiency of prepared TiO₂/zeolite on AMX degradation was attributed to the adsorption capacity of zeolite and the photocatalytic activity of TiO₂. Comparison of the degree of mineralization determined by the concentration of remaining DOC showed a removal of 25% which was lower than the degradation of parent AMX. Contributing to the lower DOC removal was the formation of degradation products compared prior to irradiation and at the end of photocatalytic treatment by LC-MS.

The other immobilization method, which was tested by immobilizing TiO₂ on Ca-alginate, performed satisfactorily with respect to the degradation of AMX. Based on the two different preparation methods adopted, the method in which TiO₂ was attached on the surface of the bio-polymer produced slightly increased degradation but was limited by fluctuation over irradiation time. TiO₂ leaching or aggregation which would have resulted in a decrease in the surface area could possibly have attributed to these results.

8.3. Recommendations for future research

The photochemical methods applied in this study using the chosen setups have resulted in both batch photoreactors showing great potential for degrading the APIs. This study, although providing useful insights into the photochemical degradation of APIs, is by no means conclusive and highlights the need for further development of the technology before it can be successfully applied for pharmaceutical-contaminated wastewater treatment. Foremost is the need to scale-up these photochemical processes to deal with the complex nature of such wastewaters.

Due to the complex nature of contaminated wastewater, which often contains industrial pollutants and high levels of organic matter, combinations with other AOP methods such as ozonation and photo-Fenton to enhance the degradation rates as well to improve the biodegradability of wastewater should be investigated.

Potential extensions of the studies summarised in this chapter are proposed in this section, indicating possible future research areas.

8.3.1. Photochemical degradation of diclofenac, naproxen and their mixtures by UV light

Based on the results obtained, the mechanism of API degradation in aqueous mixtures thereof is more complex than that for individual APIs only, and is not clearly understood. Therefore, further effort is required to fully characterise the degradation pathway of such mixtures in order to develop more effective and efficient wastewater treatment. While NSAIDs were the focus of this study, other classes of commonly used APIs such as antibiotics, β -blockers and antidepressant can be considered suitable candidates. Furthermore, more robust chromatographic methods (i.e. HPLC, LC-MS, LC-MS/MS) enabling simultaneous detection of APIs during the degradation process needs to be developed.

In addition, this study should be further extended to include other type of raw water such as secondary wastewater effluents as the water quality (e.g. organic matter and pH) may vary and thus affect the degradation process in different ways.

It is also a recommendation of this study to measure TOC as it provides more comprehensive information about the mineralization of degradation products and parent APIs. In addition, bioassay tests could be used alongside chemical detection methods to closely monitor the toxicity of the photochemically treated water, enabling the development of safer water treatment technologies. Bioassay tests should take into account toxicity towards beneficial microorganisms, fish, plants,

algae and invertebrates, ensuring that the treatment process and treated water are both safe for humans and the environment.

Degradation studies should be further extended to include those metabolites excreted as by-products of pharmaceutical metabolism in the human body.

8.3.2. Solar photolytic and TiO₂ photocatalytic degradation of pharmaceuticals

Future large-scale investigations would require suitable, flexible solar hardware. A CPC solar reactor, which uses symmetrically shaped mirrors (“round-W”) to harvest direct and diffuse light, could be used to optimise solar illumination conditions to increase API degradation efficiency. Tropical regions such as Townsville have favourable climatic conditions with over 300 days of sunshine per year, providing a unique opportunity to develop more suitable solar technology and test and implement novel methods.

8.3.3. Identification of photoproducts and elucidation of degradation pathways

Instrumentation such as LC-QTOF, which allows chromatographic separation of individual compounds and tandem MS_n ionization with accurate mass measurement, should be considered for any future chemical detection. Additionally, isolation of compounds from large scale reactions would enable for structural elucidation and confirmation by NMR.

The water matrix and its composition affect the rate and abundance of degradation product formation during TiO₂ photocatalysis and direct photolysis. As a result, it is important to develop and, where possible incorporate chemical measurements to enable photoproduct monitoring and early detection during the course of treatment. This early detection may provide information regarding the type of degradation products formed, providing a better indication about the pathway degradation which in turn would enable early intervention and further optimisation of the treatment.

8.3.4. Integrated photocatalytic adsorbent for the degradation of amoxicillin

It has been shown that the combined acid-alkali treatment of zeolite yielded a better performing IPA material. However, cations or other impurities that might be present in the zeolite were deemed to be responsible for the suppression of TiO₂ crystal growth. Treatment with different concentrations of acid and alkali would be needed to be examined in order to overcome this problem. While, natural zeolite was not found to participate in the degradation of AMX, it is possible that interactions

between its surface and TiO_2 may affect the process; therefore, further effort is required to minimise these variations.

To improve the photocatalytic activity of TiO_2 loaded on natural zeolite, metal doping (e.g. Pt, Au, Ag) might be also incorporated. The effect of other parameters affecting the AMX degradation such as solution pH and the presence of dissolved oxygen should be explored.

The prepared IPA materials can be also used for AMX solar degradation studies or tested on other environmentally important APIs such as analgesics (e.g. ibuprofen) and antibiotics (e.g. sulfamethoxazole).

To improve the performance of TiO_2 -gel beads prepared from this method, parameters such as concentration of NaAlg, CaCl_2 and TiO_2 P25 can be altered. Characterization studies of the surface using SEM, XRD and surface area measurements would enable the improved understanding of the fluctuations of results observed in this study.

Separation of AMX degradation products could be investigated using different mobile phases possibly with different additives or by modifying existing gradients. For example, MeOH and ACN, both commonly used solvents in reverse phase HPLC, may give rise to differences in the elution order or elution strength of specific by-products enabling chromatographic separation. Likewise, different solid phases may influence compound adsorption and elution.

References

- [1] S.D. Richardson, T.A. Ternes, *Anal. Chem.* 83 (2011) 4614-4648.
- [2] S.K. Khetan, T.J. Collins, *Chem. Rev.* 107 (2007) 2319-2364.
- [3] J.Q. Jiang, Z. Zhou, V.K. Sharma, *Microchemical Journal* 110 (2013) 292-300.
- [4] S. Mompelat, B. Le Bot, O. Thomas, *Environ. Int.* 35 (2009) 803-814.
- [5] D. Fatta-Kassinos, S. Meric, A. Nikolaou, *Anal. Bioanal. Chem.* 399 (2011) 251-275.
- [6] B. Halling-Sørensen, S.N. Nielsen, P.F. Lanzky, F. Ingerslev, H.C.H. Lützhof, S.E. Jørgensen, *Chemosphere.* 36 (1998) 357-394.
- [7] L.H.M.L.M. Santos, A.N. Araújo, A. Fachini, A. Pena, C. Delerue-Matos, M.C.B.S.M. Montenegro, *J. Hazard. Mater.* 175 (2010) 45-95.
- [8] O.K. Dalrymple, D.H. Yeh, M.A. Trotz, *J. Chem. Technol. Biotechnol.* 82 (2007) 121-134.
- [9] M. Klavarioti, D. Mantzavinou, D. Kassinos, *Environ. Int.* 35 (2009) 402-417.
- [10] A.Y.C. Tong, R. Braund, D.S. Warren, B.M. Peake, *Cent. Eur. J. Chem* 10 (2012) 989-1027.
- [11] M.N. Chong, B. Jin, C.W.K. Chow, C. Saint, *Water Res.* 44 (2010) 2997-3027.
- [12] C.D. Metcalfe, *Environ. Toxicol. Chem.* 32 (2013) 1683-1684.
- [13] S. Esplugas, D.M. Bila, L.G.T. Krause, M. Dezotti, *J. Hazard. Mater.* 149 (2007) 631-642.
- [14] A. Nikolaou, S. Meric, D. Fatta, *Anal. Bioanal. Chem.* 387 (2007) 1225-1234.
- [15] J.P. Bound, N. Voulvoulis, *Environ. Health Perspect.* 113 (2005) 1705-1711.
- [16] S. Suárez, M. Carballa, F. Omil, J.M. Lema, *Rev. Environ. Sci. Biotechnol.* 7 (2008) 125-138.
- [17] A. Ziyilan, N.H. Ince, *J. Hazard. Mater.* 187 (2011) 24-36.
- [18] B. Ferrari, N. Paxéus, R. Lo Giudice, A. Pollio, J. Garric, *Ecotox. Environ. Safe.* 55 (2003) 359-370.
- [19] P. Verlicchi, M. Al Aukidy, E. Zambello, *Sci. Total Environ.* 429 (2012) 123-155.
- [20] K. Kümmerer, *J. Environ. Manage.* 90 (2009) 2354-2366.
- [21] T.A. Ternes, *Water Res.* 32 (1998) 3245-3260.
- [22] Z. Moldovan, *Chemosphere.* 64 (2006) 1808-1817.
- [23] J.E. Drewes, T. Heberer, K. Reddersen, *Wat. Sci. Technol.* 46 (2002) 73-80.
- [24] R. López-Serna, A. Jurado, E. Vázquez-Suñé, J. Carrera, M. Petrović, D. Barceló, *Environ. Pollut.* 174 (2013) 305-315.
- [25] T. Heberer, *J. Hydrol.* 266 (2002) 175-189.
- [26] R. Andreozzi, R. Marotta, N. Paxeus, *Chemosphere.* 50 (2003) 1319-1330.
- [27] M. Carballa, F. Omil, J.M. Lema, M. Llombart, C. García-Jares, I. Rodríguez, M. Gomez, T. Ternes, *Water Res.* 38 (2004) 2918-2926.
- [28] N. Lindqvist, T. Tuhkanen, L. Kronberg, *Water Res.* 39 (2005) 2219-2228.
- [29] S.J. Khan, J.E. Ongerth, *Chemosphere.* 54 (2004) 355-367.
- [30] O. Braga, G.A. Smythe, A.I. Schäfer, A.J. Feitz, *Environ. Sci. Technol.* 39 (2005) 3351-3358.
- [31] A.J. Watkinson, E.J. Murby, S.D. Costanzo, *Water Res.* 41 (2007) 4164-4176.
- [32] A.J. Watkinson, E.J. Murby, D.W. Kolpin, S.D. Costanzo, *Sci. Total Environ.* 407 (2009) 2711-2723.
- [33] N. Le-Minh, R.M. Stuetz, S.J. Khan, *Talanta.* 89 (2012) 407-416.
- [34] A. Pal, K.Y.H. Gin, A.Y.C. Lin, M. Reinhard, *Sci. Total Environ.* 408 (2010) 6062-6069.
- [35] K. Kümmerer, *Chemosphere.* 75 (2009) 417-434.
- [36] I. Michael, L. Rizzo, C.S. McArdell, C.M. Manaia, C. Merlin, T. Schwartz, C. Dagot, D. Fatta-Kassinos, *Water Res.* 47 (2013) 957-995.
- [37] V. Calisto, V.I. Esteves, *Chemosphere.* 77 (2009) 1257-1274.
- [38] K. Kümmerer, A. Al-Ahmad, V. Mersch-Sundermann, *Chemosphere.* 40 (2000) 701-710.
- [39] J.L. Oaks, M. Gilbert, M.Z. Virani, R.T. Watson, C.U. Meteyer, B.A. Rideout, H.L. Shivaprasad, S. Ahmed, M.J.I. Chaudhry, M. Arshad, S. Mahmood, A. Ali, A.A. Khan, *Nature.* 427 (2004) 630-633.
- [40] T. Brodin, J. Fick, M. Jonsson, J. Klaminder, *Science.* 339 (2013) 814-815.

- [41] K. Kümmerer, *Chemosphere*. 75 (2009) 435-441.
- [42] Th. Heberer, K. Reddersen, A. Mechlinski, *Water Sci. Technol.* 46 (2002) 81-88.
- [43] T.A. Ternes, M. Meisenheimer, D. McDowell, F. Sacher, H.J. Brauch, B.H. Gulde, G. Preuss, U. Wilme, N.Z. Seibert, *Environ. Sci. Technol.* 36 (2002) 3855-3863.
- [44] O.A. Jones, J.N. Lester, N. Voulvoulis, *Trends. Biotechnol.* 23 (2005) 163-167.
- [45] D.J. Lapworth, N. Baran, M.E. Stuart, R.S. Ward, *Environ. Pollut.* 163 (2012) 287-303.
- [46] S. Carbonaro, M.N. Sugihara, T.J. Strathmann, *Appl. Catal. B-Environ.* 129 (2013) 1-12.
- [47] K. Fent, A.A. Weston, D. Caminada, *Aquat. Toxicol.* 76 (2006) 122-159.
- [48] I. Oller, S. Malato, J.A. Sánchez-Pérez, *Sci. Total. Environ.* 409 (2011) 4141-4166.
- [49] H. Yamamoto, Y. Nakamura, S. Moriguchi, Y. Honda, I. Tamura, Y. Hirata, A. Hayashi, J. Sekizawa, *Water Res.* 43 (2009) 351-362.
- [50] E. Donner, T. Kosjek, S. Qualmann, K.O. Kusk, E. Heath, D.M. Revitt, A. Ledin, H.R. Andersen, *Sci. Total. Environ.* 443 (2013) 870-876.
- [51] F.A. Caliman, M. Gavrilesu, *Clean-Soil Air Water.* 37 (2009) 277-303.
- [52] P. Drillia, K. Stamatelidou, G. Lyberatos, *Chemosphere*. 60 (2005) 1034-1044.
- [53] M. Petrovic, D. Barceló, *TrAC Trends. Anal. Chem.* 26 (2007) 486-493.
- [54] Y.J. Zhang, S.U. Geißen, C. Gal, *Chemosphere*. 73 (2008) 1151-1161.
- [55] R. Andreozzi, V. Caprio, A. Insola, R. Marotta, *Catal. Today*. 53 (1999) 51-59.
- [56] O. Legrini, E. Oliveros, A.M. Braun, *Chem. Rev.* 93 (1993) 671-698.
- [57] P.R. Gogate, A.B. Pandit, *Adv. Environ. Res.* 8 (2004) 501-551.
- [58] J.L. Wang, L.J. Xu, *Crit. Rev. Environ. Sci. Technol.* 42 (2012) 251-325.
- [59] R.F. Dantas, C. Sans, S. Esplugas, *J. Environ. Eng.-ASCE*. 137 (2011) 754-759.
- [60] Y. Wang, H. Zhang, J.H. Zhang, C. Lu, Q.Q. Huang, J. Wu, F. Liu, *J. Hazard. Mater.* 192 (2011) 35-43.
- [61] F. Ay, F. Kargi, *J. Hazard. Mater.* 179 (2010) 622-627.
- [62] A.G. Trovó, R.F.P. Nogueira, A. Agüera, A.R. Fernandez-Alba, S. Malato, *Water Res.* 45 (2011) 1394-1402.
- [63] M. Sturini, A. Speltini, F. Maraschi, A. Profumo, L. Pretali, E. Fasani, A. Albin, *Environ. Sci. Technol.* 44 (2010) 4564-4569.
- [64] C. Baeza, D.R.U. Knappe, *Water Res.* 45 (2011) 4531-4543.
- [65] Y.J. Jung, W.G. Kim, Y. Yoon, J.W. Kang, Y.M. Hong, H.W. Kim, *Sci. Total Environ.* 420 (2012) 160-167.
- [66] E. De Bel, C. Janssen, S. De Smet, H. Van Langenhove, J. Dewulf, *Ultrason. Sonochem.* 18 (2011) 184-189.
- [67] G.T. Güyer, N.H. Ince, *Ultrason. Sonochem.* 18 (2011) 114-119.
- [68] Y.X. Lin, C. Ferronato, N.S. Deng, J.M. Chovelon, *Appl. Catal. B-Environ.* 104 (2011) 353-360.
- [69] E. Regulska, J. Karpińska, *Appl. Catal. B-Environ.* 117-118 (2012) 96-104.
- [70] N. Klammerth, L. Rizzo, S. Malato, M.I. Maldonado, A. Agüera, A.R. Fernández-Alba, *Water Res.* 44 (2010) 545-554.
- [71] J. Radjenović, C. Sirtori, M. Petrović, D. Barceló, S. Malato, *Chemosphere*. 79 (2010) 368-376.
- [72] C. Sirtori, A. Zapata, W. Gernjak, S. Malato, A. Lopez, A. Agüera, *Water Res.* 45 (2011) 1736-1744.
- [73] H. Dimitroula, V.M. Daskalaki, Z. Frontistis, D.I. Kondarides, P. Panagiotopoulou, N.P. Xekoukoulotakis, D. Mantzavinos, *Appl. Catal. B-Environ.* 117 (2012) 283-291.
- [74] F. Méndez-Arriaga, R.A. Torres-Palma, C. Pétrier, S. Esplugas, J. Gimenez, C. Pulgarin, *Water Res.* 43 (2009) 3984-3991.
- [75] J. Madhavan, F. Grieser, M. Ashokkumar, *J. Hazard. Mater.* 178 (2010) 202-208.
- [76] F.J. Rivas, F.J. Beltrán, A. Encinas, *J. Environ. Manage.* 100 (2012) 10-15.
- [77] R. Andreozzi, M. Canterino, R. Marotta, N. Paxeus, *J. Hazard. Mater.* 122 (2005) 243-250.
- [78] K. Ikehata, N.J. Naghashkar, M.G. Ei-Din, *Ozone-Sci. Eng.* 28 (2006) 353-414.
- [79] P. Bautista, A.F. Mohedano, J.A. Casas, J.A. Zazo, J.J. Rodriguez, *J. Chem. Technol. Biotechnol.* 83 (2008) 1323-1338.

- [80] S. Malato, J. Blanco, A. Vidal, C. Richter, *Appl. Catal. B-Environ.* 37 (2002) 1-15.
- [81] L.A. Pérez-Estrada, S. Malato, W. Gernjak, A. Agüera, E.M. Thurman, I. Ferrer, A.R. Fernández-Alba, *Environ. Sci. Technol.* 39 (2005) 8300-8306.
- [82] A.G. Trovó, S.A.S. Melo, R.F.P. Nogueira, *J. Photochem. Photobiol. A-Chem.* 198 (2008) 215-220.
- [83] I. Michael, E. Hapeshi, C. Michael, A.R. Varela, S. Kyriakou, C.M. Manaia, D. Fatta-Kassinos, *Water Res.* 46 (2012) 5621-5634.
- [84] I. Kim, N. Yamashita, H. Tanaka, *J. Hazard. Mater.* 166 (2009) 1134-1140.
- [85] F. Méndez-Arriaga, R.A. Torres-Palma, C. Pétrier, S. Esplugas, J. Gimenez, C. Pulgarin, *Water Res.* 42 (2008) 4243-4248.
- [86] I. Sirés, E. Brillas, *Environ. Int.* 40 (2012) 212-229.
- [87] Y. Liu, X. Gan, B. Zhou, B. Xiong, J. Li, C. Dong, J. Bai, W. Cai, *J. Hazard. Mater.* 171 (2009) 678-683.
- [88] T. Oppenländer, *Photochemical Purification of Water and Air-Advanced Oxidation Processes (AOPs): Principles, Reaction Mechanisms, Reactor Concepts*, Wiley-VCH, New York, 2003.
- [89] O. Shvydkiv, *Microphotochemistry - A New Resources-Efficient Synthesis Tool Approach*. PhD Thesis. The School of Chemical Sciences, Dublin City University, 2012.
- [90] D.E. Moore, *J. Pharm. Biomed. Anal.* 5 (1987) 441-453.
- [91] R. Salgado, V.J. Pereira, G. Carvalho, R. Soeiro, V. Gaffney, C. Almeida, V.V. Cardoso, E. Ferreira, M.J. Benoliel, T.A. Ternes, A. Oehmen, M.A.M. Reis, J.P. Noronha, *J. Hazard. Mater.* 244-245 (2013) 516-527.
- [92] V.J. Pereira, K.G. Linden, H.S. Weinberg, *Water Res.* 41 (2007) 4413-4423.
- [93] W.Z. Li, S.G. Lu, Z.F. Qiu, K.F. Lin, *Environ. Technol.* 32 (2011) 1063-1071.
- [94] N. De la Cruz, R.F. Dantas, J. Giménez, S. Esplugas, *Appl. Catal. B-Environ.* 130 (2013) 249-256.
- [95] J. Blanco-Galvez, P. Fernández-Ibáñez, S. Malato-Rodríguez, *J. Sol. Energy Eng-Trans ASME.* 129 (2007) 4-15.
- [96] E.M. Rodríguez, G. Fernández, P.M. Alvarez, F.J. Beltrán, *Water Res.* 46 (2012) 152-166.
- [97] S.E. Braslavsky, *Pure Appl Chem* 79 (2007) 293-465.
- [98] V. Homem, L. Santos, *J. Environ. Manage.* 92 (2011) 2304-2347.
- [99] R. Bauer, G. Waldner, H. Fallmann, S. Hager, M. Klare, T. Krutzler, S. Malato, P. Maletzky, *Catal. Today.* 53 (1999) 131-144.
- [100] S.A. Parsons, M. Williams, in: S. Parsons (Ed.), *Advanced Oxidation Processes for Water and Wastewater Treatment*, IWA Publishing, London, 2005.
- [101] I. Kim, H. Tanaka, *Environ. Int.* 35 (2009) 793-802.
- [102] F. Yuan, C. Hu, X.X. Hu, J.H. Qu, M. Yang, *Water Res.* 43 (2009) 1766-1774.
- [103] T.E. Doll, F.H. Frimmel, *Chemosphere.* 52 (2003) 1757-1769.
- [104] L. Carlos, D.O. Mártire, M.C. Gonzalez, J. Gomis, A. Bernabeu, A.M. Amat, A. Arques, *Water Res.* 46 (2012) 4732-4740.
- [105] J. Peuravuori, *Int. J. Environ. Anal. Chem.* 92 (2012) 1470-1492.
- [106] V. Calisto, M.R.M. Domingues, V.I. Esteves, *Water Res.* 45 (2011) 6097-6106.
- [107] A. Fujishima, X.T. Zhang, D.A. Tryk, *Surf. Sci. Rep.* 63 (2008) 515-582.
- [108] D.S. Bhatkhande, V.G. Pangarkar, A.A.C.M. Beenackers, *J. Chem. Technol. Biotechnol.* 77 (2002) 102-116.
- [109] S. Malato, P. Fernández-Ibáñez, M.I. Maldonado, J. Blanco, W. Gernjak, *Catal. Today.* 147 (2009) 1-59.
- [110] O. Carp, C.L. Huisman, A. Reller, *Prog. Solid State Chem.* 32 (2004) 33-177.
- [111] C.S. Turchi, D.F. Ollis, *J. Catal.* 122 (1990) 178-192.
- [112] M.R. Hoffmann, S.T. Martin, W. Choi, D.W. Bahnemann, *Chem. Rev.* 95 (1995) 69-96.
- [113] B. Ohtani, *Chem. Lett.* 37 (2008) 217-229.
- [114] T.A. Kandiel, L. Robben, A. Alkaim, D. Bahnemann, *Photochem. Photobiol. Sci.* 12 (2013) 602-609.
- [115] C.G. Silva, J.L. Faria, *Photochem. Photobiol. Sci.* 8 (2009) 705-711.

- [116] A. Achilleos, E. Hapeshi, N.P. Xekoukoulotakis, D. Mantzavinos, D. Fatta-Kassinos, *Chem. Eng. J.* 161 (2010) 53-59.
- [117] D. Dimitrakopoulou, I. Rethemiotaki, Z. Frontistis, N.P. Xekoukoulotakis, D. Venieri, Mantzavinos, *J. Environ. Manage.* 98 (2012) 168-174.
- [118] M.A. Fox, M.T. Dulay, *Chem. Rev.* 93 (1993) 341-357.
- [119] A. Mills, S. Le Hunte, *J. Photochem. Photobiol A: Chemistry.* 108 (1997) 1-35.
- [120] L.H. Hu, P.M. Flanders, P.L. Miller, T.J. Strathmann, *Water Res.* 41 (2007) 2612-2626.
- [121] A.L. Giraldo, G.A. Peñuela, R.A. Torres-Palma, N.J. Pino, R.A. Palominos, H.D. Mansilla, *Water Res.* 44 (2010) 5158-5167.
- [122] X. Van Doorslaer, P.M. Heynderickx, K. Demeestere, K. Debevere, H. Van Langenhove, J. Dewulf, *Appl. Catal. B-Environ.* 111 (2012) 150-156.
- [123] R.A. Palominos, M.A. Mondaca, A. Giraldo, G. Penuela, M. Pérez-Moya, H.D. Mansilla, *Catal. Today.* 144 (2009) 100-105.
- [124] E.S. Elmolla, M. Chaudhuri, *Desalination.* 252 (2010) 46-52.
- [125] C. Sirtori, A. Agüera, W. Gernjak, S. Malato, *Water Res.* 44 (2010) 2735-2744.
- [126] F. Méndez-Arriaga, J. Gimenez, S. Esplugas, *J. Adv. Oxid. Technol.* 11 (2008) 435-444.
- [127] L. Yang, L.E. Yu, M.B. Ray, *Water Res.* 42 (2008) 3480-3488.
- [128] R.K. Szabó, C.S. Megyeri, E. Illés, K. Gajda-Schranz, P. Mazellier, A. Dombi, *Chemosphere.* 84 (2011) 1658-1663.
- [129] J. Kockler, D. Kanakaraju, B. D. Glass, M. Oelgemöeller, *J. Sustain Sc. Manage.* 7 (2012) 23-29.
- [130] T.E. Doll, F.H. Frimmel, *Water Res.* 38 (2004) 955-964.
- [131] T.E. Doll, F.H. Frimmel, *Catal. Today.* 101 (2005) 195-202.
- [132] A. Achilleos, E. Hapeshi, N.P. Xekoukoulotakis, D. Mantzavinos, D. Fatta-Kassinos, *Sep. Sci. Technol.* 45 (2010) 1564-1570.
- [133] D.A. Lambropoulou, M.D. Hernando, I.K. Konstantinou, E.M. Thurman, I. Ferrer, T.A. Albanis, A.R. Fernández-Alba, *J. Chromatogr. A.* 1183 (2008) 38-48.
- [134] W. Li, S. Lu, Z. Qiu, K. Lin, *J. Hazard. Mater.* 176 (2010) 1051-1057.
- [135] V. Romero, N. De la Cruz, R.F. Dantas, P.M.J. Giménez, S. Esplugas, *Catal. Today.* 161 (2011) 115-120.
- [136] S. Fukahori, T. Fujiwara, R. Ito, N. Funamizu, *Chemosphere.* 89 (2012) 213-220.
- [137] D. Friedmann, C. Mendive, D. Bahnemann, *Appl. Catal. B-Environ.* 99 (2010) 398-406.
- [138] J.F. García-Araya, F.J. Beltrán, A. Aguinaco, *J. Chem. Technol. Biotechnol.* 85 (2010) 798-804.
- [139] A. Agüera, L.A.P. Estrada, I. Ferrer, E.M. Thurman, S. Malato, A.R. Fernandez-Alba, *J. Mass Spectrom.* 40 (2005) 908-915.
- [140] D. Fatta-Kassinos, M.I. Vasquez, K. Kümmerer, *Chemosphere.* 85 (2011) 693-709.
- [141] U.I. Gaya, A.H. Abdullah, *J. Photochem. Photobiol. C-Photochem. Rev.* 9 (2008) 1-12.
- [142] F. Méndez-Arriaga, S. Esplugas, J. Giménez, *Water Res.* 42 (2008) 585-594.
- [143] R. Rosal, A. Rodríguez, M.S. Gonzalo, E. García-Calvo, *Appl. Catal. B-Environ.* 84 (2008) 48-57.
- [144] R. Molinari, F. Pirillo, V. Loddo, L. Palmisano, *Catal. Today.* 118 (2006) 205-213.
- [145] A.F. Martins, F. Mayer, E.C. Confortin, C.D. Frank, *Clean-Soil Air Water.* 37 (2009) 365-371.
- [146] J.M. Herrmann, *Top. Catal.* 34 (2005) 49-65.
- [147] J.M. Herrmann, *Catal. Today.* 53 (1999) 115-129.
- [148] T.E. Doll, F.H. Frimmel, *Water Res.* 39 (2005) 403-411.
- [149] C. Martínez, M. Canle, M.I. Fernandez, J.A. Santaballa, J. Faria, *Appl. Catal. B-Environ.* 107 (2011) 110-118.
- [150] N. Zhang, G.G. Liu, H.J. Liu, Y.L. Wang, Z.W. He, G. Wang, *J. Hazard. Mater.* 192 (2011) 411-418.
- [151] L. Rizzo, S. Meric, D. Kassinos, M. Guida, F. Russo, V. Belgiorno, *Water Res.* 43 (2009) 979-988.

- [152] C. Lacey, G. McMahon, J. Bones, L. Barron, A. Morrissey, J.M. Tobin, *Talanta*. 75 (2008) 1089-1097.
- [153] A.C. Mehinto, E.M. Hill, C.R. Tyler, *Environ. Sci. Technol.* 44 (2010) 2176-2182.
- [154] L. Feng, E.D. van Hullebusch, M.A. Rodrigo, G. Esposito, M.A. Oturan, *Chem. Eng. J.* 228 (2013) 944-964.
- [155] T. Heberer, *Toxicol. Lett.* 131 (2002) 5-17.
- [156] T. Heberer, A. Mechlinski, B. Fanck, A. Knappe, G. Massmann, A. Pekdeger, B. Fritz, *Ground Water Monit. Remediat.* 24 (2004) 70-77.
- [157] R. Salgado, R. Marques, J.P. Noronha, G. Carvalho, A. Oehmen, M.A.M. Reis, *Environ. Sci. Pollut. Res.* 19 (2012) 1818-1827.
- [158] A.L. Boreen, W.A. Arnold, K. McNeill, *Aquat. Sci.* 65 (2003) 320-341.
- [159] T. Poiger, H.R. Buser, M.D. Müller, *Environ. Toxicol. Chem.* 20 (2001) 256-263.
- [160] J.L. Packer, J.J. Werner, D.E. Latch, K. McNeill, W.A. Arnold, *Aquat. Sci.* 65 (2003) 342-351.
- [161] P. Bartels, W. von Tümpling, *Sci. Total Environ.* 374 (2007) 143-155.
- [162] D.E. Moore, S. Robertsthomson, D. Zhen, C.C. Duke, *Photochem. Photobiol.* 52 (1990) 685-690.
- [163] L. Minetto, F.M. Mayer, C.A. Mallmann, A.F. Martins, *Clean-Soil Air Water.* 40 (2012) 950-957.
- [164] Z. Shu, J.R. Bolton, M. Belosevic, M. Gamal El Din, *Water Res.* 47 (2013) 2881-2889.
- [165] P. Calza, V.A. Sakkas, C. Medana, C. Baiocchi, A. Dimou, E. Pelizzetti, T. Albanis, *Appl. Catal. B-Environ.* 67 (2006) 197-205.
- [166] L.A. Pérez-Estrada, M.I. Maldonado, W. Gernjak, A. Agüera, A.R. Fernández-Alba, M.M. Ballesteros, S. Malato, *Catal. Today.* 101 (2005) 219-226.
- [167] A. Bernabeu, R.F. Vercher, L. Santos-Juanes, P.J. Simón, C. Lardin, M.A. Martínez, J.A. Vicente, R. Gonzalez, C. Llosa, A. Arques, A.M. Amat, *Catal. Today.* 161 (2011) 235-240.
- [168] D. Vogna, R. Marotta, A. Napolitano, R. Andreozzi, M. d'Ischia, *Water Res.* 38 (2004) 414-422.
- [169] V. Naddeo, V. Belgiorno, D. Kassinos, D. Mantzavinos, S. Meric, *Ultrason. Sonochem.* 17 (2010) 179-185.
- [170] A. Aguinaco, F.J. Beltrán, J.F. García-Araya, A. Oropesa, *Chem. Eng. J.* 189-190 (2012) 275-282.
- [171] J. Eriksson, J. Svanfelt, L. Kronberg, *Photochem. Photobiol.* 86 (2010) 528-532.
- [172] P. Grenni, L. Patrolecco, N. Ademollo, A. Tolomei, A. Barra Caracciolo, *Microchem. J.* 107 (2013) 158-164.
- [173] A. Jelic, M. Gros, A. Ginebreda, R. Cespedes-Sánchez, F. Ventura, M. Petrovic, D. Barcelo, *Water Res.* 45 (2011) 1165-1176.
- [174] R. Marotta, D. Spasiano, I. Di Somma, R. Andreozzi, *Water Res.* 47 (2013) 373-383.
- [175] M. Cleuvers, *Ecotox. Environ. Safe.* 59 (2004) 309-315.
- [176] N. Klammerth, S. Malato, A. Agüera, A. Fernández-Alba, *Water Res.* 47 (2013) 833-840.
- [177] E. Felis, D. Marciocha, J. Surmacz-Gorska, K. Miksch, *Water Sci. Technol.* 55 (2007) 281-286.
- [178] F. Boscá, M.A. Miranda, L. Vañó, F. Vargas, J. Photochem. Photobiol. A: Chemistry 54 (1990) 131-134.
- [179] M. Isidori, M. Lavorgna, A. Nardelli, A. Parrella, L. Previtiera, M. Rubino, *Sci. Total Environ.* 348 (2005) 93-101.
- [180] F. Boscá, M.L. Marin, M.A. Miranda, *Photochem. Photobiol.* 74 (2001) 637-655.
- [181] M. DellaGreca, M. Brigante, M. Isidori, A. Nardelli, L. Previtiera, M. Rubino, F. Temussi, *Environ. Chem. Lett.* 1 (2004) 237-241.
- [182] J.V. Castell, M.J. Gomez-Lechon, C. Grassa, L.A. Martinez, M.A. Miranda, P. Tarrega, *Photochem. Photobiol.* 57 (1993) 486-490.
- [183] E. Felis, K. Miksch, *Wat. Sci. Technol.* 2009 2253-2259.
- [184] L. Prieto-Rodriguez, S. Miralles-Cuevas, I. Oller, A. Agüera, G.L. Puma, S. Malato, J. Hazard. Mater. 211 (2012) 131-137.

- [185] C. Tixier, H.P. Singer, S. Oellers, S.R. Muller, *Environ. Sci. Technol.* 37 (2003) 1061-1068.
- [186] R. Andreozzi, V. Caprio, C. Ciniglia, M. De Champdoré, R. Lo Giudice, R. Marotta, E. Zuccato, *Environ. Sci. Technol.* 38 (2004) 6832-6838.
- [187] H. Xu, W.J. Cooper, J. Jung, W. Song, *Water Res.* 45 (2011) 632-638.
- [188] E.S. Elmolla, M. Chaudhuri, *Desalination*. 256 (2010) 43-47.
- [189] E.S. Elmolla, M. Chaudhuri, *J. Hazard. Mater.* 173 (2010) 445-449.
- [190] D. Klauson, J. Babkina, K. Stepanova, M. Krichevskaya, S. Preis, *Catal. Today*. 151 (2010) 39-45.
- [191] J.H.O.S. Pereira, A.C. Reis, O.C. Nunes, M.T. Borges, V.J.P. Vilar, R.A.R. Boaventura, *Environ. Sci. Pollut. Res.* (2013) 1-12.
- [192] C. Mavronikola, M. Demetriou, E. Hapeshi, D. Partassides, C. Michael, D. Mantzavinos, D. Kassinos, *J. Chem. Technol. Biotechnol.* 84 (2009) 1211-1217.
- [193] A. Pérez-Parada, A. Agüera, M.D. Gómez-Ramos, J.F. García-Reyes, H. Heinzen, A.R. Fernández-Alba, *Rapid Commun. Mass Spectrom.* 25 (2011) 731-742.
- [194] E. Nägele, R. Moritz, *J. Am. Soc. Mass Spectrom.* 16 (2005) 1670-1676.
- [195] D.M. Pavlović, S. Babić, A.J.M. Horvat, M. Kaštelan-Macan, *TrAC - Trends Anal Chem.* 26 (2007) 1062-1075.
- [196] E.K. Putra, R. Pranowo, J. Sunarso, N. Indraswati, S. Ismadji, *Water Res.* 43 (2009) 2419-2430.
- [197] A.M. Braun, M.T. Maurette, E. Oliveros, *Photochemical Technology*, Wiley-VCH:Weinheim, 1991.
- [198] Heraeus, Operation Instructions UV-RS-1. No 4510 3400.
- [199] ARPANSA. Australian Radiation Protection and Nuclear Safety Agency. <http://www.arpansa.gov.au>. Date accessed: 18 June 2013.
- [200] Standard Methods for the Examination of the Water and Wastewater, 18th Edition ed., American Public Health Association, Washington D.C, 1992.
- [201] ICH, Harmonised Tripartite Guideline 2005 Validation of Analytical Procedures: Text and Methodology Q2 (R1). www.ich.org. Date accessed: 20 May 2013.
- [202] Y.H. Hsu, Y.B. Liou, J.A. Lee, C.Y. Chen, A.B. Wu, *Biomed. Chromatogr.* 20 (2006) 787-793.
- [203] M.W. Dong, *Modern HPLC for Practicing Scientists*, John Wiley & Sons, New Jersey, 2006.
- [204] USEPA, Fate, Transport and Transformation Test Guidelines, OPPTS 835.2210: Direct photolysis rate in water by sunlight, 1998.
- [205] F.J. Benitez, F.J. Real, J.L. Acero, G. Roldan, *J. Chem. Technol. Biotechnol.* 84 (2009) 1186-1195.
- [206] J. Pérez-Prieto, R.E. Galian, M.C. Morant-Miñana, *Chem. Phys. Chem.* 7 (2006) 2077-2080.
- [207] N. Guettaï, H.A. Amar, *Desalination*. 185 (2005) 439-448.
- [208] J. Choina, H. Kosslick, C. Fischer, G.U. Flechsig, L. Frunza, A. Schulz, *Appl. Catal. B-Environ.* 129 (2013) 589-598.
- [209] J.H.O.S. Pereira, V.J.P. Vilar, M.T. Borges, O. González, S. Esplugas, R.A.R. Boaventura, *Sol. Energy*. 85 (2011) 2732-2740.
- [210] B. Zheng, Z. Zheng, J. Zhang, Q. Liu, J. Wang, X. Luo, L. Wang, *Environ. Eng. Sci.* 29 (2012) 386-391.
- [211] H. Yang, G.Y. Li, T.C. An, Y.P. Gao, J.M. Fu, *Catal. Today* 153 (2010) 200-207.
- [212] L.A. Ioannou, E. Hapeshi, M.I. Vasquez, D. Mantzavinos, D. Fatta-Kassinos, *Sol. Energy*. 85 1915-1926.
- [213] I. Michael, E. Hapeshi, C. Michael, D. Fatta-Kassinos, *Water Res.* 44 (2010) 5450-5462.
- [214] P. Calza, E. Pelizzetti, *Pure Appl. Chem.* 73 (2001) 1839-1848.
- [215] D.C. Schmelling, K.A. Gray, P.V. Kamat, *Water Res.* 31 (1997) 1439-1447.
- [216] M.N. Chong, B. Jin, G. Laera, C.P. Saint, *Chem. Eng. J.* 174 (2011) 595-602.
- [217] J.H.O.S. Pereira, A.C. Reis, D. Queirós, O.C. Nunes, M.T. Borges, V.P. Vilar, R.A.R. Boaventura, *Sci. Total Environ.* 463-464 (2013) 274-283.
- [218] M. Ziegmann, T. Doll, F.H. Frimmel, *Acta Hydroch. Hydrob.* 34 (2006) 146-154.

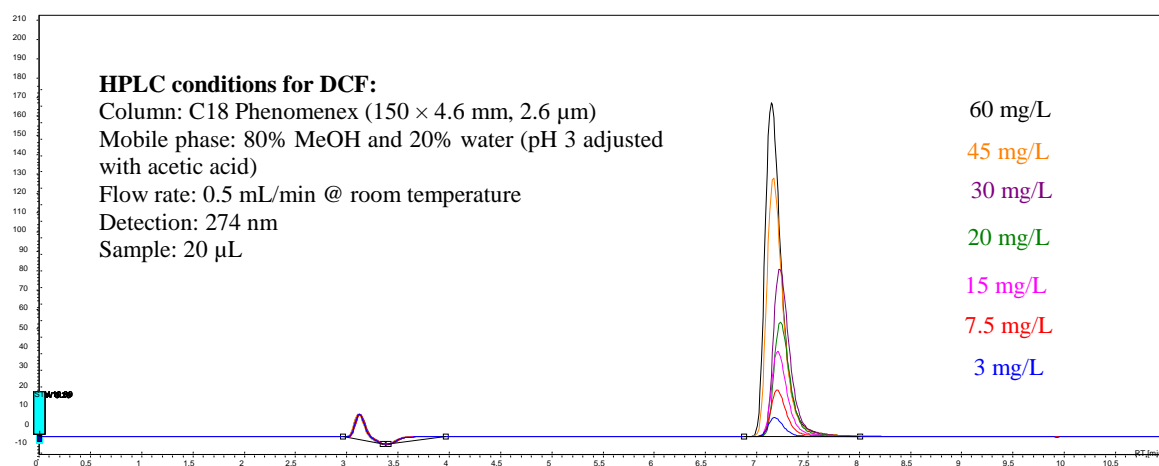
- [219] C. Sirtori, A. Zapata, I. Oller, W. Gernjak, A. Agüera, S. Malato, *Water Res.* 43 (2009) 661-668.
- [220] H.Y. Chen, O. Zahraa, M. Bouchy, *J. Photochem. Photobiol. A: Chemistry* 108 (1997) 37-44.
- [221] C. Rodrigues-Silva, M.G. Maniero, S. Rath, J.R. Guimarães, *Chem. Eng. J.* 224 (2013) 46-52.
- [222] D. Nasuhoglu, V. Yargeau, D. Berk, *J. Hazard. Mater.* 186 (2011) 67-75.
- [223] J. Radjenović, C. Sirtori, M. Petrović, D. Barceló, S. Malato, *Appl. Catal. B-Environ.* 89 (2009) 255-264.
- [224] S. Loiselle, D. Vione, C. Minero, V. Maurino, A. Tognazzi, A.M. Dattilo, C. Rossi, L. Bracchini, *Water Res.* 46 (2012) 3197-3207.
- [225] L. Rizzo, S. Meric, M. Guida, D. Kassinos, V. Belgiorno, *Water Res.* 43 (2009) 4070-4078.
- [226] F. Méndez-Arriaga, M.I. Maldonado, J. Gimenez, S. Esplugas, S. Malato, *Catal. Today.* 144 (2009) 112-116.
- [227] S. Chiron, C. Minero, D. Vione, *Environ. Sci. Technol.* 40 (2006) 5977-5983.
- [228] M.H. Priya, G. Madras, *Ind. Eng. Chem. Res.* 45 (2006) 482-486.
- [229] J. Pereira, V.J.P. Vilar, M.T. Borges, O. González, S. Esplugas, R.A.R. Boaventura, *Sol. Energy* 85 (2011) 2732-2740.
- [230] A. Agüera, M.J. Martínez Bueno, A.R. Fernández-Alba, *Environ. Sci. Pollut. Res.* 20 (2013) 3496-3515.
- [231] I. Ferrer, E.M. Thurman, *TrAC - Trends Anal Chem.* 22 (2003) 750-756.
- [232] M.C. Jiménez, M.A. Miranda, R. Tormos, *J. Photochem. Photobiol A: Chemistry.* 104 (1997) 119-121.
- [233] J. Sádecká, J. Netriová, *J. Liq. Chromatogr. Related. Technol.* 28 (2005) 2887-2894.
- [234] W. Zhang, L.D. Zou, L.Z. Wang, *Appl. Catal. A-Gen.* 371 (2009) 1-9.
- [235] F. Haque, E. Vaisman, C.H. Langford, A. Kantzas, *J. Photochem. Photobiol. A: Chemistry.* 169 (2005) 21-27.
- [236] Q.M. Kang, B.L. Yuan, J.G. Xu, M.L. Fu, *Catal. Lett.* 141 (2011) 1371-1377.
- [237] A.Y. Shan, T.I.M. Ghazi, S.A. Rashid, *Appl. Catal. A-Gen.* 389 (2010) 1-8.
- [238] S. Basha, C. Barr, D. Keane, K. Nolan, A. Morrissey, M. Oelgemöller, J.M. Tobin, *Photochem. Photobiol. Sci.* 10 (2011) 1014-1022.
- [239] M.E. Fabiyi, R.L. Skelton, *J. Photochem. Photobiol. A: Chemistry.* 132 (2000) 121-128.
- [240] S. Gelover, P. Mondragón, A. Jiménez, *J. Photochem. Photobiol. A: Chemistry.* 165 (2004) 241-246.
- [241] M.N. Chong, V. Vimonses, S. Lei, B. Jin, C. Chow, C. Saint, *Microporous. Mesoporous Mater.* 117 (2009) 233-242.
- [242] Z. Shi, S. Yao, C. Sui, *Catal. Sci. Tech.* 1 (2011) 817-822.
- [243] N.F. Zainudin, A.Z. Abdullah, A.R. Mohamed, *J. Hazard. Mater.* 174 (2010) 299-306.
- [244] E.P. Reddy, L. Davydov, P. Smirniotis, *Appl. Catal. B-Environ.* 42 (2003) 1-11.
- [245] W.J. Zhang, K.L. Wang, Y. Yu, H.B. He, *Chem. Eng. J.* 163 (2010) 62-67.
- [246] F. Li, S. Sun, Y. Jiang, M. Xia, M. Sun, B. Xue, *J. Hazard. Mater.* 152 (2008) 1037-1044.
- [247] M. Nikazar, K. Gholivand, K. Mahanpoor, *Desalination.* 219 (2008) 293-300.
- [248] M. Huang, C. Xu, Z. Wu, Y. Huang, J. Lin, J. Wu, *Dyes Pigments.* 77 (2008) 327-334.
- [249] S. Wang, Y. Peng, *Chem. Eng. J.* 156 (2010) 11-24.
- [250] K.Y. Foo, B.H. Hameed, *Adv. Colloid. Interface. Sci.* 162 (2011) 22-28.
- [251] S. Gomez, C.L. Marchena, L. Pizzio, L. Pierella, *J. Hazard. Mater.* 258-259 (2013) 19-26.
- [252] A. Ates, C. Hardacre, *J. Colloid. Interface. Sci.* 372 (2012) 130-140.
- [253] M.C. Kimling, R.A. Caruso, *J. Mater. Chem.* 22 (2012) 4073-4082.
- [254] S.K. Papageorgiou, F.K. Katsaros, E.P. Favvas, G.E. Romanos, C.P. Athanasekou, K.G. Beltsios, O.I. Tziaila, P. Falaras, *Water Res.* 46 (2012) 1858-1872.
- [255] J.Q. Albarelli, D.T. Santos, S. Murphy, M. Oelgemöller, *Water. Sci. Technol.* 60 (2009) 1081-1087.

- [256] C.G. Silva, Synthesis, Spectroscopy and Characterization of Titanium Dioxide based Photocatalysts for the Degradative Oxidation of Organic Pollutants, PhD Thesis. Departamento de Engenharia Quimica, Universidade do Porto, 2008.
- [257] B. Zhu, L. Zou, *J. Environ. Manage.* 90 (2009) 3217-3225.
- [258] C.R. Oliveira, J. Rubio, *Miner. Eng.* 20 (2007) 552-558.
- [259] M.E. Trujillo, D. Hírales, M.E. Rincón, J.F. Hinojosa, G.L. Leyva, F.F. Castellón, *J. Mater. Sci.* 48 (2013) 6778-6785.
- [260] M.V.P. Sharma, V. Durgakumari, M. Subrahmanyam, *J. Hazard. Mater.* 160 (2008) 568-575.
- [261] J. Burana-osot, S. Hosoyama, Y. Nagamoto, S. Suzuki, R.J. Linhardt, T. Toida, *Carbohydr. Res.* 344 (2009) 2023-2027.
- [262] I. Gozlan, A. Rotstein, D. Avisar, *Chemosphere.* 91 (2013) 985-992.

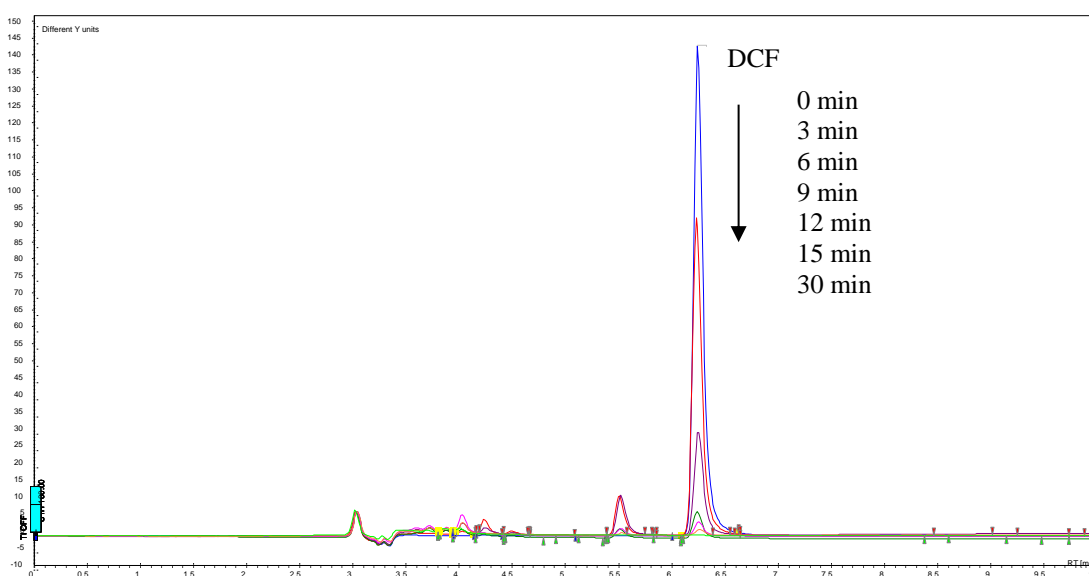
Appendix

Selected HPLC chromatogram

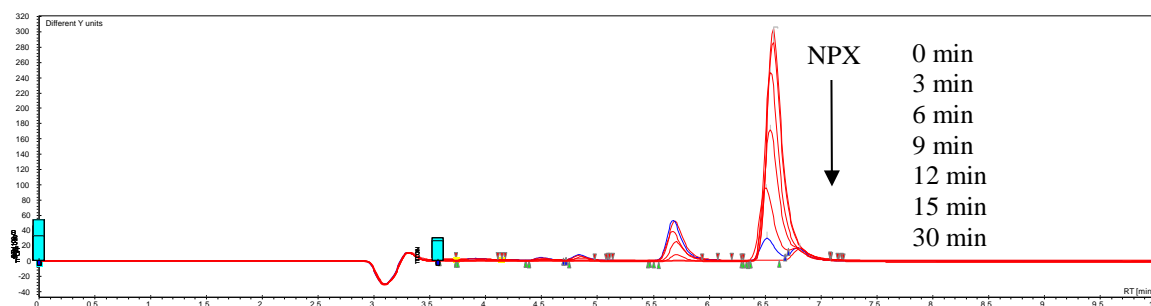
DCF calibration (standard concentrations 3-60 mg/L) (section 4.2.1)



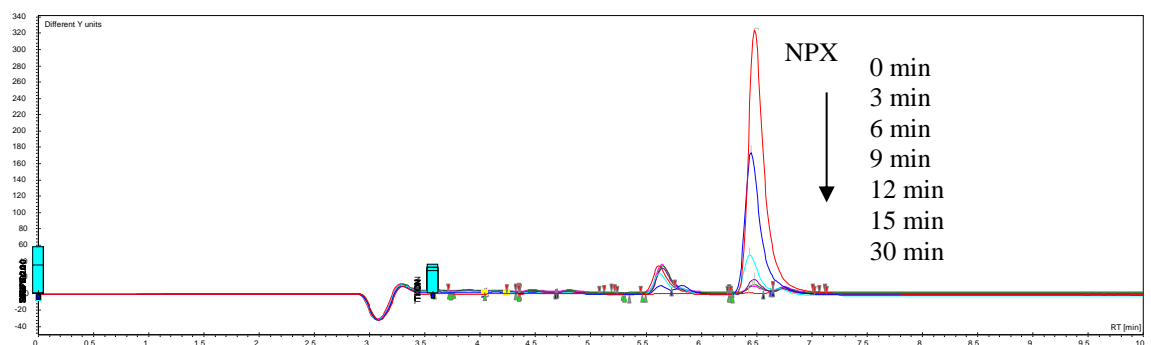
Photocatalysis of DCF in distilled water by medium pressure Hg lamp in immersion-well reactor (section 4.5)



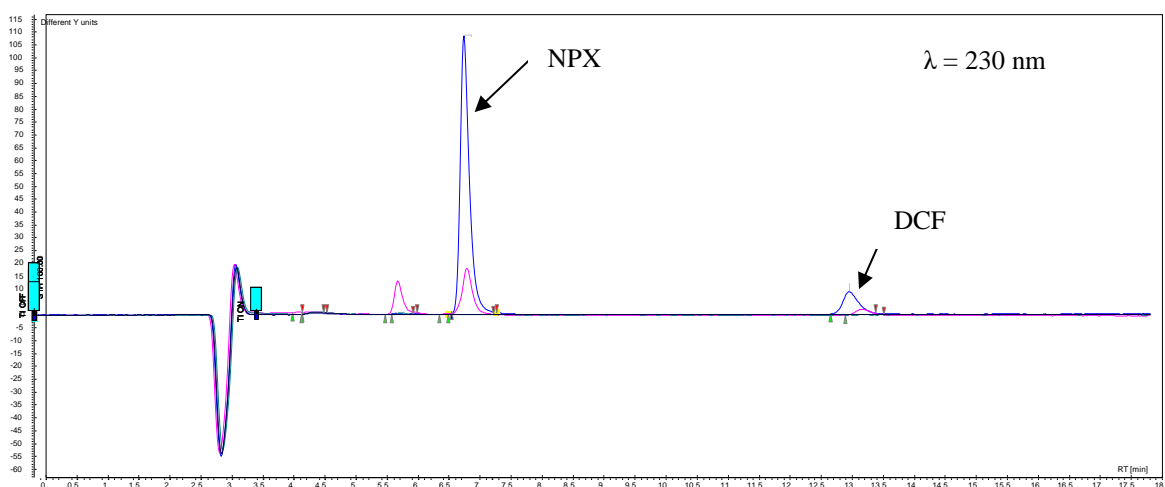
Direct photolysis of NPX in drinking water in immersion-well reactor (section 4.4)



Photocatalysis of NPX in distilled water by medium pressure Hg lamp in immersion-well reactor (section 4.6)



Photocatalysis of DCF and NPX mixtures in distilled water under sunlight (section 5.4)



FT-ICR-MS data (section 6.3)

NPX degradation product (ESI-)

Compound **48***: $C_{26}H_{25}O_5^- = 417$ ($t_R = 4.9$ min), Error Δ ppm = 5 ppm

CONFIRMATION

Molecular Formula: C₂₆H₂₅O₅ (-1)

Monoisotopic Mass: 417.1707
Average Mass: 417.4752
Most Abundant Mass: 417.1708

OK

